université de BORDEAUX

THÈSE PRÉSENTÉE

POUR OBTENIR LE GRADE DE

DOCTEUR DE

L'UNIVERSITÉ DE BORDEAUX

ÉCOLE DOCTORALE DES SCIENCES CHIMIQUES

SPÉCIALITÉ: CHIMIE ORGANIQUE

Par Cristiano Matteo MASTRODONATO

Elaboration of Fluorescent Molecular Probes and Molecular-Based Nanoparticles for Bioimaging Purposes

Sous la direction de: Mireille BLANCHARD-DESCE

Soutenue le 31/08/2017

Membres du jury:

M. LEMERCIER, Gilles	Professeur des Université, Univ. Reims	Rapporteur
Mme. SASAKI, Isabelle	Chargé de Recherche, Univ. Tolouse	Rapporteur
M. MONGIN, Olivier	Maître de Conférences, Univ. Rennes	Examinateur
M. VAULTIER, Michel	Directeur de Recherche Émérite, Univ. Bordeaux	Président du Jury
Mme. BLANCHARD-DESCE, Mireille	Directeur de Recherche, Univ. Bordeaux	Directrice de Thèse

Elaboration of fluorescent molecular probes and molecular-based nanoparticles for bioimaging purposes

Fluorescence-based techniques are popular tools for the study and understanding of biological processes. This has prompted continuous research aimed at the development of a wide range of fluorescent probes specifically designed for specific applications. Among them, fluorescent pH probes are of much interest as pH variations or gradients are involved in many biological events and anomalous alterations are often related to the onset of dysfunctions and diseases. In this framework we have developed a series of promising two-photon pH fluorescent molecular probes. These quadrupolar bolaamphiphilic probes are of great interest, as they combine a steep pH-dependence of their optical properties close to neutral pH, ratiometric behavior and large response to two-photon (2P) excitation in the NIR region. As such they offer much promise for ratiometric detection of the pH in biological environments and in situ monitoring of acidification. In parallel, we have been interest in the design of ultrabright nanoparticles for bioimaging purpose (in particular highly sensitive optical imaging). We chose to focus on Fluorescent Organic Nanoparticles made of organic molecules with low molecular weight (FONs) as they offer a flexible route and promising alternatives to toxic quantum dots. In this case the design of the dye used as building blocks of the FONs is of crucial importance and strongly influence the chemical and physical properties of the nanoparticles generated, such as their one and two-photon brightness and both their structural and colloidal stability. In that context a library of novel dipolar chromophores have been synthesized and used to prepare FONs using the nanoprecipitation method. Their properties were thoroughly investigated in order to determine the relationship between the molecular design of the isolated dye and the overall properties of the nanoparticles made of these dyes. As a result, Hyperbright FONs emitting in the green to NIR region and combining giant brightness and remarkable stability have been achieved. They offer major promise for bioimaging based on both excitation and detection in the NIR region.

Keywords: Organic synthesis, fluorescent probes, nanoparticles, two-photon absorption

Elaboration de sondes moléculaires fluorescentes et de nanoparticules organiques fluorescentes pour l'imagerie du vivant

Les techniques de fluorescence sont des outils de choix pour l'étude et la compréhension fine des processus biologiques. Ceci requiert toutefois l'utilisation de sondes fluorescentes parfaitement adaptées au but visé et répondant aux différentes exigences requises pour l'application visée. Dans ce cadre, nous nous sommes plus particulièrement intéressés à l'élaboration de sondes biphotoniques de pH adaptées à une mesure très sensible de faibles variations de pH autour du pH neutre. Les variations et gradients de pH sont en effet impliqués dans un certain nombre de processus biologiques importants et peuvent être associées à des dysfonctionnements liés à certaines maladies. Dans ce cadre, nous avons développé de nouvelles sondes fluorescentes de pH fluorescentes présentant à la fois un comportement ratiométrique, une forte sensibilité autour du pH neutre et facilement excitables dans le proche IR par absorption à deux photons. Ces sondes de structure quadrupolaire et bolamamphiphile permettent ainsi la détection ratiométrique du pH dans des environnements biologiques au moyen d'une excitation biphotonique dans le proche IR. En parallèle, nous nous sommes intéressés à l'élaboration de nanoparticules hyperbrillantes dédiées à l'imagerie biologique par microscopie de fluorescence induite par excitation à deux photons. Nous nous sommes plus particulièrement attachées au design de nanoparticules organiques fluorescentes constituées de molécules organiques de bas poids moléculaire (FONs). Cette approche offre en effet une grande flexibilité et la possibilité d'accéder à des nanosondes ayant des brillances comparables aux très populaires quantum dots mais moins toxiques et plus facilement dégradables. L'ingénierie moléculaire des fluorophores utilisés pour la préparation des FON est cruciale puisqu'elle influence fortement à la fois les propriétés photophysiques (brillance, couleur…) et leur propriétés physico-chimiques (stabilité chimique et structurale, stabilité colloïdale). Dans ce contexte, une librairie de nouveaux chromophores dipolaires a été synthétisée et utilisées pour la préparation de FON par la méthode de nano-précipitation. Leurs propriétés ont été étudiées afin de déterminer la relation entre la structure du chromophore et les propriétés globales des nanoparticules constituées de ces colorants. Ce travail a permis d'identifier les paramètres structuraux permettant d'accéder à des nanoparticules présentant à la fois une brillance exceptionnelle, une émission modulable du vert au rouge et proche IR et une remarquable stabilité colloïdale. Ces nanoparticules présentent des potentialités majeures pour l'imagerie *in vivo* par excitation et détection dans le proche IR.

Mots clés: Synthèse organique, sondes fluorescent, nanoparticules, absorption à deux photons

UMR 5255

[ISM, équipe Imagerie et photonique moléculaires, 351 Cours de la Libération, 33405 Talence, France]

In Loving Memory of Antonio

Acknowledgements

At the end of this trip, I would like to thank all those who walked with me.

I want to thank my supervisor, Dr. Mireille Blanchard-Desce, who for the first time I just call Mireille. Thank you for welcoming me in your group, giving me this chance, and for your scientific teachings. Above all, thank you for your life lessons.

I would like to thank Dr. Michel Vaultier for his support during my organic synthesis work, it was a big honor to have worked alongside you.

A warm thanks goes to Pr. Verhlac, for his extreme friendliness and kindness. Smoking a cigarette with you was a relief moment in times of stress. Probably the "healthiest" cigarettes I have ever smoked.

Many thanks to Pr. G. Lemercier, Dr. I. Sasaki and Dr. O. Mongin, who accepted to be member of the jury and revised this manuscript.

A big hug to my "laboratory" friends. To Seb, who took over one year before to start to share wash bottles with me. To Maximus, who took less than one year to start to steal my bulb rubbers. To Nino for the pleasant conversations we had together. To Guillaume with his wonderful smile. To the people that I met during this experience and I shared nice moments with: Vincent, Ludovic (the Master of tartiflette), Imanol, Talia, Magali, Petra, Adina and Judith.

Thanks to the Nano2Fun members: Davide, Antonio, Domna, Paolo, Somananda, Siarhei, Sergio, Slava, Silvia, Dmitrii, Dzmitryi, Valentina, Laura and Luca, my best wishes to all of you. Many thanks to Pr. J. Veciana, Dr. N. Ventosa, Dr. I. Ratera and Dr. S. Sala for their hospitality during my secondment in Barcelona, as well as Pr. S. George, Pr. S. Pati and Harpan for my period in Bangalore.

Special thanks to Edu, simply a Great Friend. I can imagine you are very happy after the last final match of Champions League; I hope we will watch the next one together.

A lovely hug to the big PP…Big Man with Big Heart… Thank you my friend, for your support and your outstanding organizational skills. I wish you all the best for the future. Next time we will meet, I really would like to be on the passenger seat of your car, going for a nice dinner (magari da Orazio).

And JD? I wasn't forgetting my "camembert devouring" friend. But before to thank you, I want to clarify our situation about Hearthstone, because I think it's a good thing to point out that you have not won a game for last 2 years now. Matter of luck? I don't think so, not in the game. My luck has been to find you on my way. Thank you for your unique attitude to be a superb Leader, always honest and helpful, ready to reply: "Let's have a look!". I wish you to never lose that spark. Thank you.

Finally, I would like to thank my family: my parents, my sisters Agata and Soccorsa and my beloved brother Tato.

A kiss to the women of my life, my mother Maria, my wife Angela and our little Greta.

Hi Dad, we started many years ago…We've done it.

Thank you all.

LIST OF ABBREVIATIONS

1P	One-photon
2P	Two-photon
2PA	Two-photon absorption
ACQ	Aggregation-caused quenching
CV	Cresyl violet
DCV	Dicyanovinyl
DCM	4-(Dicyanomethylene)-2-methyl-6-(4-dimethylaminostyryl)-4*H*-pyran
DETB	1,3-Diethyl-2-thiobarbiturate
DSC	Differential scanning calorimetry
FONs	Fluorescent organic nanoparticles
GUVs	Giant unilamellar vesciscles
HRMS	High resolution mass spectrometry
HW	Horner-Wittig
HWE	Horner-Wadsworth-Emmons
IC	Internal conversion
ICT	Internal charge transfer
ISC	Intersystem crossing
NBS	*N*-Bromosuccinimide
NIR	Near infrared region
NMR	Nuclear magnetic resonance
NPs	Nanoparticles
SDS	Sodium dodecyl sulfate
PET	Photoinduced electron transfer
PLGA	Poly(lactic-*co*-glycolic acid)
RRM	Routine reprecipitation method
TEM	Transmission electron microscopy
TLC	Thin layer chromatography

Table of Contents

1. Introduction 1

1.1 Photoluminescence 3
1.2 Absorption 3
1.3 Fluorescence 7

1.3.1 Effect of the environment 9
1.3.2 Quenching 10
1.3.3 Chemical sensing by fluorescence 13

1.4 Bioimaging by fluorescence microscopy 14
1.5 Two-photon absorption 16
1.6 Structure-property relationship 19
1.7 Nanoparticles 21

1.7.1 Upconversion nanoparticles (UCNPs) 22
1.7.2 Quantum dots (Q-dots) 23
1.7.3 Noble metal NPs 24
1.7.4 Silica nanoparticles (SiNPs) 24
1.7.5 Carbon dots (C-dots) 25
1.7.6 Dendrimers 26
1.7.7 Polymeric NPs 26
1.7.8 Fluorescent organic nanoparticles by low molecular weight molecules (FONs) 27

Bibliographic references 30

2. Design of New Two-photon pH Probes 33

2.1 Introduction and goal of the work 35

2.1.1 Importance of pH in biological environment 35
2.1.2 Fluorescent pH-probes 38
2.1.3 Dual emission ratiometric pH probes 42
2.1.4 Ratiometric pH probes for two-photon excitation techniques 42

2.2 Design of the probes 45
2.3 Synthesis 47
2.4 pH dependence of the photophysical properties 50

2.4.1 Absorption and emission 51
2.4.2 pKa determination 53
2.4.3 Two-photon absorption 56
2.4.4 pKa determination under two-photon excitation 57

2.5 Applications 58

2.5.1 Imaging 58
2.5.2 Investigation of PLGA stability by pH monitoring using pH probes 60

2.6 Conclusion 62
Bibliographic references 63

3. Dipolar dyes and Nanoparticles 67
3.1 Objectives 69
3.2 Design and ideas 69
3.3 Synthesis 71
3.4 Photophysical properties in organic solvent solution 76
3.4.1 Linear optical properties 76
3.4.2 Non linear optical properties 79
3.5 Morphological characterizations of FONs 81
3.6 Photophysical properties of chromophores in aggregated state 82
3.6.1 Linear optical properties 83
3.6.2 Non linear optical properties 86
3.7 Chemical stability of the FONs 90
3.8 Conclusions 93
Bibliographic references 95

4. Towards Efficient Energy Transfer Process in NPs Exploiting Hydrogen bond 97
4.1 Hydrogen-bond (H-bond) 99
4.2 Design of the chromophores 105
4.3 Synthesis 106
4.3.1 Synthesis of the intemediate 107
4.3.2 Synthesis of the uracile derivative 108
4.3.3 Synthesis of the triazine derivative 110
4.4 Linear optical properties in organic solvent 112
4.5 Non linear optical properties in organic solvent 115
4.6 Aggregated state 116
4.7 Energy transfer in two components NPs 119
4.8 Conclusion 123
Bibliographic references 124

General Conclusion 127
Target Molecules 131
Experimental Part 133
Annex: Organic Synthesis Review 175

Chapter 1

Introduction

1.1 Photoluminescence

The word fluorescence was coined by G. G. Stokes[1], who was the first one to observe that a solution of quinine sulfate glowed blue after irradiation with the UV part of solar light splitted by a prisma. Today we know that the fluorescence is just one of the possible paths in the luminescence field. The luminescence consists in a phenomenon in which a species is excited to a higher energy electronic state and than comes back to the ground state with emission of light. When the excitation is achieved by light irradiation, the de-excitation process is named photoluminescence (Figure 1.1).

Figure 1.1 General scheme for photoluminescence

1.2 Absorption

When a photon of suitable energy interacts with a molecule, it can be absorbed inducing an electronic transition; one electron in the ground state configuration, in a bonding (σ, π) or non-bonding orbital (n), can be promoted into an anti-bonding one (π*, σ*). In the field of the UV-Vis spectroscopy, the transition which requires the less energy involves the Highest (in energy) Occupied (by electrons) Molecular Orbital (HOMO) and the Lowest Unoccupied one (LUMO) according to the following scheme (Scheme 1.1), and the moiety of the molecule responsible for this process is called chromophore.

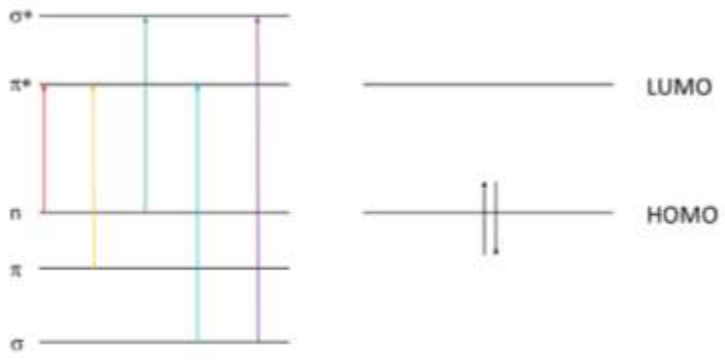

Scheme 1.1 Electronic transitions allowed by UV-Visible irradiation

The absorption of one photon occurs on a timescale of 10^{-15} s and it induces a redistribution of electron density in the molecule, whereas the positions of nuclei in the molecule and in the solvent around it

remain unchanged due to their high mass comparing to electrons (i.e., Born-Oppenheimer approximation). The rate of the absorption leads to a *vertical transition* often referred to an electronic transition with "frozen" positions of the nuclei (i.e., Franck-Condon principle, Figure 1.2).

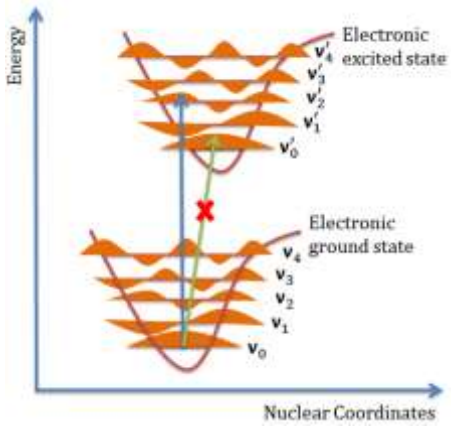

Figure 1.2 Illustration of a vertical transition[2] during the absorption of one photon

Each electronic state is composed by several vibrational levels that can be described by wavefunctions. These levels are populated as a function of the temperature according to Boltzmann's distribution and, at room temperature, the lowest one is the most filled. Upon absorption of a photon, the intensity of the transition is proportional to the square power of the overlap integral between the vibrational wavefunctions of the two states that are involved[3], determining a vibrational structure of the absorption band as depicted in Figure 1.3.

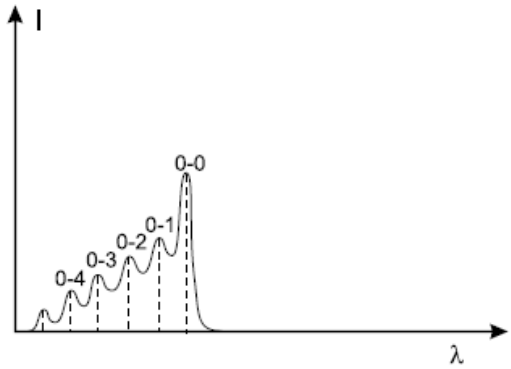

Figure 1.3 Vibronical structure of an absorption band[3]

From a practical point of view, the ability of a molecule to absorb light at a given wavelength (λ) and conditions (e.g., solvent), is expressed by its absorbance. One can consider the model described in Figure

1.4, wherein P_0 and P are respectively the intensity of the light beam which enters and leaves the solution, b is the optical pathlength and S is the surface of the considered volume.

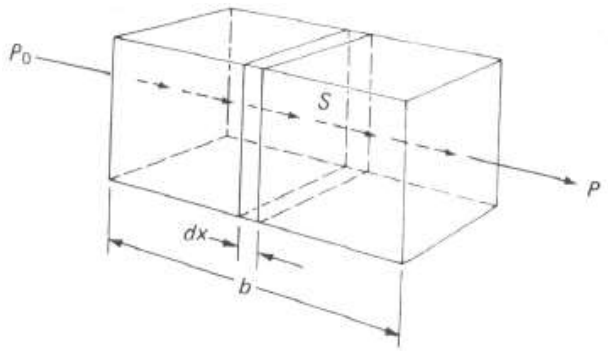

Figure 1.4 Representation of a light beam through a defined volume

Assuming the system homogeneus and continuous, the light beam monochromatic and the rays of the beam perpendicular to the surface S, the Lambert law defines the amount of light which cross the infinitesimal volume S·dx (Equation 1.1):

$$\frac{dP_x}{P_x} = -k\,dx$$

Equation 1.1

wherein k is a constant which depends on the wavelength of the beam, temperature, nature of the species and is directly proportional to its concentration (c), according to the Beer relation (Equation 1.2):

$$k = k'c$$

Equation 1.2

Introducing the last equation in the Lambert law and integrating, the new equation is:

$$\int_{P_0}^{P} dP_x/P_x = -\int_{0}^{b} k'c\,dx \quad => \quad \ln\frac{P}{P_0} = -k'b\,c$$

Equation 1.3

Shifting to decimal logaritm and rearranging, one can obtain the Lambert-Beer law (Equation 1.4):

$$\log P_0/P = \frac{k' b\, c}{2.303} \quad => \quad A(\lambda) = \varepsilon\, b\, c$$

Equation 1.4

wherein A(λ) is the absorbance, b is the optical pathlength and ε(λ) = *k'*/2.303 is called molar absorption coefficient, typically expressed as $L \cdot mol^{-1} \cdot cm^{-1}$. The equation 1.4 shows that the absorbance is proportional to the concentration but however several factors can produce some deviations from this condition; for the purpose of this manuscript, it's important to point out that a deviation can occur at high concentration of compound and therefore for quantitative measurements is necessary to work in diluted conditions (tipically less than 10^{-4} M).

It is important to observe that electronic transitions follow some criteria called selection rules, which consist in restrictions that rule the process. The first one is about the conservation of the total spin number, therefore singlet-triplet or vice-versa transitions are forbidden (Scheme 1.2).

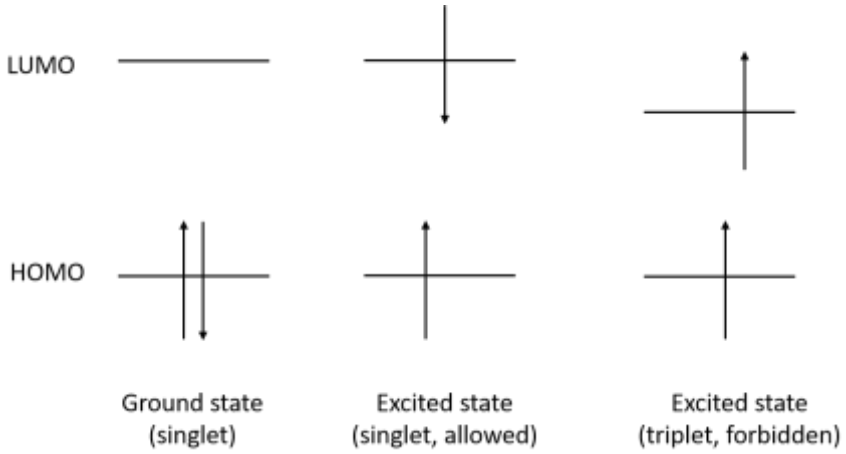

Scheme 1.2 HOMO-LUMO transition

Anyway the term forbidden means the probability for a forbidden transition to occur is low but not impossible and thanks to spin-orbit coupling between the wavefunctions with different multiplicity of spins, forbidden transitions can be observed, but with low molar absorption coefficients. The second selection rule concerns the transition forbidden by symmetry, in which there is no overlap between the orbitals involved in the transition, as for n→π*. However, as in the previous case, vibronic coupling can

lead to distorsions which break the symmetry, making these transitions observable, but with low molar absorption coefficients too.

1.3 Fluorescence

A comfortable way to articulate the discussion on fluorescence, consists in starting from the Perrin-Jablonsky diagram, which allows a quick and general view of the possible phenomena (Figure 1.5).

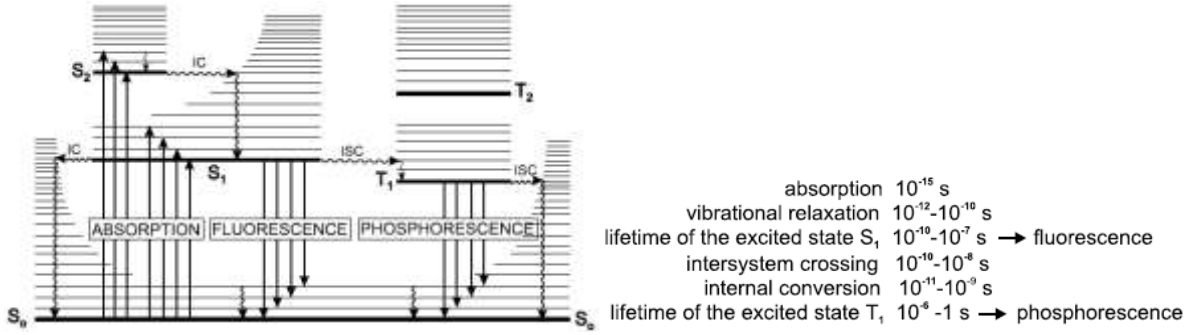

Figure 1.5 Perrin-Jablonsky diagram[3]

The radiative paths for de-excitation are fluorescence and phosphorescence, which happen with the emission of a photon respectively from singlet and triplet state. The population of the triplet state occurs after intersystem crossing (ISC) upon excitation and, indeed the transition $T_1 \rightarrow S_0$ is forbidden, the spin-orbit coupling makes the process possible; thus heavy atoms (e.g., bromine, iodine) usually promote these transitions. It's important to observe that vibrational relaxation happens on a timescale shorter than lifetimes of singlet or triplet excited states (Figure 1.5); this means that, upon excitation, the emission comes from the lowest vibrational level of the excited state. Considering the absorption and, observing that the energy difference between the vibrational level in the ground and excited state are similar, the emission upon excitation often looks like a mirror image of the absorption spectrum (Figure 1.6).

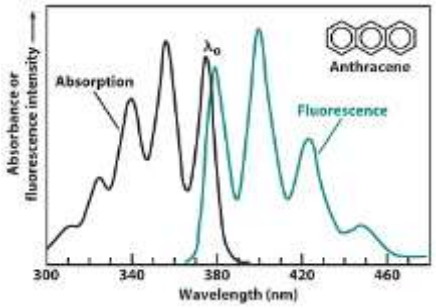

Figure 1.6 Absorption and emission spectra of anthracene in cyclohexane[4]

The internal conversion (IC) represents a non-radiative path which involves a transition between levels with the same multiplicity of spin and it's more efficient when the energy of these levels are close; it follows that IC $S_n \rightarrow S_1$ is more efficient than $S_1 \rightarrow S_0$ and this is the reason why the probability is low to observe fluorescence due to high energetic transitions. The difference between the maximum of absorption and emission spectra, usually expressed as wavelength or wavenumber, is called Stokes shift.

Focusing the attention on fluorescence one can imagine a solution of a chromophore which is excited to S_1 state upon light irradiation, then the molecules can relax by radiative or non-radiative paths; the temporal features of the process can be described according to the following equation:

$$[M^*] = exp\left(-{}^{t}/_{\tau}\right)[M^*]_0$$

Equation 1.5

wherein $[M^*]_0$ and $[M^*]$ are the concentrations of the specie in the excited state S_1, respectively at initial time and after a generic period of time t, and τ is the lifetime of the excited state, which is also equal to:

$$\tau = 1/(k_r + k_{nr})$$

Equation 1.6

wherein k_r is the rate constant for radiative process and k_{nr} is the sum of rates of radiationless de-excitation pathways. It is easy to observe that ideally, if the excited state would de-excite only through fluorescence emission, the equation 1.6 is reduced to the following (Equation 1.7):

$$\tau = \frac{1}{K_r} = \tau_r$$

Equation 1.7

wherein τ_r is commonly defined as radiative lifetime. Furthermore it worths to point out that the decay of [M*] over time follows an exponential decay (Equation 1.5).

In order to evaluate the efficiency of the fluorescence for a chromophore in a given condition, the figure of merit widely used is the fluorescence quantum yield, which represents the ratio between the number

of photons emitted by fluorescence divided by the number of photons absorbed. However this quantity can be also expressed in terms of rate constants previously described as following (Equation 1.8):

$$\Phi_F = K_r/(K_r + K_{nr})$$

Equation 1.8

From an experimentally point of view Φ_F can be absolutely measured using a so called Integrating Sphere, but most of the times it is determined by relative comparison with a reference, according to the following equation:

$$\Phi_F = \Phi_R \frac{n^2}{n_R^2} \frac{1-10^{-A_R}}{1-10^{-A}} \frac{I}{I_R}$$

Equation 1.9

wherein Φ_R is the fluorescence quantum yield of the reference (tabulated value), n is the refractive index of the solvent, A is the absorbance and I is the area of the emission spectra respectively for the specie (no subscript) and reference (denoted with R as subscript). This relation can be used only if the experimental conditions for the measurements of the parameters are the same and the absorbance of the specie as well as the reference are low, avoiding inner filter phenomena.

The fluorescence spectra of a compound in solution is affected by several parameters and, in the next section I am going to discuss some of them which are fundamental for this manuscript.

1.3.1 Effects of the environment

A molecule into solution is surrounded by solvent molecules and the intermolecular interactions are also responsible for the energy of the levels involved in the electronic transition. Upon excitation, a redistribution of the electronic density in the dye occurs, resulting in an instantaneous variation of the dipole moment of the dye. This means that the original configuration of the solvent shell around the excited molecule rearranges in order to stabilize the excited state of the chromophore; usually this effect is larger as the polarity of the solvent increases, because commonly the dipole moment of the dye in the excited state is enhanced. Similarly, when the excited molecule comes back to the ground state (e.g.,

after emission of a photon), a new variation of the dipole moment occurs, followed by another reorganization of the solvatation shell (Figure 1.7).

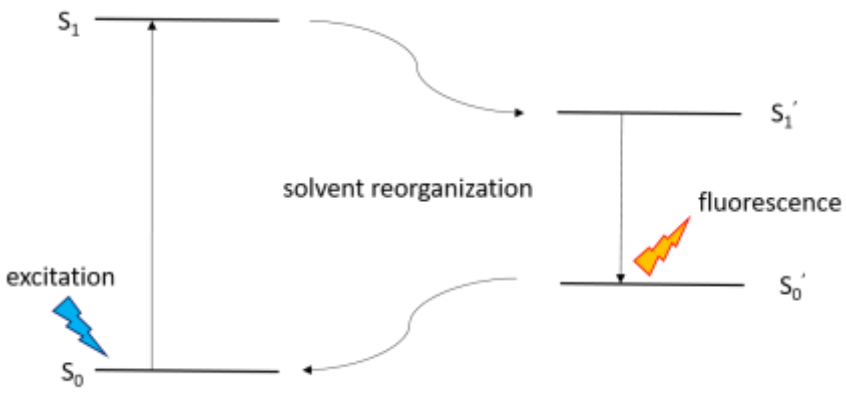

Figure 1.7 Effect of solvent reorganization after the absorption and the emission of a photon

The process described is responsible for the shift of the emission to lower energies as the polarity of the solvent increases. However the effects of the environment depends by several factors related to the nature of the fluorophore, the solvent and their interactions. For example the viscosity of the solvent determines the rate of the reorganization of the solvent shell to the variation of the dipole moment of the fluorophore, in particular if the viscosity is high, the fluorescence emission can happen before of the reorganization, without substantial modification of the energy of the excited state. Thus for very viscous solvents, the emission is low affected by the rearrangement of the solvent. Vice versa, when the timescale of the reorganization of the solvent shell is comparable with the fluorescence emission one, the energy of the excited state will be more influence. More generally one can say that fluorescence emission of a certain fluorophore into a solution is usually connected to the nature of its environment and therefore it depends on several parameters (e.g., polarity of the solvent, viscosity, pH); this concept, which will be renewed in the following subchapters, is really important and makes fluorescence useful for several kind of applications in bioimaging (e.g., pH or polarity probes).

1.3.2 Quenching

According to the IUPAC Gold Book[5], the word quenching is referred to: “Deactivation of an excited molecular entity intermolecularly by an external environmental influence (such as a quencher) or

intramolecularly by a substituent through a non-radiative process". This can be splitted theoretically into two phenomena, which are defined as following:

A) When the external environmental influence (quencher) interferes with the behavior of the excited state after its formation, the process is referred to *dynamic quenching*.
B) When the environmental influence inhibits the excited state formation, the process is referred to *static quenching*.

The dynamic quenching occurs when the chromophore in the excited state (M*) is able to approach to a molecule of quencher (Q), promoting a non-radiative decay path, leading to a decrease of the Φ_F (Equation 1.8). It follows that the concept of approaching is related to the parameters which influence the motion of the molecules (i.e., viscosity of the medium, temperature, size of the molecules) and the probability that the collisions will happen during the excited state of the dye (i.e., concentration of the quencher and lifetime of the excited state). Some of dynamic quenching processes are depicted in Figure 1.8.

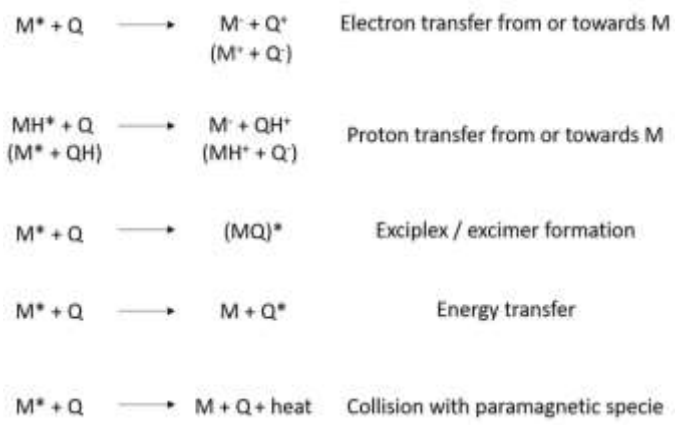

Figure 1.8 Dynamic quenching processes

It can be demonstrated that for a pure dynamic quenching, the process is ruled by the Stern-Volmer relation as following:

$$\frac{F_0}{F} = \frac{\tau_0}{\tau} = 1 + K_{SV}[Q]$$

Equation 1.10

where F and τ are respectively the fluorescence intensity and the lifetime in presence of the quencher, F_0 and τ_0 are the same but in absence of the latter one, [Q] is the concentration of the quencher and K_{SV} is known as the Stern-Volmer constant.

Anyway chromophores can associate into non-fluorescent complexes in the ground state, resulting in a static quenching; for such a process, it can be derived that the ratio of fluorescence intensity in absence and presence of quencher is given by:

$$\frac{F_0}{F} = 1 + K_{AS}[Q]$$

Equation 1.11

where K_{AS} is the formation constant for the non-fluorescent complex. One can observe that in both cases, the ratio F_0/F is linear with [Q], therefore there are no differences in the trend. In order to distinguish between the two kinds of quenching, a common approach is the evaluation of the ratio τ_0/τ, which increases for dynamic quenching whereas is equal to one in static process (because the non-fluorescent complex is not observed and therefore the lifetime of the fluorescent specie is still τ_0). Furthermore in some cases, the quenching is induced by the combination of the two processes.

1.3.3 Chemical sensing by fluorescence

As previously discussed, the fluorescence of a molecule is strictly affected by its environment and the parameters which are able to influence this system, thus represents one of the fundamental ideas behind the *fluorescence sensing*. In brief, the concept that rules the topic consists in determining information about the molecular environment of a a dye, such as chemical-physical parameters (i.e., temperature, viscosity, pH) and/or composition (i.e., concentration of a specific specie), by means of the variations of the fluorescence response that the latter are able to induce. The species which are used for this purpose are commonly known as *fluorescent probe*. Several biological processes and onset of diseases are related to changes of concentration of chemical species and therefore the ability to monitor them represents an important issue in the scope of medicine and biology.

Fluorescent probes can be classified according to the mechanism of interaction with the analyte and therefore according to several criteria. In the first instance they can be splitted into two classes, depending on the presence or not of a recognition unit then, according to the kind of interaction with probed specie (Figure 1.9).

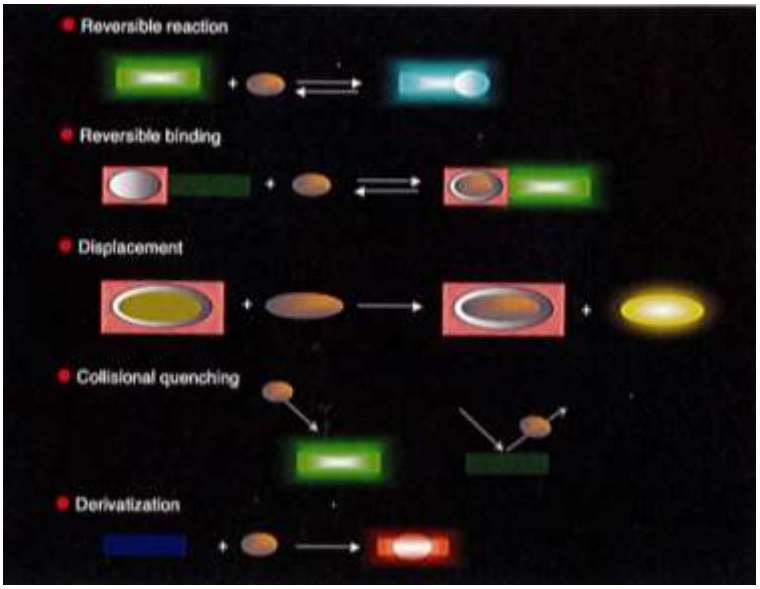

Figure1.9 Chemical sensing by fluorescence[3]

1) Reversible reaction: the analyte is involved in a reversible reaction with the fluorophore, leading to a variation of the fluorescence features of the latter;
2) Collisional quenching: the analyte collisionally quenches the fluorophore;
3) Derivatization: the analyte reacts irreversibly with a non-fluorescent specie leading to the formation of a fluorescent one;
4) Reversible binding: the analyte interacts with a recognition unit linked to the fluorophore with changes in its fluorescence characteristics;
5) Displacement: the analyte displaces the fluorophore by its complex, in which it isn't covalently linked to the recognition unit.

Intuitively upon these interactions some variations in fluorescence occur, and the ones which are monitored (Figure 1.10), for instance lifetime, contribute to determine the kind of analytical technique used for the purpose, such as Fluorescence-Lifetime Imaging Microscopy (FLIM) for the cited example.

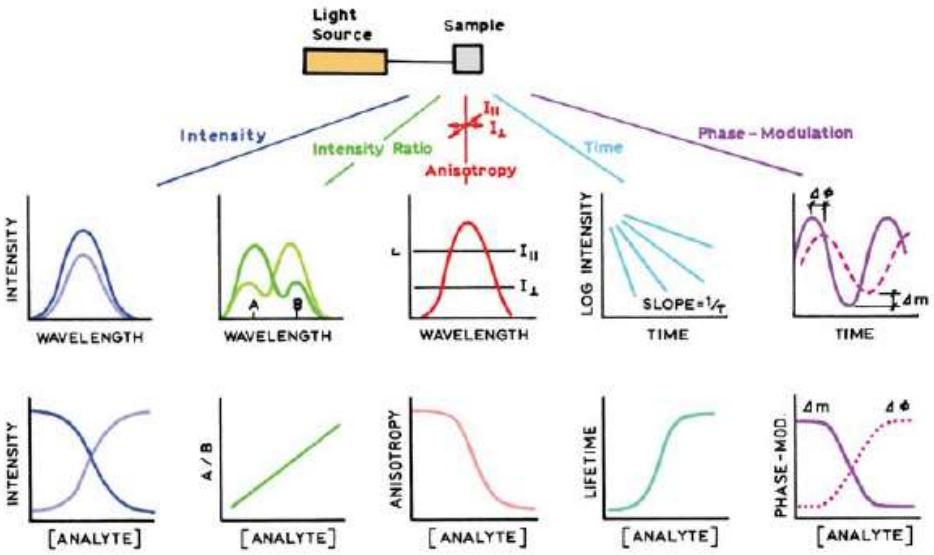

Figure 1.10 Spectral properties monitorable in fluorescence sensing[6]

1.4 Bioimaging by fluorescence microscopy

Bioimaging comprises all the techniques which are able to produce a two-dimensional picture[7] of a biological sample (spanning from subcellular structures up to whole organisms). There are several methods for the purpose, such as atomic force microscopy[8-9], ultrasound[8-10], magnetic resonance[8-9], positron emission tomography[8-9] and many others; among these, fluorescence microscopy finds its place with its fascinating features.

In principle when an analyte is fluorescent, it's determination in cells or tissues can be achieved directly by spectroscopy (direct methods), but many components are not fluorescent or not concentrated enough. In this quest, the advantages offered by the possibility to make these elements fluorescent by means of exogenous fluorophores is valuable and made fluorescence microscopy more and more attractive over time. In parallel, progress in technology led to the development of devices capable of high resolution and three-dimensional analysis (i.e., confocal laser scanning microscope[11-14]) and techniques in super-resolution (e.g., STimulated Emission Depletion[15-16]), making the fluorescence microscopy one of the main tools for bioimaging. In this view however, there are some drawbacks to face, related to the nature of the sample.

Generally speaking, cells and biological tissues are mainly constituted by water, lipids and proteins and their optical properties can not be neglected (Figure 1.11).

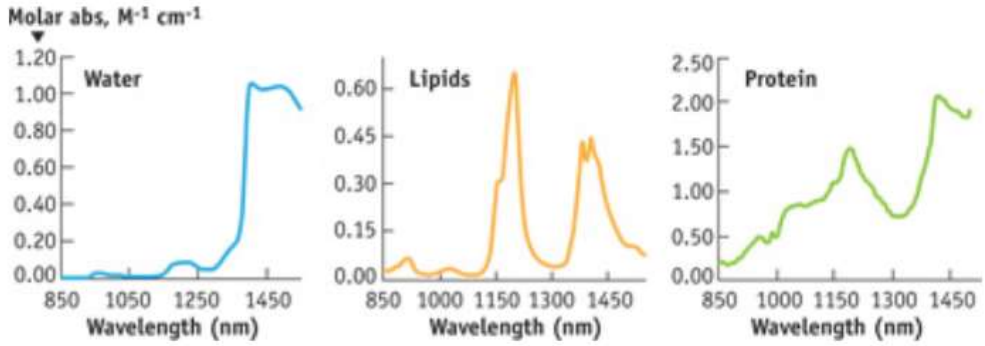

Figure 1.11 Absorption spectra in the NIRof major tissue components: water, lipids and proteins (here albumine)[17]

Moreover biological tissues are naturally populated by endogenous chromophores (Figure 1.12) of different nature, which are responsible for so called autofluorescence, representing a large source of noise.

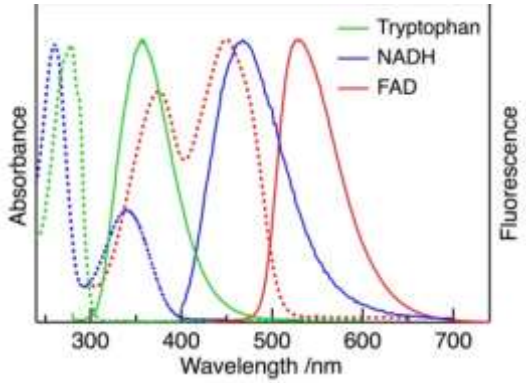

Figure 1.12 Absorption (dotted lines) and emission (solid lines) spectra of some endogenous species in neutral acqueous solution[18]

Another important parameter to consider is the scattering of the light, induced by interaction with objects with size comparable to the wavelength of the radiation. In this view biological samples (according to their nature) are able to scatter the light[19-21], resulting in a global attenuation of the intensity both in excitation and collection of fluorescence.

Comparing to excitation by means of UV-Visible light, the utilization of longer wavelength leads to deeper penetration of biological samples due to lower scattering and lower absorption by the main tissue

components and, furthermore, the absorption of light by endogenous chromophores is also reduced, avoiding autofluorescence.

1.5 Two-photon absorption

From the previous considerations it emerges that for fluorescence bioimaging purpose, the NIR window, and therefore the multiphotonic excitation techniques, seems optimal; among these, the most common and used is the two-photon one.

The two-photon absorption (2PA) phenomena was theorized for the first time in 1931 by Maria Goppert-Mayer[22] and experimentally observed in 1961 by Kaiser[23]. It consists in the excitation of a molecule by the simultaneous absorption of two photons; in most of the cases, due to experimental simplicity of the instrument setup, the photons are degenerate and their energy is half of the one required in one-photon process (Figure 1.13).

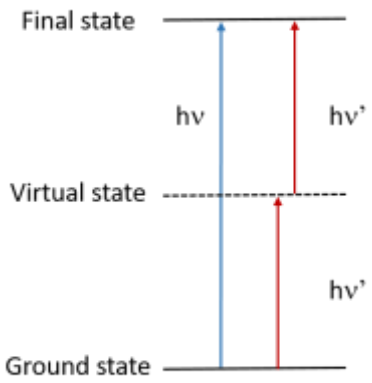

Figure 1.13 One and two-photon transitions

Between one-photon and two-photon processes there are some substantial differences; according to the essential state model[24], for centrosymmetric molecules an inversion of the Laporte rule occurs (Figure 1.14), therefore the transitions allowed through two-photon excitation are forbidden in one-photon and vice versa.

Centrosymmetric molecules

One-photon	*Two-photon*
$g \leftrightarrow u$	$g \not\leftrightarrow u$
$g \not\leftrightarrow g$	$g \leftrightarrow g$
$u \not\leftrightarrow u$	$u \leftrightarrow u$

Figure 1.14 Selection rule for one and two-photon transition[25]

Another important difference is the dependency of the phenomena with the intensity of the light; for one-photon excitation the absorption is linear to the light intensity, whereas for two-photon it is quadratic, according to Equation 1.12.

$$N = \sigma_2 I^2$$

Equation 1.12

Wherein N is the number of photon absorbed per second, I is the intensity of the light and σ_2 is the two-photon absorption cross section, which is measured in Goppert-Mayer units (1 GM= 10^{-50} cm^4 second $photons^{-1}$) and represents a figure of merit to evaluate the responsivity of a specie towards two-photon absorption process. From the fluorescence point of view , it worths to remark that upon excitation by one or two-photon, the emission spectrum of the species doesn't change.

Two-photon absorption process found its place in fluorescence microscopy in 1990 thanks to W. Denk, J. H. Strickler and W. W. Webb, who developed the first two-photon laser scanning microscope[26] (Figure 1.15).

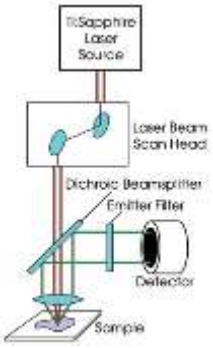

Figure 1.15 Skech of a two-photon laser scanning microscope[27]

As well as the possibility to use NIR light for excitation, one of the main feature that makes two-photon microscopy so attractive, is its intrinsic confocality. As already mentioned in order to get two-photon transition, a high density of photons is required (Equation 1.12), which is achieved by means of suitable sources (i.e., pulsed laser) and system of lens which focus the light beam on the specimen. However whereas in one-photon techniques the excitation is extended through the optical path, in two-photon it is limited just to the focal volume (Figure 1.16), where the intensity of the light is high enough to produce the excitation.

Figure 1.16 Illumination with one-photon (upper beam, 532 nm) and two-photon wavelengths (lower beam, 1057 nm)[28]

This feature also affects photobleaching of the chromophore and photodamage of the sample, that result confined in space, making two-photon excitation useful also in other fields such as microfabrication by photopolymerization[29-30] (Figure 1.17) and photodynamic therapy[31].

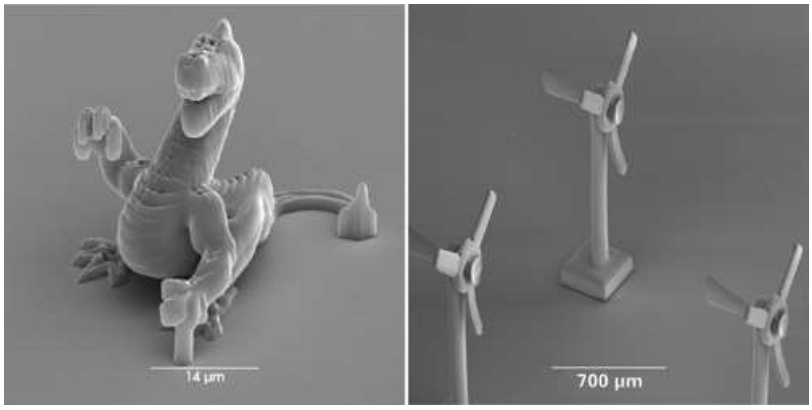

Figure 1.17 Scanning Electron Microscopy (SEM) images of micro-objects made by two-photon polymerization[32]

Coming back on fluorescence imaging, a figure of merit to evaluate the optical properties of general probe is its brightness, defined as following:

$$\text{one-photon brightness} = \varepsilon \Phi_F$$

$$\text{two-photon brightness} = \sigma_2 \Phi_F$$

Equations 1.13

It's intuitive that having probes with high values of two-photon brightness represents a benefit for imaging, therefore over time several researches have been done in order to understand what is the relation between the structure of a two-photon absorber and its σ_2: the structure-property relationships[24, 33-34].

1.6 Structure-property relationship

In this paragraph the discussion will be centered on the class of compounds described in this manuscript, which are dipolar and quadrupolar systems (Figure 1.18).

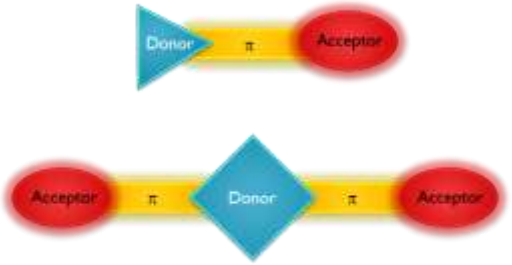

Figure 1.18 Sketch for dipolar and quadrupolar structures in this manuscript

The studied dipolar structures can be splitted into three parts, a donor moiety (D) conjugated to an acceptor one (A) through an electron rich path (π-bridge). Upon excitation these molecules undergo an intramolecular charge transfer (ICT) from the donor to the acceptor group[33], usually accompained by a large variation of the dipole moment. For such molecules, increasing the dipolar strength by means of strong donor and/or acceptor moietes can lead into an enhancement of σ_2[35] (Figure 1.19). Concerning the quadrupoles the situation must be through; for the structure depicted in Figure 1.18, the ICT can occur from the donor group to the acceptor end-ones too, however the situation concerning the strength of the donor and/or the acceptor is very complex and usually a fine tuning of the features of these moieties is required.

Another important parameter is the extension and the conjugation of the π-electrons. It's been observed that electron rich dyes present a higher response in two-photon absorption processes than analogous electron poor ones[35] (Figure 1.19); this effect can be so influential that a figure of merit used to evaluate the response in such case is σ_2/Ne, wherein Ne is the number of π-electrons.

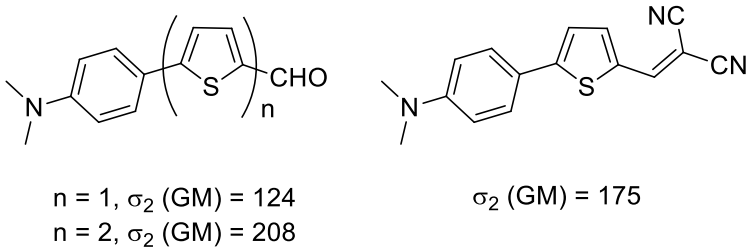

Figure 1.19 Effect of enhancement of dipolar strength and extension of the π-system on σ_2 at λ_{2PA}^{max}[35]

As mentioned it's also important that the π-system is well conjugated, meaning that the overall molecular architecture must be able to ensure a planar conformation which enhances the overlap of the orbitals (Figure 1.20).

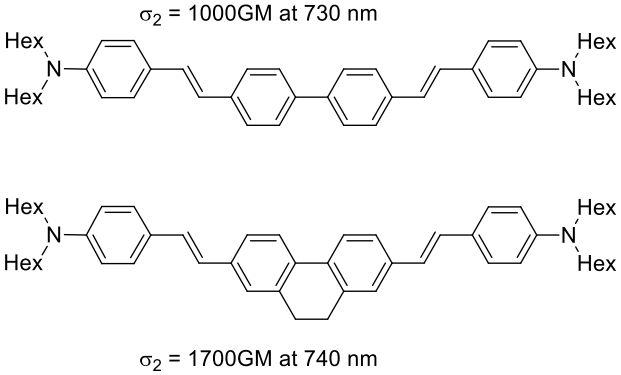

Figure 1.20 Enhancement of σ_2 by forcing planar conformation[24]

So far we have discussed how two-photon excitation techniques can be useful for fluorescence bioimaging in the NIR window and how the molecular structure of a compound can be engineered in order to improve its properties for such applications; however, according to the kind of usage, there are several parameters that must be taken into account (i.e., chemical/photostability in biological environment, absence of toxicity).

1.7 Nanoparticles

The definition of nanoparticles (NPs) have several nuances in literature (Table 1.1), but they commonly refer to objects whose dimensions range between 1 and 100 nm.

	Nanoparticle
ISO	A particle spanning 1–100 nm (diameter)
ASTM	An ultrafine particle whose length in 2 or 3 places is 1–100 nm
NIOSH	A particle with diameter between 1 and 100 nm, or a fiber spanning the range 1–100 nm.
SCCP	At least one side is in the nanoscale range.
BSI	All the fields or diameters are in the nanoscale range.
BAuA	All the fields or diameters are in the nanoscale range.

Table 1.1 Definitions of nanoparticles[36] according to different standards

Considering the nature of their constituents, NPs can be classified in inorganic (e.g., Q-dots, metal oxide based, silica) and organic ones (e.g., molecular aggregates, dendrimers, polymeric). Very often organic and/or inorganic compounds with interesting optical features suffer of problems such as low solubility, drop of fluorescence quantum yield in acqueous medium and photobleaching. In this view the use of nanoparticles represents an approach to partially overcome these drawbacks[37]; moreover the possibility to confine a high number of fluorophores per nanoparticle results in an object with higher brightness than single constituent[38]. For that reason in the last decades the topic has been deeply investigated, leading to a wide bunch of nanomaterials; here it is a briefly description of the most common nanoparticles studied in fluorescence bioimaging field.

1.7.1 Upconversion nanoparticles (UCNPs)

This class of NPs are based on rare earth elements; tipically they consist of $NaYF_4$ nanocrystals doped with lanthanide species such as Er^{3+}, Tm^{3+} and Yb^{3+}. These NPs have emission based on the upconversion process[39], through which two or more excitation photons are converted in one emission

photon with higher energy, leading to an anti-Stokes shift. Furthermore UCNPs absorb in the NIR window, usually between 750 and 1000 nm, and they can exhibit (most of the times) sharp multicolor emission (Figure 1.21). They are also characterized by very high photostability[40] but suffer of some drawbacks such as low fluorescence quantum yield[39].

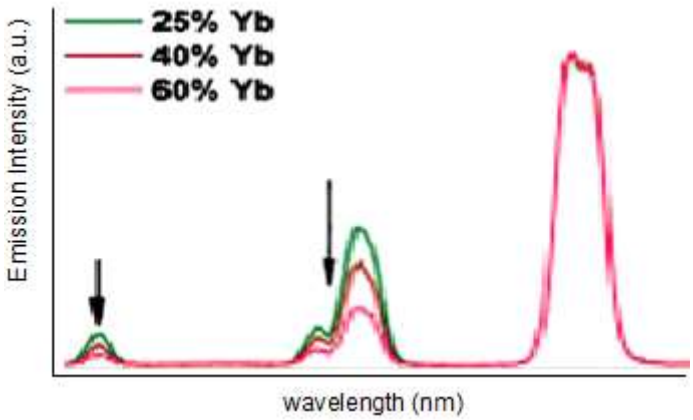

Figure 1.21 Upconversion emission spectra UCNPs $NaYF_4$: Yb/Er (25-60/2 mol%) exciting at 980 nm[39]

1.7.2 Quantum dots (Q-dots)

This class of materials consists in nanocrystals made by semiconductors of III-V group (e.g., GaAs, InP), II-VI group (e.g., CdS, CdSe) and IV-VI one (e.g., PbS, PbTe). They show unique optical properties due to the quantum confinement, which determines a relationship between the size and the emission spectra[41-42]; when increasing their size, the quantum effect induces a red shift of the fluorescence of the Q-dots (Figure 1.22).

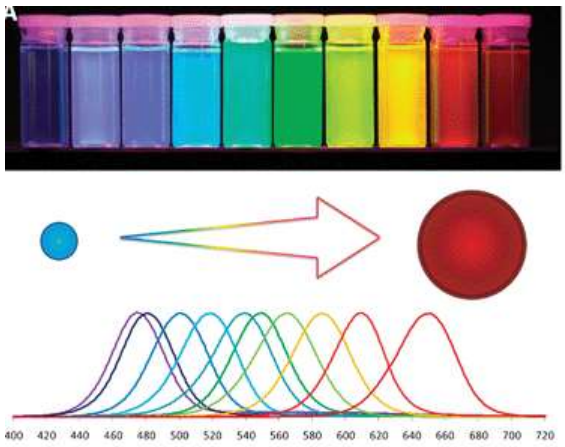

Figure 1.22 Size-emission relation in Q-dots[43]

Cadmium based ones are the most studied, with high brightness (expecially after encapsulation with ZnS layer[44-45]) and photostability, but for biological applications, they suffer of drawbacks such as toxicity and low biocompatibility. In this view several efforts have been done to improve Q-dots' properties, such as development of Q-dots without toxic heavymetals (e.g., $CuInS_2/ZnS$[46]) and surface passivation and functionalization techniques[37, 47]; for instance in 2012 Ye et al.[48] carried out an in vivo pilot study on rhesus macaques using phospholipid micelle-encapsulated CdSe/CdS/ZnS Q-dots, without evidence of toxicity.

1.7.3 Noble metal NPs

Among noble metals, gold (Au) and silver (Ag) have been highly investigated in biological field. AuNPs offer advantages such as low toxicity[49], high photostability[50] and tunability of their optical properties according to their shape and size[51], that can be adjusted on the base of the method used for their preparation[52] (usually wet methods such as citrate reduction of $HAuCl_4$[53]). They also exhibit high potential in terms of bioconjugation, taking advantage from thiol chemistry which offer a wide range of possibilities for surface modification (Figure 1.23).

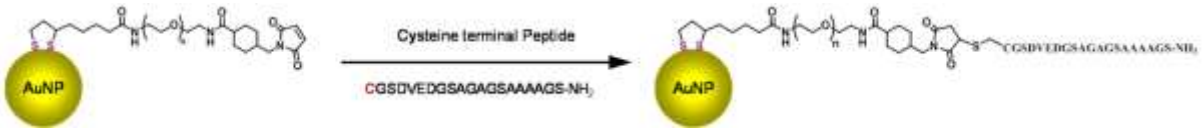

Figure 1.23 Peptide conjugation of surface functionalized AuNPs[51]

AgNPs can be also prepared by several ways, the most common ones are based on reduction of $AgNO_3$ (e.g., polyol synthesis[54]) which offer control on shape and size on produced NPs and, therefore, on their optical properties as well as AuNPs. AgNPs exhibit interesting antimicrobial properties[51, 55], but they suffer some limitations due to oxydability of silver surface[51, 56].

1.7.4 Silica nanoparticles (SiNPs)

This class comprises nanoparticles based on silicon dioxide (silica, SiO_2), that aroused a lot of interest due to their non toxicity and biocompatibility. Their size and structure can be modulated according to the methods used for the preparation; for instance the Stober method[57], which is the most commonly

used nowadays, allows to get almost monodisperse NPs. A variation of this method by means of surfactant templating agent (e.g., cetyltrimethylammonium bromide) leads to monodisperse mesoporous NPs with high porosity (i.e., MCM-41, Figure 1.24) and useful loading capabilities for cargo applications. Exploiting the well established silicon chemistry, fluorescent SiNPs can be readily obtained by grafting of fluorophores[51].

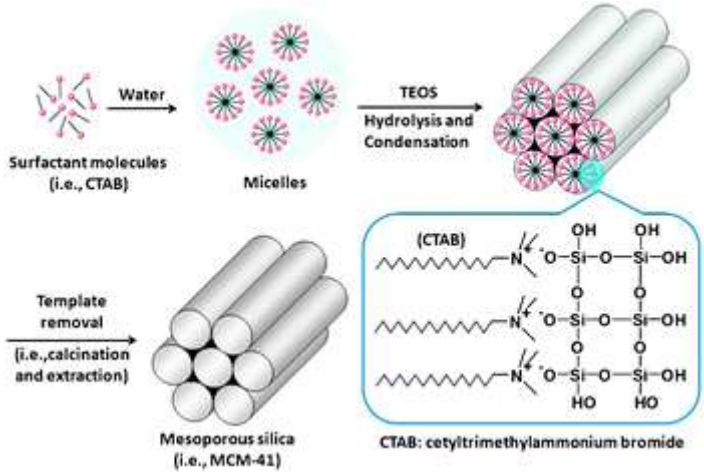

Figure 1.24 Formation of MCM-41[58]

1.7.5 Carbon dots (C-dots)

C-dots are made mainly by sp^2-carbon atom and can contain different amount of hydrogen, oxygen and nitrogen. They become interesting in fluorescence bioimaging thanks to their low toxicity[59-60], good biocompatibility[7] and good chemical and photostability[61]. Tipically they can be prepared by top-down approach (e.g., arc-discharge, electrochemical method, laser ablation), by cleavage of other carbonaceous materials (e.g., graphite) or by bottom-up approach (e.g., thermal methods), by treatment of small precursors (e.g., sugar[60]). Their optical properties are also very interesting and can be tuned in strictly relation with their nature and methods used for preparation[61]; for instance some C-dots exhibit emission (intensity and wavelength) dependency by excitation wavelength (Figure 1.25).

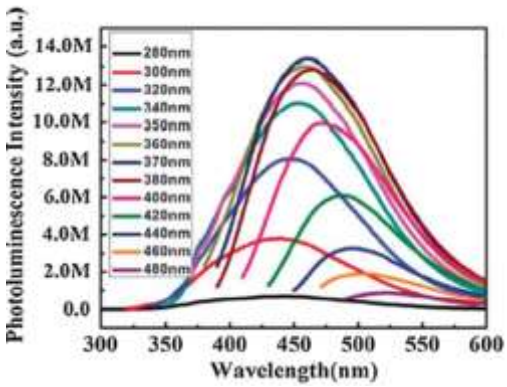

Figure 1.25 Emission spectra of C-dots upon excitation at different wavelenghts[62]

1.7.6 Dendrimers

These molecules are characterized by highly ramified structures and ideally, they are monodisperse. Dendrimers are made by a core linked to repetition units (that can induce different ramifications) which end with terminal groups. In general their properties are highly tunable and strictly related to the nature of the building blocks involved and backbone of the architecture (e.g., tunability of hydrophilicity by surface modifications). Usually they are made fluorescent by means of dyes which are covalently linked in the structure and, one of the main effect of the hyperbranched organization, is the amplification of the properties comparing to the single dye. For instance Blanchard-Desce et al.[63] reported a series of two-photon absorbing dendrimers (different generations) bringing fluorene-based dyes on their surface, observing a linear enhancement of σ_2 with the number of chromophores grafted, up to 56000 GM (4th generation, Figure 1.26).

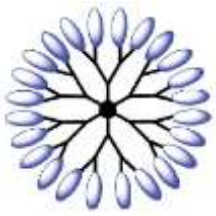

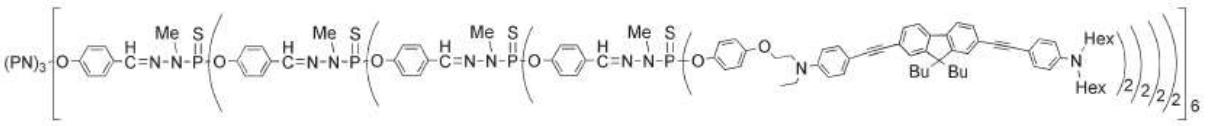

Figure 1.26 Schematic representation (up) of the chemical structure (bottom) of a two-photon absorbing dendrimer[63]

1.7.7 Polymeric NPs

This class is rather wide and comprises several materials and strategies aiming to get fluorescent nanostructures (Figure 1.27).

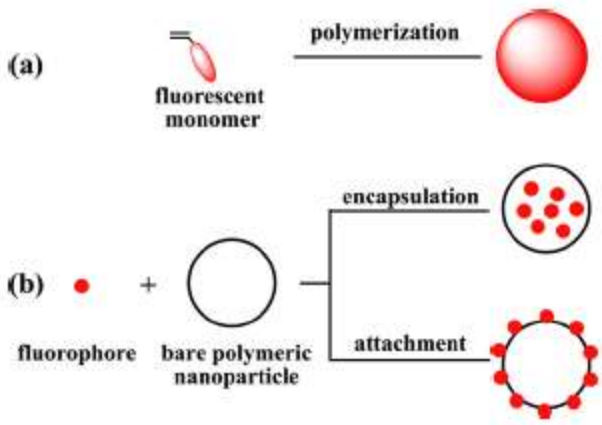

Figure 1.27 Common strategies for fluorescent polymeric NPs[37]

In the first approach of the Figure 1.27, the idea is to use a fluorescent monomer, by covalent binding of a fluorophore to a polymerizable moiety, that upon polymerization leads to fluorescent NPs[37, 64]. The second strategy represent an easier way to dope NPs, which doesn't require the synthesis of the fluorescent monomer. In this view the doping can be achieved by entrapment of the fluorophore inside the scaffold[37, 65] or by chemical binding on the surface of the NPs[37], which must be suitable functionalized for the purpose. Several kind of polymers have been investigated, such as hydrophilic ones (e.g., polyethylenglycols based[66], N-(2-hydroxypropyl)methacrylamide (HPMA)[67]) or hydrophobic ones (e.g., polystyrene[68], polyacrilonitrile[66]), however always aiming to biocompatibility and lack of toxicity[7].

1.7.8 Fluorescent organic nanoparticles by low molecular weight molecules (FONs)

Fluorescent organic nanoparticles is a wide class that, for definition, comprises nanoparticles made by organic compounds, and exhibiting fluorescence properties. I will focus my attention on the kind of nanoparticles studied in this manuscript and therefore the acronym FONs will be referred to ones made by organic molecules with low molecular weight, designed for bioimaging applications. The hydrophobicity of the dyes involved is able to induce the formation of nano-aggregates in water, in order

to minimize the contact of fluorophores with it, resulting in confinement of a huge number of molecules in a small volume[38]. Their properties can be widely tuned according to the nature of the fluorophores involved and, therefore, the engineering of their molecular structures is a key parameter. An interesting example of this concept is what so called aggregation-caused quenching (ACQ), which consists in quenching of the fluorescence (Φ_F), due to increased non radiative de-excitation paths upon aggregation. In 2001 Tang et al.[69] observed that the silole in Figure 1.28 had an opposite trend, exhibiting emissive properties shifting from solution to aggregated state, a phenomenon called aggregation-induced emission (AIE)[69].

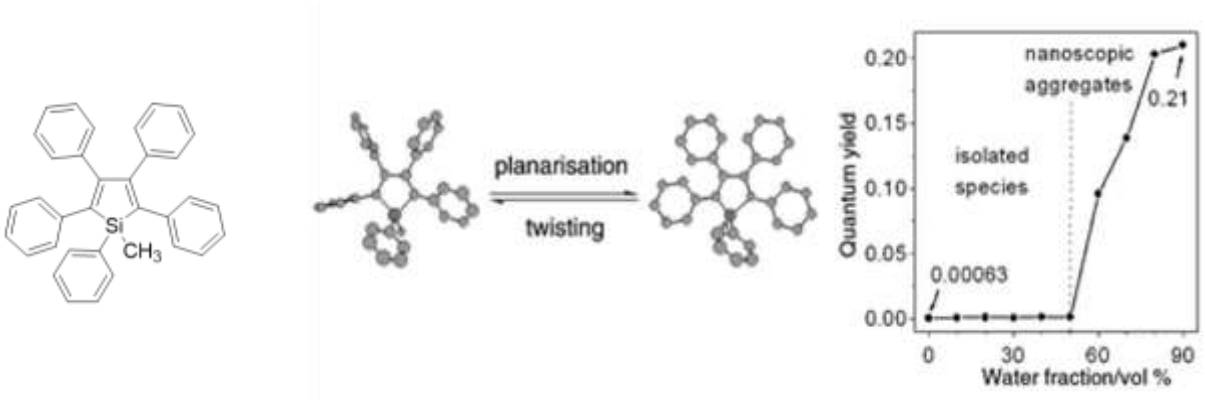

Figure 1.28 Molecular structure (left), conformational rotamers (middle) and variation of the Φ_F of 1-methyl-1,2,3,4,5-pentaphenylsilole in different ratio water-ethanol mixture (right)[69]

The silole in the previous figure, can be visualized as a rotor-stator like molecule, in which the phenyl rings are the rotor moieties. In confined state, a planarization of the structure can happen, leading to an improvement of the conjugation; however, the rotational motions of phenyl rings are not totally prevented, but reduced to a small extent, which is howsoever enough to avoid the formation of excimer specie and quenching of the fluorescence.

1.7.8.1 Preparation of FONs

The FONs described in this manuscript were prepared by routine reprecipitation method (RRM)[70]; there are many ways to prepare them (i.e., laser ablation, vapor deposition), but among those, the reprecipitation represents the quickest and cheapest approach.

In the reprecipitation method adopted in this manuscript, the fluorophores (not soluble in water by test) are dissolved in a water-miscible solvent (e.g., acetone, ethanol, DMSO, THF), aiming to a

concentration about 10^{-3}M; then a small aliquote of this solution is injected into a large volume of milliQ water under vigorous stirring. The process results into a fast solvent displacement, leading to the formation of a colloidal dispersion as following depicted (Figure 1.29).

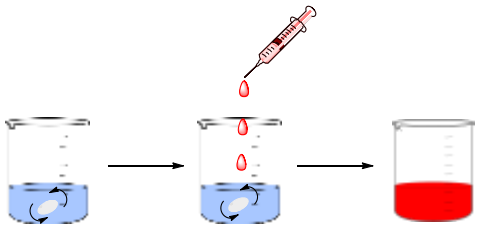

Figure 1.29 Routine reprecipitation method for FONs' preparation

Moreover the parameters that affect the growth of the particles (e.g., temperature, concentrations) can be changed, offering a tunability of properties such as size and shape[38, 70] (Figure 1.30)

Figure 1.30 SEM images of poly(1,6-di(*N*-carbazolyl)-2,4-hexadiyne) nanocrystals made by RRM at different water temperatures: 0°C (left), 20°C (middle). 50°C (right); the sizes of the crystals are 150nm, 100nm and 70 nm, respectively.[70]

Bibliographic references

[1] G. G. Stokes, *Philos. Tr. Soc. Lond.* **1852**, *142*, 463-562.

[2]http://chem.libretexts.org/core/physical_and_theoretical_chemistry/spectroscopy/fundamentals/selection_rules_and_transition_moment_integral.

[3] B. Valeur, M. N. Berberan-Santos, *Molecular Fluorescence - Principles and Applications*, WILEY-VCH, **2012**.

[4] http://archive.cnx.org/contents/81bb0311-98ee-4cfc-b3c8-0eab6aeace37@2/photoluminescence-spectroscopy-and-its-applications.

[5] A. D. McNaught, A. Wilkinson, *IUPAC. Compendium of Chemical Terminology, 2nd ed. (the "Gold Book")* Blackwell Scientific Publications, Oxford, **1997**.

[6] J. R. Lakowicz, *Principles of Fluorescence Spectroscopy*, Third ed., Springer, **2010**.

[7] O. S. Wolfbeis, *Chem. Soc. Rev.* **2015**, *44*, 4743-4768.

[8] A. R. Kherlopian, T. Song, Q. Duan, M. A. Neimark, M. J. Po, J. K. Gohagan, A. F. Laine, *BMC Systems Biology* **2008**, *2*, 74.

[9] T. F. Massoud, S. S. Gambhir, *Gene. Dev.* **2003**, *17*, 545-580.

[10] J. A. Jensen, *Prog. Biophys. Mol. Bio.* **2007**, *93*, 153-165.

[11] M. Minsky, *Scanning* **1988**, *10*, 128-138.

[12] P. Davidovits, M. D. Egger, *Nature* **1969**, *223*, 831-831.

[13] P. Davidovits, M. D. Egger, *Appl. Opt.* **1971**, *10*, 1615-1619.

[14] I. J. Cox, C. J. R. Sheppard, *Appl. Opt.* **1983**, *22*, 1474-1478.

[15] S. W. Hell, J. Wichmann, *Opt. Lett.* **1994**, *19*, 780-782.

[16] T. A. Klar, S. W. Hell, *Opt. Lett.* **1999**, *24*, 954-956.

[17] D. Salo, D. Kim, Q. Cao, M. Y. Berezin, http://www.bioopticsworld.com/articles/print/volume-7/issue-1/features/multispectral-imaging-deep-tissue-imaging-extended-near-infrared-a-new-window-on-in-vivo-bioimaging.html

[18] M. S. Islam, M. Honma, T. Nakabayashi, M. Kinjo, N. Ohta, *Int. J. Mol. Sci.* **2013**, *14*, 1952-1963.

[19] J. V. Frangioni, *Curr. Opin. Chem. Biol.* **2003**, *7*, 626-634.

[20] A. M. Smith, M. C. Mancini, S. Nie, *Nat. Nanotechnol.* **2009**, *4*, 710-711.

[21] L. J. Steven, *Phys. Med. Biol.* **2013**, *58*, R37.

[22] M. Göppert-Mayer, *Ann. Phys. (Berl.)* **1931**, *401*, 273-294.

[23] W. Kaiser, C. G. B. Garrett, *Phys. Rev. Lett.* **1961**, *7*, 229-231.

[24] M. Pawlicki, H. A. Collins, R. G. Denning, H. L. Anderson, *Angew. Chem. Int. Edit.* **2009**, *48*, 3244-3266.

[25] http://photonicswiki.org/index.php?title=Two_Photon_Absorption.

[26] W. Denk, J. Strickler, W. Webb, *Science* **1990**, *248*, 73-76.

[27] http://www.photonics.com/Article.aspx?AID=43009, **2006**.

[28] R. Homma, B. J. Baker, L. Jin, O. Garaschuk, A. Konnerth, L. B. Cohen, D. Zecevic, *Phil. Trans. R. Soc., B, Biol. Sci.* **2009**, *364*, 2453.

[29] K.-S. Lee, R. H. Kim, D.-Y. Yang, S. H. Park, *Prog. Polym. Sci.* **2008**, *33*, 631-681.

[30] S. Wu, J. Serbin, M. Gu, *J. Photochem. Photobiol., A, Chem.* **2006**, *181*, 1-11.

[31] H. A. Collins, M. Khurana, E. H. Moriyama, A. Mariampillai, E. Dahlstedt, M. Balaz, M. K. Kuimova, M. Drobizhev, X. D. YangVictor, D. Phillips, A. Rebane, B. C. Wilson, H. L. Anderson, *Nat. Photonics* **2008**, *2*, 420-424.

[32] A. Ostendorf, B. N. Chichkov, in *Photonics Spectra*, **2006**.

[33] M. Barzoukas, M. Blanchard-Desce, *J. Chem. Phys.* **2000**, *113*, 3951-3959.

[34] H. Myung Kim, B. Rae Cho, *Chem. Commun.* **2009**, 153-164.

[35] E. Genin, V. Hugues, G. Clermont, C. Herbivo, M. C. R. Castro, A. Comel, M. M. M. Raposo, M. Blanchard-Desce, *Photochem. Photobiol. Sci.* **2012**, *11*, 1756-1766.

[36] S. Horikoshi, N. Serpone, in *Microwaves in Nanoparticle Synthesis*, Wiley-VCH Verlag GmbH & Co. KGaA, **2013**, pp. 1-24.

[37] M. Chen, M. Yin, *Prog. Polym. Sci.* **2014**, *39*, 365-395.

[38] S. Fery-Forgues, *Nanoscale* **2013**, *5*, 8428-8442.

[39] Y. Yang, *Microchim. Acta* **2014**, *181*, 263-294.

[40] Y. I. Park, J. H. Kim, K. T. Lee, K.-S. Jeon, H. B. Na, J. H. Yu, H. M. Kim, N. Lee, S. H. Choi, S.-I. Baik, H. Kim, S. P. Park, B.-J. Park, Y. W. Kim, S. H. Lee, S.-Y. Yoon, I. C. Song, W. K. Moon, Y. D. Suh, T. Hyeon, *Adv. Mater.* **2009**, *21*, 4467-4471.

[41] D. Bera, L. Qian, T.-K. Tseng, P. H. Holloway, *Materials* **2010**, *3*.

[42] A. P. Alivisatos, *Science* **1996**, *271*, 933.

[43] P. Zrazhevskiy, M. Sena, X. Gao, *Chem. Soc. Rev.* **2010**, *39*, 4326-4354.

[44] M. A. Hines, P. Guyot-Sionnest, *J. Phys. Chem.* **1996**, *100*, 468-471.

[45] J. Li, J.-J. Zhu, *Analyst* **2013**, *138*, 2506-2515.

[46] D. Deng, Y. Chen, J. Cao, J. Tian, Z. Qian, S. Achilefu, Y. Gu, *Chem. Mater.* **2012**, *24*, 3029-3037.

[47] J. K. Oh, *J. Mater. Chem.* **2010**, *20*, 8433-8445.

[48] L. Ye, K.-T. Yong, L. Liu, I. Roy, R. Hu, J. Zhu, H. Cai, W.-C. Law, J. Liu, K. Wang, J. Liu, Y. Liu, Y. Hu, X. Zhang, M. T. Swihart, P. N. Prasad, *Nat. Nanotechnol.* **2012**, *7*, 453-458.

[49] N. Khlebtsov, L. Dykman, *Chem. Soc. Rev.* **2011**, *40*, 1647-1671.

[50] X. Huang, M. A. El-Sayed, *Journal of Advanced Research* **2010**, *1*, 13-28.

[51] K. E. Sapsford, W. R. Algar, L. Berti, K. B. Gemmill, B. J. Casey, E. Oh, M. H. Stewart, I. L. Medintz, *Chem. Rev.* **2013**, *113*, 1904-2074.

[52] Y.-C. Yeh, B. Creran, V. M. Rotello, *Nanoscale* **2012**, *4*, 1871-1880.

[53] J. Turkevich, G. Garton, P. C. Stevenson, *J. Colloid Sci.* **1954**, *9*, 26-35.

[54] X. Lu, M. Rycenga, S. E. Skrabalak, B. Wiley, Y. Xia, *Annu. Rev. Phys. Chem.* **2009**, *60*, 167-192.

[55] M. Tuominen, E. Schultz, M. Sillanpää, in *Nanomaterials and the Environment, Vol. 1*, **2013**, p. 48.

[56] J.-S. Lee, A. K. R. Lytton-Jean, S. J. Hurst, C. A. Mirkin, *Nano Lett.* **2007**, *7*, 2112-2115.

[57] W. Stöber, A. Fink, E. Bohn, *J. Colloid Interface Sci.* **1968**, *26*, 62-69.

[58] P. Yang, S. Gai, J. Lin, *Chem. Soc. Rev.* **2012**, *41*, 3679-3698.

[59] N. Li, X. Liang, L. Wang, Z. Li, P. Li, Y. Zhu, J. Song, *J. Nanopart. Res.* **2012**, *14*, 1177.

[60] M. Havrdova, K. Hola, J. Skopalik, K. Tomankova, M. Petr, K. Cepe, K. Polakova, J. Tucek, A. B. Bourlinos, R. Zboril, *Carbon* **2016**, *99*, 238-248.

[61] Y. Song, S. Zhu, B. Yang, *RSC Adv.* **2014**, *4*, 27184-27200.

[62] J. Wang, J. Qiu, *J. Mater. Sci.* **2016**, *51*, 4728-4738.

[63] O. Mongin, T. R. Krishna, M. H. V. Werts, A.-M. Caminade, J.-P. Majoral, M. Blanchard-Desce, *Chem. Commun.* **2006**, 915-917.

[64] M. Dossi, R. Ferrari, L. Dragoni, C. Martignoni, P. Gaetani, M. D'Incalci, M. Morbidelli, D. Moscatelli, *Macromol. Mater. Eng.* **2013**, *298*, 771-778.

[65] S. M. Buck, H. Xu, M. Brasuel, M. A. Philbert, R. Kopelman, *Talanta* **2004**, *63*, 41-59.

[66] X.-d. Wang, R. J. Meier, O. S. Wolfbeis, *Adv. Funct. Mater.* **2012**, *22*, 4202-4207.

[67] K. D. Jensen, P. Kopečková, J. H. B. Bridge, J. Kopeček, *AAPS PharmSciTech* **2001**, *3*, 62-75.

[68] X.-d. Wang, D. E. Achatz, C. Hupf, M. Sperber, J. Wegener, S. Bange, J. M. Lupton, O. S. Wolfbeis, *Sens. Actuators B Chem.* **2013**, *188*, 257-262.

[69] J. Luo, Z. Xie, J. W. Y. Lam, L. Cheng, H. Chen, C. Qiu, H. S. Kwok, X. Zhan, Y. Liu, D. Zhu, B. Z. Tang, *Chem. Commun.* **2001**, 1740-1741.

[70] H. Masuhara, H. Nakanishi, K. Sasaki, *Single Organic Nanoparticles*, **2003**.

Chapter 2

Design of New Two-Photon pH Probes

2.1 Introduction and goal of the work

In the first section of this chapter some basic concepts about the biological relevance of the pH, and fluorescent pH probes will be introduced. This will be helpful in understanding the context in which this work fits.

2.1.1 Importance of pH in biological environment

In biological field pH is a fundamental parameter for the normal carrying out of biochemical processes in living organisms. For example just think of chemiosmotic coupling[1] in oxidative and photophosphorilation that takes place in mitochondria and chloroplasts, where the electron transport chains are coupled to the formation of a protonic gradient across membranes, which is used as driving force for the phosphorylation of the ADP (Figure 2.1).

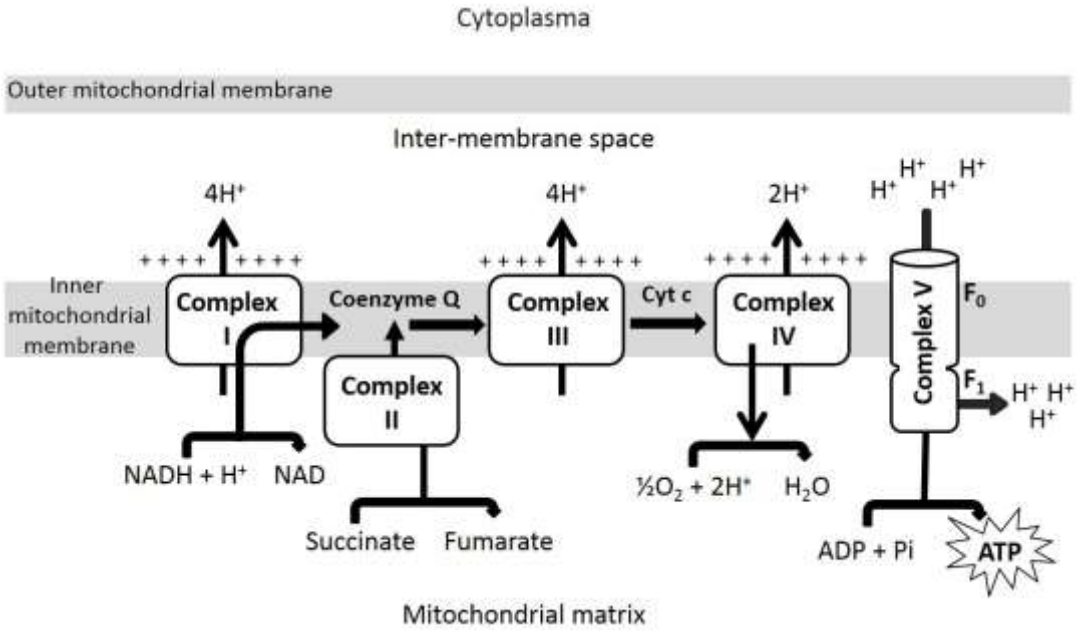

Figure 2.1 Oxidative phosphorylation[2]

The processes that can take place inside a cell are varied and often require dissimilar conditions, among which the pH is one of the most relevant and, in order to ensure the best situation for the biological activities, eukariotic cells are highly compartimentalized[3].

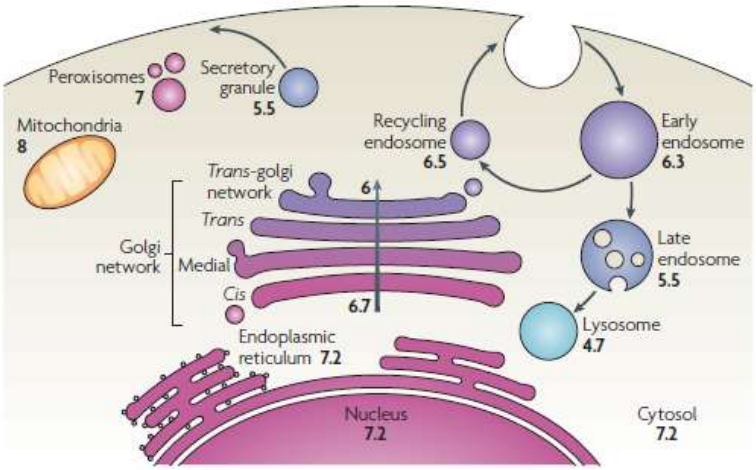

Figure 2.2 pH of different subcellular compartments[3]

As shown in the previous figure, pH is not constant over the whole cell, but changes according to the compartments[3], from more acidic organelles such as lysosomes up to alkaline ones such as mitochondria. In the absence of compartmentalization by membrane delimitation, many processes could not be carried out properly: for instance the degradation of lipids occurs thanks to the action of lipase which are enzymes contained in lysosomes, that are active at acidic pH (i.e., about 5.0), whereas they are unactive in neutral condition, ensuring the safety of the cells in case of lysosomes rupture[3] and possible release in the cytosol (pH≈ 7.2). Moreveor following metabolic activities, such as the production of ATP by glycolysis, the pH of the cytosol tends to decrease; however the homeostasis condition, which is a key factor for the proper functioning of the cell, is ensured by means of appropriate regulatory mechanisms, such as exchangers and co-transporters[3].

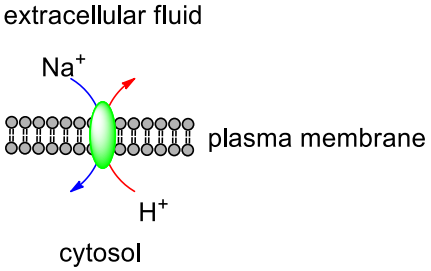

Figure 2.3 Antiporting mechanism of Na^+/H^+ exchanger

The example in the previous figure shows the antiporting mechanism of a sodium-proton exchanger (NHE), a transmembrane protein present in mammalian cells that is responsible for exchanging intracellular H^+ with extracellular Na^+, contributing to enhance of the intracellular pH level.

However pH regulation does not only affect the intracellular environment. In fact, as mentioned above, the regulatory mechanisms for intracellular pH homeostasis involve transmembrane processes between the cytosol and the interstitial space. Then pH outside of the cellular compartment (pHe) is regulated by biological processes involving the action of organs such as kidneys and lungs[4]. The alteration of normal pH conditions is often related to a variety of disorders and pathologies. For example lysosomal pH alterations[5] are related to the intracellular metabolism of Amyloid-β Protein Precursor, which is involved in the onset of Alzheimer's disease; acidification of cytosol in cardiac myocite leads to an overload of intracellular Ca^{2+}, resulting in alteration of their contractility that can lead to arrhytmias and cardiac failure[3, 6-7].

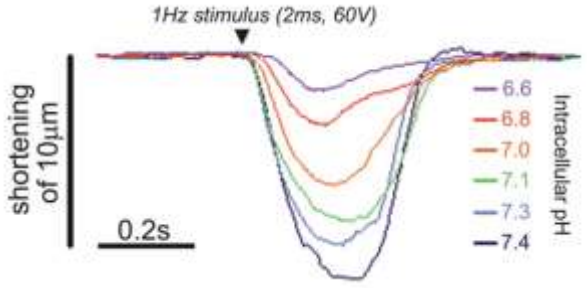

Figure 2.4 Effect of uncompensated intracellular acidosis on myocyte contractility[6]

As for the diseases associated with variations of extracellular pH, tumors are a representative case. Generally, due to the low vascularization, they exhibit a remarkable glycolytic activity which is accompanied by an equally efficient homeostasis process. In this way their physiological intracellular pH is preserved at the expense of the extracellular environment which is significantly acidified, as low as 6.5[8]. In fact, while in normal tissue the pHe (≈ 7.4) is generally higher than intracellular one (pHi≈ 7.2), in tumors the situation is reversed (pHe < pHi).

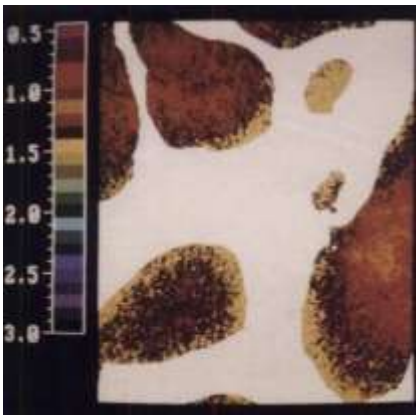

Figure 2.5 Pseudocolor-image of fluorescence-ratio profile between microvessels in tumor tissue. *White regions*, vascular space. The values of 1.0, 1.5 and 2.0 correspond to pH of 6.38, 6.92 and 7.5 respectively. *Color scale height*, 150 μm[9]

It follows that the ability to measure and/or monitor pH in cellular environment, especially close to membranes, is of great importance both in the biological field, in order to understand what are the biochemical mechanisms that induce pH changes, and in the medical ambit, taking advantage of the close correlation between pH alterations and the onset and development of pathologies.

2.1.2 Fluorescent pH-probes

In this section we will introduce a brief excursion of fluorescein based probes, which is a frequently used family of pH probes, in order to better understand feautures and requirements for fluorescence bioimaging purposes.

Fluorescein can exist in water solution into several forms, according to the pH-dependant equilibriums depicted in Figure 2.6[10].

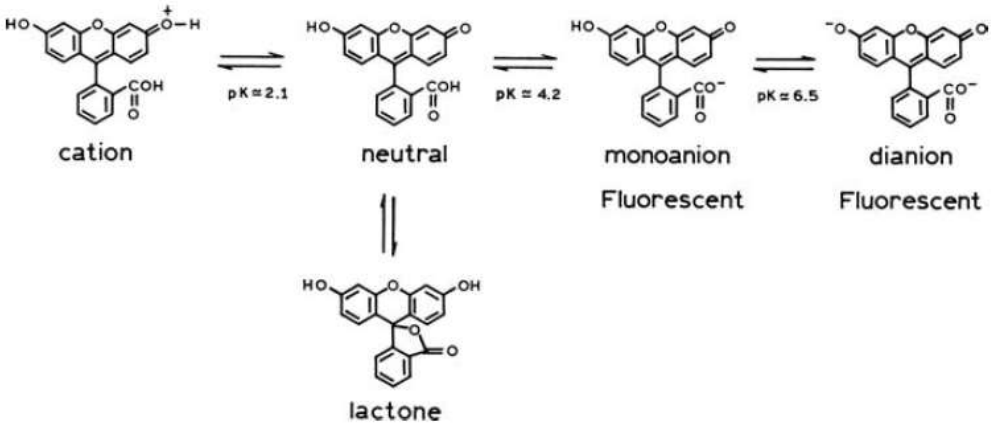

Figure 2.6 pH-dependent equilibriums of fluorescein[10]

In a range of pH between 5.0 and 8.0, the absorption spectrum is basically constituted by the anionic and dianionic species; the first one exhibits two peaks with roughly the same molar absorption at 453 and 472 nm, whereas the dianionic form display a main band at 490 nm[11]. The emission of the two species is widely overlapped and, upon excitation at a suitable wavelength (488 nm in figure 2.7) in different pH conditions, the fluorescence emission show a clear intensity reduction of the band at about 515 nm.

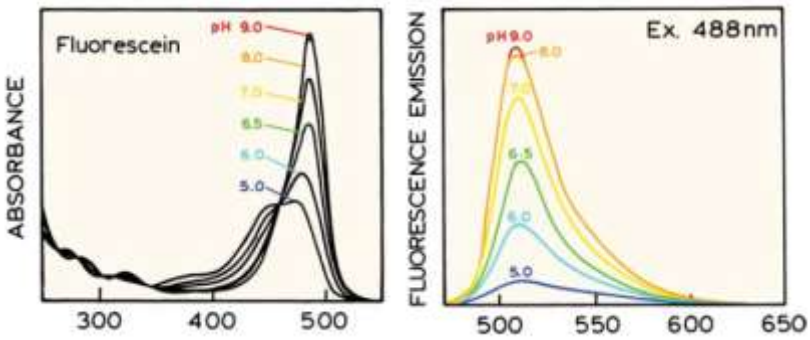

Figure 2.7 Absorption and emission spectra of fluorescein in different pH conditions[10]

The pH dependence of absorption and emission, due to the equilibrium among the species present at a given pH, allows ratiometric properties that can be exploited for pH determination with advantage. In particular the ratio of fluorescence intensities registered at a single wavelength upon excitation at two different ones (usually about 450 and 490 nm for fluorescein) is strictly related to the ratio of the two conjugated emissive forms, which in turn is determined by the pH of the solution (Figure 2.8). This relationship allows to perform pH measurements from fluorescence intensity ones, and the method is known as dual excitation ratiometric approach.

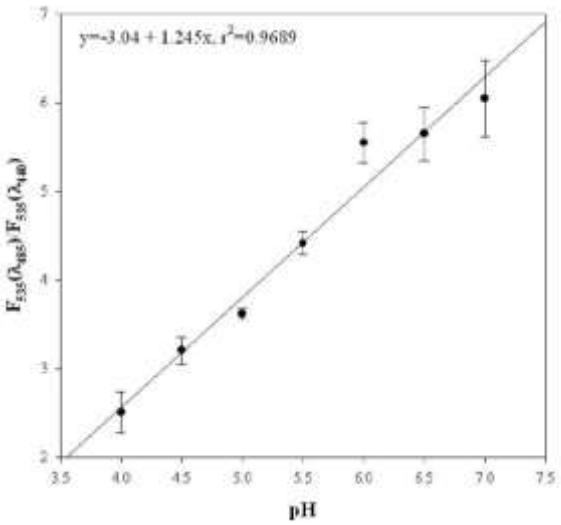

Figure 2.8 *In vivo* pH calibration curve of fluorescein-dextran ratio against pH)[12]

The main advantage of this mode is that the fluorescence intensity ratios are independent on parameters such as local concentration of the probe, optical path length and photobleaching, which therefore do not affect the pH measurement. These features have made many fluorescein-based dual excitation ratiometric probes widely used for pH determination in biological environment.

Fluorescein (and in general charged compounds) is usually loaded into cells by means of cell-permeant ester derivatives; the idea consists in enabling cell loading (avoiding invasive techniques such as microinjection) by means of fluorescein diacetate (FDA, Figure 2.9) that is less polar and, upon internalization, is converted to fluorescein by action of intracellular esterase[13].

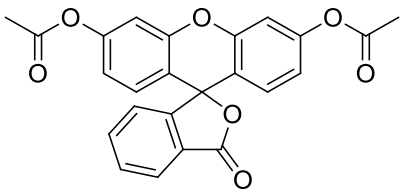

Figure 2.9 FDA

To date this kind of approach has been highly developed and acetoxymethyl esters (AM), which are hydrolyzed into the cell by non specific esterase, are largely used to mask polar functional groups in pH-probes[14].

However FDA suffers of high leakage rate[15], making it difficult to use especially for studies over time. Usually this problem is addressed by enhancing the retention time of the probe inside cells by increasing

its polarity by means of functionalization of the chemical structure. For instance carboxyfluorescein released upon hydrolysis of its diacetate (CFDA, Figure 2.10) or AM esters, contains a carboxyl group on position 5 or 6 which increase the retention inside cells[16].

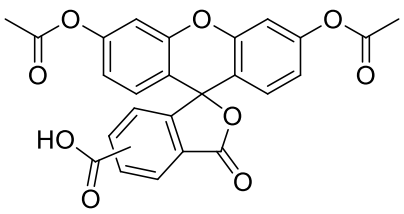

Figure 2.10 CFDA

Another important issue to take into account for pH probing is its pKa value; in order to get sensitivity to pH variation around neutrality, the probe must have a pKa very close to it and ideally pKa≈ pH should be satisfied[14]. In this condition a little variation of the pH induces a significative change of the analytical response related to the ratiometric property monitored, getting high sensitivity. For these reasons several researches have been done to develop ratiometric pH probes with pKa close to neutrality. In this view, 2',7'-Bis-(2-carboxyethyl)-5-(6)carboxyfluorescein (BCECF, Figure 2.11), introduced by Rink et al.[17] (in its AM ester form) represents an improvement of CFDA and, with a pKa equals to 7.0, it is one of the most used probes for pH measurements[14].

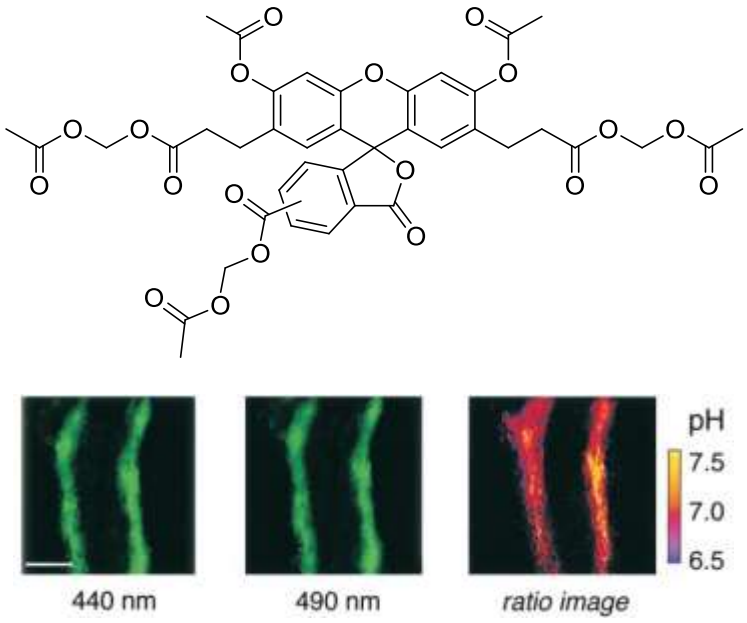

Figure 2.11 Top: AM ester of BCECF; bottom[18]: Fluorescence images of BCECF-dextran-stained distal airway taken at 440 nm (left) and 490 nm (middle) excitation wavelengths. Spatial map of pH shown as pseudocolored ratio image (right). Bar, 100 μm.

2.1.3 Dual emission ratiometric pH probes

However the development of pH probes followed also the specific requirements of other techniques and the development of other technologies. For instance several common devices used in biological field, such as flow cytometers and microplate readers, work with one excitation source setup[14], therefore in this view dual excitation probes suffer of some limitations. Furthermore the appearance of confocal microscopes represented another reason to research on ratiometric pH probes exhibiting pH dependancy of fluorescence spectra in terms of shift of the λ_{ems}^{max}, meaning that the conjugated species of the probe are able to exhibit fluorescence in different spectral regions. Similarly to dual excitation probes, compounds that show two emission bands upon excitation at one wavelength, are known as dual emissive ratiometric pH ones. In this view benzoxanthene derivatives, such as seminaphthorhodafluors (SNARFs), are the most common and representative ones[14]. They usually exhibit dual excitation and dual emission ratiometric behavior, long absorption and emission wavelengths and pKa close to neutrality (pKa= 7.5[10] for Carboxy SNARF-1 in Figure 2.12[19]).

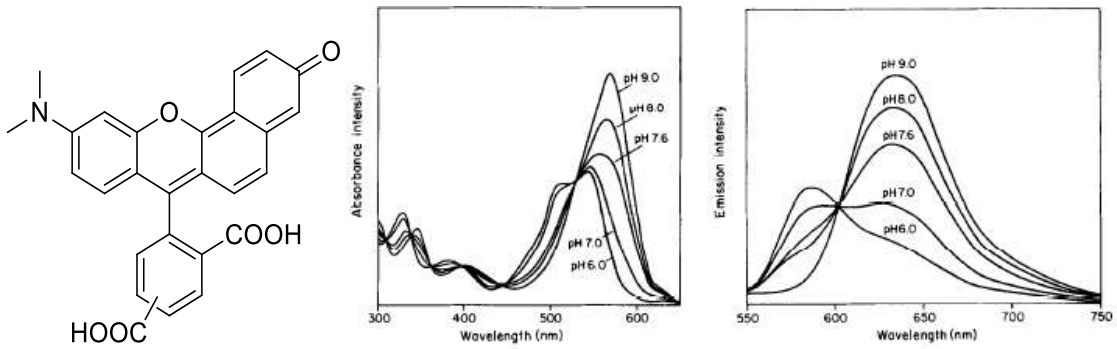

Figure 2.12 C.SNARF-1: structure (left); absorption (middle) and emission spectra (right, sample excited at 534nm) in 50 mM potassium phosphate buffered solutions[19]

2.1.4 Ratiometric pH probes for two-photon excitation techniques

The development of two-photon microscopy stimulated the research and investigations for ratiometric pH probes suitable for two-photon (2P) excitation techniques. In general 2P pH probes must be characterized by high values of two-photon brightness ($\sigma_2\Phi_F$), which allows to get high quality 2P image and in principle to work with low power lasers, reducing photodamage and enabling long time experiments. In the view of the ratiometric approach this feature must be extended to both the forms at the pH dependant equilibrium. In 2004 Blanchard-Desce et al.[20] reported the two push-pull-push

quadrupoles depicted in Figure 2.13, which show strong modulation of non linear optical properties upon (de)protonation.

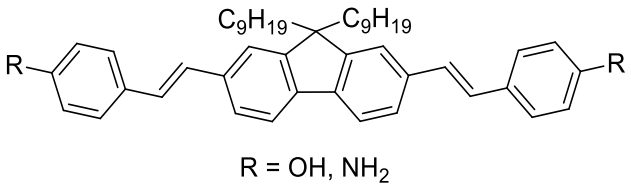

Figure 2.13

Both compounds undergo significative spectral changes upon deprotonation of the acidic forms, with a bathochromic shift of the emission bands that are accompained by a reduction of fluorescence quantum yields values. However in parallel, the enhancement of the internal charge transfer (ICT) character (that is enhanced from phenol to phenolate and from anilinium to aniline) induces an increase of two photon cross section (σ_2), with beneficial consequences for brightness, a concept which will be renewed in the next sections. The pKa values measured for these compounds were 9.5 and 3.5 respectively for phenol and aniline derivative.

Several works can be found in literature about small-molecule based 2P ratiometric pH probes[21] for bioimaging purpose, some of them following quoted.

In 2006 Jullien et al.[22] reported some work on optical properties on dipolar 5-aryl-2-pyridyloxazole derivatives, studying their optical properties upon one and two-photon excitation. These compounds exhibit tunable pKa values ranging from 2.0 to 8.0, by playing on the stuctures of donor and acceptor moieties and some of them, such as 4-PYMPO-NH_2 (Figure 2.14) show dual emissive ratiometric behavior.

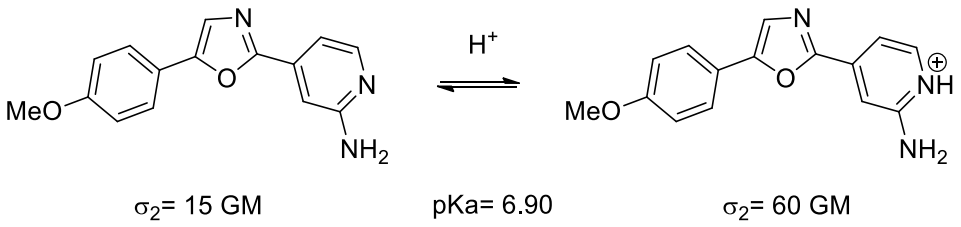

Figure 2.14

In 2012 Cho et al.[23] reported a 2-methoxy-6-(5-oxazolyl)naphtalene derivative with a pKa about 4.4, which was successfully used for ratiometric pH estimation in live cells and human tissues by means of two-photon microscopy (Figure 2.15).

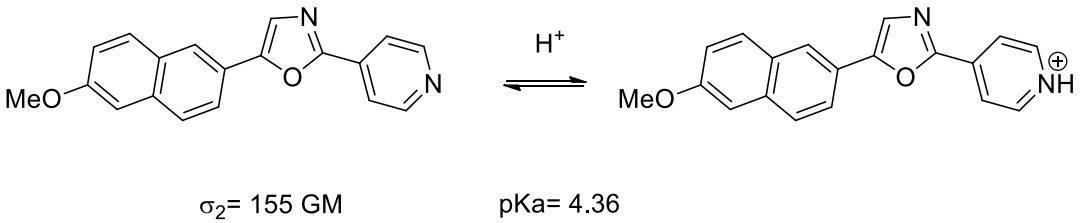

Figure 2.15

A series of benzimidazole derivative (Figure 2.16) with pKa values between 4.9 and 6.1, was prepared by Kim et al.[24] and employed for ratiometric two-photon imaging of live cells and mice brain tissues.

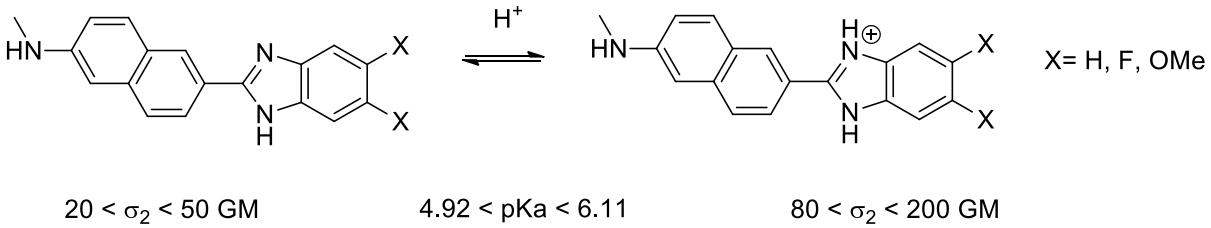

Figure 2.16

A benzo[d]thiazole derivative (Figure 2.17) with pKa about 5.0 was reported by Zhao et al.[25] and used for intracellular pH determination of HeLa cells.

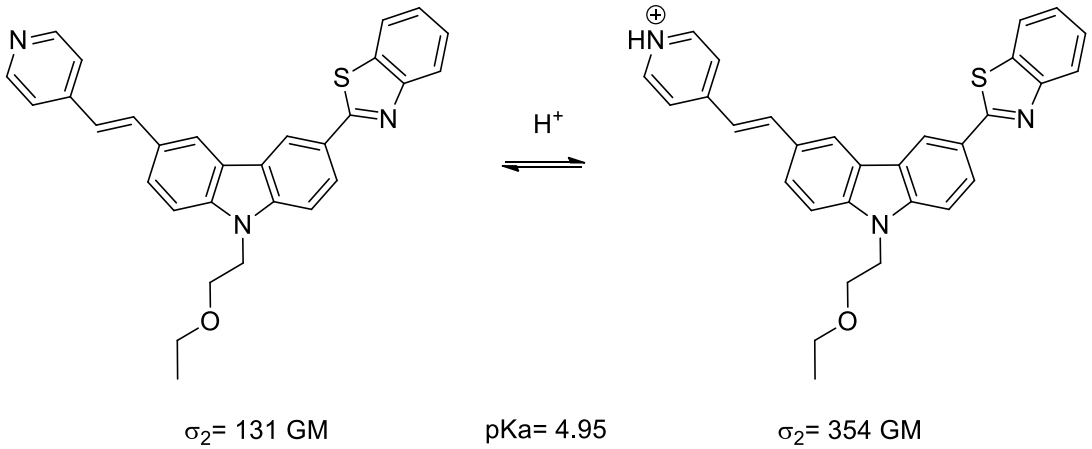

Figure 2.17

From the previous examples it is possible to note that the combination of some pH probes properties is rather complicated. Often compounds having pKa close to neutral pH, and therefore very sensitive to little pH variations in physiological conditions, lack of suitable two-photon cross section for one or both conjugated forms or vice versa; in this context the purpose of this work finds its position.

The aim is to prepare ratiometric pH probes for cell membranes:

- characterized by pKa close to neutrality, in order to get high sensitivity to little variations around physiological pH;
- exhibiting dual emission ratiometric behavior;
- showing large two-photon cross section, therefore suitable for pH probing by two-photon excitation techniques;
- able to stain cell membranes, aiming to measure pH close to them, where we have seen a variety of important biochemical processes take place.

2.2 Design of the probes

The target chromophores are quadrupoles of the type type A-π-D-π-A (Figure 2.18) and their molecular structure are following described.

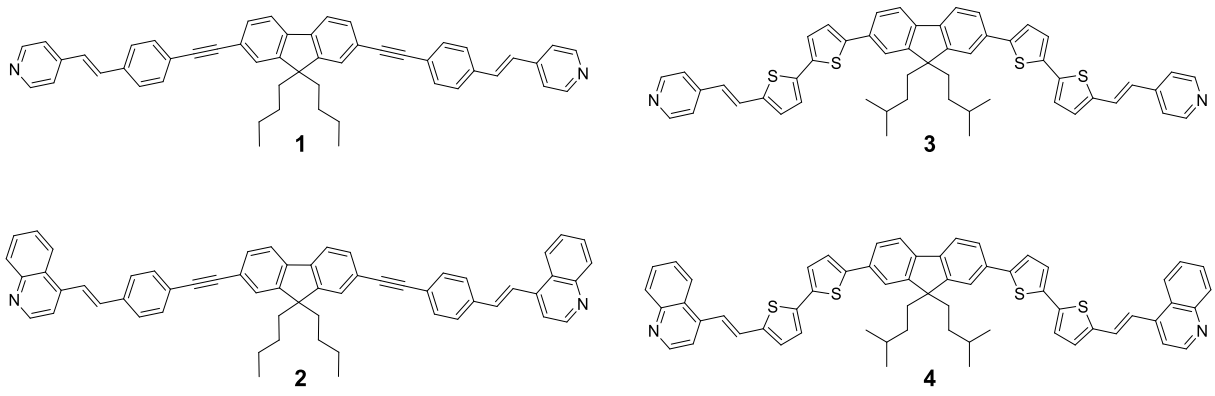

Figure 2.18 pH probes synthesized

The donor core chosen is fluorene, a deeply studied[26-37] scaffold involved in synthesis of several dipolar and quadrupolar systems, usually exhibiting high Φ_F and good non linear optical properties. It worths to point out that, according to the principles given in the first chapther, fluorene represents a planarization

of biphenyl, aiming to improve two-photon cross section by better electron conjugation in the molecular structure. Moreover fluorene can be easily functionalized on the positions 2 and 7 of the aromatic rings, which exhibit good reactivity towards electrophilic substitutions, and on position 9 by exploiting the acidity of the protons in that position (pKa= 22.6 in DMSO[38]) due to aromatic stabilization of conjugated anion.

The π-bridges selected consists of ethynylene-phenylene-vinylene and 2,2'-bithiophene moieties, according to which the chromophores will be named distinctly as first and second family respectively. The idea behind the variation of the conjugative element, is to achieve a tunability of the optical properties. In particular the replacement with the bithiophene motif represents an extension of the π-system which should provoke a desirable enhancement of σ_2 because of the increase of the charge transfer character of the dye. Furthermore heterocycles are often used in the field of two-photon materials as conjugation path, because comparing to carbon-carbon double bonds they usually enhance photostability[39] and induce red-shift of absorption and emission[39]. Finally, aiming to get probes for cell membranes, the two chosen π-bridges contributes to get length of about 3.4 nm (distance between the two nitrogen atoms in each chromophore), matching the main thickness of biological membranes[40], in order to get incorporation within the cell membranes (Figure 2.19).

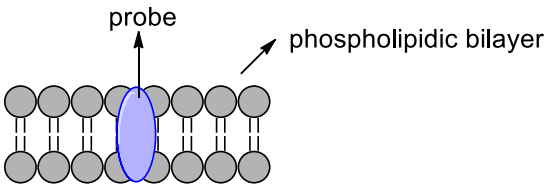

Figure 2.19 Transmembrane incorporation of the probe in the lipidic bilayer.

In this view the lipophylic character of the inner part of the chromophores is enhanced by functionalization on position 9 of the core with two alkyl chains; usually this kind of modification doesn't affect optical properties[41].

The acceptor end-groups chosen are pyridine and quinoline ones; they show a weak basicity thanks to the electron pairs on the nitrogen atoms, resulting in pKa about equal to 5.2 and 4.8 for pyridinium and quinolinium respectively. However a modulation of their basicity (i.e., enhanced), due to cross

conjugation with the donor core is expected, which may eventually result in a shift of pKa values towards 7.

2.3 Synthesis

From synthetic point of view it's comfortable to take advantage from the symmetry of the molecules (Figure 2.20).

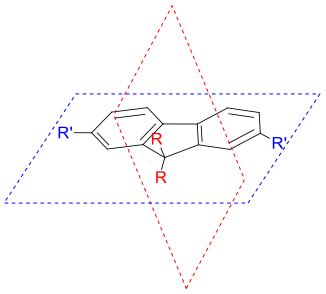

Figure 2.20 Sketch of substituted fluorene core with symmetry planes.

In particular one can identify a mirror plane on which the fluorene scaffold lies (blue one in the previous figure), containing the substituents on positions 2 and 7, and a mirror plane perpendicular to the first one which contains the other two substituents on position 9 (red one in the previous figure). It follows that planning a synthesis made by two-fold steps, one for the introduction of the alkyl chains and the other one for the functionalization of the positions 2 and 7, seems advantageous. According to the latter idea and, in order to perform a cheap synthesis using simple and commercially available materials, chromophores **1** and **2** were prepared by means of the retrosynthetic route depicted as following (Scheme 2.1).

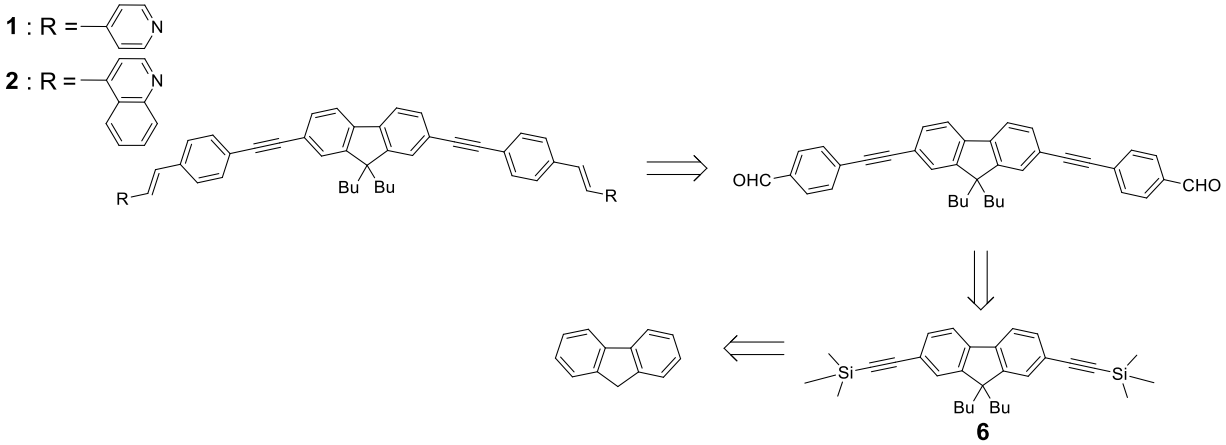

Scheme 2.1 Retrosynthesis of target molecules **1** and **2**

The intermediate **6** was already present in our laboratory as previously synthesized[42], [i], however the description of the synthesis also includes the steps used for the preparation of such, highlighting the convenience of the synthetic route chosen.

Commercially available fluorene was iodinated via aromatic electrophilic substitution by iodine in acidic conditions (Scheme 2.2)[43].

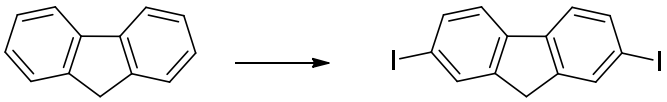

5

Scheme 2.2 Bis-iodination of fluorene; reagents and conditions: I_2, HIO_4, H_2SO_4, AcOH, 75 °C, 2 h, 80%.

The butyl chains were introduced by nucleophilic substitutions of the carbanion generated by deprotonation of **5** on butyl bromide; the reaction was performed in biphasic conditions using a phase transfer agent (Scheme 2.4)[44].

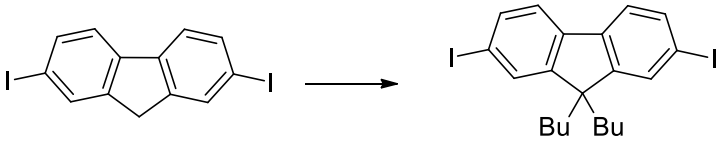

5 **6**

Scheme 2.3 Bis-alkylation of **5**; reagents and conditions: tetrabutylammonium bromide, KOH, n-butyl bromide, $PhMe/H_2O$ (2:1), 65 °C, 1 h, 90%.

Thus the iodine atoms were replaced by Sonogashira cross-coupling with ethynyltrimethylsilane, protecting one side of each ethynyl moiety, getting the intermediate **7** (Scheme 2.4)[42].

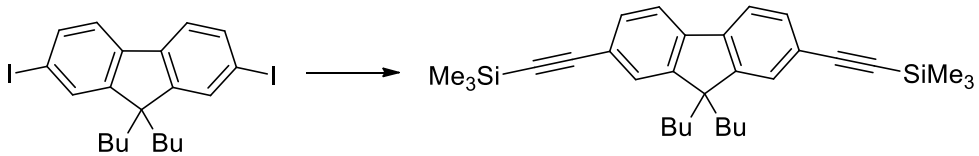

6 **7**

Scheme 2.4 Two-fold Sonogashira cross-coupling; reagents and conditions: ethynyltrimethylsilane, CuI, $Pd(PPh_3)_2Cl_2$, $PhMe/Et_3N$ (1:1), 40 °C, overnight, 79%.

[i] Compounds **1** and **2** were previously prepared and studied by A. Sourdon, J.-M. Vabre and J. Daniel, that I warm thank.

The triple bonds were quickly deprotected by methanolysis in basic conditions (Scheme 2.5), activating the terminal carbon bonds in view of the next step.

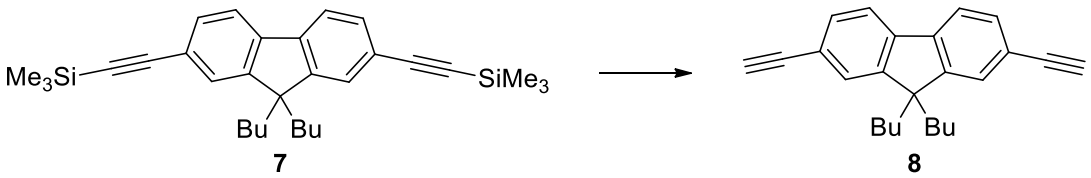

Scheme 2.5 Methanolysis of the silane; reagents and conditions: 1N KOH, THF/MeOH (3:1), rt, 30 min, 84%.

At this point the common precursor of the target molecules was achieved by a second two-fold Sonogashira cross coupling with 4-bromobenzaldehyde, another commercially available and cheap reagent (Scheme 2.6).

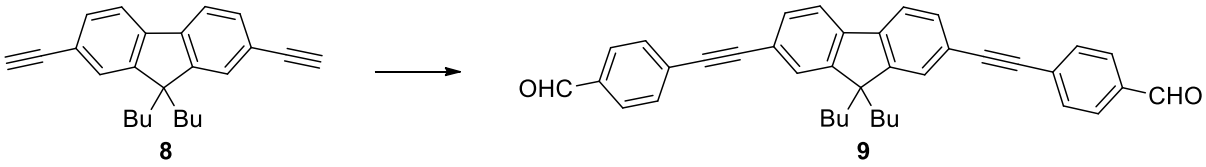

Scheme 2.6 Two-fold Sonogashira cross-coupling; reagents and conditions: 4-bromobenzaldehyde, CuI, $Pd(PPh_3)_2Cl_2$, Toluene/Et_3N (4:1), 40 °C, overnight, 75%.

Target molecules **1** and **2** were finally prepared by Wittig-Horner reaction with 4-(diphenylphosphinoylmethyl)pyridine (**10**)[45] and 4-(diphenylphosphinoylmethyl)quinoline (**11**)[42] as following reported.

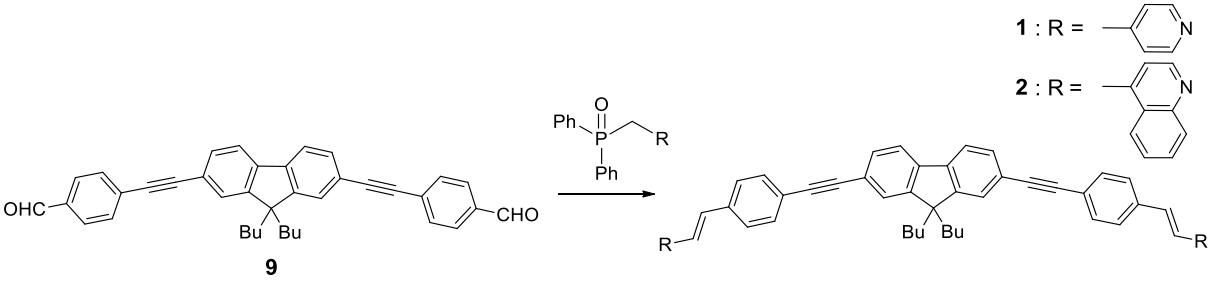

Scheme 2.7 Two-fold Wittig-Horner reaction; reagents and conditions R-CH_2-P(O)Ph_2, NaH, THF, rt, 24 h, 81% (**1**), 79% (**2**).

It worths to point out the stabilizing effect of pyridine and quinoline moieties on the phosphorus α-carbanion generated after deprotonation of the phosphine oxide derivatives, which allows to get **1** and **2** with high *E*,*E* stereoselectivity[46].

The synthesis of **3** and **4** were performed using a strategy similar to the one adopted for the first family of probes (Scheme 2.8).

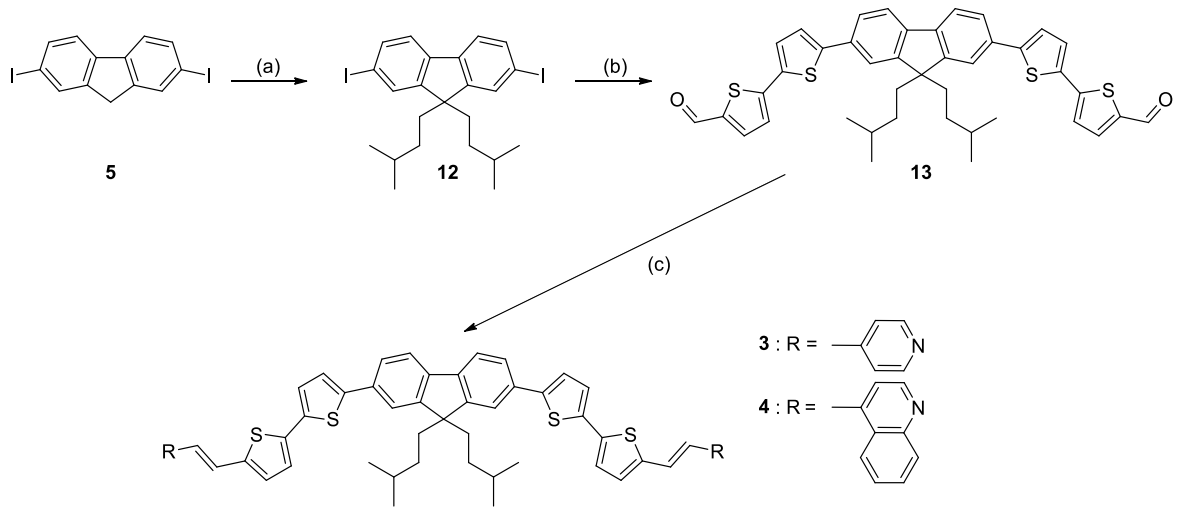

Scheme 2.8 Synthesis of the second family of probes; (a) n-Bu_4NBr, KOH_{aq}, 1-bromo-3-methylbutane, Toluene, 65°C, 2h then rt, 24h (44%); (b) (5'-formyl-[2,2'-bithiophen]-5-yl)boronic acid, K_2CO_3, Pd(dppf)Cl_2,Toluene/MeOH=2:1, 70°C, 48h (39%); (c) **10** or **11** (1.02 eq.), NaH, THF, rt, 24h (**3**, 64%; **4**, 59%).

Starting from **5**, double alkylation by means of isopentyl bromide allows to get compound **12**. Isopentyl chains were used instead of butyl ones because **12** was an intermediate involved in another project in our laboratory, whereas for the purpose of this work, the variation should not affect the optical properties of the probes but at most it should increase their lipophylic behavior. At this point the π-bridge was introduced by a two-fold Suzuki cross-coupling with commercially available (5'-formyl-[2,2'-bithiophen]-5-yl)boronic acid getting compound **13**, the common precursor of the target molecules. Finally, Wittig-Horner condensations of the latter one with **10** and **11** allow to get respectively **3** and **4**.

2.4 pH dependence of the photophysical properties

The study of the absorption and emission properties was carried out on diluted solutions (10^{-6} M) of the chromophores in sodium dodecyl sulfate (SDS) micellar water (SDS:BuOH:water = 6:5:89 wt%). In fact the bolamphiphilic feature of these compounds makes them soluble in the colloidal environment. The pH of the solutions was regulated by small addition of aqueous hydrochloric acid or sodium hydroxide solutions. Data concerning absorption and emission properties are summarized in Table 2.1 and following discussed.

	λ_{abs}^{max} [nm]	λ_{em}^{max} [nm]	Φ_F	λ_{2PA}^{max} [nm]	σ_2^{max} [c] [GM]	$\sigma_2^{max}\Phi_F$ [d] [GM]	pKa
1[a]	380	417	0.67	700	260	174	7.0
1[b]	401	544	0.26	750	1070	278	
2[a]	386	436	0.52	700	700	364	6.2
2[b]	420	590	0.12	730	1260	151	
3[a]	444	500	0.35	730	400	140	6.3
3[b]	485	621	0.14	820	1740	244	
4[a]	446	554	0.10	800	1000	100	6.8
4[b]	515	679	0.04	820	3900	156	

Spectroscopic data were collected using diluted solutions of chromophores in micellar water (SDS/butanol/water, 6:5:89 wt%) under basic[a] (10^{-3} M NaOH; pH = 11) or acidic[b] conditions (10^{-3} M HCl; pH = 3). [c]Two-photon absorption cross section given in GM (1 GM = 10^{-50} cm^4 s $photon^{-1}$). [d]Two-photon brightness defined as the product of the maximum 2PA cross-section and of the fluorescence quantum yield (Φ_F).

Table 2.1 Absorption and emission properties of chromophores **1**, **2**, **3** and **4** in micellar water

2.4.1 Absorption and emission

Absorption and emission spectra of the chromophores, in basic and acidic conditions, are reported in the following figure.

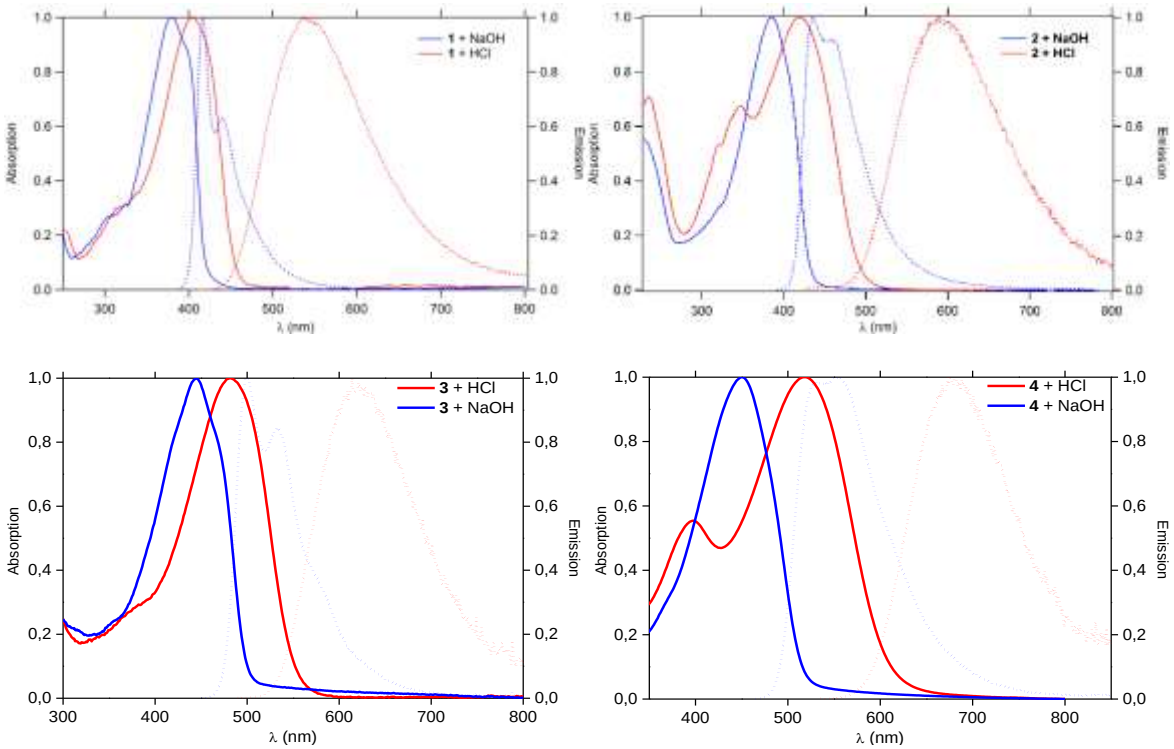

Figure 2.21 Normalized absorption (solid line) and emission (dotted line) spectra in basic (blue) and acidic (red) conditions

At basic pH compounds **1** and **2** exhibit absorption in the near UV-Visible (λ_{abs}^{max}= 380 nm and 386 nm respectively for **1** and **2**), whereas their emission are in the violet (λ_{ems}^{max}= 417 nm and 436 nm respectively for **1** and **2**). Upon acidification of the medium, the absorption bands are slightly red-shifted in the violet region (λ_{abs}^{max}= 401 nm and 420 nm respectively for **1** and **2**) whereas the emission bands undergo more pronounced red-shift up to green (**1**, λ_{ems}^{max}= 544 nm) and yellow (**2**, λ_{ems}^{max}= 590 nm). From this data is possible to draw some considerations. The replacement of the pyridine group with the quinoline one, being an extension of the π-system, results in a red-shift of the absorption and emission bands (more pronounced for the latter). Moving from basic to acidic conditions, the protonation of the acceptor moieties leads to an enhancement of their electron withdrawing character, that results into a red-shift of absorption and emission bands too.

Concerning the chromophores **3** and **4**, in basic conditions they show absorption in the violet-blue region ($\lambda_{abs}^{max}\approx$ 445 nm), then turquoise (**3**, λ_{ems}^{max}= 500 nm) or yellow-green (**4**, λ_{ems}^{max}= 554 nm) fluorescence. Upon acidification of the solutions, the absorption bands are shifted up to cyan (**3**, λ_{abs}^{max}= 485 nm) and green region (**4**, λ_{abs}^{max}= 515 nm), whereas the emission bands move to orange-red (**3**, λ_{ems}^{max}= 621 nm) and deep-red-near infrared region (**4**, λ_{abs}^{max}= 679 nm). The trends observed are similiar to the previous ones.

At this point it is possible to compare the chromophores of the first family (**1** and **2**) with those of the second one (**3** and **4**). As mentioned the elongation of the π-bridge, through the replacement of the ethynylene-phenylene moiety with the 2,2'-bithiophene one, induces a red-shift of the optical bands, both in basic and acidic pH conditions.

Furthermore, the protonation of the acceptor groups (e.g., from $\mathbf{1}_{basic}$ to $\mathbf{1}_{acid}$), the replacement of the pyridine moiety with the quinoline (e.g., from **1** to **2**) or the elongation of the π-bridge (e.g., from **1** to **3**), are accompanied by a reduction of the fluorescence quantum yield.

Eventually all the chromophores display a remarkable spectral shift in the emission spectra further to protonation, that represents a signature for dual emission ratiometric pH probes.

2.4.2 pKa determination

The pH dependancy of the emission spectra was deeply investigated (Figure 2.22) recording spectra spanning a large pH window.

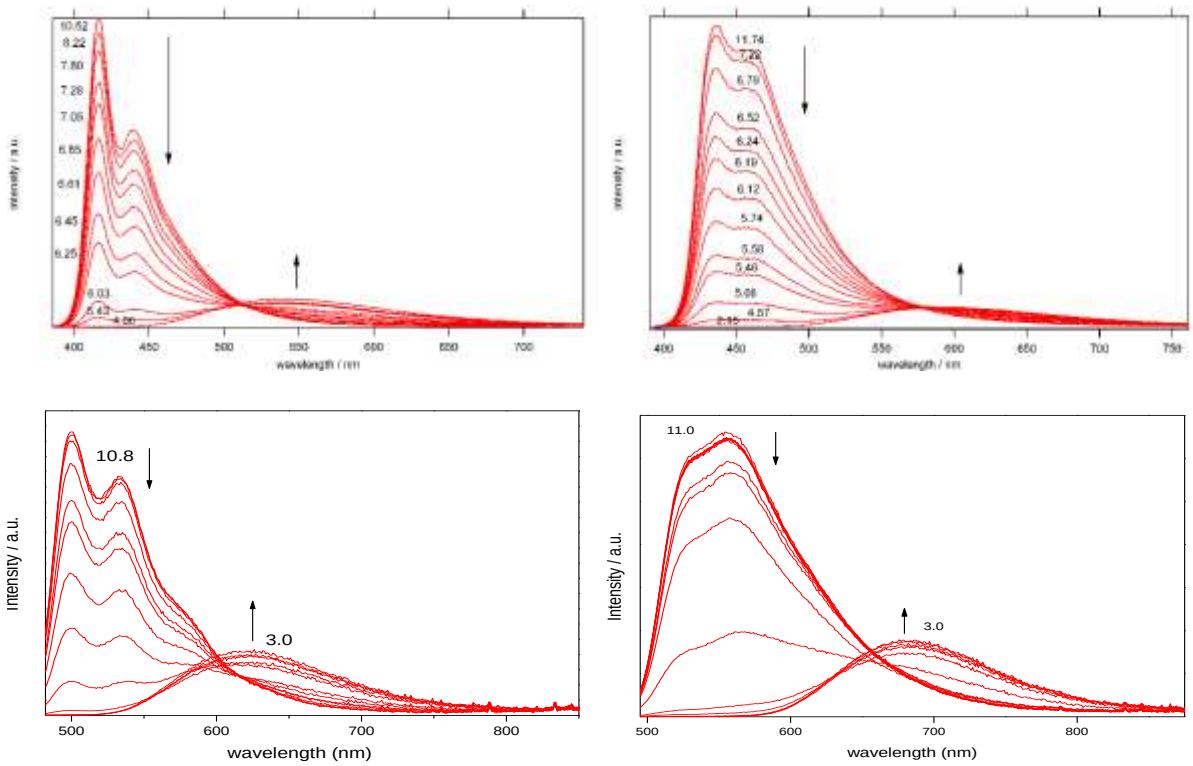

Figure 2.22 pH dependancy of emission spectra in micellar water. Top: **1** (left, λ_{exc}= 380 nm), **2** (right, λ_{exc}= 386 nm); bottom: **3** (left, λ_{exc}= 460 nm)**, 4** (right, λ_{exc}= 486 nm).

From the graphs one can observe that decreasing pH induces a reduction of fluorescence intensity of the basic forms concomitant to an enhancement of the intensity of acidic ones. The behavior reflects the mutual variation of the concentrations of the two conjugated species as a function of the pH.

At this point we moved towards measurements of the pKa of the chromophores. For this purpose we performed fluorimetric titration experiments on diluted solutions (10^{-6} M) of dyes in micellar water. Upon excitation by 1P irradiation, fitting the ratios of fluorescence intensity as a function of pH led to classical sigmoidal curves (Figure 2.23). The fitting data are reported in Table 2.2.

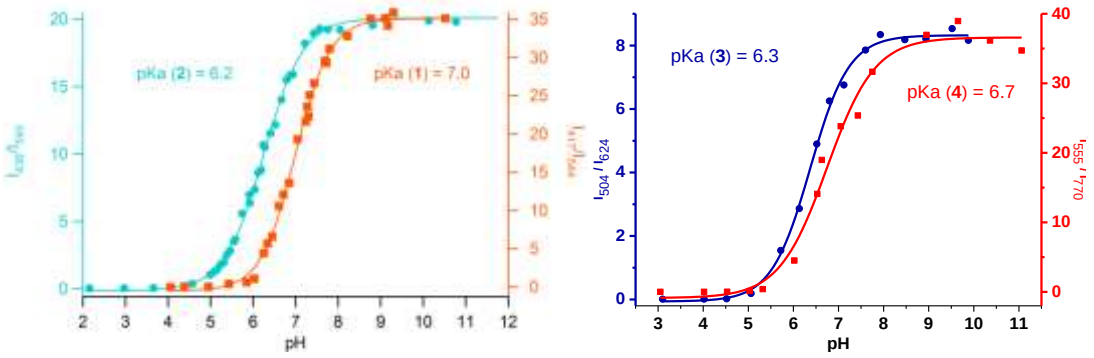

Figure 2.23 pKa determination via fluorimetric ratiometric titration

Cpd	λ_{exc}	Intensity Ratio (nm/nm)	Adj-R^2	pKa_{obs}
1	380	417/544	0.998	7.0 ± 0.1
2	386	436/590	0.998	6.2 ± 0.1
3	470	504/624	0.998	6.3 ± 0.1
4	486	555/770	0.985	6.7 ± 0.1

Table 2.2

The pKa observed (pKa_{obs}) lie in the range between 6.2 and 7.0, making them suitable for pH determination in physiological conditions. Recalling that pKa of pyridinium and quinolium are respectively 5.2 and 4.8, is possible to appreciate the large shift of the values. This can be readily understood by the analysis of the resonance structures in Figure 2.24.

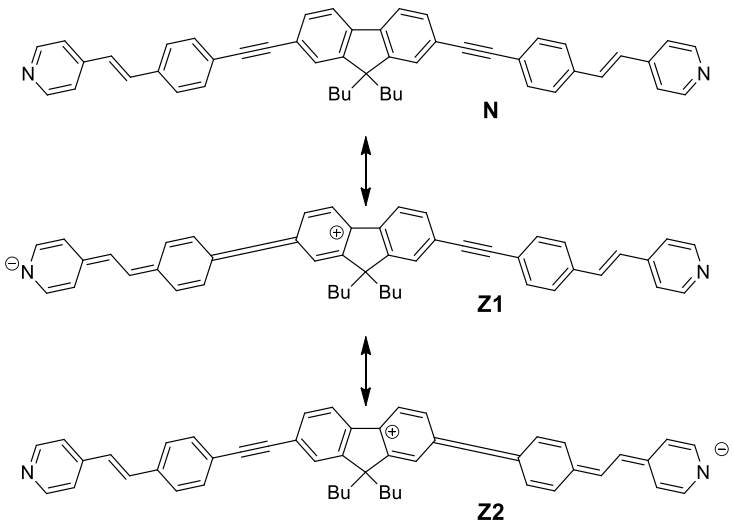

Figure 2.24 Resonance structures of **1**; neutral one (N, top) and two zwitterionic ones (Z1 and Z2, below).

The properties of a molecule are strictly related to its chemical architecture; according to the principles of the resonance theory, the structure closest to the real one is given by the hybrid of the resonance ones which can be written, keeping into account their relative stability. It follows that the most stable resonance forms are the ones in Figure 2.24 (compound **1** used as model), the neutral one with no charge separation and, among all the possible zwitterionic forms, the ones with the negative charge on nitrogen atom (more electronegative than carbon). As a consequence the basicity of the acceptor end-groups are increased due to the quadrupolar effect, resulting in a reduction of the acidity of their conjugated acidic forms (protonated specie) and enhanced pKa values comparing to simple pyridine and quinoline. This leads to a pKa tuning of the acceptor moieties circumventing modifications of their chemical structures.

Moreover, due to difficulties in getting measurements close to the inflection points of the curves (higher slopes), the pH range was spanned several times and practically the same values of emission intensities were found in correspondence of the same pH values, highlighting the stability of the probes through the passage from acidic to basic conditions and vice versa.

The bithiophene motif induces a prominent bathochromic effect of the absorption bands from basic to acidic pH, that could also enable spectrophotometric ratiometric behavior for **3** and **4**. An investigation of pH dependancy of absorption spectra was carried out similarly to emission ones (Figure 2.25).

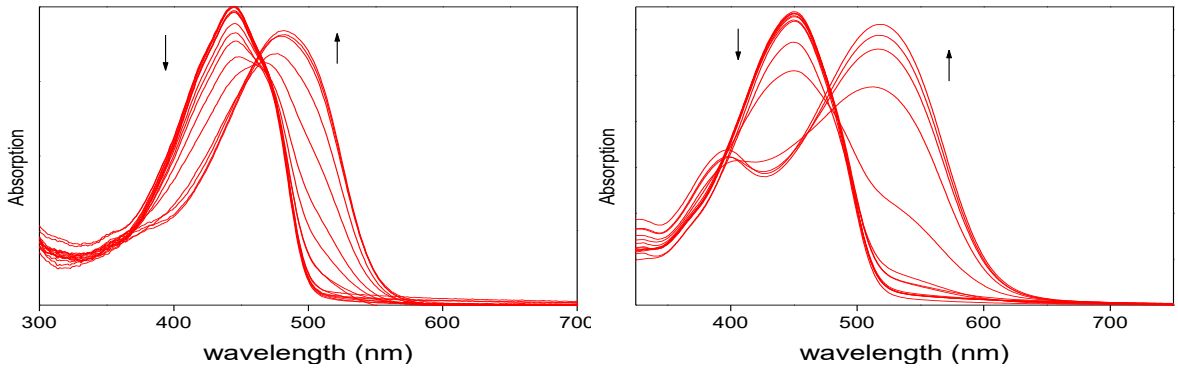

Figure 2.25 pH dependancy of absorption spectra of **3** (left) and **4** (right) in micellar water

Lowering the pH induces a reduction of the absorption of the deprotonated forms of **3** and **4**, with simultaneous enhancement of the acidic ones, pointing out a trend fully analogous to the one observed

in their emission spectra. Ratiometric spectrophotometric titrations of **3** and **4** were performed too, leading to pKa_{obs} in very good agreement with the ones previously obtained.

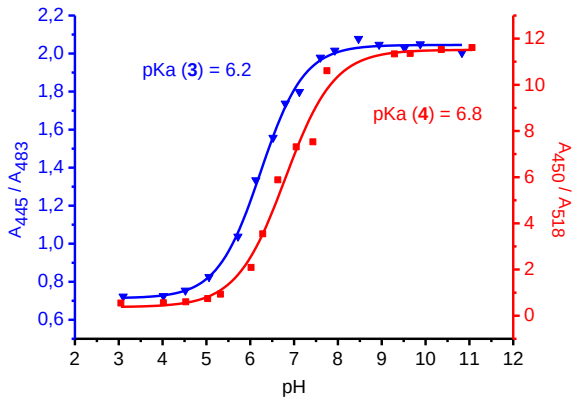

Cpd	Intensity Ratio (nm/nm)	Adj-R^2	pKa_{obs}
3	445/483	0.998	6.2 ± 0.1
4	450/518	0.986	6.8 ± 0.1

Figure 2.26 Spectrophotometric titration curves of **3** (blue) and **4** (red) and related data

2.4.3 Two-photon absorption

In order to verify their potential as 2P ratiometric pH probes, 2PA spectra of the chromophores (10^{-4}M in micellar water) were determined (Figure 2.27) by means of 2P excited fluorescence technique[ii].

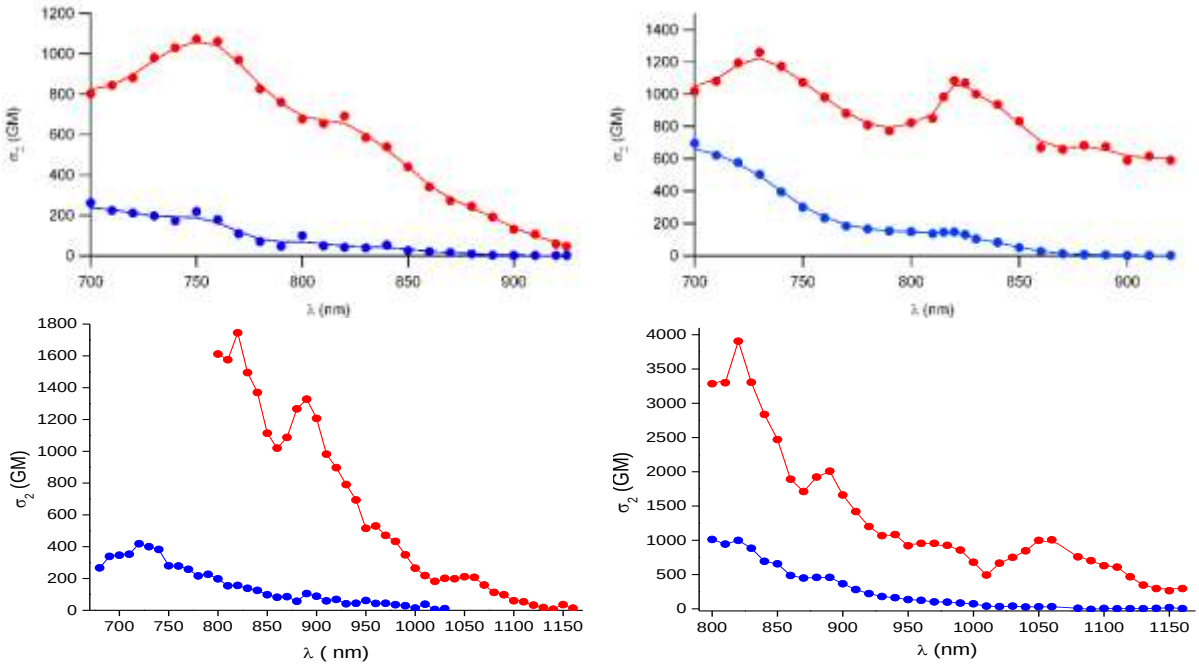

Figure 2.27 2PA spectra in basic (blue) and acidic (red) conditions. Top: **1** (left), **2** (right); bottom: **3** (left), **4** (right).

[ii] The measurements were carried out by O. Mongin and G. Clermont, that I warm thank.

Concerning the first family, in basic conditions **1** and **2** exhibit λ_{2PA}^{max} = 700 nm, with σ_2^{max} equals to 260 and 700 GM respectively. According to the evoked principles one can observe that the quinoline group induces an enhancement of σ_2 due to the extension of the π-system. Upon acidification λ_{2PA}^{max} are slightly red-shifted up to 750 and 730 nm respectively for **1** and **2**. The protonation of the end-groups make them stronger acceptors, inducing an enhancement of the ICT followed by the rise of the σ_2^{max}[47], that turns equal to 1070 and 1260 GM respectively for **1** and **2**.

For the second family of the chromophores, the effects previously observed are still valid. At basic pH **3** and **4** display λ_{2PA}^{max} = 730 and 800 nm respectively, with σ_2^{max} = 400 and 1000 GM. Upon acidification λ_{2PA}^{max} are shifted up to 820 nm, where σ_2^{max} = 1740 and 3900 GM respectively for **3** and **4**.

A comparison between the two families clearly point out that the replacement of the ethynylene-phenylene moiety with the 2,2'-bithiophene one results in a strong modulation of the 2PA response, which is enhanced when comparing **1** to **3** and **2** to **4**, especially for the acidic forms.

It worths to underline that the mentioned effects are accompanied by a reduction in fluorescence quantum yield (Table 2.1). However in terms of two-photon brightness ($\sigma_2\Phi_F$) this detrimental effect is very well counterpoised by the enhancement of σ_2, holding $\sigma_2\Phi_F$ over 100 GM for all the probes, both in basic and acidic conditions.

2.4.4 pKa determination under two-photon excitation

After having investigated the 2PA response of the chromophores, we decided to perform pKa ratiometric determination under 2P excitation. A first study on compound **1** was already performed in our laboratory and the obtained results are reported in the following figure.

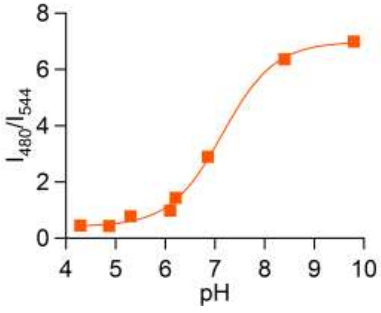

Figure 2.28 Ratiometric fluorimetric titration of **1** under 2P excitation (λ_{exc}= 750 nm)

Fitting the ratios of fluorescence intensity as a function of pH led to pKa_{obs} very close to the one determined under 1P excitation. In the same way fluorimetric titrations of **3** and **4** were carried out (Figure 2.29).

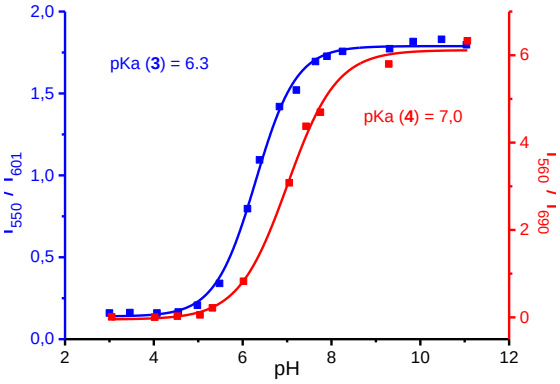

Cpd	λ_{exc}	Intensity Ratio (nm/nm)	Adj-R^2	pKa_{obs}
3	820	550/601	0.997	6.3 ± 0.1
4	820	555/770	0.996	7.0 ± 0.1

Figure 2.29 Ratiometric fluorimetric titration of **3** and **4** under 2P excitation

Fitting of the fluorescence intensity ratios led to sigmoidal curves and pKa_{obs}= 6.3 ± 0.1 and 7.0 ± 0.1 respectively for **3** and **4**. It worths to observe that for **3** the fitting gave exactly the same value of pKa observed under 1P excitation (6.3), while for compound **4** the value of pKa observed by 2P irradiation (7.0) is slightly higher than the one determined by 1P excitation.

2.5 Applications

In this section we are going to discuss some applications of the prepared chromophores as ratiometric pH probes.

2.5.1 Imaging

Due to its pKa_{obs}, closer to neutrality, **1** was selected for imaging experiments on living cells. However before this, its potential to stain biological membranes was tested by means of a preliminary study carried out Giant Unilamellar Vescicles (GUVs)[iii], which are largely used as models that emulates biological membranes[48-49]. GUVs were prepared by electroformation in presence of **1**, both in basic (pH= 8.1) and neutral (pH= 7.2) conditions. Imaging by confocal microscopy exhibited that the chromophore is able to stain the membranes and, in both the cases, the fluorescence emission was delimited just to them. In particular in basic conditions only the fluorescence of the deprotonated form

[iii] The experiments were carried out by B. Goudeau, H. Voldoire, S. Arbault, that I warm thank.

was observed (collected between 415 and 500 nm, Figure 2.30), whereas close to the neutrality, according to the pKa_{obs} measured in previous experiments, the emission of the protonated form (collected between 550 and 700 nm) was observed too, proving the presence of the two species at the equilibrium.

Figure 2.30 Overlap of bright field and fluorescence images (λ_{exc}= 405 nm) of GUVs stained with **1** in basic conditions (artificial colours)

After these results, experiments on living cells were performed[iv]. For the purpose COS-7 cells were incubated with **1** and imaged under continuous irradiation (Figure 2.31). The conditions of the experiments were set up exciting at 405 nm and collecting fluorescence from 390 to 645 nm, in order to excite and observe both the two conjugated species.

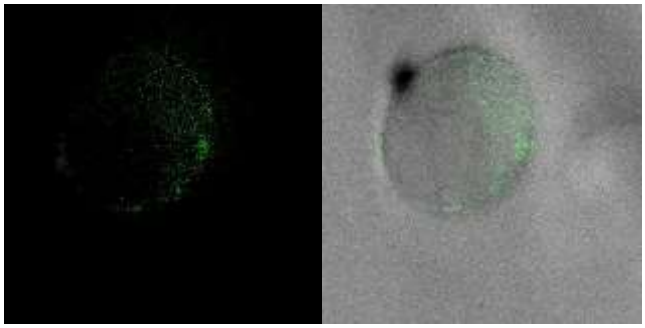

Figure 2.31 Fluorescence imaged COS-7 cell incubated with chromophore **1** (left) and overlap with bright field (right)

As displayed the chromophore was found able to stain the tested cells allowing their imaging.Thus it was tested also by 2P irradiation, exciting both the conjugated species at 700 nm and collecting the fluorescence signal between 390 and 688 nm (Figure 2.32).

[iv] The experiments were carried out by J. Daniel, that I warm thank.

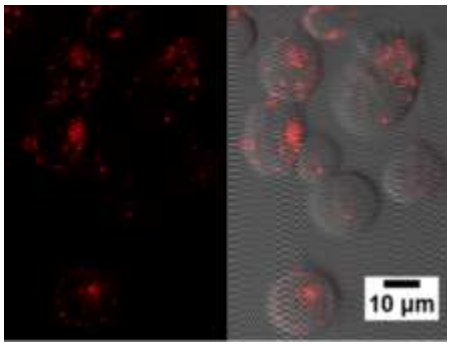

Figure 2.32 2P images of COS-7 cells incubated with **1** (left) and overlap with bright field one (right)

Also this time the results were positive, getting images of cells by 2P excitation. Finally the ratiometric behavior of the probe allowed the determination of an overall pH equals to 6.8, by means of the fluorimetric titration curve (Figure 2.23) determined in micellar environment under 1P excitation.

2.5.2 Investigation of PLGA stability by pH monitoring using pH probes

In this section the pH probing ability of chromophore **2** was tested for pH monitoring over time in specific NPs made from poly(lactic-co-glycolic acid) (PLGA, Figure 2.33).

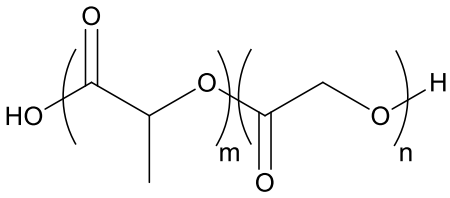

Figure 2.33 PLGA chemical structure

PLGA exhibits high biocompatibility and biodegradability[50-51], in fact it is approved by Food and Drug Administration in several applications, and it is object of intense study as drug delivery systems[50-51]. However one of the main practical drawbacks is related to the acidic environment that is generated inside the PLGA matrix upon hydrolysis of the ester linkages of its structure, that can affect the stability of the delivered chemicals[52-53]. Thus several researches have been done for monitoring of pH microclimate[54-56] in PLGA-based materials as well as techniques to counterpoise its decrease upon hydrolysis(e.g., use of neutralizing excipients such as inorganic bases[57]). Furthermore it must be pointed out that the microclimate pH is strictly influenced not only by the nature of the polymer (i.e.,

ratio of the monomers used for the polymerization) but also by the size and the morphology of the materials[54-56] and therefore it is dependant by the method used for their preparations.

Taking into account the above mentioned hydrolysis phenomena that induces acidic environments, the probe chosen for such experiences was **2**, due to its low value of observed pKa (6.2) comparing to the other synthesized probes, with a dynamic range for pH detection in more acidic window (5.2-7.2) and therefore more suitable for this specific application. Thus **2** was encapsulated inside PLGA 50:50 NPs prepared by nanoprecipitation and the batch was splitted into three parts, which were stored respectively at room temperature, 4°C and 40°C, aiming to observe the effect of the temperature on the hydrolysis of the copolymer.

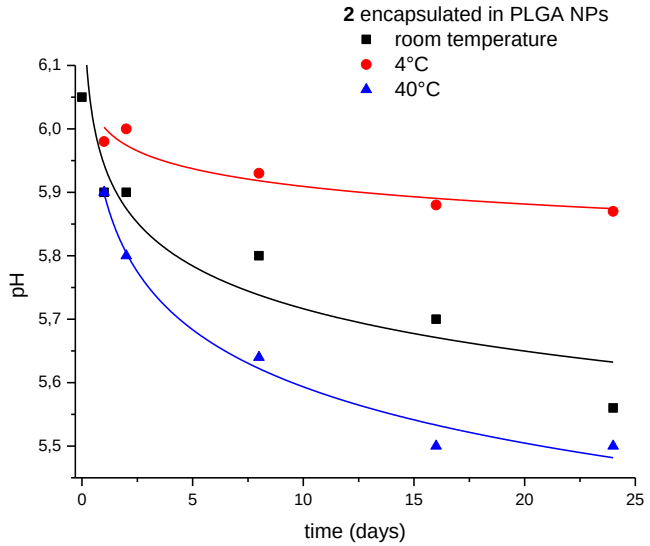

Figure 2.34 Microclimate pH monitoring over time in PLGA NPs

The observed pH was measured by means of the calibration curve achieved in micellar water using the same ratio of fluorescence intensity (I_{436}/I_{590}) and excitation wavelength (386 nm). Considering the batch stored at room temperature, one can observe the reduction of the pH as a function of the time due to hydrolysis of ester linkages. Furthermore as expected, a low temperature (4°C) is able to slow down the kinetic of the process, whereas the opposite behavior is observed for the batch stored at 40°C. As mentioned observed pH depends on several parameters such as the nature of polymer used (e.g., composition, molecular weight) and the size of the particles. In similar studies about microclimate pH monitoring by confocal laser scanning microscopy carried out on PLGA 50/50 microspheres with

diameter ranging from 50 to 120 μm, the hydrolysis of PLGA resulted in peaks of acidity corresponding to pH of 3.0[56], with higher acidity for larger particles. Instead the NPs prepared by reprecipitation in the conditions adopted, which are characterized by spherical shape and a diameter ranging from 50 to 100 nm[58], the values of pH registered for all the batches change lie in between about 6.0 and 5.5. This behavior can be explained in terms of particles size; in particular for small particles the diffusion of hydrolysis products outside the polymer matrix is facilitate comparing to larger ones, leading to a less pronounced decrease of pH[56].

2.6 Conclusion

In this chapter a series of interesting pH probes has been synthesized and studied. The chromophores **1** and **2** (first family) display dual emission ratiometric behavior with pKa_{obs}, estimated by fluorimetric titrations, founded equal to 7.0 and 6.2 respectively, as consequence of the quadrupolar effect induced by the molecular architecture. The ability of **1** to stain lipophilic membranes was tested on GUVs, giving back good preliminary results in view of imaging on living cells. These studies, achieved on COS-7 cells, exhibited positive feedback, allowing imaging under 2P and 1P excitation with ratiometric determination of the pH. Moreover compound **2** was used for microclimate pH monitoring in PLGA 50:50 NPs, allowing to follow small variation of pH due to hydrolysis process, for batches stored at different temperatures. The second family of probes (**3** and **4**) was prepared with the idea to improve the optical properties of the first one, getting more red-shifted emitters by means of variation of the structure of the π-bridge in the molecular scaffold. This change also led to an enhancement of the two-photon cross sections, comparing to the analogous compounds of the first family, which allows to hold good two-photon brightness nevertheless the decrease of the fluorescence quantum yields. They also exhibit dual emission ratiometric behavior that, concurrently with pKa_{obs} close to neutrality (6.3 for **3** and 6.7 for **4**), make them good candidates as near-neutral dual emission ratiometric pH-probes for 1P and 2P applications.

Bibliographic references

[1] P. Mitchell, *Biol. Rev.* **1966**, *41*, 445-501.

[2] T. D. Correa, S. M. Jakob, J. Takala, *Critical Care Horizons* **2015**, *1*, 31-41.

[3] J. R. Casey, S. Grinstein, J. Orlowski, *Nat. Rev. Mol. Cell. Biol.* **2010**, *11*, 50-61.

[4] B. Alberts, A. Johnson, J. Lewis, *Molecular Biology of the Cell*, Garland Science, New York, **2002**.

[5] A. A. Golabek, E. Kida, M. Walus, W. Kaczmarski, M. Michalewski, K. E. Wisniewski, *Mol. Genet. Metab.* **2000**, *70*, 203-213.

[6] R. D. Vaughan-Jones, K. W. Spitzer, P. Swietach, *J. Mol. Cell. Cardiol.* **2009**, *46*, 318-331.

[7] M. Vassalle, C. Lin, *J. Biomed. Sci.* **2004**, *11*, 542-565.

[8] M. Damaghi, J. Wojtkowiak, R. Gillies, *Front. Physiol.* **2013**, *4*, 370.

[9] G. R. Martin, R. K. Jain, *Cancer Res.* **1994**, *54*, 5670.

[10] J. R. Lakowicz, *Principles of Fluorescence Spectroscopy*, Third ed., Springer, **2010**.

[11] R. Sjöback, J. Nygren, M. Kubista, *Spectrochim. Acta Mol. Biomol. Spectrosc.* **1995**, *51*, L7-L21.

[12] C.-S. Chen, *BMC Cell Biol.* **2002**, *3*, 21.

[13] L. Karmazsin, G. Balla, J. Szöllösi, *Acta Paediatr. Hung.* **1979**, *20*, 249-253.

[14] J. Han, K. Burgess, *Chem. Rev.* **2010**, *110*, 2709-2728.

[15] *The Molecular Probes Handbook: A Guide to Fluorescent Probes and Labeling Technologies*, 11th ed., Life Technologies Corporation, **2010**.

[16] S. Mordon, J. M. Devoisselle, V. Maunoury, *Photochem. Photobiol.* **1994**, *60*, 274-279.

[17] T. J. Rink, R. Y. Tsien, T. Pozzan, *J. Cell Biol.* **1982**, *95*, 189-196.

[18] Y. Song, J. Thiagarajah, A. S. Verkman, *J. Gen. Physiol.* **2003**, *122*, 511-519.

[19] J. E. Whitaker, R. P. Haugland, F. G. Prendergast, *Anal. Biochem.* **1991**, *194*, 330-344.

[20] M. H. V. Werts, S. Gmouh, O. Mongin, T. Pons, M. Blanchard-Desce, *J. Am. Chem. Soc.* **2004**, *126*, 16294-16295.

[21] H. M. Kim, B. R. Cho, *Chem. Rev.* **2015**, *115*, 5014-5055.

[22] S. Charier, O. Ruel, J.-B. Baudin, D. Alcor, J.-F. Allemand, A. Meglio, L. Jullien, B. Valeur, *Chem. Eur. J.* **2006**, *12*, 1097-1113.

[23] H. J. Park, C. S. Lim, E. S. Kim, J. H. Han, T. H. Lee, H. J. Chun, B. R. Cho, *Angew. Chem., Int. Ed.* **2012**, *51*, 2673-2676.

[24] H. J. Kim, C. H. Heo, H. M. Kim, *J. Am. Chem. Soc.* **2013**, *135*, 17969-17977.

[25] J. Wang, Y. Sun, W. Zhang, Y. Liu, X. Yu, N. Zhao, *Talanta* **2014**, *129*, 241-248.

[26] B. A. Reinhardt, L. L. Brott, S. J. Clarson, A. G. Dillard, J. C. Bhatt, R. Kannan, L. Yuan, G. S. He, P. N. Prasad, *Chem. Mater.* **1998**, *10*, 1863-1874.

[27] R. Kannan, G. S. He, L. Yuan, F. Xu, P. N. Prasad, A. G. Dombroskie, B. A. Reinhardt, J. W. Baur, R. A. Vaia, L.-S. Tan, *Chem. Mater.* **2001**, *13*, 1896-1904.

[28] G. S. He, J. Swiatkiewicz, Y. Jiang, P. N. Prasad, B. A. Reinhardt, L.-S. Tan, R. Kannan, *J. Phys. Chem. A* **2000**, *104*, 4805-4810.

[29] A. R. Morales, K. J. Schafer-Hales, C. O. Yanez, M. V. Bondar, O. V. Przhonska, A. I. Marcus, K. D. Belfield, *Chemphyschem* **2009**, *10*, 2073-2081.

[30] K. D. Belfield, M. V. Bondar, I. Cohanoschi, F. E. Hernandez, O. D. Kachkovsky, O. V. Przhonska, S. Yao, *Appl. Opt.* **2005**, *44*, 7232-7238.

[31] M. Charlot, N. Izard, O. Mongin, D. Riehl, M. Blanchard-Desce, *Chem. Phys. Lett.* **2006**, *417*, 297-302.

[32] O. Mongin, L. Porrès, L. Moreaux, J. Mertz, M. Blanchard-Desce, *Org. Lett.* **2002**, *4*, 719-722.

[33] M. H. V. Werts, S. Gmouh, O. Mongin, T. Pons, M. Blanchard-Desce, *J. Am. Chem. Soc.* **2004**, *126*, 16294-16295.

[34] S. Yao, K. D. Belfield, *J. Org. Chem.* **2005**, *70*, 5126-5132.

[35] O. K. Kim, K. S. Lee, Z. Huang, W. B. Heuer, C. S. Paik-Sung, *Opt. Mater.* **2003**, *21*, 559-564.

[36] K. D. Belfield, A. R. Morales, B.-S. Kang, J. M. Hales, D. J. Hagan, E. W. Van Stryland, V. M. Chapela, J. Percino, *Chem. Mater.* **2004**, *16*, 4634-4641.

[37] O. Mongin, L. Porrès, M. Charlot, C. Katan, M. Blanchard-Desce, *Chem. Eur. J.* **2007**, *13*, 1481-1498.

[38] F. G. Bordwell, *Acc. Chem. Res.* **1988**, *21*, 456-463.

[39] H. Myung Kim, B. Rae Cho, *Chem. Commun.* **2009**, 153-164.

[40] K. Mitra, I. Ubarretxena-Belandia, T. Taguchi, G. Warren, D. M. Engelman, *Proc. Natl. Acad. Sci. U.S.A.* **2004**, *101*, 4083-4088.

[41] S. Marder, D. Neher, *Photoresponsive Polymers I*, Springer Berlin Heidelberg, **2008**.

[42] J. Daniel, C. Mastrodonato, A. Sourdon, G. Clermont, J.-M. Vabre, B. Goudeau, H. Voldoire, S. Arbault, O. Mongin, M. Blanchard-Desce, *Chem. Commun.* **2015**, *51*, 15245-15248.

[43] O. Mongin, M. Sankar, M. Charlot, Y. Mir, M. Blanchard-Desce, *Tetrahedron Lett.* **2013**, *54*, 6474-6478.

[44] E. J. Cueto Díaz, S. Picard, V. Chevasson, J. Daniel, V. Hugues, O. Mongin, E. Genin, M. Blanchard-Desce, *Org. Lett.* **2015**, *17*, 102-105.

[45] M. Blanchard-Desce, T. S. Arrhenius, J. M. Lehn, *Bull. Soc. Chim. Fr.* **1993**, *130*, 266-272.

[46] M. Edmonds, A. Abell, in *Modern Carbonyl Olefination*, Wiley-VCH Verlag GmbH & Co. KGaA, **2003**, pp. 1-17.

[47] H. M. Kim, B. R. Cho, *Chem. Rev.* **2015**, *115*, 5014-5055.

[48] C. Peetla, A. Stine, V. Labhasetwar, *Mol. Pharm.* **2009**, *6*, 1264-1276.

[49] D. L. Richmond, E. M. Schmid, S. Martens, J. C. Stachowiak, N. Liska, D. A. Fletcher, *Proc. Natl. Acad. Sci. U.S.A.* **2011**, *108*, 9431-9436.

[50] H. K. Makadia, S. J. Siegel, *Polymers* **2011**, *3*, 1377-1397.

[51] K. E. Uhrich, S. M. Cannizzaro, R. S. Langer, K. M. Shakesheff, *Chem. Rev.* **1999**, *99*, 3181-3198.

[52] A. Giteau, M. C. Venier-Julienne, A. Aubert-Pouëssel, J. P. Benoit, *Int. J. Pharm.* **2008**, *350*, 14-26.

[53] G. Zhu, S. R. Mallery, S. P. Schwendeman, *Nat. Biotechnol.* **2000**, *18*, 52-57.

[54] Y. Liu, A. H. Ghassemi, W. E. Hennink, S. P. Schwendeman, *Biomaterials* **2012**, *33*, 7584-7593.

[55] L. Li, S. P. Schwendeman, *J. Control. Release* **2005**, *101*, 163-173.

[56] A. G. Ding, S. P. Schwendeman, *Pharm. Res.* **2008**, *25*, 2041-2052.

[57] W. Jiang, S. P. Schwendeman, *Mol. Pharm.* **2008**, *5*, 808-817.

[58] M. Bourdenx, J. Daniel, E. Genin, F. N. Soria, M. Blanchard-Desce, E. Bezard, B. Dehay, *Autophagy* **2016**, *12*, 472-483.

Chapter 3

Dipolar dyes and Nanoparticles

3.1 Objectives

Nowadays fluorescent organic nanoparticles prepared by aggregation of low molecular weight molecules (FONs) are of considerable interest in the field of biological applications such as imaging[1-7]. In particular they represent a very promising alternative to other nanotechnologies such as quantum dots (QDs), especially due to the absence of heavy metals, that provide an efficient response to biocompatibility issues[8-10]. Consequently in the last decades many efforts have been made by the scientific community in order to understand what are the phenomena and principles that govern the properties of these nanotools[1, 11], in such a way to tune and make them appropriate for the applications in which they are required.

The physical and chemical properties of FONs is a very complex topic in which the chemical structure of the chromophores involved plays a crucial role[1, 10-14]; in particular it is responsible not only for the properties of the chromophores themeselves, but it also affects the interactions among the chromophoric subunits that can take place in the aggregated state[10-11, 15-17]. Though the latter represents a further level of complexity, it also represents a further level of adjustability of the features of the FONs that is well worth studying.

In this view the objective of the introduced work consists in the synthesis of a series of new dipolar chromophores and the investigation of the effects that some chemical modifications can have on their properties, both in molecular and aggregated state.

3.2 Design and ideas

The main scaffold of the compounds studied is reported in the following figure.

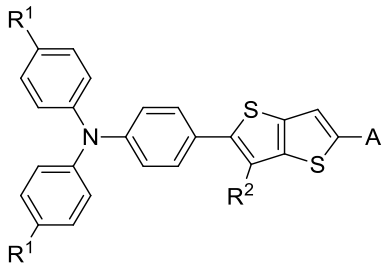

Figure 3.1

The donor group is a triphenylamine moiety, which has been involved in the synthesis of many others chromophores[11, 18-20], often dipolar and octupolar, with good response to 2PA process. In particular its propeller shape contributes to avoid stacking in the aggregated state[21] and therefore prevents fluorescence quenching processes. Moreover it is a versatile building block that can be easily functionalized on the para positions by aromatic electrophilic substitutions[22-23], such as halogenation or formylation, and then readily used to build up conjugated structures (e.g., through cross coupling or condensations reactions).

The π-bridge for the electron conjugation between the donor and the acceptor group is a thieno[3,2-b]thiophene unit. Compared to bis-thiophene the fused scaffold ensure a planarization of the system by preventing the twist between the thiophene rings (Figure 3.2) and should concur to lower the fluorescence quenching by internal conversion.

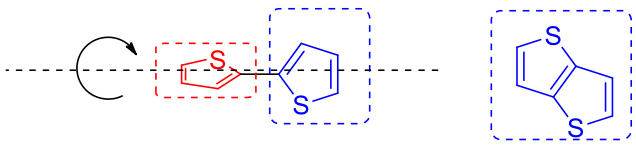

Figure 3.2 Planarization of the π-system by fused rings

The acceptor groups are selected with increasing electronwithdrawing nature, in the order formyl, dicyanovinyl (DCV) and diethylthiobarbiturate (DETB), aiming to adjust the optical properties of the chromophores by playing on their ground-state dipolar moment[24]. Furthermore, we will subsequently present the synthetic advantages provided by the possibility of exploiting condensations of the aldehyde moiety with precursors with active α-hydrogens.

The functionalizations on the triphenylamine unit are performed by means of *tert*-butylphenyl (*t*-BuPh) groups and bromine atoms. The idea consists in using bulky groups with opposite electronic effects, respectively aiming to avoid stacking in the aggregated state and get fine tuning of the optical properties by slight modulation of the donating strength of the triphenylamine.

In order to get the discussion and the analysis of the data more comfortable, for the identification of the compounds as well as to a numeric code (Arabic numbers, corresponding to that adopted in the

manuscript), will also be used a binary code, with lowercase letters which identify the nature of the acceptor group and Roman numbers for the remaining substitutions (Table 3.1 and Figure 3.3).

Acceptor	R^1, R^2	Cpd	Binary code
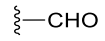	H, H	**14**	**Ia**
	H, Br	**15**	**IIa**
	Br, Br	**16**	**II'a**
	tert-butyl-C_6H_4, H	**17**	**IIIa**
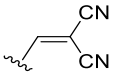	H, H	**18**	**Ib**
	H, Br	**19**	**IIb**
	Br, Br	**20**	**II'b**
	tert-butyl-C_6H_4, H	**21**	**IIIb**
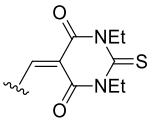	H, H	**22**	**Ic**
	H, Br	**23**	**IIc**
	Br, Br	**24**	**II'c**
	tert-butyl-C_6H_4, H	**25**	**IIIc**

Table 3.1 Numeric and binary code for the chromophores studied

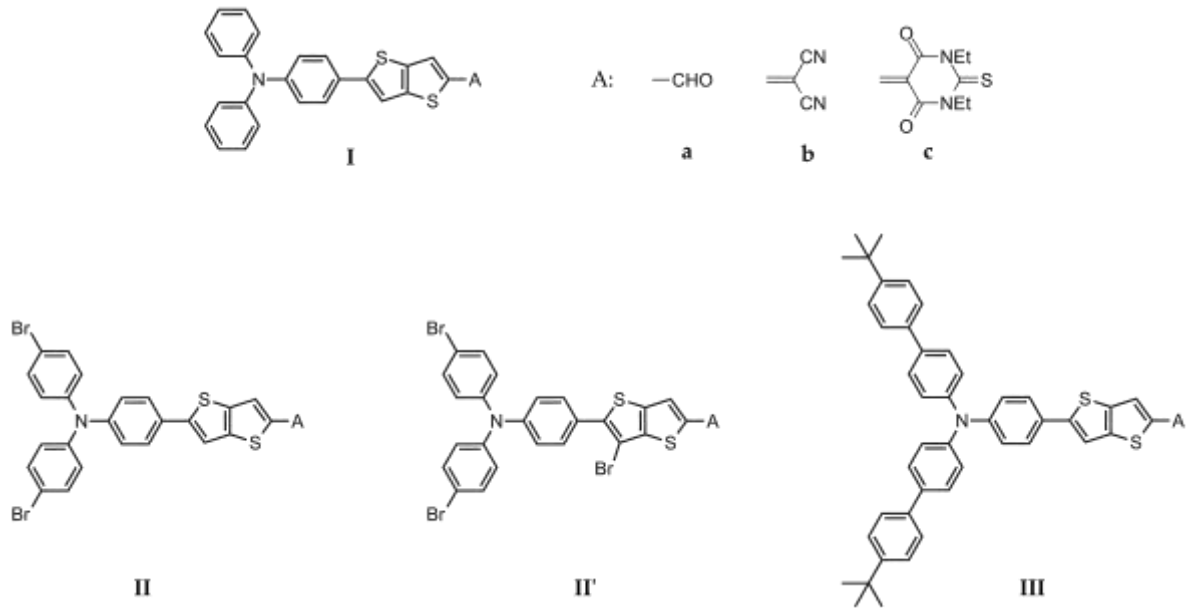

Figure 3.3 Chemical structures and binary codes of the studied chromophores

After having analyzed the structure of the chromophores studied and the reasons that led to such molecular architectures we are going to present the synthetic strategy.

3.3 Synthesis

The first part of the synthesis consists in the preparation of the series with formyl group as acceptor moiety (**a** serie). The prime step is the link of the donor to the π-bridge, which was achieved by means

of a Suzuki cross coupling between commercially available (4-(diphenylamino)phenyl)boronic acid and 5-bromothieno[3,2-b]thiophene-2-carbaldehyde (already present in our laboratory), according to the following scheme.

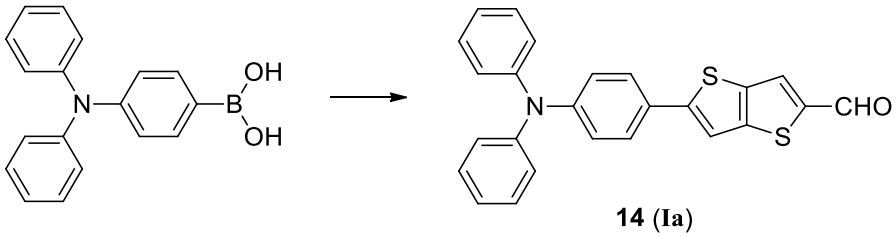

14 (**Ia**)

Scheme 3.1 Suzuki cross coupling; reagents and conditions: (4-(diphenylamino)phenyl)boronic acid, 5-bromothieno[3,2-b]thiophene-2-carbaldehyde, K_2CO_3, $Pd(dppf)Cl_2$, toluene:MeOH=1:1, 75°C, overnight (76%, **14**)

At this point the idea was to perform the bis-bromination on the two para available positions of the triphenylamine moiety, in order to get compound **IIa**, then replacement of the latter ones with *t*-BuPh by means of cross coupling. It worths to point out that in the original synthetic route, the bromination on the thienothiophene unit leading to the serie **II'** in Figure 3.3 was not planned, but it came out from experimental results and observations. Practically a first attemp of bis-bromination was performed using 2.2 eq of NBS (freshly purified) according to protocols performed other times in our research group[9] (Scheme 3.2).

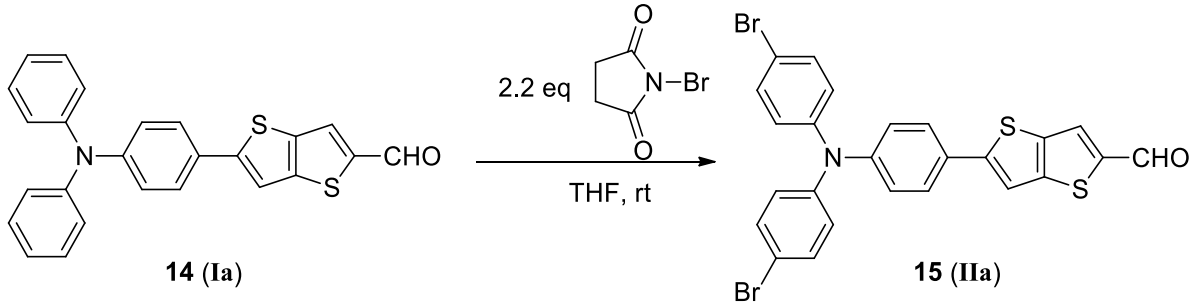

Scheme 3.2 First attempt bis-bromination; reagents and conditions: **14**, 2.2 eq NBS, THF, rt

NBS works as a source of bromine which is able to give the electrophilic substitutions on the activated para positions of the phenyl rings (whereas functionalizations on the ortho ones are inhibited for steric reasons). However after reacting one day, a TLC (silica gel) monitoring showed the situation sketched in the following figure.

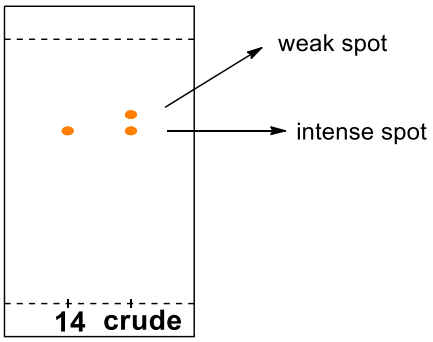

Figure 3.4 Sketch of the TLC monitoring of the bis bromination reaction after one day

A first inspection of the TLC plate exhibits a stain with the same retention factor (Rf) of the starting material and another spot very close to the first one. Both turned orange upon treatment with 2,4-dinitrophenylhydrazine highlighting, in each one, the presence of the carbonyl group that led to the formation of the corresponding hydrazones. These considerations induced to think about a partial conversion of **14**, then the reaction was left reacting for another night. A second TLC control showed unchanged pattern, therefore some more NBS (0.5 eq) was added and the reaction was kept in the same conditions for another night. Then TLC control exhibited similar scenario, the only difference was in the intensity of the stains of the crude spot, that turned very close by naked eye inspection. An aliquote of the sample was treated in order to perform a control by ^{1}H NMR, which exhibited the presence of two compounds with formyl groups but no **14** anymore. Due to these results, the reaction was quenched and the two compounds were isolated by means of chromatography and their analysis displayed the formation of the bis (**15**) and tris (**16**) brominated compounds. However this failing attempt of total conversion of starting material into bis-brominated derivative had its positive features, demonstrating the electronic communication between the donor and the position brominated on the π-bridge. In fact, according to the mechanism of the electrophilic substitution, the reactivity on the thiophene ring can be explained in terms of stabilization of the Wheland intermediate as depicted in the following scheme.

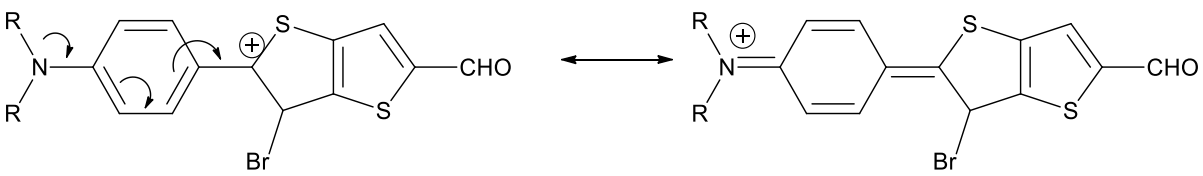

Scheme 3.3 Stabilization of the Wheland intermediate

Moreover it's interesting to observe that no bromination on the thiophene ring bearing the formyl group was observed, most likely due to the deactivating effect of the latter one. With these informations, the bis-bromination on the triphenylamine moiety was performed again, slightly changing the reaction conditions in order to enhance the selectivity towards the more reactive positions and avoiding the third bromination (Scheme 3.4).

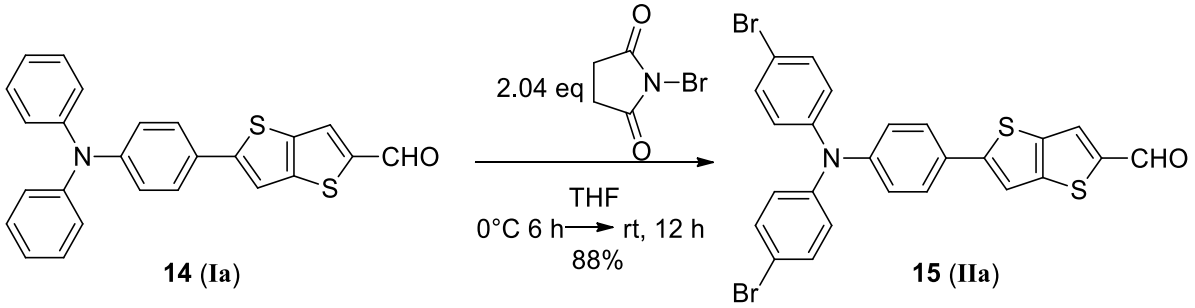

Scheme 3.4 Bis-bromination (performed conditions); reagents and conditions: **14**, 2.04 eq NBS, THF, 0°C for 6 hours, then rt for 12 hours (88%, **15**)

However, having synthesized the target compound, the possibility of obtaining an additional one to study was appealing. Moreover, considering the overall synthetic scheme for the chromophores, the possibility to prepare a number of compounds with a bromine atom on the thiophene ring (series **II'**) was concrete. In view of these considerations, the reactivity observed was exploited to get **16** as target compound with good yield too (Scheme 3.5).

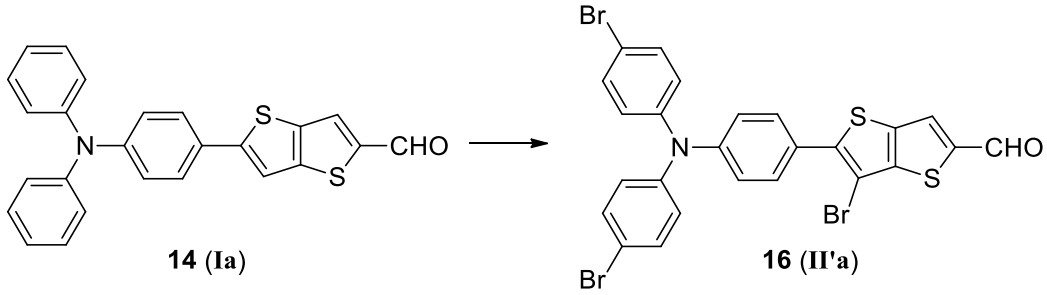

Scheme 3.5 Tris-bromination; reagents and conditions: **14**, 3.3 eq NBS, THF, rt, overnight (89%, **16**)

The last compound of the serie **a** (**17**) was synthesized through Suzuki cross coupling between **15** and commercialy available 4-*tert*-butylphenylboronic acid (Scheme 3.6).

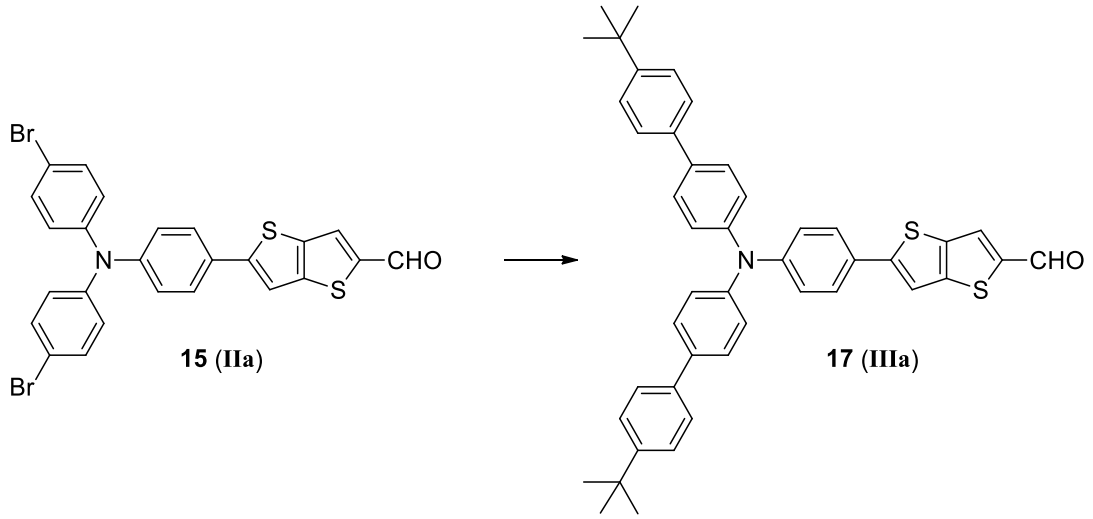

Scheme 3.6 Suzuki cross coupling; reagents and conditions: **15**, 4-*tert*-butylphenylboronic acid, K_2CO_3, $Pd(dppf)Cl_2$, toluene:MeOH=1:1, 75°C, overnight (71%, **17**)

At this point the serie **a** was completed and it was used as precursor for the preparation of the **b** and **c** series through Knoevenagel condensations, respectively with malononitrile and 1,3-diethyl-2-thiobarbituric acid (Scheme 3.7).

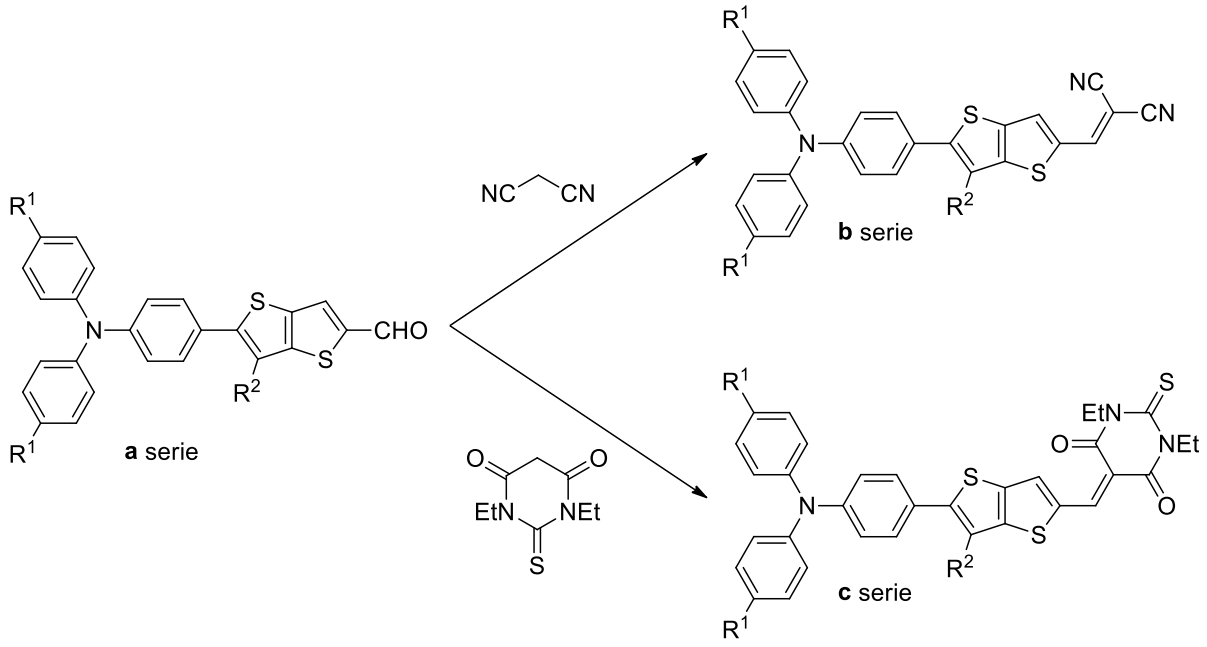

Scheme 3.7

These reactions were performed by means of a protocol developed in order to make purifications easy and quick. Practically the transformations were carried out by means of β-alanine as catalyst and by tuning of the solvent mixture (toluene/ethanol) in order to achieve precipitation of condensed products during the reactions, whereas starting reagents were kept into solution and thus allowing to collect the desired compounds by simple filtration and wash. Few exceptions were observed for some malononitrile

derivatives whose ^{1}H NMR spectra exhibit the presence of little amount of impurities that were removed by further chromatography column, probably due to formation of dimer of malononitrile[25]. The conditions and results of the condensations are reported in the following table.

cpd	R_1, R_2	Eq[1]	Solvents	Duration [h]	Yield [%]
18 (Ib)	H, H	2.0	Tol:EtOH = 1.5:1.0	24	91
19 (IIb)	Br, H	2.2	EtOH	48	87
20 (II'b)	Br, Br	1.1	EtOH	72	66
21 (IIIb)	*tert*-butyl-C_6H_4, H	9.3	Tol:EtOH = 1.7:1.0	24	75
22 (Ic)	H, H	1.1	EtOH	24	83
23 (IIc)	Br, H	1.0	EtOH	24	86
24 (II'c)	Br, Br	1.1	EtOH	24	81
25 (IIIc)	*tert*-butyl-C_6H_4, H	1.1	Tol:EtOH = 1.0:1.3	24	77

[1]Number of equivalent used for malononitrile (**b**) or 1,3-diethyl-2-thiobarbituric acid (**c**)

Table 3.2 Conditions of Knoevenagel condensations

After chemical characterizations of the isolated species (experimental part), their optical features were investigated[I]. The first part of this work is the study of structure-property relationships in organic solvent solution.

3.4 Photophysical properties in organic solvent solution

In order to make the discussion easier and more comfortable, the study of the photophysical features of the compounds (**Ia-IIIc**), recorded in $CHCl_3$ solution, will be articulated before analyzing the linear optical properties and later the non linear ones.

3.4.1 Linear optical properties

Recorded absorption and emission spectra are diplayed in the following figure.

[I] 1P photophysical study of dyes in solution and FONs was carried out in collaboration with P. Pagano, that I warm thank, who also performed the 2P absorption studies and the morphological characterizations of FONs.

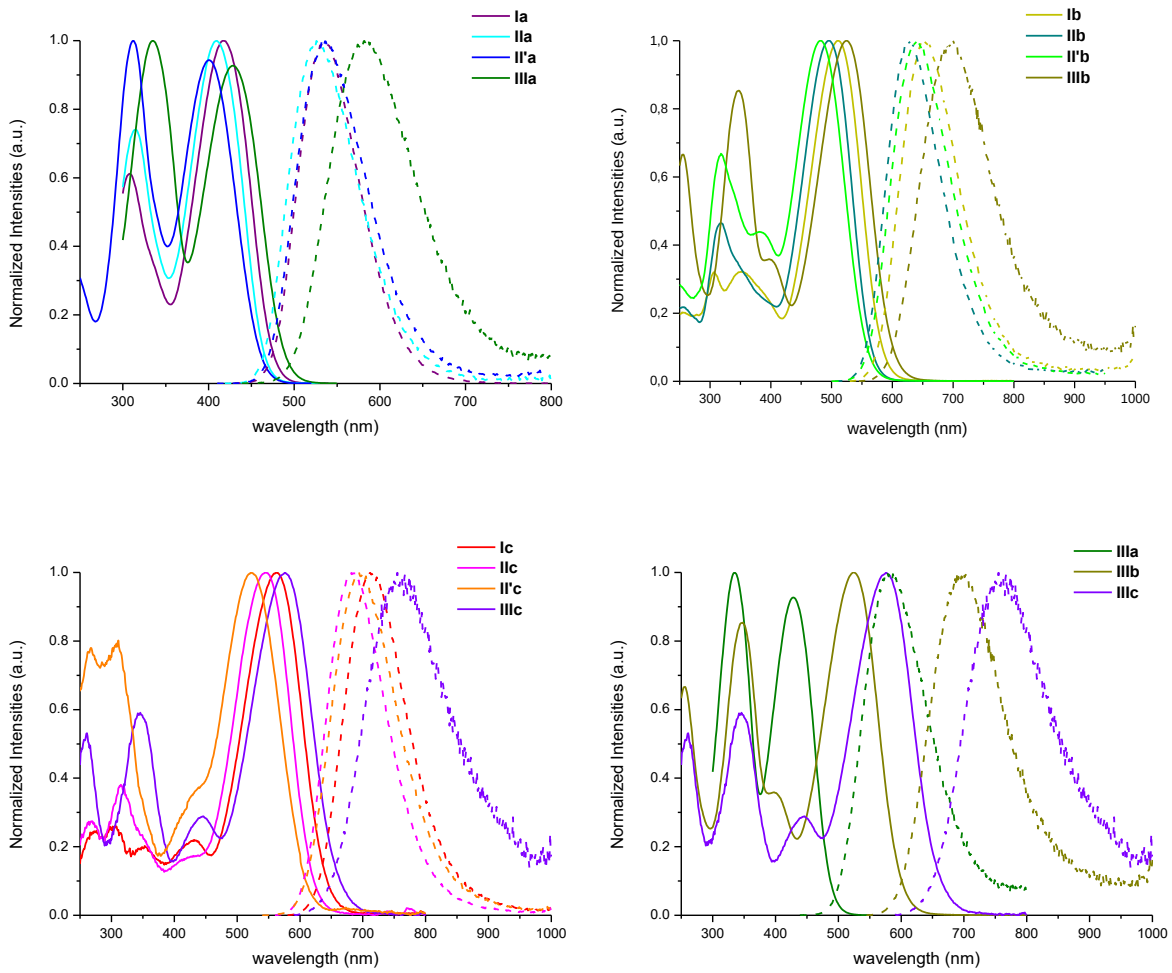

Figure 3.5 Normalized absorption (solid line) and emission (dotted line) spectra in $CHCl_3$ of series **a**, **b** and **c** (respectively top-left, top-right and bottom-left) and serie **III** (bottom-right)

Concerning the absorption spectra, one can observe that all the chromophores exhibit an intense band in the near UV or visible region with molar absorption coefficients ranging from about $3.0 \cdot 10^4$ and $7.0 \cdot 10^4$ $M^{-1}cm^{-1}$. A first analysis concerning the strength of the acceptor moieties point out that moving from formyl group, to dicyanovinyl (DCV) and diethylthiobarbiturate (DETB), therefore from the weakest to the strongest electronwithdrawing group, the bands undergo a bathochromic effect according to an enhacement of the ICT character, due to increased polarization of the ground state[13, 24]; in other words the enhancement of the push-pull strength is responsible for the observed red shift of the optical bands. In this view the trend for the substitutions on the donor moiety is very similar; moving from bromine (electron acceptor) to hydrogen and *tert*-butylphenyl group (electron donor), a bathochromic effect related to the increase of the ICT is observed too.

Concerning the emission spectra the behavior between the position of the optical bands and the strength of the push-pull system is analogous to the one recognized from the absorption spectra. Moreover the enhancement of the dipolar moment upon excitation induces a stabilization of the excited states by the solvatation shell, which leads to a pronounced positive solvatochromism as depicted in the following figure.

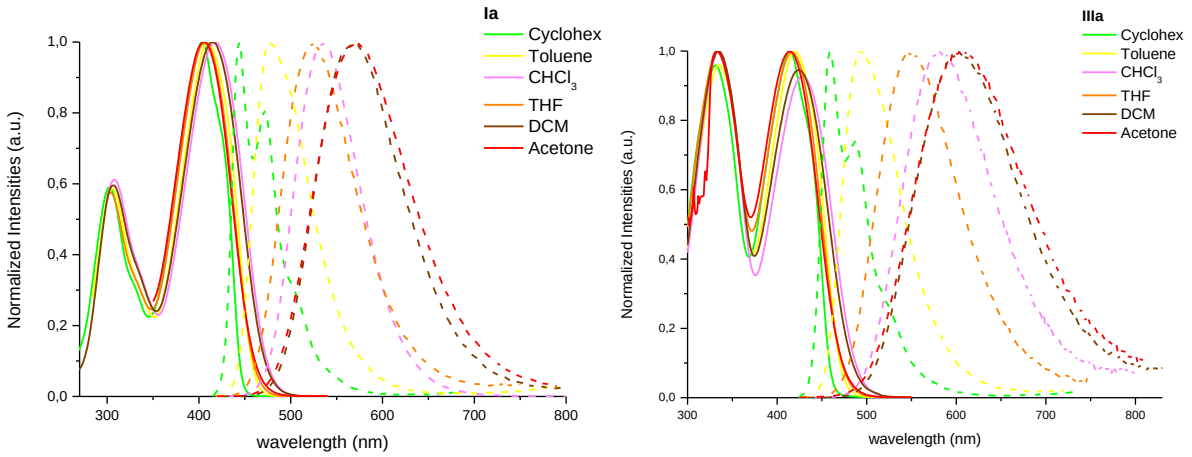

Figure 3.6 Examples of observed positive solvatochromism (**Ia**, left and **IIIa**, right)

One can observe that the variation of the acceptor group in the order formyl, DCV and DETB, is accompained by a decrease of the fluorescence quantum yields and the measured lifetimes (Table 3.3). However an analysis of the rates of radiative and non radiative decays provides more information. Considering the series **b** and **c**, the substitutions on the donor moiety with *tert*-butylphenyl groups (from **Ib** to **IIIb** and from **Ic** to **IIIc**) are accompained by a reduction of the radiative decay rates concomitant to a marked increase of the non radiative decay ones, whereas in the **a** series this behavior is not observed. This phenomenon could be explained in terms of quenching of the fluorescence by photoinduced electron transfer (PET), which is more pronounced in molecules with high push-pull character, and in this case, for compounds with strongest acceptor and donor moieties **IIIb** and **IIIc**.

Cpd	λ_{max}^{1PA} [nm]	ε^{max} [10^4 $M^{-1}cm^{-1}$]	λ_{max}^{ems} [nm]	Φ_f	Stokes Shift [10^3 cm^{-1}]	$\varepsilon^{max}\Phi_F$ [10^4 $M^{-1}cm^{-1}$]	τ [ns]	k_r [$10^9 s^{-1}$]	k_{nr} [$10^9 s^{-1}$]
Ia	417	3.9	534	0.84	5.2	3.3	2.8	0.30	0.06
IIa	409	3.7	526	0.84	5.4	3.1	2.5	0.34	0.06
II'a	401	2.9	538	0.76	6.3	2.2	2.6	0.29	0.09
IIIa	429	3.9	582	0.73	6.1	2.8	3.3	0.22	0.08
Ib	511	4.2	652	0.47	4.2	2.0	2.6	0.18	0.20
IIb	495	5.4	629	0.31	4.3	1.7	1.5	0.21	0.46
II'b	482	4.5	638	0.42	5.1	1.9	2.4	0.18	0.24
IIIb	525	4.5	700	0.24	4.8	1.1	1.9	0.13	0.40
Ic	563	6.0	712	0.37	3.7	2.2	1.9	0.19	0.33
IIc	547	6.8	681	0.28	3.6	1.9	1.2	0.23	0.60
II'c	522	5.5	694	0.30	4.7	1.65	1.6	0.19	0.44
IIIc	576	5.5	755	0.06	4.1	0.33	0.6	0.10	1.57

Table 3.3 Linear photophysical properties in $CHCl_3$ solution

Concerning the substitutions with bromine atoms on the triphenylamine moiety, in the series **b** and **c** (from **Ib** to **IIb** and from **Ic** to **IIc**), they induce a decrease of fluorescence quantum yields, probably due to intersystem crossing, with concomitant enhancement of the non radiative decay rates. Strickingly the introduction of a third bromine atom on the π-bridge (**II'b** and **II'c**) induces an increase of fluorescence quantum yields comparing with analogous bis-brominated derivatives (**IIb** and **IIc**), probably due to a reduction of the PET process previously mentioned; in fact a reduction of the non radiative decay rates is observed too.

The properties measured so far will serve as a reference for understanding what are the consequences of molecular confinement in aggregated state; in a similar way in the next subchapter the study of the non-linear optical properties of the chromophores in $CHCl_3$ solution will be exposed.

3.4.2 Non linear optical properties

2PA spectra for the chromophores in $CHCl_3$ solution are reported in the following figure.

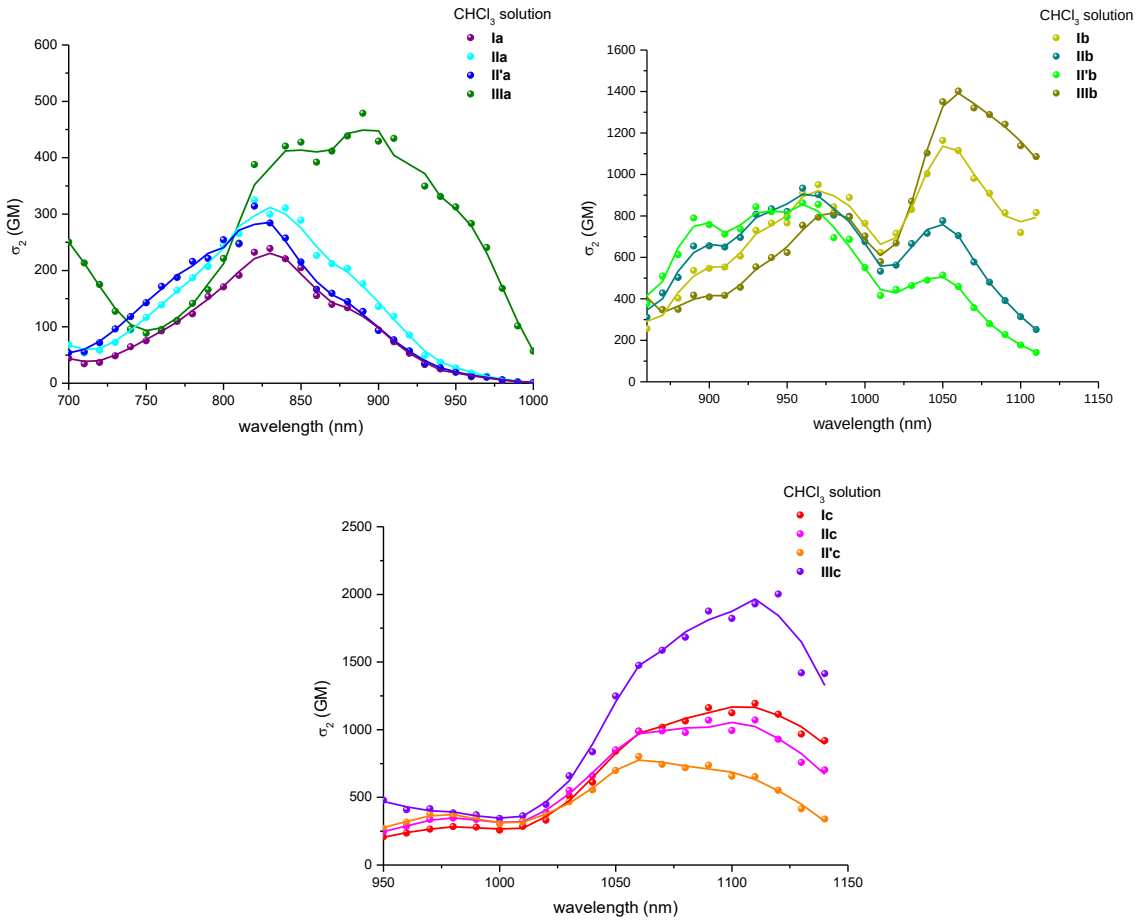

Figure 3.7 2PA spectra of compounds of **a** (top-left), **b** (top-right) and **c** (bottom) series in $CHCl_3$ solution

A first view of the spectra shows that under 2P excitation all the chromophores display λ_{max}^{2PA} about twice λ_{max}^{1PA}, which is related to their dipolar nature. Concerning the effects due to the variations of the acceptor group, when its electronwithdrawing character increases, from formyl to DCV to DETB moiety, respectively **a**, **b**, **c** series, a red shift of the optical band is observed. As expected this trend is concomitant to an enhancement of the σ_2^{max} values, which is more pronounced from formyl to DCV serie (Table 3.4).

Cpd	$2\lambda_{max}^{1PA}$ [nm]	λ_{max}^{2PA} [nm]	$\sigma_2{}^{max}$ [GM]
Ia	834	830	240
IIa	818	820	330
II'a	802	820	314
IIIa	858	890	480
Ib	1022	1050	1164
IIb	990	960	934
II'b	964	960	862
IIIb	1050	1060	1402
Ic	1126	1110	1194
IIc	1094	1110	1072
II'c	1044	1060	802
IIIc	1152	1120	2002

Table 3.4 Non linear photophysical properties of dyes **Ia-IIIc** in $CHCl_3$ solution

Regarding the effect due to the functionalizations on the triphenylamine moiety, when the electron donor character of the substituents increases, respectively in the order bromine, hydrogen and *tert*-butylphenyl (i.e., **I**, **II**, **III** series), a red shift of the optical bands is observed too, which is accompanied by an enhancement of σ_2^{max} values (except for **Ia** and **IIa**). The serie **II'** instead, always diplay a reduction of σ_2^{max} comparing to its bis-brominated analogous **II**.

At this point the synthesized chromophores (**Ia-IIIc**) were used for preparation of NPs by routine reprecipitation method (RRM), thus beginning the study of the properties of FONs made from them.

3.5 Morphological characterizations of FONs

A first characterization was performed by transmission electron microscopy (TEM, Figure 3.8) and ζ-potential and the obtained data are reported in the Table 3.5.

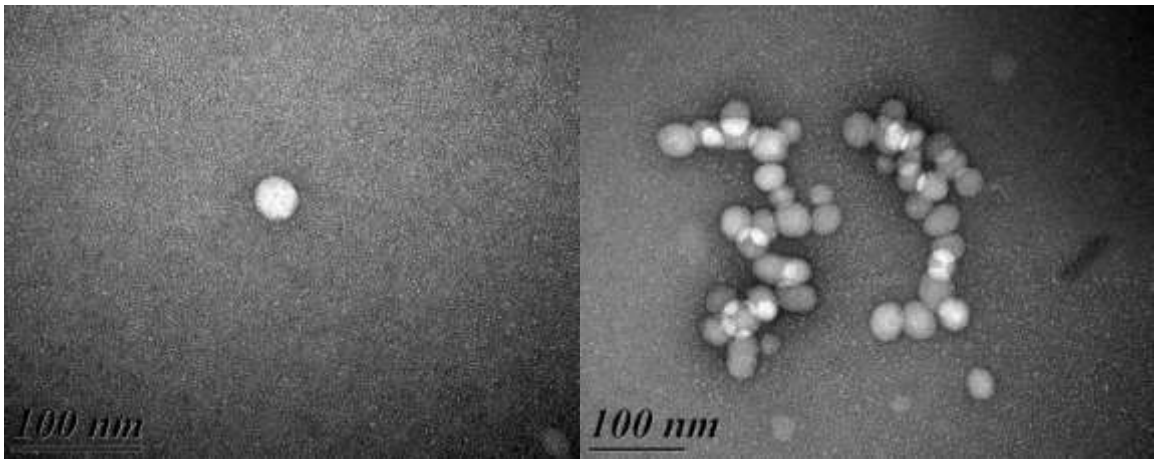

Figure 3.8 TEM image of FONs made from **IIIc** (left) and **IIc** (right)

cpd	d_{TEM} [nm]	ζ-potential [mV]	N[a] [10^4]
Ia	42	-70	5.7
IIa	37	-85	2.8
II'a	35	-74	2.0
IIIa	27	-72	0.9
Ib	21	-74	0.6
IIb	39	-75	3.0
II'b	43	-56	3.5
IIIb	32	-79	1.5
Ic	30	-67	1.4
IIc	29	-75	1.0
II'c	26	-70	0.6
IIIc	32	-72	1.2

[a]Number of dyes per single nanoparticles

Table 3.5 Structural properties of FONs

All the NPs prepared exhibit spherical shape, with diameter ranging from about 20 to 45 nm by TEM and average number of molecules per each NP was estimated between 0.6 10^4 and 5.7 10^4. All of them display negative zeta potentials (ζ-potential), which let figure out an organization of the chromophores with electron withdrawing groups (acceptor ones) pointing towards the water interface, with possibility to establish interactions such as hydrogen bonds.

3.6 Photophysical properties of chromophores in aggregated state

Similarly to what has been done previously, the discussion starts with description of the linear optical properties; furthermore for each NP the obtained results are compared with the ones got in $CHCl_3$ solution, in order to understand what are the aftermaths that such state induces.

3.6.1 Linear optical properties

Absorption and emission spectra of the NPs are displayed in the following figure.

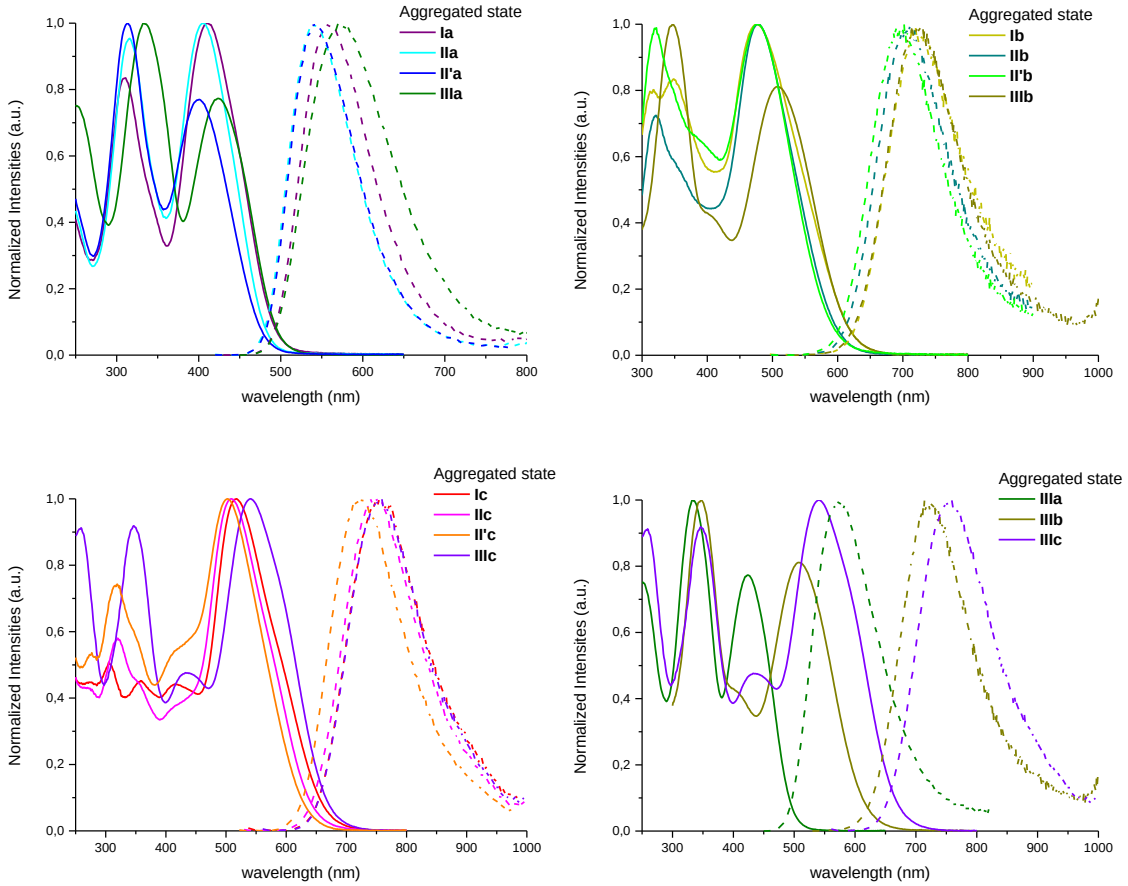

Figure 3.9 Normalized absorption (solid line) and emission (dotted line) spectra of serie **a** (top-left), **b** (top-right), **c** (bottom-left) and **III** (bottom-right) as NPs in water

Concerning the absorption spectra, one can observe that the aggregated state induces an hypsochromic effect concomitant to a hypochromic one (except for **IIb** and **IIIb**) comparing with $CHCl_3$ solution and the position of the bands is tuned by the variations of the chemical structure. In particular, the enhancement of the electron withdrawing character of the acceptor group determines a bathochromic effect, resulting in absorption in the violet, cyan-green and green-yellow region respectively for the series **a**, **b** and **c**. In each series the functionalization of the donor moiety with *tert*-butylphenyl groups (from **I** to **III**) induces a bathochromic effect, whereas the one with bromine atoms (from **I** to **II** or **II'**) induces a slight hypsochromic one, except for **IIb** and **II'b** (Table 3.6) that exhibit almost the same position of the bands. It's interesting to point out that comparing the spectra in solution with ones in aggregated state, the absorption spectra of the latter ones appear rather broadened, probably due to

excitonic coupling allowed by proximity of the molecules in such state In fact this effect is more pronounced in absorption spectra of the series **b** and **c** that, bearing the strongest acceptor group, are more prone to the phenomenon. In this way the aforementioned exception about the functionalization of **Ib** to get **IIb** or **II'b** can be also explained, considering that the enhancement of steric hindrance should provoke a reduction of the excitonic coupling by increasing of the intermolecular distance.

cpd	$\lambda_{abs}^{max}(\Delta\lambda^{max})$[a] [nm]	$\varepsilon^{max}(\Delta\varepsilon^{max})$[a] [$10^4$ $M^{-1}cm^{-1}$]	$\lambda_{ems}^{max}(\Delta\lambda^{max})$[a] [nm]	Φ_F	Stokes Shift [$10^3 cm^{-1}$]	τ_1/τ_2 [ns]
Ia	410 (-7)	3.4 (-0.5)	557 (+23)	0.05	6.4	1.2 (0.46) / 3.9 (0.54)
IIa	407 (-2)	3.6 (-0.1)	541 (+15)	0.05	6.1	0.9 (0.57) / 2.8 (0.43)
II′a	401 (0)	2.5 (-0.4)	540 (+2)	0.04	6.4	0.8 (0.71) / 2.4 (0.29)
IIIa	424 (-5)	3.3 (-0.6)	570 (-12)	0.06	6.0	0.9 (0.59) / 3.8 (0.41)
Ib	476 (-35)	3.5 (-0.7)	719 (+67)	0.01	7.1	1.5 (0.58) / 4.0 (0.42)
IIb	478 (-17)	6.1 (+0.7)	711 (+82)	0.01	6.9	1.1 (0.73) / 3.5 (0.27)
II′b	478 (-4)	/	702 (+64)	0.01	6.7	1.1 (0.84) / 3.5 (0.16)
IIIb	507 (-18)	5.0 (+0.5)	714 (+14)	0.02	5.7	1.5 (0.50) / 4.6 (0.50)
Ic	517 (-46)	5.2 (-0.8)	754 (+42)	0.004	6.1	0.9 (0.80) / 2.7 (0.20)
IIc	509 (-38)	5.5 (-1.3)	752 (+71)	0.007	6.3	1.0 (0.80) / 2.9 (0.20)
II′c	502 (-20)	5.2 (-0.3)	725 (+30)	0.006	6.1	0.7 (0.84) / 2.2 (0.16)
IIIc	541 (-35)	4.9 (-0.6)	749 (-6)	0.005	5.1	1.0 (0.76) / 3.0 (0.24)

[a]Inside round brackets the variation observed upon confinement in aggregated state

Table 3.6 Liner photophysical properties of dyes as FONs chromophoric subunits in deionized water

Considering the fluorescence spectra one can observe again that the enhancement of the electron withdrawing character of the acceptor results in a marked red shift, leading to the emission from green to yellow of the series **a**, up to deep red to near infrared region respectively for the series **b** and **c**. The effect of the substitutions on the donor moiety are instead more complex In particular, making a comparison with the series **I**, the introduction of bromine atoms induces a blue shift of the emission bands (**II** and **II'**), whereas the *tert*-butylphenyl groups (**III**) determines a red shift in the series **a** and a blue one in the serie **b** and **c**. Moreover one can note the effect of the structural variations on the fluorescence quantum yields. As expected when the electronwithdrawing feature of the acceptor group increase, Φ_F decrease; however in each series (**a**, **b** and **c**) the NPs of the kind **III** don't exhibit the least

fluorescence quantum yield but, in spite of this, they diplay values among the best in each series. To better understand this, we can consider the λ_{max}^{ems} recorded in different solvents and reported in the following table.

Cpd	Cyclohex	Tol	$CHCl_3$	THF	DCM	Acetone	DMSO
Ia	455	477	524	534	573	573	609
IIa	435	467	509	526	540	551	589
II'a	444	476	528	523	557	580	608
IIIa	459	493	549	579	605	605	653
Ib	534	584	657	665	680	723	/
IIb	520	565	626	647	660	705	740
II'b	524	571	638	666	683	729	747
IIIb	550	601	696	709	743	766	/
Ic	583	627	711	710	740	766	/
IIc	565	608	683	690	709	752	810
II'c	656	612	691	714	731	779	/
IIIc	596	646	757	757	792	/	/

Table 3.7 Emission maxima of the dyes **Ia**-**IIIc** in different polarity solvents

In the series **a** the compounds **I**, **II** and **II'** display an emission similar to the one in DCM, whereas for **III** it is more similar to the one acquired in THF, a less polar solvent. In a similar way for the series **b** and **c**, the emissions due to the species **II'** and **III** correspond to a less polar environment of the ones for **I** and **II**. This result can be explained again in terms of intermolecular interactions, in particular in the aggregated state the molecular confinement allows that a chromophoric unit can experience the local field generated by an adjacent molecule, thus the introduction of bulky substituents, which increase the distance between them, tends to reduce this effect and as aftermath the chromophores experience a less polar environment. Furthermore the steric hindrance could also result in a reduction of exciton coupling, with positive outcomes on fluorescence quantum yields.

Some more information about the structure of the NPs can be achieved by some considerations on the values of lifetime registered. Whereas in $CHCl_3$ solution the chromophores exhibit a mono exponential decay, prepared NPs show a biexponential one. This can be ascribed to different environments that dyes can experience in the aggregated state. In particular one can figure out the structure of the NPs

constituted by an external layer which is directly in touch with water, and therefore more prone to non radiative decay processes and an internal part which is not, to whom one can attribute respectively the shortest and the longest lifetime observed.

Finally, despite the quenching of the fluorescence in aggregated state, the great number of chromophores per NPs contributes to their large 1P brightness, that ranges from 10^6 to 10^8 M^{-1} cm^{-1} for **a** serie and hold about 10^7 M^{-1} cm^{-1} for deep red emitter **IIIb**, nevertheless the reduction of Φ_F. This behavior make these FONs very promising as bright deep red emitter for imaging by 1P excitation techniques.

From now on it is possible to shift on the study of the non linear optical properties, observing what are the aftermaths that molecular confinement induces and what are the effects of the variations of the chemical structures.

3.6.2 Non linear optical properties

The non linear optical features of the NPs made from chromophores **Ia-IIIb** are reported in the Table 3.8; unfortunately the serie **c** is characterized by too low fluorescence quantum yield to get reliable data in 2PEF experiments, therefore it is omitted.

Cpd	λ_{abs}^{max} [nm]	λ_{max}^{2PA} [nm]	$\sigma_2^{max}(\Delta\sigma_2^{max})$ [a, b] [GM]
Ia	410	910	395 (+155)
IIa	407	820	457 (+127)
		890	557 (+227)
II′a	401	830	165 (-149)
IIIa	424	910	182 (-298)
Ib	476	1070	300 (-864)
IIb	478	1060	921 (-13)
II′b	478	1060	739(-123)
IIIb	507	1080	726 (-676)

[a]Inside the round brackets the variation observed upon confinement in NPs comparing to $CHCl_3$ solution
[b]Referred to chromophoric subunits

Table 3.8 Non linear photophysical data of dyes **Ia-IIIb** as FONs in deionized water

All the FONs exhibit 2PA bands in the NIR with λ_{max}^{2PA} which is close or slightly red shifted comparing to $2\lambda_{max}^{1PA}$, which represents a typical behavior of dipolar 2P absorbers, in which the transition to the excited state is possible both under 1P or 2P irradiation.

From investigation of the 2PA spectra registered in aggregated state (Figure 3.10), it is evident that the scenario is more complex than the one for $CHCl_3$ solution. In particular the molecular proximity promoted in NPs has great influence on the through-space interchromophoric interactions, that depend on several parameters related to the nature of the chromophores and to their reciprocal arrangements (i.e., dipole orientation, distance), leading to strong modulation of the 2PA response in terms of two-photon cross section and spectral shape.

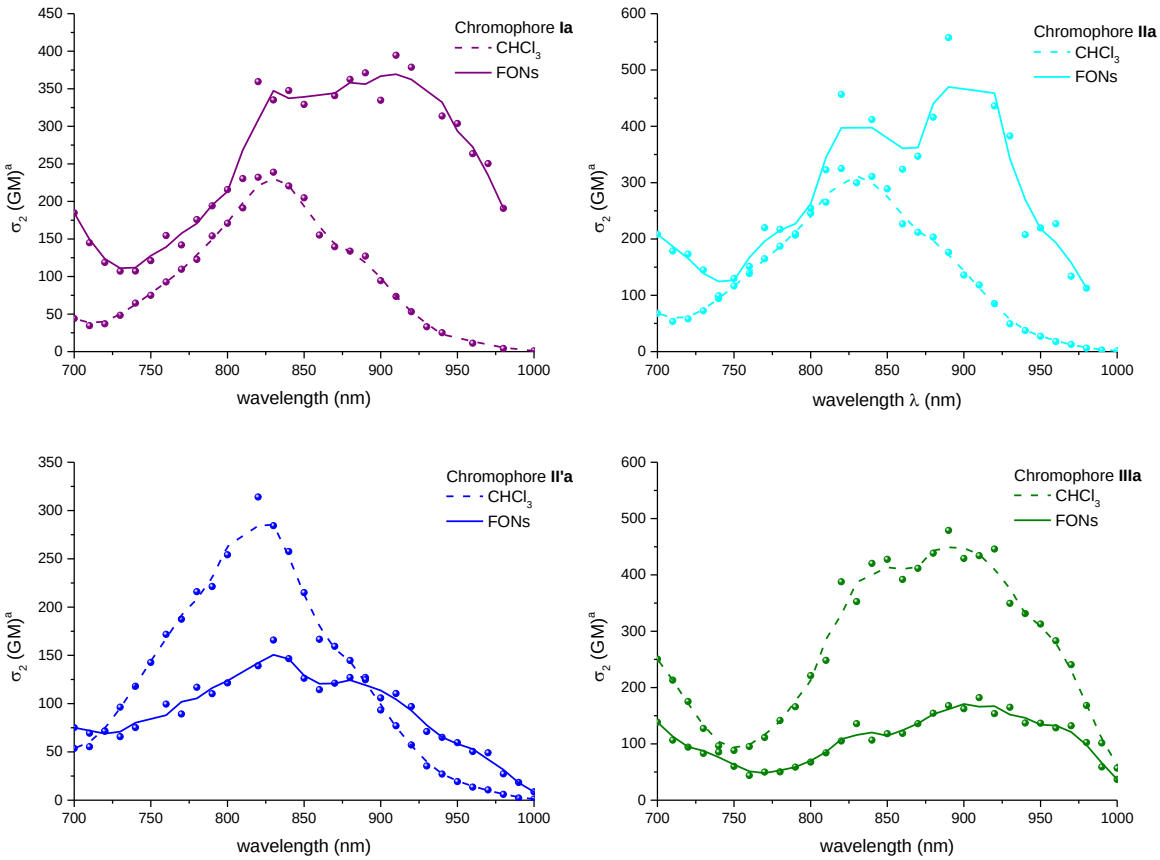

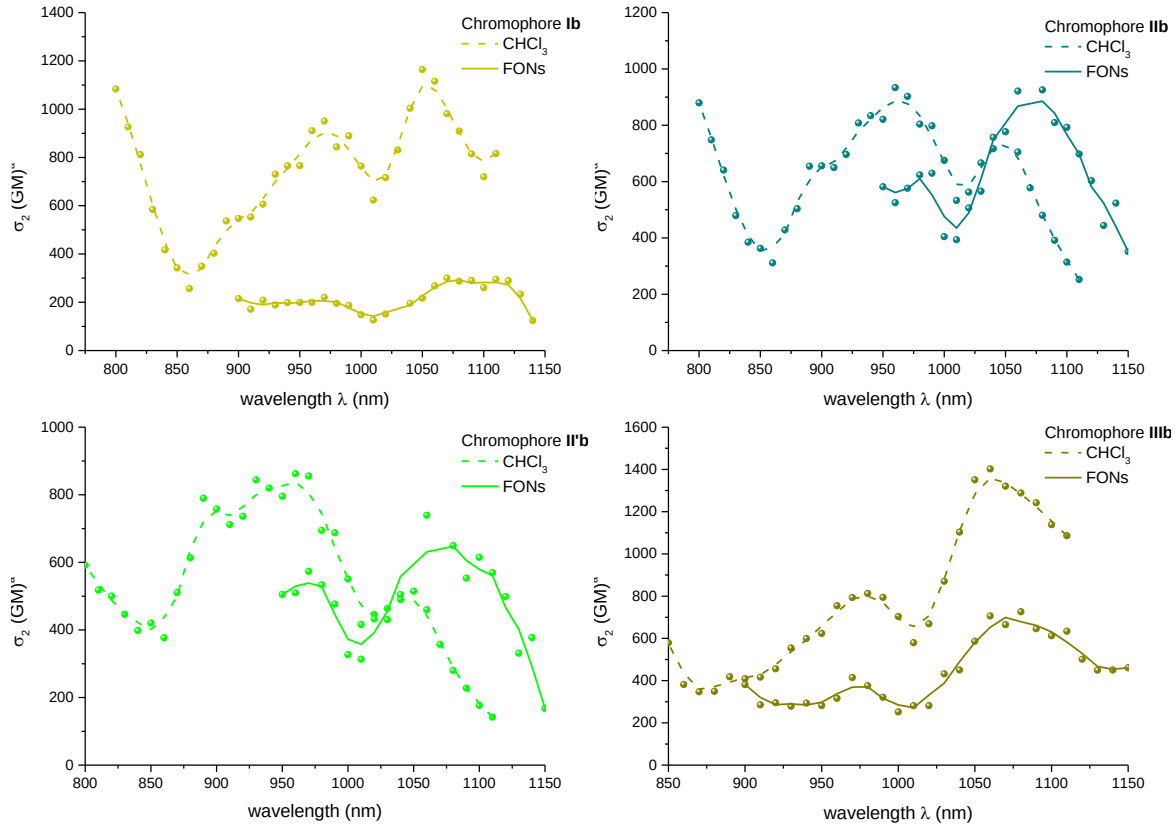

[a]Referred to chromophoric subunits

Figure 3.10 2PA spectra of chromophores in $CHCl_3$ (dotted line) solution and in aggregated state (solid line)

Considering the structural variations of the chromophores, the greater electron withdrawing character of the DCV moiety compared with the formyl one, results in a bathochromic effect of the absorption bands concomitant to an enhancement of the 2P cross sections (except for **I**), as depicted in the following figure.

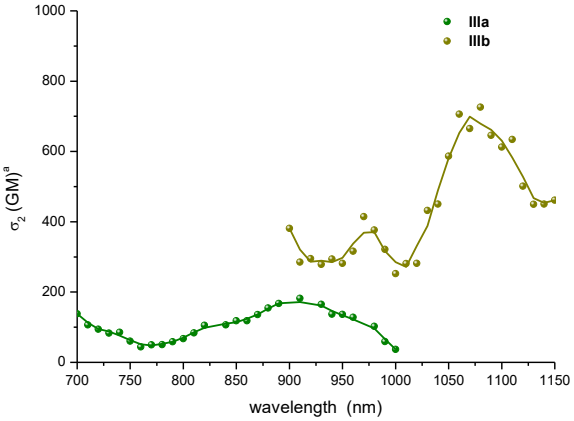

[a]Referred to chromophoric subunit

Figure 3.11 2PA spectra of **IIIa** (green) and **IIIb** (dark yellow)

About the functionalizations on the donor moiety, as expected the interchromophoric interactions have a great effect on the σ_2^{max} values. In particular both in the serie **a** and **b**, the species **III**, which bear the strongest electron donor group, don't exhibit the largest 2P cross section as registered in solution, but in contrast the best ones are observed for the species **II**, with reduced electron donor feature comparing to **I** and **III**, due to bromine substitutions. As mentioned this could be ascribed to the arrangement of the dye molecules in the confined state that, in the case of the species **II**, favours the 2PA response (Figure 3.12).

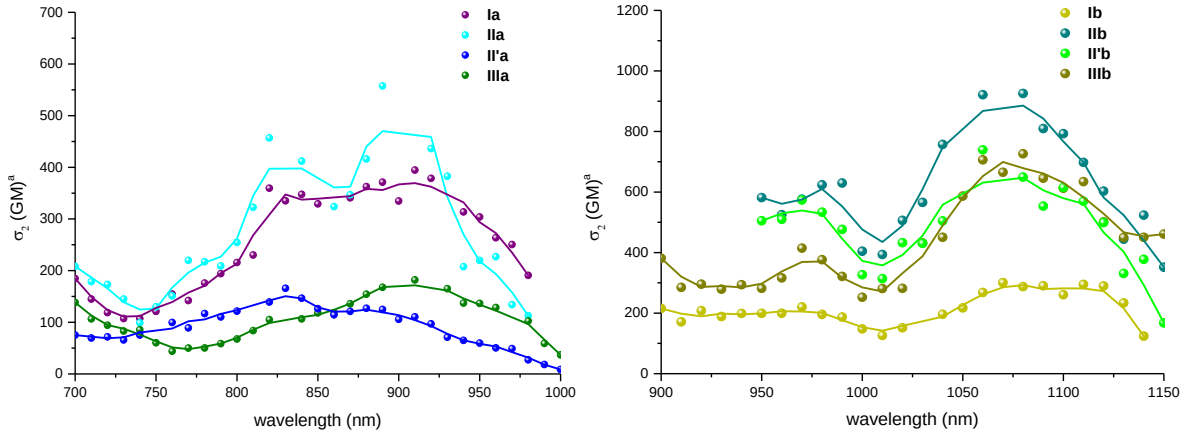

[a]Referred to chromophoric subunit

Figure 3.12 2P absorption spectra of serie **a** (left) and **b** (right) in aggregated state in water

From a general point of view it worths to consider the high 2P brightness of the NPs prepared, which ranges from 10^5 to 10^6 GM and, for biological applications, to remind that the ones belonging to the **b** serie are also deep red-near infrared emitters, making them very appealing for 2P imaging.

The properties described so far are referred to freshly prepared NPs, meaning that they were measured immediately after their manufacture. However NPs must not be intended like static objects, in fact they can undergo several processes such as surface rearrangement and coalescence, resulting in changes of their optical properties. These phenomena are strictly related to the nature of the chromophores, making possible their tunability by playing on their chemical structures. Therefore in the following subchapter the consequences of the different chemical functionalitazions will be examined by means of overtime monitoring experiments.

3.7 Chemical stability of the FONs

The stability of NPs was studied by means of monitoring their absorption and emission spectra overtime; the obtained results are reported in the following figure.

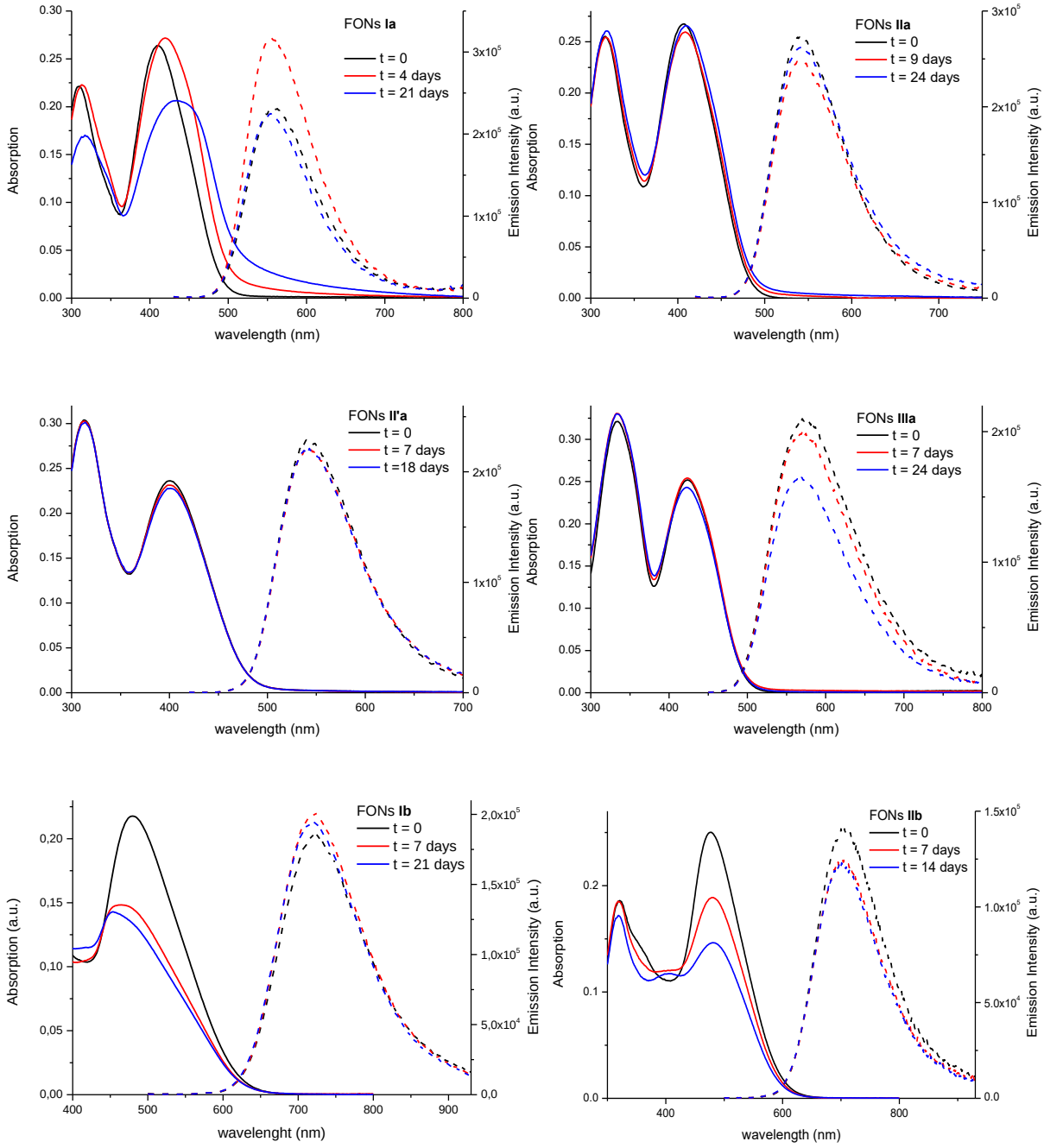

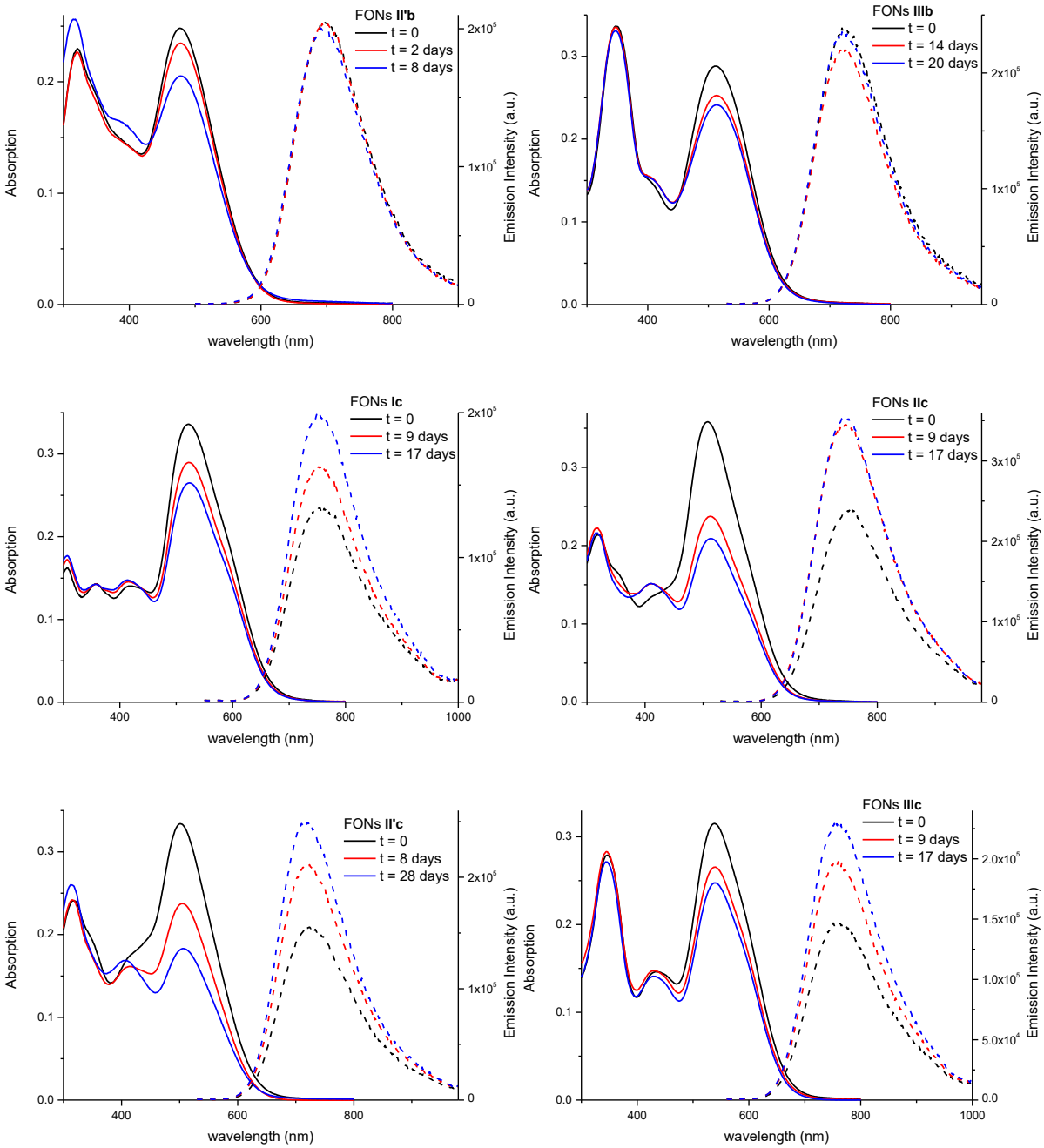

Figure 3.13 Evolution of the absorption and emission spectra of FONs in water over time

A first analysis of the spectra can be carried on by observing NPs made from **Ia**; their absorption spectra undergo a pronounced broadening and flattening overtime due to aggregation processes. The introduction of the bulky groups instead (**IIa**, **II'a** and **IIIa**), induces a big enhancement of the colloidal stability, holding absorption spectra almost unchanged overtime. Furthermore these NPs also exhibit a good retention of the fluorescence properties over about three weeks, especially in the case of brominated species, pointing out that for this series, the bromine atoms ensure a better structural stability

than *tert*-butylphenyl groups. Regarding to the series **b** the trend is similar, getting the best colloidal stability for NPs made from **II'b** and **IIIb**, whereas for the series **c**, **IIIc** and **Ic** seem to be the most stable.

However for the series **b** and **c** there is also another point that must be taken into account and investigated These chromophores were synthesized by means of Knoevenagel condensations which are reversible reactions, meaning that, according to the conditions, they can undergo towards hydrolysis to give back their precursors, the aldehyde (**Ia**, **IIa**, **II'a** or **IIIa**) and the specie with active α-hydrogens (i.e., malononitrile or the barbituric acid derivatives), practically the reverse process (i.e., commonly known as retro-Knoevenagel). In this view an aliquote of **IIIb** and **IIIc** were separately dissolved in a polar solvent miscible with water (DMSO) and, to each batch, 2% of water was added and the evolution of aborption spectra were monitored overtime (Figure 3.14).

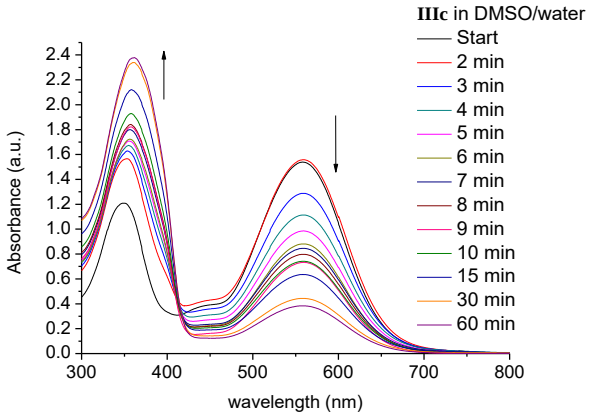

Figure 3.14 Monitoring of the evolution of the absorption spectra of dye **IIIc** in DMSO after addition of 2% of water

For **IIIc** the hydrolysis was very fast and a marked variation of the spectra, with reduction of the intensity of the its characteristic band, was observable since after few minutes. For **IIIb** the process was not appreciable in the first hour, however after one day the situation was clear too. In the next figure the measurements achieved after one day are compared with ones concerning the NPs made from the same dyes over a longer time window (three days, Figure 3.15).

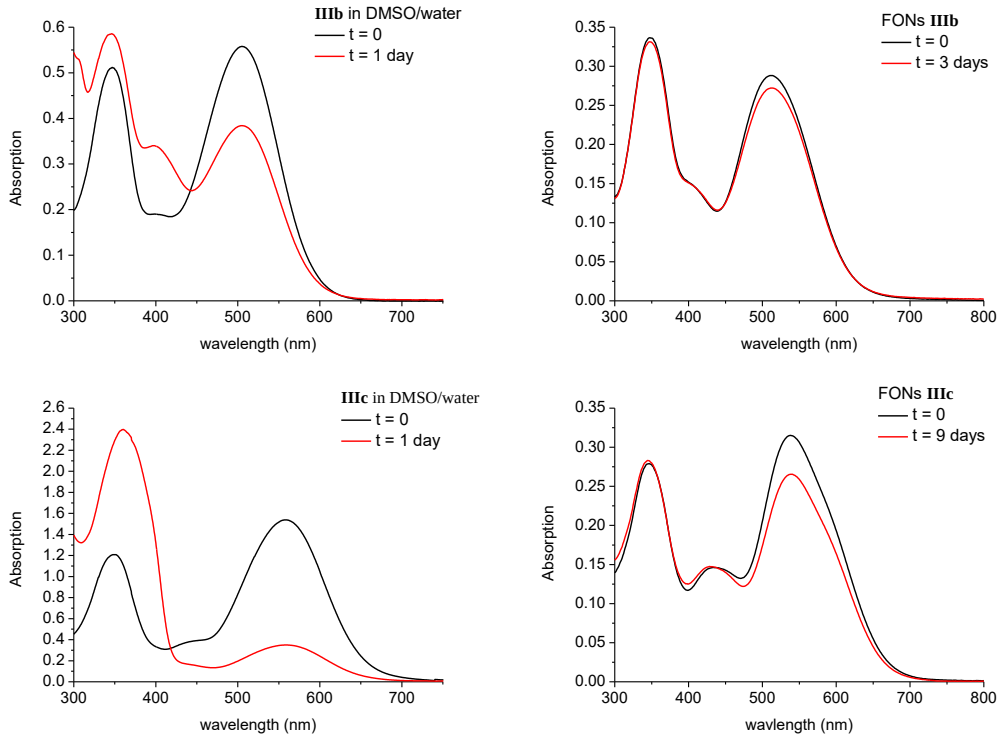

Figure 3.15 Chemical stabilization of dyes **IIIb** and **IIIc** within FONs

As the spectra display, whereas in DMSO containing 2% of water the retro-Knoevenagel occurs in a short time window (minutes for **IIIc**), in the NPs this process is prevented, or at least slowed down, meaning that the aggregated state works as a chemical protection towards the hydrolysis process; such behavior has been observed also for other chromophores developed in our group[26]. In order to conclude this study, it worths to mention that, in terms of reactivity, **IIIc** was expected to hydrolyze faster than **IIIb**, due to the stronger electron withdrawing character of the DETB comparing to DCV.

3.8 Conclusion

Three families of new dipolar chromophores have been prepared by a simple and versatile synthetic route based on a mixed linear (serie **a**) and divergent (series **b** and **c** from **a** one by Knoevenagel condensations) approach. The engineering of their chemical architectures exhibited high impact on their photophysical properties, allowing a fine tuning of their absorption and emission spectra (that ranges from green to near infrared region in $CHCl_3$ solution), concomitant to a strong modulation of the 2PA response, with an enhancement of the 2P cross section with increasing of the polarization by playing on the electron withdrawing feature of the acceptor moiety. The dyes have been successfully used for preparation of NPs by RRM, which display spherical shape and negative ζ-potential, pointing out a

specific organization of the chromophores on the surface. Their optical properties are strictly affected by through-space interactions which are promoted in aggregated state, originating phenomena such as exciton coupling which can be tuned according to the molecular architecture of the chromophoric subunits. The latter one has demonstrated to possess also a great impact on the non linear optical properties, for instance the modulation of the two-photon cross section that, in each serie (**a** and **b**), follows a different trend comparing to the one found in $CHCl_3$ solution, with bis-brominated derivatives (**IIa** and **IIb**) that displayed best results. Moreover, as demonstrated by means of monitoring overtime of the NPs, functionalizations of the chemical scaffold have pointed out the possibility to tune and eventually enhance their colloidal stability, whereas, for the NPs made from dyes of the series **b** and **c**, the simple conversion to nanoaggregate has shown to act as chemical protection against hydrolysis process.

Bibliographic references

[1] V. Parthasarathy, S. Fery-Forgues, E. Campioli, G. Recher, F. Terenziani, M. Blanchard-Desce, *Small* **2011**, *7*, 3219-3229.

[2] S. Fery-Forgues, *Nanoscale* **2013**, *5*, 8428-8442.

[3] H.-H. Lin, S.-Y. Su, C.-C. Chang, *Org. Biomol. Chem.* **2009**, *7*, 2036-2039.

[4] B. Koichi, K. Hitoshi, M. Akito, O. Hidetoshi, N. Hachiro, *Jpn. J. Appl. Phys.* **2009**, *48*, 117002.

[5] S. Yang, D. Lu, L. Tian, F. He, G. Chen, F. Shen, H. Xu, Y. Ma, *Nanoscale* **2011**, *3*, 2261-2267.

[6] M. Breton, G. Prevel, J.-F. Audibert, R. Pansu, P. Tauc, B. L. Pioufle, O. Francais, J. Fresnais, J.-F. Berret, E. Ishow, *Phys. Chem. Chem. Phys.* **2011**, *13*, 13268-13276.

[7] A. Patra, C. G. Chandaluri, T. P. Radhakrishnan, *Nanoscale* **2012**, *4*, 343-359.

[8] X. Zhang, X. Zhang, B. Yang, Y. Zhang, M. Liu, W. Liu, Y. Chen, Y. Wei, *Colloids Surf., B* **2014**, *113*, 435-441.

[9] E. Genin, Z. Gao, J. A. Varela, J. Daniel, T. Bsaibess, I. Gosse, L. Groc, L. Cognet, M. Blanchard-Desce, *Adv. Mater.* **2014**, *26*, 2258-2261.

[10] J. Daniel, A. J. Godin, M. Palayret, B. Lounis, L. Cognet, M. Blanchard-Desce, *J. Phys. D* **2016**, *49*, 084002.

[11] J. Daniel, F. Bondu, F. Adamietz, M. Blanchard-Desce, V. Rodriguez, *ACS Photonics* **2015**, *2*, 1209-1216.

[12] K. Amro, J. Daniel, G. Clermont, T. Bsaibess, M. Pucheault, E. Genin, M. Vaultier, M. Blanchard-Desce, *Tetrahedron* **2014**, *70*, 1903-1909.

[13] M. Barzoukas, C. Runser, A. Fort, M. Blanchard-Desce, *Chem. Phys. Lett.* **1996**, *257*, 531-537.

[14] S. J. Strickler, R. A. Berg, *J. Chem. Phys.* **1962**, *37*, 814-822.

[15] F. Terenziani, M. Morone, S. Gmouh, M. Blanchard-Desce, *ChemPhysChem* **2006**, *7*, 685-696.

[16] F. Terenziani, V. Parthasarathy, A. Pla-Quintana, T. Maishal, A.-M. Caminade, J.-P. Majoral, M. Blanchard-Desce, *Angew. Chem. Int. Ed.* **2009**, *48*, 8691-8694.

[17] A. C. Robin, V. Parthasarathy, A. Pla-Quintana, O. Mongin, F. Terenziani, A.-M. Caminade, J.-P. Majoral, M. Blanchard-Desce, *Proc. SPIE* **2010**, *7774*.

[18] C. Katan, F. Terenziani, O. Mongin, M. H. V. Werts, L. Porrès, T. Pons, J. Mertz, S. Tretiak, M. Blanchard-Desce, *J. Phys. Chem. A* **2005**, *109*, 3024-3037.

[19] C. Le Droumaguet, A. Sourdon, E. Genin, O. Mongin, M. Blanchard-Desce, *Chem. Asian. J.* **2013**, *8*, 2984-3001.

[20] F. Terenziani, C. Katan, E. Badaeva, S. Tretiak, M. Blanchard-Desce, *Adv. Mater.* **2008**, *20*, 4641-4678.

[21] Y. Shirota, *J. Mater. Chem.* **2005**, *15*, 75-93.

[22] T. N. Baker, W. P. Doherty, W. S. Kelley, W. Newmeyer, J. E. Rogers, R. E. Spalding, R. I. Walter, *J. Org. Chem.* **1965**, *30*, 3714-3718.

[23] T. Mallegol, S. Gmouh, M. A. A. Meziane, M. Blanchard-Desce, O. Mongin, *Synthesis* **2005**, *2005*, 1771-1774.

[24] A. Mishra, R. K. Behera, P. K. Behera, B. K. Mishra, G. B. Behera, *Chem. Rev.* **2000**, *100*, 1973-2012.

[25] A. J. Fatiadi, *Synthesis* **1978**, *1978*, 165-204.

[26] J. B. Verlhac, J. Daniel, P. Pagano, G. Clermont, M. Blanchard-Desce, *C. R. Chim.* **2016**, *19*, 28-38.

Chapter 4

Towards Efficient Energy Transfer Process in NPs Exploiting Hydrogen bond

4.1 Hydrogen-bond (H-bond)

H-bond is a very complex subject that has experienced a deep refinement and evolution over the decades; just think that even its definition has presented many difficulties and several ones[1] have been proposed, then abandoned, changed or expanded. As proposed by Steiner in his comprehensive and thorough work[2], the hydrogen bond can be defined as an interaction of the type X-H···A, if it constitutes a local bond and if the term X-H, said donor, acts as proton donor to the specie A, said acceptor. In order to be characterized as a H-bond, some criteria (e.g., energies involved, angles between the species, distances between the latter ones) must be required[1].

H-bond can be also classified according to some conventionally parameters such as the number of acceptor centers interacting with a certain hydrogen atom, leading to normal, bifurcated or trifurcated kind of bridges, which involve respectively one, two or three acceptor groups (Figure 4.1).

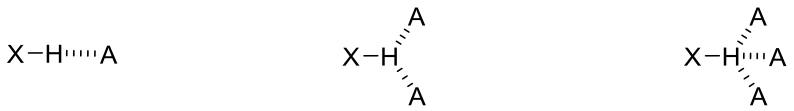

Figure 4.1 Types of H-bonds, from the left normal, bifurcated and trifurcated

Another way to classify H-bonds is based on the energy of the interaction, leading to so called strong, moderate or weak types, with different features and properties. Although the situation is not compartmentalized, with well defined limits that correspond to net changes of the properties of hydrogen bonds, but rather nuanced and continues, without precise confines. However understanding the factors that combine to determine the energy of a hydrogen bond, that lies between 0.2 and 40 kcal/mol, allows to better understand its nature. These terms consist in electrostatic, polarization, charge transfer and Van der Waals (which assembles dispersion and exchange repulsion)[2-4] and, according to their contribute, due to the chemical nature of the acceptor and donor moieties, the features of H-bond can easily change, determining, for instance, a more pronounced character of Van der Waals or covalent interaction. This concept can be well visualized in the following figure.

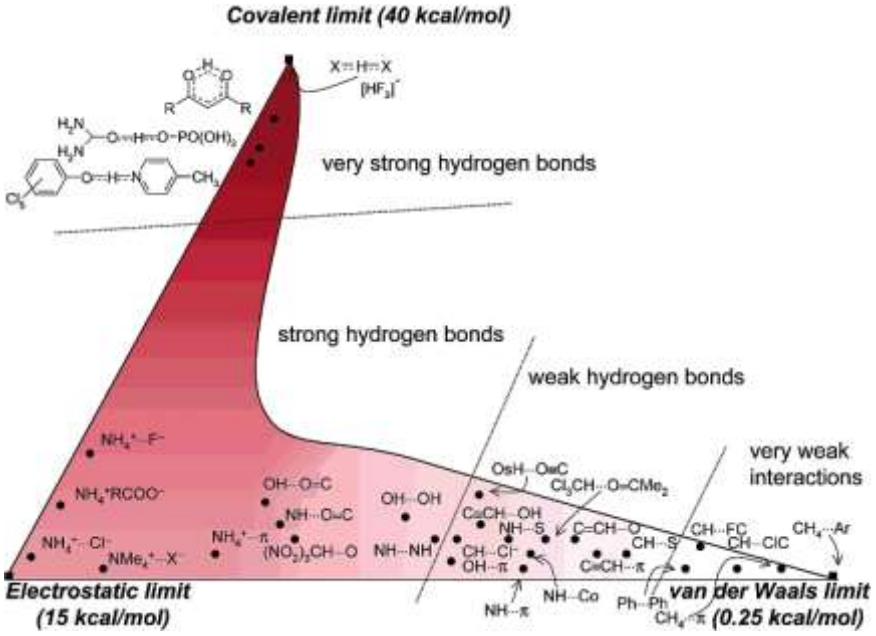

Figure 4.2 Interactions involved in H-bond[4]

According to Jeffrey[5], H-bond can be classified into three main types:

- Strong: the character of the H-bond is mainly covalent, with energy over 15 kcal/mol and strong directionality that tends to linearity.
- Moderate: the character of the bond is dominated by electrostatic term, with energy between 4 and 15 kcal/mol and discrete directionality.
- Weak: bond energy is less than 4 kcal/mol and the electrostatic contribution is less than in the case of moderate, so that Van der Waals one takes on great importance and, as a consequence, the directionality decrease.

To change the character of the hydrogen bond there are other features in addition to those listed which change too; some of the key ones are reported in the following table.

	Strong	Moderate	Weak
Interaction type	strongly covalent	mostly electrostatic	electrost. / dispers.
Bond length H···A [Å]	1.2-1.5	1.5-2.2	>2.2
Lengthening of X-H [Å]	0.08-0.25	0.02-0.08	<0.02
X-H versus H···A [Å]	X-H ≈ H···A	X-H < H···A	X-H << H···A
X···A [Å]	2.2-2.5	2.5-3.2	>3.2
Directionality	strong	moderate	weak
Bond angles [°]	170-180	>130	>90
Bond energy [kcal mol^{-1}]	15-40	4-15	<4
Relat. IR shift $\Delta\tilde{\nu}_{X\text{-}H}$ [cm^{-1}]	25%	10-25%	<10%

Table 4.1 Jeffrey's classification of H-bond[2, 5]

The hydrogen bonding is responsible for a whole series of phenomena in nature, such as the unique properties of water, like high dielectric constant, surface tension and heat of vaporization. Moreover its biological role is fundamental, contributing to the stabilization of secondary and tertiary structures of proteins[6-8] or, corcerning DNA, the pairing of purine and pyrimidine bases[9-10].

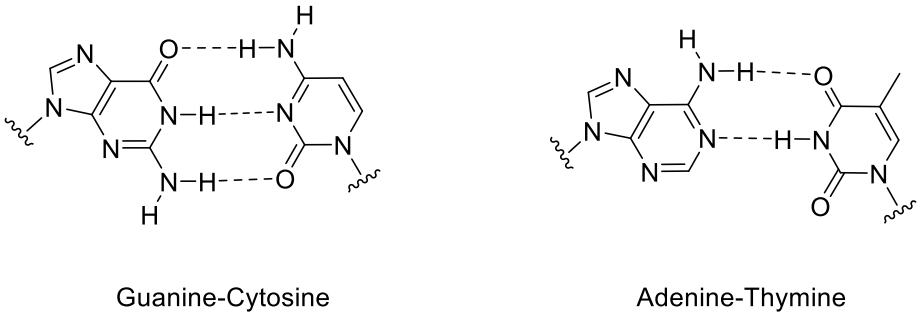

Figure 4.3 DNA base pairing

The latter one represents a natural example of molecular recognition via hydrogen bond[10]; this concept is very important in the field of supramolecular chemistry[2, 11-14] and it plays a pivotal role in crystal engineering[4], wherein non-covalent interactions are exploited to get control over the structure of a supermolecule. In this view several studies have been done in order to understand the nature and the properties of the chemical motifs[15-16] that can be used for this purpose and some of them are reported in the following figure[2, 16].

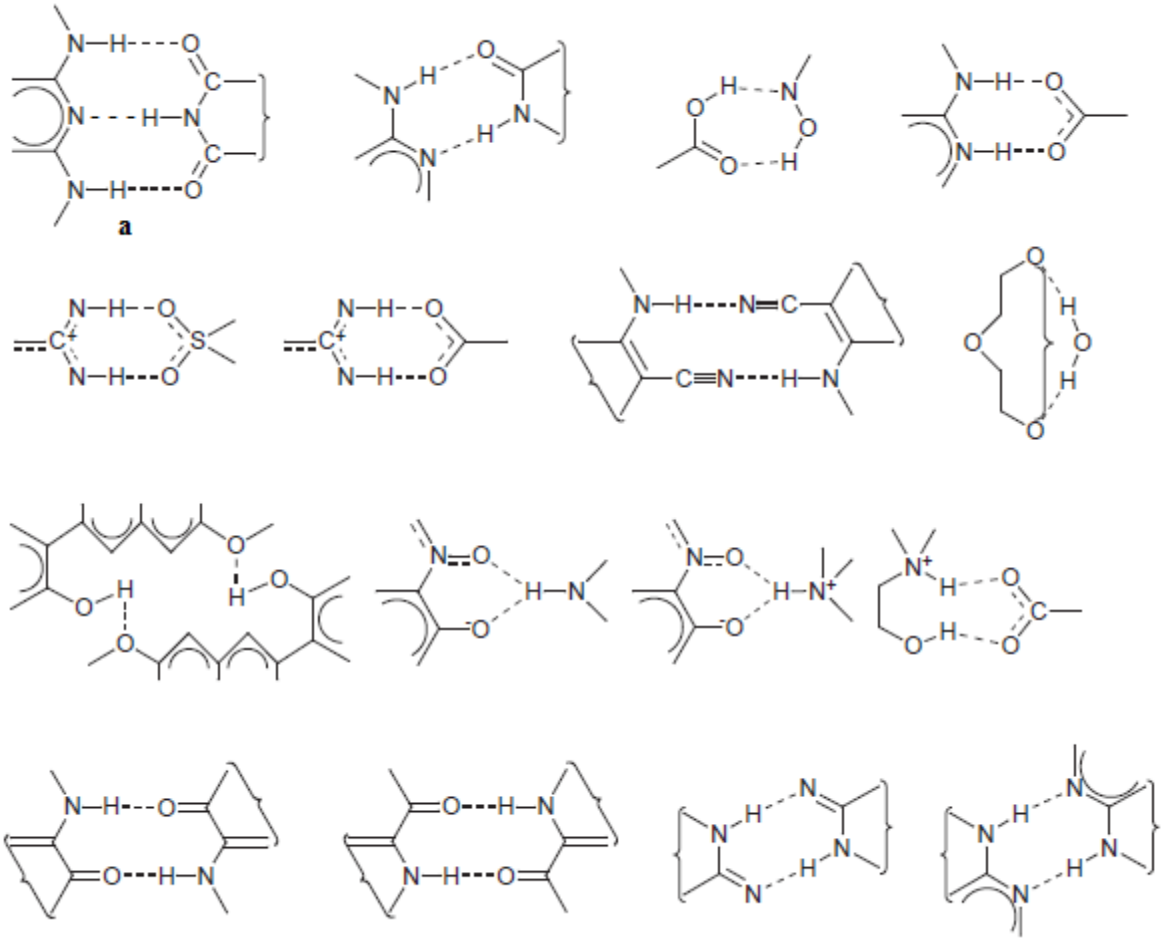

Figure 4.4 Bimolecular hydrogen-bonded ring motifs[2, 16]

The ones shown in the Figure 4.4 are bimolecular hydrogen-bonded ring motifs resulting from analysis of crystal structures in Cambridge Structural Database (CSD) conducted by Allen et al[16]. Among them the motif **a** is really interesting, in fact the author report that it occurs almost in every structure containing the two constitutive fragments and defines a probability of its formation (referred to the crystal structures stored in CSD) of 97%. This motif can be achieved by means of different molecules that contain suitable subunits able to set up the triple hydrogen bond, for instance 2,6-diaminopurine and uracil[17] or 2,4,6-triaminopyrimidine and barbituric acid derivatives[18] and others[19-24].

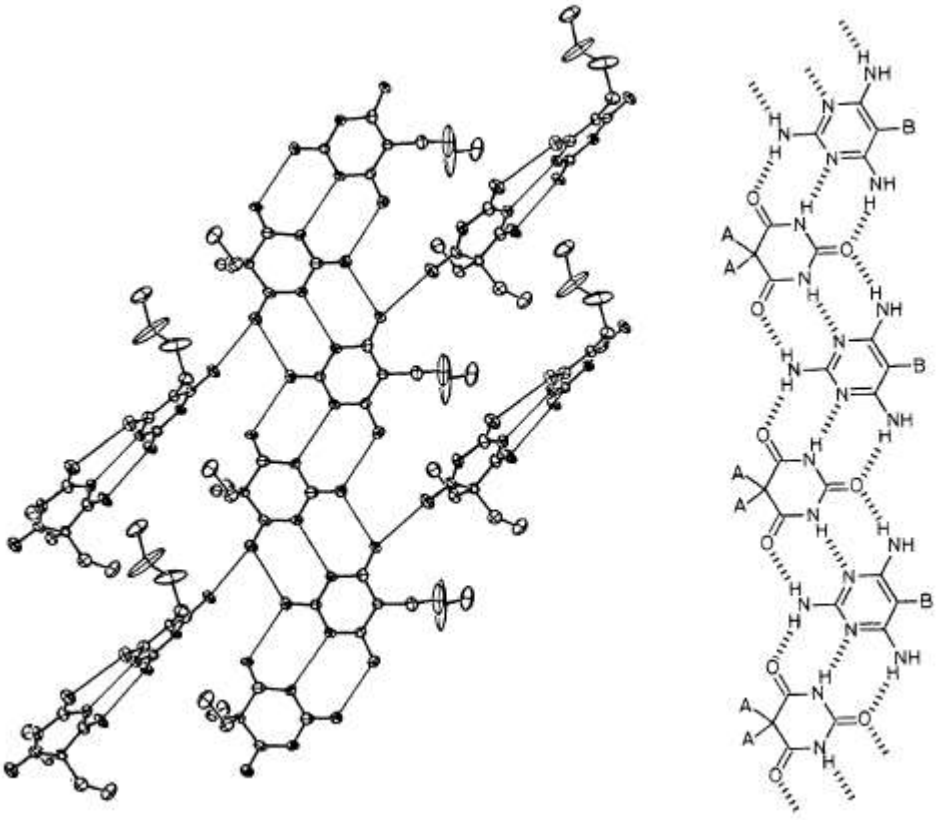

Figure 4.5 X-ray structure of cocrystals formed by 2,4,6-triaminopyrimidine and barbituric acid derivatives[18]

From a general point of view it has emerged that the nature of the H-bond can deeply affects the interaction between two species and this may induce large changes in the properties of the solid state. For instance Balan et al[25] reported a series of nanoparticles made from oligofluorene derivatives bearing different H-bonding functional groups that show specific trend of their properties (Figure 4.6), such as fluorescence quantum yield.

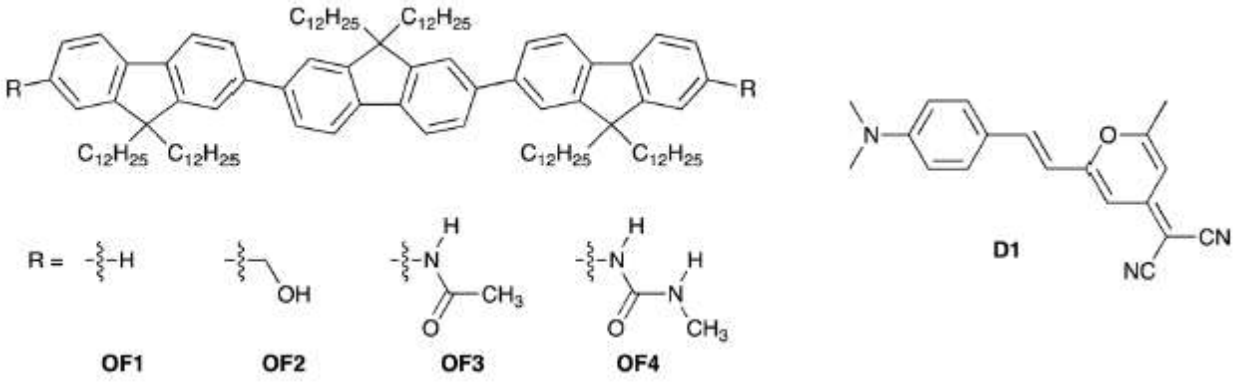

Figure 4.6 Oligofluorene derivatives and neutral dye prepared in Balan's study[25]

The species **OF1-4** have respectively 0-3 hydrogen bonding sites, and these chromophores were used to prepare NPs by reprecipitation method. The author observed that whereas in THF solution the fluorescence quantum yields for the compounds were rather similar (i.e., about 70%), in NPs state they decrease (i.e., aggregation-caused quenching), observing a more pronounced lowering from **OF1** to **OF4** (Table 4.2), ascribable to the packing of the dyes in the aggregated texture, that increases with the H-bonding capability of the chromophores.

	Φ_F in THF solution	**Φ_F in NP state**
OF1	0.71	0.68
OF2	0.72	0.65
OF3	0.70	0.32
OF4	0.79	0.11

Table 4.2

An application of these NPs is the encapsulation of a dipolar dye (**D1** in Figure 4.5) acting as acceptor in fluorescence resonance energy transfer process (whereas the **OF** dyes act as donor). Here the authors observed a more pronounced quenching of the fluorescence of the donor in the same order as previously (i.e., quenching increases from **OF1** to **OF4**), pointing out the influence of the hydrogen bond on the FRET process. It worths to remind that FRET is a non-radiative excitation transfer between two molecular entities[26], a donor and an acceptor, and its rate (k_t) depends on the distance between the two species according to the Equation 4.1.

$$k_t = (1/\tau_D)\,(R_0/r)^6$$

Equation 4.1

Wherein τ_D is the fluorescence lifetime of the donor without transfer, r is the distance between the donor and the acceptor and R_0 is called Förster radius and represents the distance at which the FRET efficiency is 50%[26]. In this view it appears more clear how the possibility of forming H-bonds, that can affect the distance among the species involved, may have a strong influence on properties of the system observed, such as the photophysical ones of the NPs mentioned in the previous example.

In this view the purpose of the work introduced in the next section consists into the synthesis of two new dipolar chromophores bearing as acceptor terminal groups a 2,4-diamino-1,3,5-triazine and an uracil moiety respectively, therefore two complementary subunits that can lead to the formation of H-bonds, and to study their properties in organic solvent solution as well as in aggregated state.

4.2 Design of the chromophores

The molecular structure of the chromophores chosen in this study are reported in the following figure.

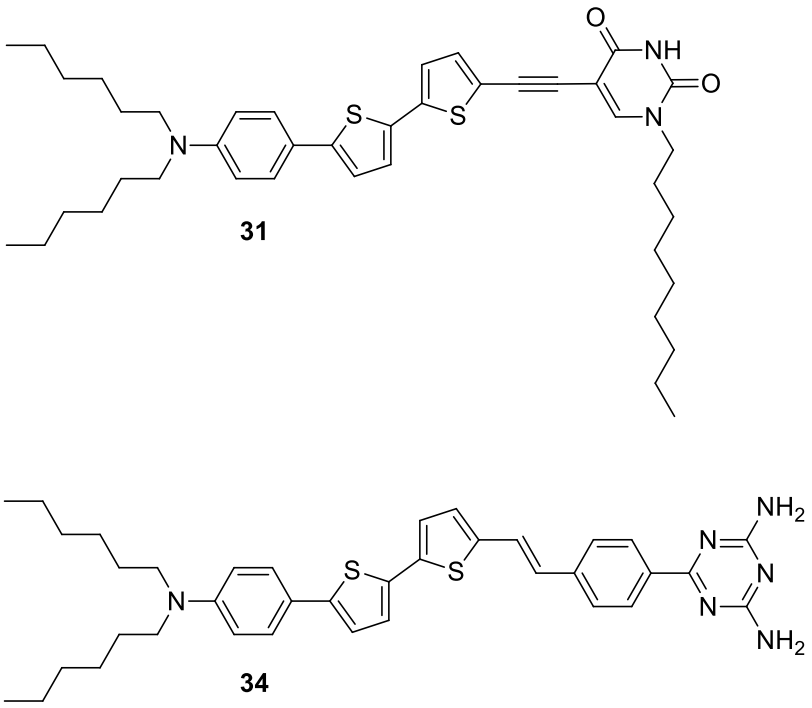

Figure 4.7 Structures and codes of the chromophores

The compounds have dipolar nature in which it is possible to identify a donor and an acceptor moieties linked by a π-bridge. Both contains *N*,*N*-dihexylaniline as donor group, wherein the two alkyl chains aim to enhance the solubility of the dyes in organic solvents.

Regarding to the π-bridges, the dyes are made by a common 2,2'-bithiophene unit, that is linked to an ethynylene moiety in **31** and to a vinylene-phenylene one in **34**; both would allow a good electron communication between the donor and the acceptor. Furthermore the choice is also related to the synthetic strategy adopted for the realization of the targets, which allows, as will be better clarified in the next section, a linear and convenient approach that originates from the same precursor.

Concerning the acceptor moiety, for **34** it consists in a 2,4-diamino-1,3,5-triazine group (also said guanamine), whereas for **31** it is an uracile derivative bearing a nonyl chain on the nitrogen atom on position one. The alkylation aims to enhance the solubility of the dye and furthermore it should decrease the chance of the nitrogen bearing the alkyl chain to get involved in hydrogen bonds with the triazine group, reducing the possibility to achieve other types of H-bonding motifs and therefore increasing the directionality of the interactions.

4.3 Synthesis

As previously mentioned the synthesis is planned in order to be quick and efficient; taking advantage from the similarity of the structures of the two compounds, the idea is to linearly prepare a common intermediate which in parallel branch out to the desired targets. In the Scheme 4.1 is reported the retrosynthetic route planned.

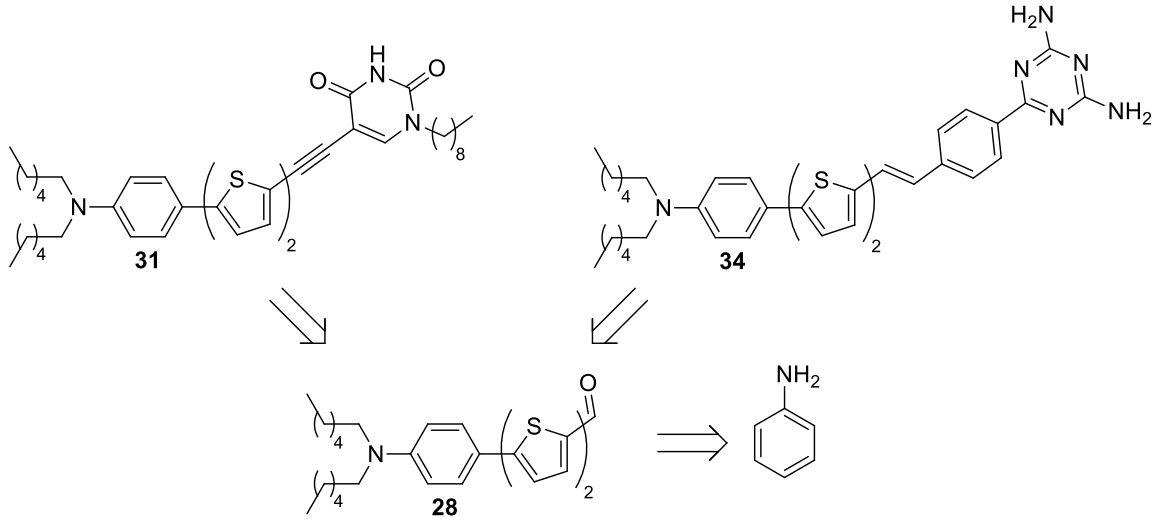

Scheme 4.1 Retrosynthetic route

According to this scheme, the synthesis can be splitted into three parts:

1) synthesis of the intermediate **28**;
2) synthesis of **31** and compounds involved in its preparation;
3) synthesis of **34** and compounds involved in its preparation.

In the following section will be discussed the first point.

4.3.1 Synthesis of the intermediate

The retrosynthesis of the intermediate **28** is shown in the Scheme 4.2.

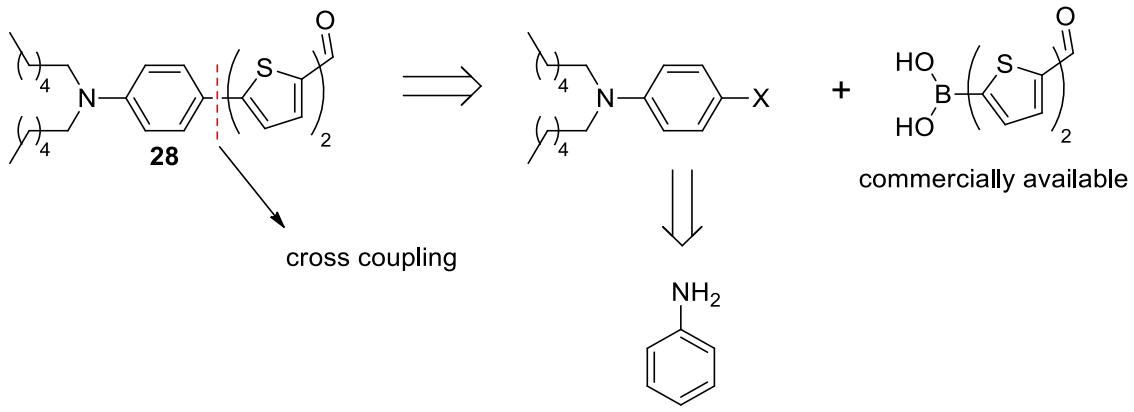

Scheme 4.2 Retrosynthesis of the intermediate **28**

The disconnection illustrated is very useful because it utilizes the cross coupling between a suitable aniline derivative and a boronic acid that is commercially available. Planning an organic synthesis involves not only the acquaintance of the chemical reactions, their mechanisms and how to perform them properly, but it entails also some other requirements which are the result of the experience; one of these is the knowledge and the use of the chemicals which are commercially available. As in this case it allows to optimize a synthetic scheme and its related costs, avoiding the preparation of chemical compounds which may be more expensive to synthesize on a laboratory scale or time-consuming or difficult to purify. After choosing the route, we can move on to the description of the synthesis of the aniline derivative.

The first step consists in a bis alkylation of aniline by means of nucleophilic substitution on hexylbromide, working in biphasic conditions and using a little amount of phase transfer agent (Scheme 4.3).

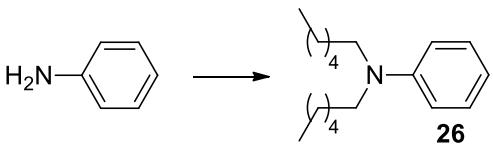

Scheme 4.3 Bis alkylation of aniline; reagents and conditions: aniline, tetrabutylammonium iodide, $NaOH_{aq}$, hexylbromide, 60°C, overnight, (91%, **26**)

Then the phenyl ring, activated towards aromatic electrophilic substitution by the dialkylamino group, was functionalized by halogenation on the para position using iodine (Scheme 4.4).

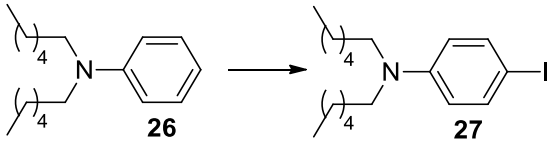

Scheme 4.4 Iodination of **26**; reagents and conditions: **26**, I_2, $NaHCO_{3aq}$, CH_2Cl_2, rt, overnight (70%, **27**)

Finally the intermediate **28** was prepared by means of a Suzuki cross coupling between **27** and the commercially available (5'-formyl-[2,2'-bithiophen]-5-yl)boronic acid according to Scheme 4.5.

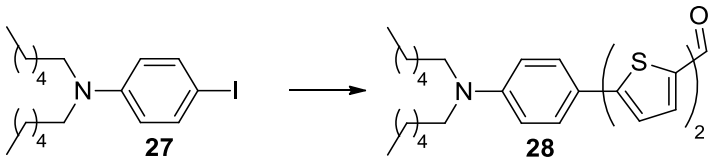

Scheme 4.5 Suzuki cross coupling; reagents and conditions: **27**, (5'-formyl-[2,2'-bithiophen]-5-yl)boronic acid, K_2CO_3, $Pd(dppf)Cl_2$, Tol:MeOH=2:1, 70°C, overnight (64%, **28**)

The used approach has advantageously led to the preparation of the compound **28** and, as well as to be useful for this work in view of the preparation of the compounds **31** and **34**, may be an efficient general method for the preparation of derivatives similar to the dialkylaniline **28** that can be readily functionalized on the carbonyl moiety (e.g., Knoevenagel condensations), thus useful as building block for more complex systems. At this point we can switch to the second part of the synthesis.

4.3.2 Synthesis of the uracile derivative

The path used for the preparation of **31** can be quickly understood by inspection of the retrosynthesis depicted in the following scheme.

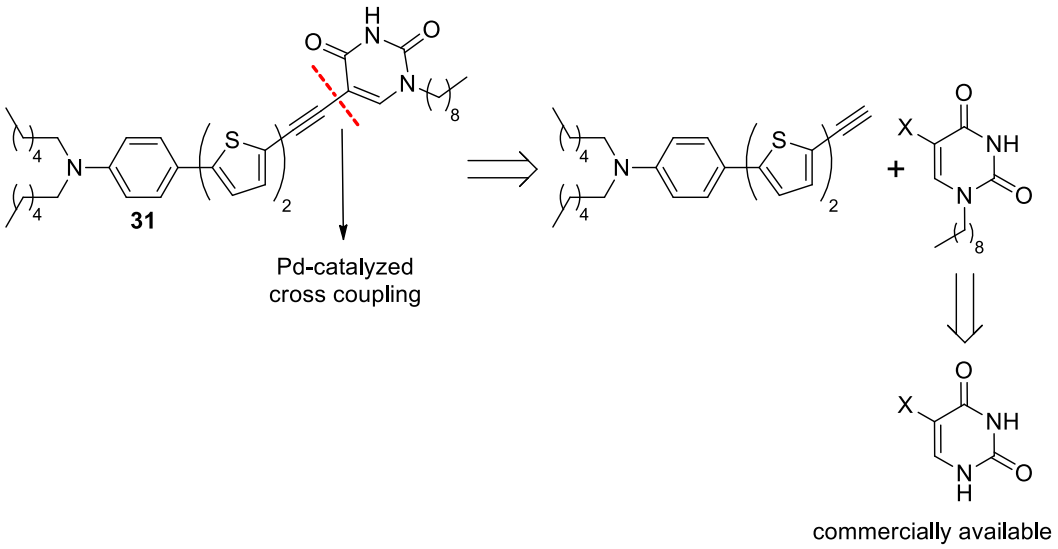

Scheme 4.6 Retrosynthetic scheme for the preparation of the compound **31**

The disconnection proposed reduces the problem to the synthesis of the shown starting materials, a *N*-alkylated uracile derivative preparable from commercially available product and a terminal alkyne derivative of **28**. The latter one can be prepared by means of a functional group interconversion (FGI) able to convert the formyl group of the compound **28** into an acetylen moiety. In this way the coupling between the donor and the acceptor is performed in two steps by means of a robust Sonogashira cross coupling.

The FGI was achieved by a Seyfert-Gilbert homologation using Ohira-Bestmann reagent according to the following scheme.

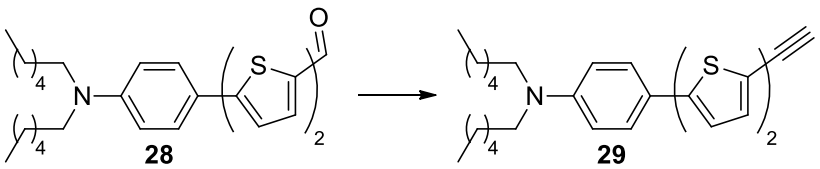

Scheme 4.7 Homologation of **28**; reagents and conditions: **28**, K_2CO_3, dimethyl (1-diazo-2-oxopropyl)phosphonate, MeOH, THF, rt, 48 hours (69%, **29**)

This method, discussed in the annex about organic synthesis, represents an alternative to other common protocols such as Corey-Fuchs, avoiding the use of hazardous species such as bromoform. Furthermore this approach leaves open a backdoor for eventually in situ transformation such as Huisgen cycloaddition, allowing click chemistry for functionalization of the triple bond.

Regarding the alkylation of 5-iodouracile, a first attempt of this transformation was tried through nucleophylic substitution on nonylbromide in basic environment (conditions 1 in Scheme 4.8), leading to low conversion and very low yield, due to the formation of a mixture of mono-alkylated products. Therefore another protocol involving the use of bis(trimethylsilyl)amine (conditions 2 in Scheme 4.8) was performed, leading to better results in terms of regioselectivity and yield (no alkylation on other positions).

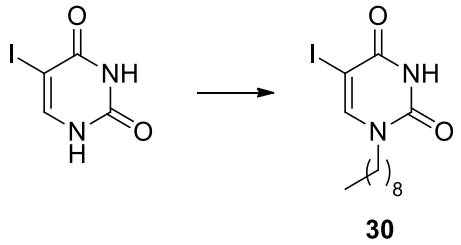

30

Scheme 4.8 Alkylation of 5-iodouracile; reagents and conditions: 1) 5-iodouracil, 1-bromononane, K_2CO_3, DMSO, 30°C, overtnight; 2) 5-iodouracil, $(NH_4)_2SO_4$, bis(trimethylsilyl)amine, reflux, overnight, then DMF, 1-bromononane, 80°C, 24 h (25%, **30**)

Finally the target molecule was achieved by means of a Sonogashira cross coupling between **29** and **30** (Scheme 4.9).

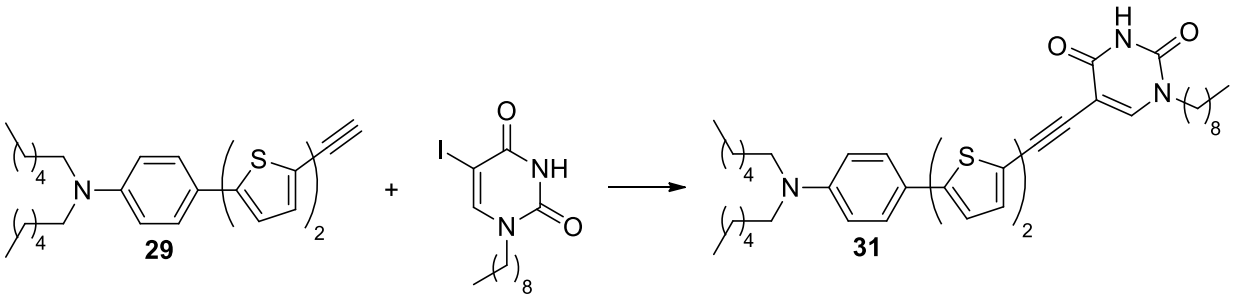

Scheme 4.9 Sonogashira cross coupling for synthesis of **31**; reagents and conditions: **29**, **30,** Pd(PPh_3)4, CuI, Et_3N, DMF, 48 h (72%, **31**)

After the preparation of the first target (**31**), we can move on the description of the synthesis of the last one, the triazine derivative (**34**).

4.3.3 Synthesis of the triazine derivative

The retrosynthetic strategy adopted is depicted in the Scheme 4.10.

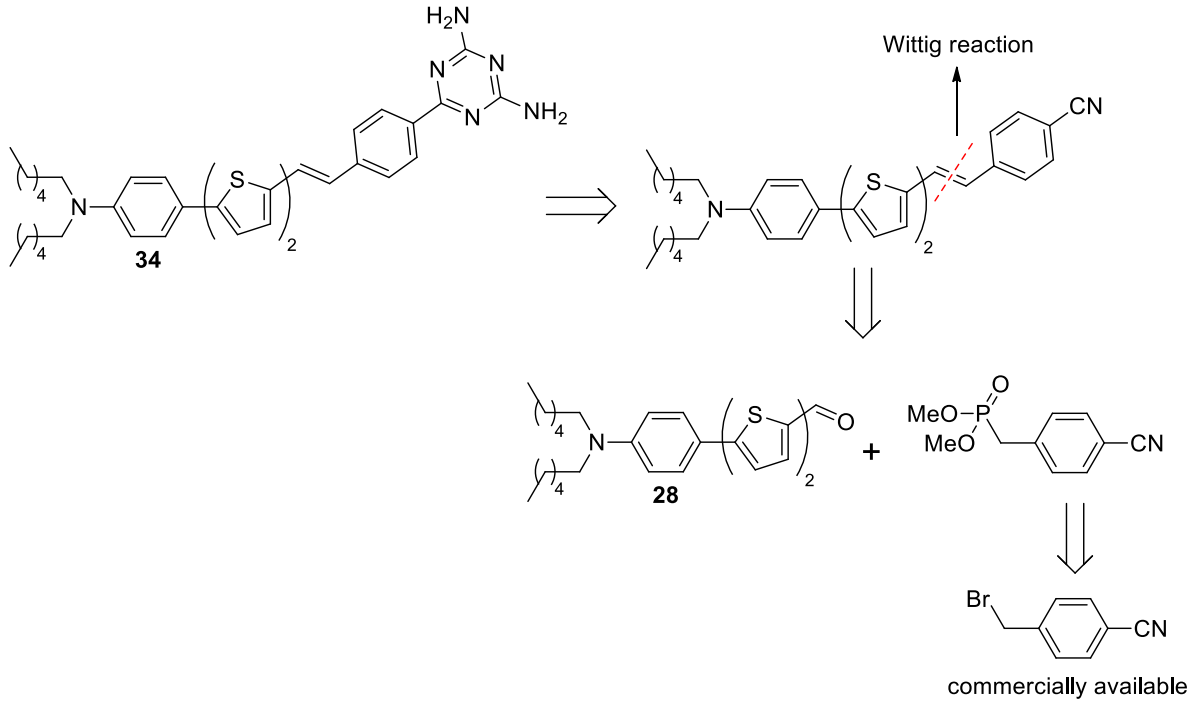

Scheme 4.10 Retrosynthetic scheme for the preparation of the compound **34**

The diaminotriazine moiety on the target compound (**34**) can be achieved by cyclization of a nitrile group with dicyandiamide, which represents a common route for the preparation of such derivatives, reducing the problem to the synthesis of the nitrile showed in the scheme. The latter one can be disconnected on the double bond and, considering a Wittig reaction, it leads to **28** as carbonyl precursor that can be reacted with the depicted phosphonate. This compound may in turn be easily prepared from commercially available 4-(bromomethyl)benzonitrile.

For this purpose a Michaelis-Arbuzov reaction by means of triethylphosphite was performed (Scheme 4.11), leading to desired phosphonate (**32**) in good yield.

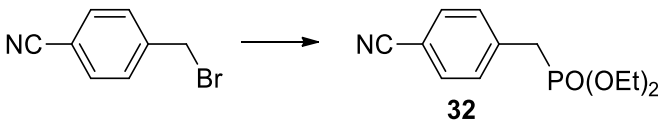

Scheme 4.11 Michaelis-Arbuzov reaction; reagents and conditions: 4-(bromomethyl)benzonitrile, triethyl phosphite, $CHCl_3$, reflux, overnight, (62%, **32**)

A Horner-Wadsworth-Emmons (HWE) reaction between **28** and **32** was achieved in the conditions reported in the Scheme 4.12, affording **33** as pure *E*-stereoisomer and in good yield.

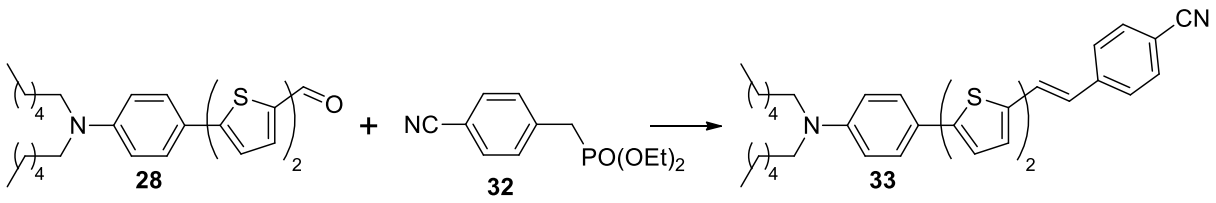

Scheme 4.12 Horner-Wadsworth-Emmons reaction; reagents and conditions: **29**, **32**, NaH, THF, room temperature, overnight (82%, **33**)

As expected the carbanion generated upon removal of the α-proton by means of the hydride is well stabilized, leading to the excellent result in terms of stereoselectivity; a typical feature of HWE reactions.

At this point the last step of the synthesis involved the formation of the 2,4-diamino-1,3,5-triazine ring by means of the cyclization of the nitrile with dicyandiamide in basic conditions (Scheme 4.13). This method represents the best and the most common way to produce guanamines[27], which are largely used in the polymers industry for the preparation of aminoformaldehyde resins as well as the manifacturing of fire-retardant additivives.

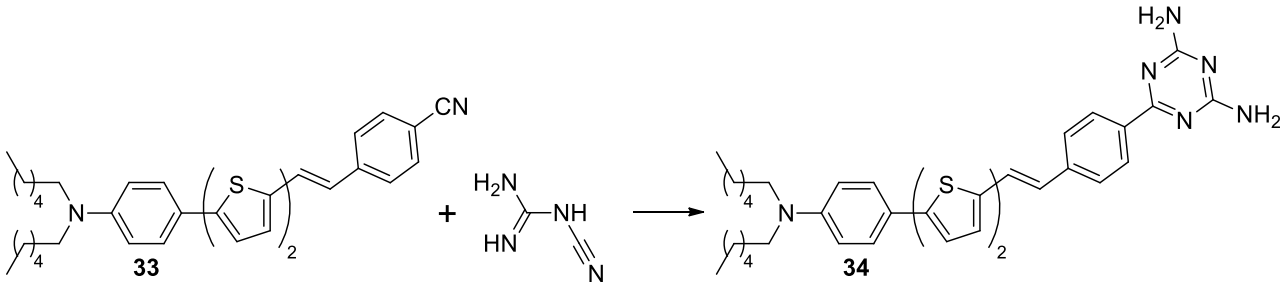

Scheme 4.13 Formation of the triazine ring; reagents and conditions: **33**, dicyandiamide, KOH, BuOH, room temperature, 48 h (66%, **34**)

In our case the reaction gave satisfactory results, leading to the desired target molecule **34** with relative good yield.

After the synthesis of the compounds and their characterizations (experimental part), we can move on the investigation of their photophysical properties.

4.4 Linear optical properties in organic solvent

The characterization of the linear photophysical features of the two chromophores was performed in THF solution; their absorption and emission spectra are following reported.

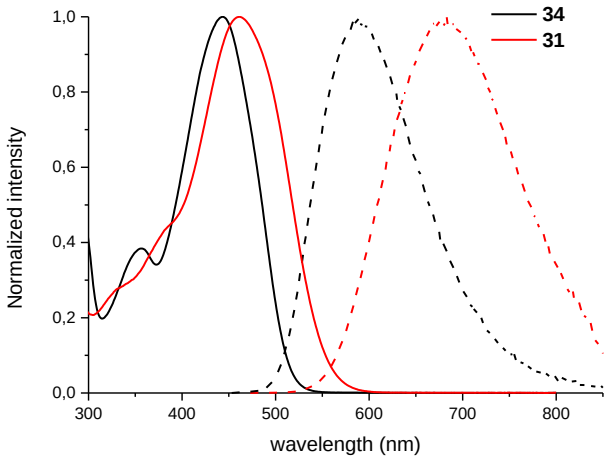

Figure 4.8 Normalized absorption (solid line) and emission (dashed line) spectra of **34** (black, λ_{exc}= 443 nm) and **31** (red, λ_{exc}= 463 nm) in THF solution

Both **34** and **31** display rather intense absorption bands in the blue region with maxima at 443 nm (ε= 7.5 10^4 $M^{-1}cm^{-1}$) and 463 nm (ε= 4.2 10^4 $M^{-1}cm^{-1}$) respectively. Upon excitation at its absorption maximum, **34** exhibits an emission band mainly located in the yellow part of the spectrum (λ_{max}^{ems}= 589 nm), whereas for **31** it lies in the red (λ_{max}^{ems}= 681 nm) region. The data are summarized in the Table 4.3.

Cpd	λ_{max}^{abs} [nm]	ε^{max} [10^4 $M^{-1}cm^{-1}$]	λ_{max}^{ems} [nm]	Φ_F	Stokes Shift [10^3 cm^{-1}]	$\varepsilon^{max}\Phi_F$ [10^4 $M^{-1}cm^{-1}$]	τ [ns]	k_r [$10^8 s^{-1}$]	k_{nr} [$10^8 s^{-1}$]
31	463	4.2	681	0.26[a]	6.9	1.1	1.9[b]	1.4	3.9
34	443	7.5	589	0.33[a]	5.6	2.5	1.1[b]	3.0	6.2

[a] Standard reference : Rhodamine 6G in EtOH (Φ=0.94); [b] λ_{exc}= 455nm

Table 4.3 Photophysical properties in THF solution

As expected, since the *N*,*N*-dihexylaniline is a good electron donor and thanks to the capacity of the triazine and the uracile to accept electrons, a dipolar character of the molecules emerged; both undergo a marked positive solvatochromism of the emission due to internal charge transfer (ICT). Being better stabilized with increasing polarity of the solvent, they display a consequent bathochromic effect on the emission maxima (Figure 4.9). The Stokes Shift are linearly dependent on the polarity-polarizability parameter (Δf) of the Lippert-Mataga relationship:

$$\nu_{abs} - \nu_{ems} = 2\,\Delta\mu^2\Delta f/hca^3 + constant$$

Equation 4.2

wherein ν is the wavenumber of absorption or emission maximum, $\Delta\mu$ is the change of the dipole moment, h is Planck's constant, c is the velocity of light, a is the radius of the Onsager cavity and Δf is the orientation polarizability, defined as:

$$\Delta f = \left(\frac{\varepsilon - a}{2\varepsilon + 1}\right) - \left(\frac{n^2 - 1}{2n^2 + 1}\right)$$

Equation 4.3

wherein ε and n are respectively the dielectric costant and the refractive index of the solvent.

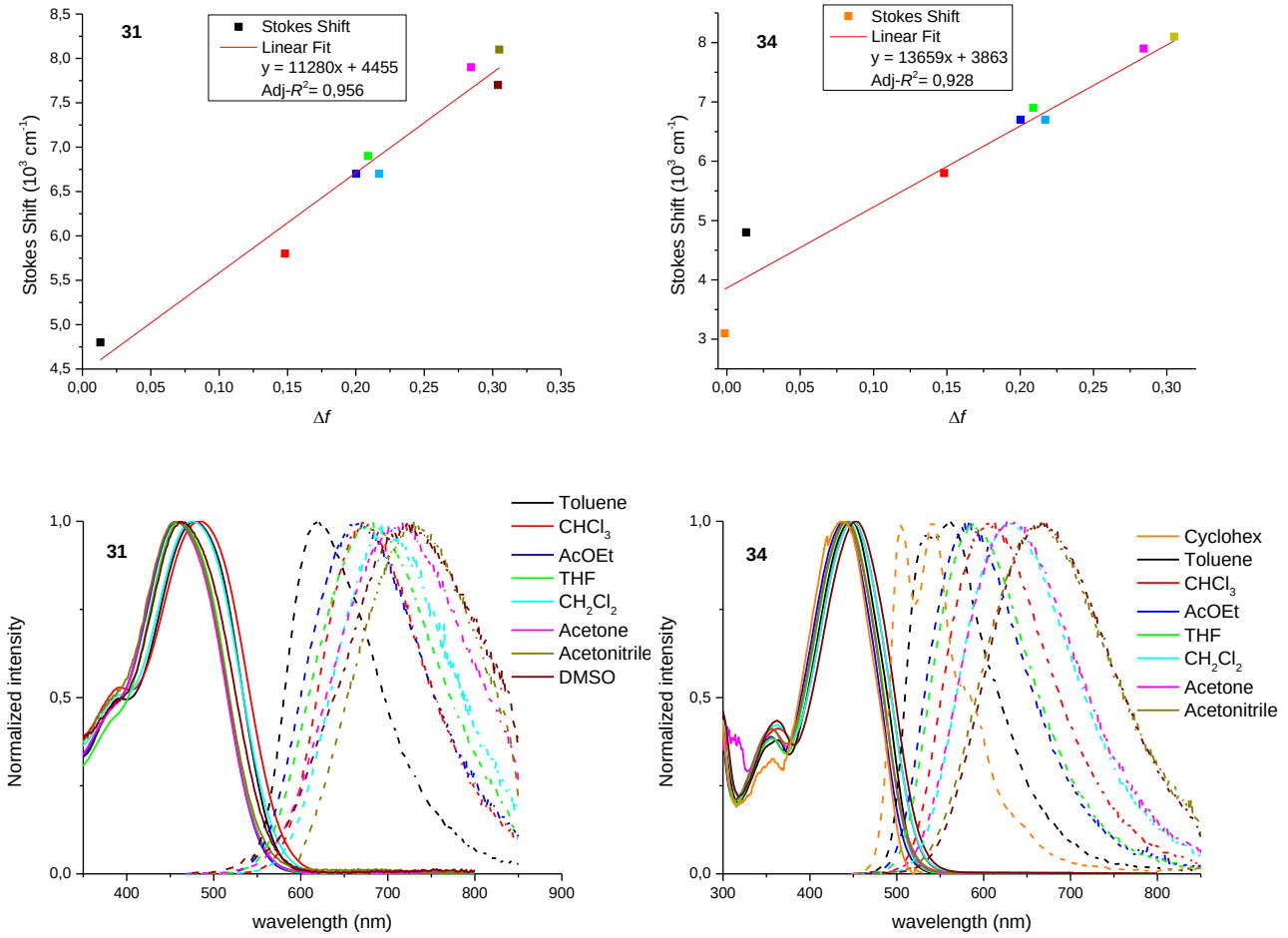

Figure 4.9 Top: Lippert's plots of **31** (left) and **34** (right). Bottom: normalized absorption (solid line) and emission spectra (dotted lines) of **31** (left) and **34** (right) in different polarity organic solvents. Consistent color code for each chromophore.

Such dipolar dyes that exhibit pronounced ICT character can be very interesting for two-photon absorption (2PA) process because, as previously discussed, two-photon cross sections can be usually enhanced by extending the π-conjugative path or increasing the difference between the ground and the excited state dipole moments, by playing on the nature of the donor and acceptor groups. Furthermore the large Stokes shift displayed by the chromophores is highly recommended for bioimaging. That, combined to red-shifted emission

in polar solvent (e.g., over 700 nm for **31** in DMSO, Figure 4.9), make them potentially useful for imaging application as red-NIR emitters and therefore worthy of investigation about their nonlinear optical properties.

4.5 Non linear optical properties in organic solvent

2PA spectra of **31** and **34** in THF solutions are reported in the following figure.

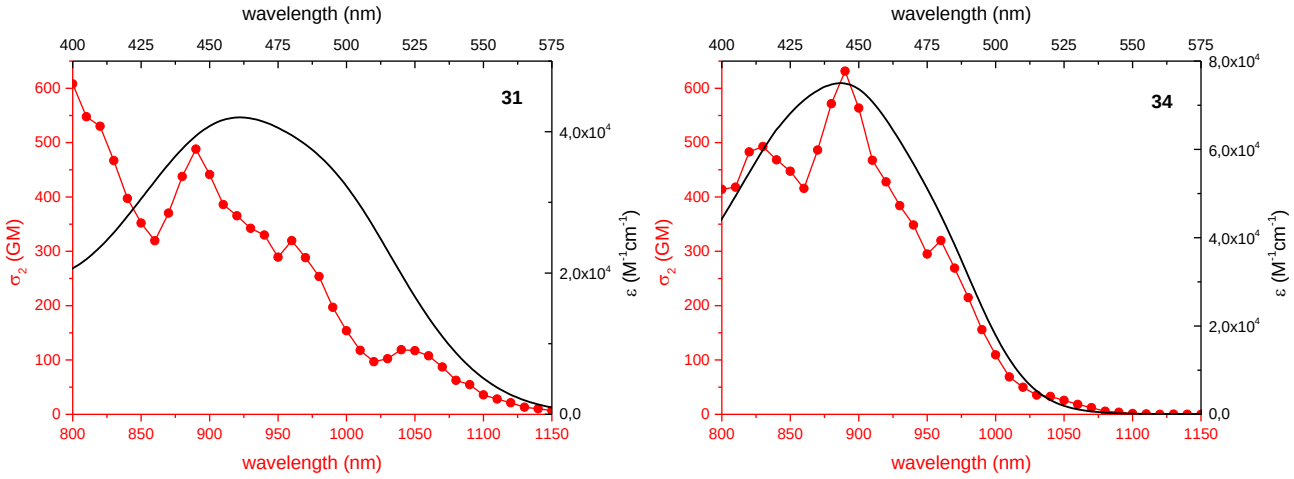

Figure 4.10 2P (red lines) and 1P (black lines) absorption spectra of **31** (left) and **34** (right)

Due to its dipolar nature the chromophore **34** exhibits structured two-photon absorption bands at about twice λ_{max}^{1PA}, corresponding to charge transfer transition with maximum at 890 nm, to which the two-photon cross section is equal to 640 GM (Table 4.4).

Cpd	$2\lambda_{max}^{1PA}$ [nm]	λ_{max}^{2PA} [nm]	$\sigma_2{}^{max}$ [GM]
31	926	890	480
		960	320
		1050	115
34	886	830	490
		890	640

Table 4.4

Concerning **31**, it displays absolute maximum below 800 nm, that could be ascribed to a transition allowed both under 1P and 2P irradiation. It seems less probable than the ICT band under 1P excitation and more probable than the latter one under 2P irradiation. In fact 1P absorption spectrum of **31** in THF solution clearly

displays a shoulder at about 390 nm; however the 2PA spectrum was not recorded below 800 nm due to technical reasons. Regarding its more intense band in 1PA spectrum (with maximum at 463 nm), the 2PA spectrum exhibits a structured band at about twice λ_{max}^{1PA}, with a relative maximum at 890 nm and two-photon cross section equals to 480 GM. Both compounds exhibited a certain response towards 2PA process which represents a positive feature, leaving room for any structural modifications, aiming to improve their efficiency as red-NIR emitting 2P absorbers.

In the following section we are going to discuss the consequences of the confinement in aggregated state of the two chromophores in water, and the photophysical properties of their NPs.

4.6 Aggregated state

The possibility to achieve an H-bond between **31** and **34** aims to promote the molecular proximity in aggregated state, thus it could play an important role in the packing of the molecules in NPs. As mentioned in the example in the section 4.1[25], this could also affect possible energy transfer processes between the chromophores in confined state. Moreover the opportunity of H-bond could favor the formation of NPs made from both chromophores by direct reprecipitation method (one step), providing an alternative to the sequential reprecipitation (two steps) used for the preparation of core-shell NPs[28]. Absorption and emission spectra of NPs made from **31** and **34** by the routine reprecipitation method are reported in the following figure.

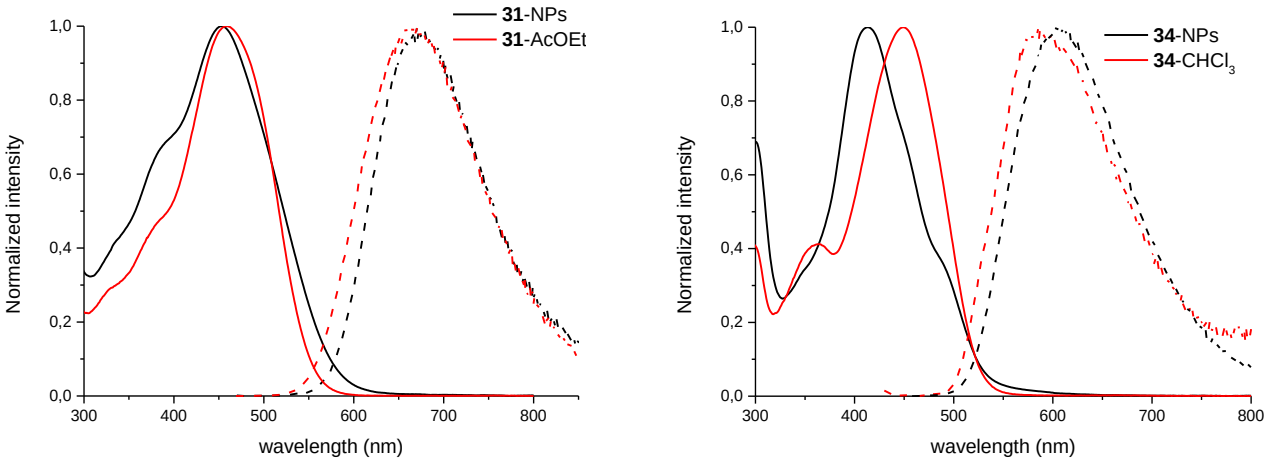

Figure 4.11 Normalized absorption (solid line) and emission (dotted line) spectra of **31** (left) and **34** (right) in aggregated state (black) and organic solvent solution (red)

One can observe that in aggregated state compound **31** exhibits broad absorption band from violet to green region with maximum at 452 nm and emission in the red part of the spectrum with its maximum at 666 nm (Table 4.5). Comparing the emission spectra obtained in NPs in water with the ones of the dye in ethyl acetate, one can notice that they show high similarity, suggesting that in aggregated state dye molecules experience an environment with polarity similar to ethyl acetate (Figure 4.9). Furthermore the broadening of the absorption band in NPs can be ascribed to exciton coupling in the aggregated state, which is promoted by molecular proximity.

Cpd	λ_{max}^{abs} [nm]	ε^{max} [10^4 $M^{-1}cm^{-1}$]	λ_{max}^{ems} [nm]	Φ_F	Stokes Shift [10^3 cm^{-1}]	$\tau^{(e)}$ [ns]	ζ-pot [mV]
31	452	4.7	666	0.02[a, b]	7.1	0.6 (70%) 2.0 (27%)	-67
34	413	6.2	607	0.01[c, d]	7.7	0.4 (88%) 2.4 (12%)	-37

Standard reference : [a]DCM in EtOH (Φ_F=0.437); [b]CV in Methanol (Φ_F=0.54); [c]Rhodamine 6G in EtOH (Φ_F=0.94); [d]Fluorescein in NaOH 0.1M (Φ_F=0.90); [e]λ^{exc} =455nm

Table 4.5

Concerning compound **34**, its absorption is located in the violet-blue region with its maximum at 413 nm, whereas its emission is mainly located in the orange region with its maximum at 607 nm, which corresponds to the emission registered in chloroform solution. In this case the shape of the absorption spectrum is most changed, in particular it can be observed that the absorption maximum underwent a net blue shift. It is also possible to distinguish two shoulders, one at about the same wavelength of the maximum registered in $CHCl_3$ and the other slightly red-shifted. This leaves hypothesize an exciton coupling with prevalence of H-type aggregates. This situation appears to be more pronounced for the chromophore **34**, in fact in its case the reduction of fluorescence quantum yield from organic solvent solution to NPs in water is more pronounced compared to **31** (which has lower Φ_F in solution). Note that for both, the passage to the aggregated state determines an increase of the Stokes shift (comparing to the data registered in THF solution). The hypothesis of dominating H-aggregates may be rationalized by considering the structures of the dyes; in particular the fact that the uracile moiety of **31** bears a nonyl chain on a nitrogen atom that may prevent the molecular packing, could lead to lower formation of H-aggregates.

Finally considering the absorption molar coefficients in THF solution (the solvent chosen for the characterization of the chromophores), the shift to NPs in water determines an hypochromic effect for **34** and a slight hyperchromic one for **31** (Figure 4.12).

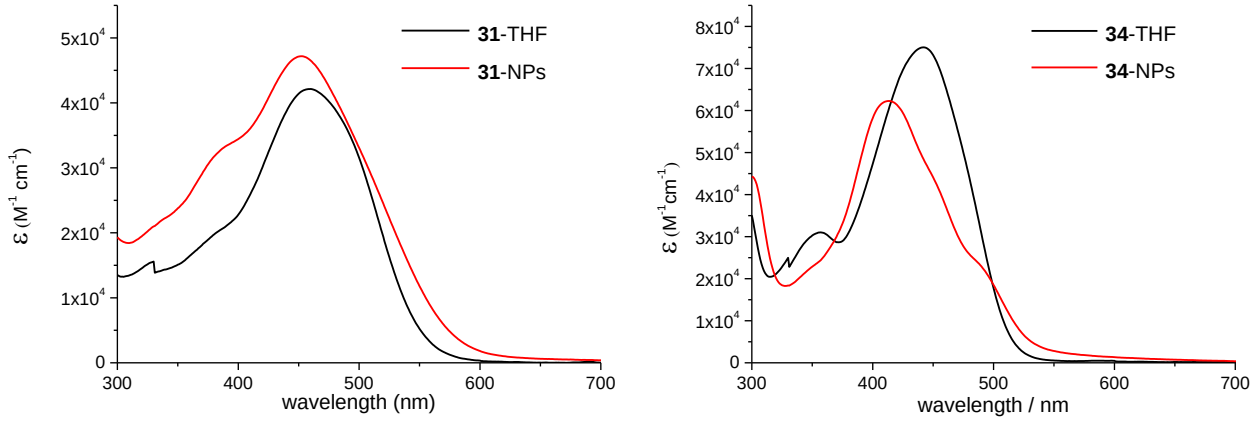

Figure 4.12 Molar absorptivity of dyes in THF solution (black lines) and NPs state (red lines)

These NPs, as well as the ones studied in the second chapter, exhibit biexponential lifetime decays, suggesting the presence of an external layer in contact with water characterized by shorter lifetime, and an internal region which is not in touch with the latter, and therefore displaying a longer lifetime.

Both the NPs show negative values of ζ-potential (more pronounced for NPs made from **31**) which suggest an organization of the external layer with triazine and uracil moieties pointing towards interface, with possibility to establish H-bonds with water. As a consequence a study of the stability of these NPs was performed by monitoring of absorption and emission spectra overtime (Figure 4.13).

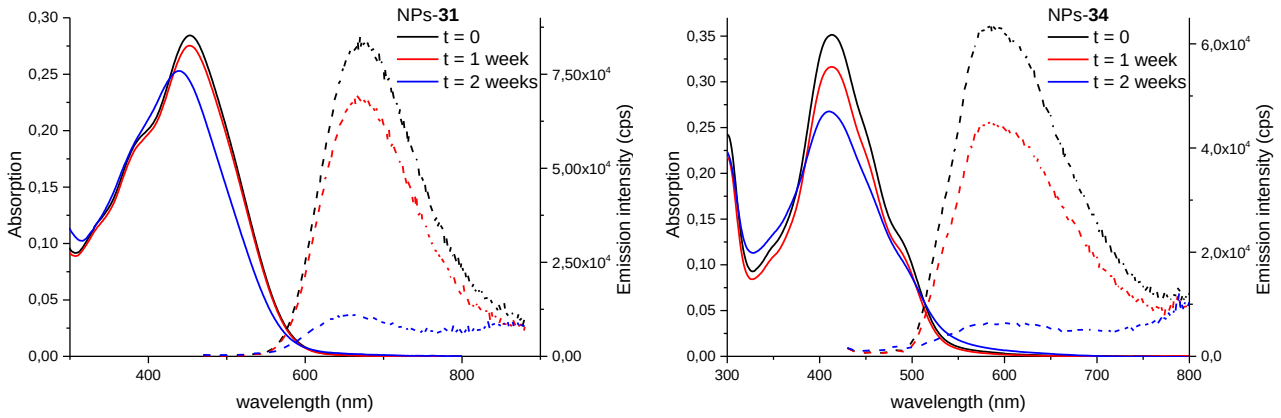

Figure 4.13 Monitoring overtime of NPs

NPs made from **34** display a certain colloidal stability over two weeks, with a moderate flattening of the absorption spectra, concomitant to a pronounced reduction of the emission intensity. Concerning the NPs made from **31** the situation is rather similar, but with less flattening of the absorption spectra than in the previous case, in agreement with the higher value of ζ-potential measured (Tab. 4.5)

As previously mentioned (section 4.1) the overlap of the emission spectra of the donor with the absorption one of the acceptor is a critical requirement in order to get energy transfer between two species; this condition is satisfied in the case of the two dyes under study, in particular the emission spectra of **34** partially overlaps the absorption one of **31**, both in aggregated state (Figure 4.14).

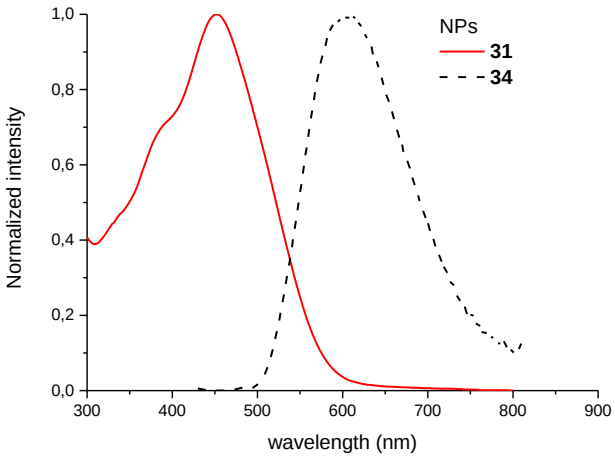

Figure 4.14 Normalized absorption (solid red line) spectrum of **31** and emission (dotted black line) one of **34**, both in aggregated state

Thus we have tried to prepare nanoparticles containing both chromophores **31** and **34** and study their chemical and physical properties.

4.7 Energy transfer in two components NPs

The protocol for the preparation of the NPs from the two components (NPs-**2C**) is an adaptation of the reprecipitation method used for the other NPs in this manuscript. An equimolar solution of the two chromophores in THF was made and then was slowly added to a large volume of milliQ water. In the Figure 4.15 is reported the absorption spectra of the NPs so produced, with the ones of NPs made from pure **31** and **34**. It's important to underline that according to the procedures used, the concentrations of **31** and **34** in the THF solution used for the manufacturing of the NPs-**2C** are the half of the ones used for the single component

NPs, whereas the conditions of the reprecipitation are the same, including the volume of THF added to water (same volume too). Thus the preparation of NPs-**2C** was done by means of a THF solution of **31** and **34** (0.5 mM each), whereas for NPs-**31** or NPs-**34**, the concentration of chromophore was 1 mM. The phenomena that leads to the formation of the nanoparticles by reprecipitation method are rather wide and complex, involving thermodynamic and kinetic features[29], and depends by several factors (e.g., nature of the organic solvent used, temperature, concentration of the chromophore). Moreover in the case of the batch **2C** the scenario is complicated by the presence of two chemical species, therefore the approach described for the preparation of NPs-**2C** aims to maintain these conditions as similar as possible to those used for the preparation of the batches NPs-**31** and NPs-**34**, in order to allow some comparisons between their photophysical properties.

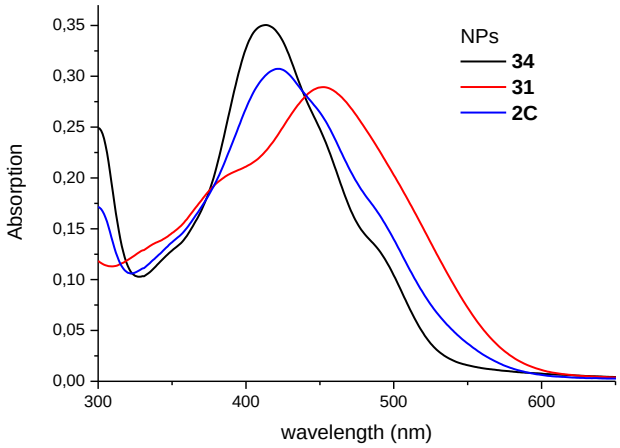

Figure 4.15 Absorption spectra of NPs made from pure one (**31**, **34**) and two components (**2C**)

The absorption spectra of the NPs-**2C** exhibits λ_{max}^{abs}= 423 nm and it clearly recalls the sum of the ones of NPs made from **31** and **34**; however in the hypothesis that the NPs-**2C** are formed by both components, we need some more investigations. In particular we must consider that if the NPs-**2C** are constituted by both the chromophores, it means that each of these experiences a different environment than the one in the respective NPs made from single component (precisely because there is also the presence of the other chromophore). In order to study this idea, a new batch of NPs (NPs-**mix**) was prepared by mixing equal volumes of pure NPs-**31** and pure NPs-**34**. Note that its absorption spectrum is compared with ones of NPs-**2C** and to a computed one (NPs-**computed**) obtained by the average of the absorption spectra of NPs-**31** and NPs-**34**.

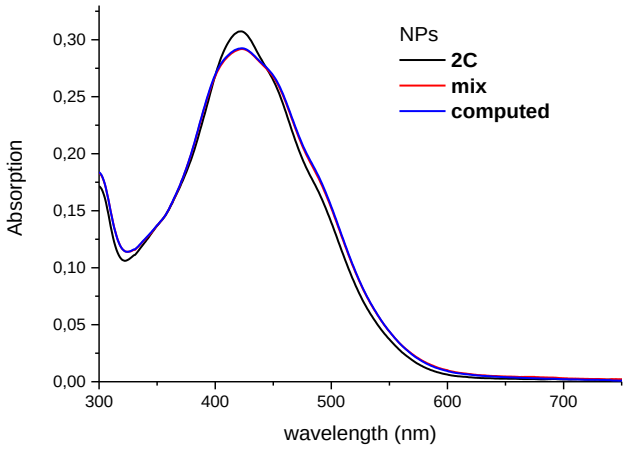

Figure 4.16 Absorption spectra of **2C** and **mix** NPs batches with the **computed** one

The figure 4.16 suggests that the nanoparticles of the **2C** type could be composed of both chromophores **31** and **34**. In fact its absorption spectrum although similar to that of the **mix** batch displays some deviations, while the latter turns out to be perfectly superimposable to the **computed** one. This effect may be due to the confinement of the two dyes in the same nanoparticles, resulting in a good spatial proximity. At this point one can proceed with investigation of the fluorescence properties, looking at emission spectrum of NPs-**2C** compared to the ones of NPs made from **31** and **34**.

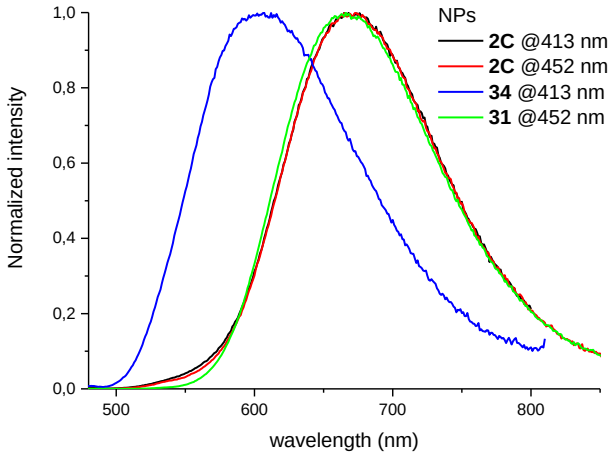

Figure 4.17 Normalized emission spectra of NPs made from single component (excited at their respectively λ_{max}^{abs}) and **2C** type

From the normalized spectra one can observe that exciting the **2C** batch at 413 nm and 452 nm (respectively the absorption maxima registered for NPs made from **34** and **31**) the emission in both cases clearly recalls the

one obtained from NPs-**31**, with λ_{max}^{ems}= 672 nm. For completeness it is reported that the fluorescence quantum yield for the NPs-**2C** as a result of excitation at 413 nm or 452 nm, in both cases is equal to 0.02 (standard: DCM in EtOH, Φ_F= 0.437).

Further information can be drawn from the analysis of the same non normalized emission spectra reported in the figure 4.18, wherein it has been added also the emissions related to the batch NPs-**mix**, excited in the same illumination conditions and at the same wavelengths used for the batch **2C**, in order to allow a comparison.

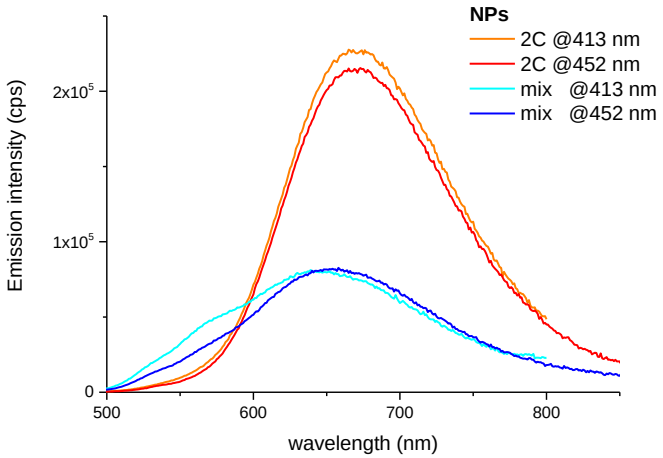

Figure 4.18 Emission spectra of NPs-**2C** and **mix** ones

The spectra related to the **mix** batch are more flat and broad than the **2C** ones and, upon excitation at absorption maxima of **31** and **34** in aggregated state, they clearly display an emission given by the sum of the two dyes, which are confined in different NPs and therefore spatial separated. In fact upon excitation at 452 nm (λ_{max}^{abs} of NPs-**31**) both the chromophores have similar molar extinction coefficients, respectively 4.3 10^4 $M^{-1}cm^{-1}$ for **34** and 4.7 10^4 $M^{-1}cm^{-1}$ for **31** (Figure 4.12). Then the emission spectra (blue one) is dominated by the fluorescence of **31**, which has the higher fluorescence quantum yield (in single component NPs, Table 4.4), with a small shoulder below 600 nm due to the emission of **34**. Upon excitation at 413 nm (λ_{max}^{abs} of NPs-**34**) the difference between the molar extinction coefficients increases, becoming equal to about 6.2 10^4 $M^{-1}cm^{-1}$ for **34** and 3.7 10^4 $M^{-1}cm^{-1}$ for **31** (Figure 4.12), inducing an enhancement of the shoulder below 600 nm (cyan spectrum) comparing to the previous one (blue). Here the emission spectra is composed of the emissions of both species, but in a more balanced manner.

Concerning the **2C** batch, upon excitation at 452 nm, one can observe the enhancement of the emission intensity (red spectrum) comparing to the **mix** one (blue spectrum), furthermore it appears rather sharp, without evidence of the shoulder below 600 nm ascribable to the emission of the specie **34**; in practice, as mentioned, the emission seems to be given only by the species **31**. So far it could be argued that the emission of **34** in the **2C** NPs type, could simply be quenched by processes such as photoinduced proton transfer. About that the emission spectrum of the **2C** batch upon excitation at 413 nm gives clues about the situation, especially considering that the chromophore **31** exhibits, at this wavelength, lower molar extinction coefficient than at 452 nm, whereas a similar emission intensity is observed upon excitation at the two mentioned wavelenghts. All these factors point out an energy transfer process from the donor (**34**) to the acceptor (**31**) in aggregated state, due to promoted proximity between the donor-acceptor pair that could be ascribable to H-bond between the species.

4.8 Conclusion

In this chapter two new dipolar chromophores bearing two H-bonding complementary subunits have been prepared and characterized. The synthetic approach was based on a linear path that started from simple aniline and led to the common aldehyde precursor (**28**); thus the triazine derivative (**34**) was obtained with high stereoselectivity by means of a HWE reaction followed by cyclization of nitrile group. Instead the uracil derivative (**31**) involved the use of an homologation followed by a Sonogashira cross coupling. The optical properties of the species were investigated in organic solvents. Then they have been used for the preparation of NPs in water by the reprecipitation method. In aggregated state the two chromophores display suitable properties for energy transfer process, exhibiting partial overlap of the emission spectra of **34** with the absorption one of **31**. Two components NPs (**2C**) were prepared by reprecipitation too, and simple photophysical studies of their absorption and emission spectra compared to the ones of single component NPs, suggest an energy transfer process between the two chromophores in the aggregated state. This leads to believe that the strategy to use two molecules that could be able to interact with each other by H-bond, to promote energy transfer in NPs made from them, seems to work. However some more studies must be performed in order to better understand the nature of the H-bond between the dyes and its effect on the properties of two components NPs.

Bibliographic references

[1] E. Arunan, R. Desiraju Gautam, A. Klein Roger, J. Sadlej, S. Scheiner, I. Alkorta, C. Clary David, H. Crabtree Robert, J. Dannenberg Joseph, P. Hobza, G. Kjaergaard Henrik, C. Legon Anthony, B. Mennucci, J. Nesbitt David, in *Pure Appl. Chem.* **2011**, *83*, 1619.

[2] T. Steiner, *Angew. Chem. Int. Ed.* **2002**, *41*, 48-76.

[3] K. Morokuma, *Acc. Chem. Res.* **1977**, *10*, 294-300.

[4] G. R. Desiraju, *Acc. Chem. Res.* **2002**, *35*, 565-573.

[5] G. A. Jeffrey, *An Introduction to Hydrogen Bonding*, Oxford University Press: New York and Oxford, **1997**.

[6] R. E. Hubbard, M. Kamran Haider, *Hydrogen Bonds in Proteins: Role and Strength*, John Wiley & Sons, Ltd, **2001**.

[7] J. K. Myers, C. N. Pace, *Biophys. J.* **1996**, *71*, 2033-2039.

[8] C. N. Pace, H. Fu, K. L. Fryar, J. Landua, S. R. Trevino, D. Schell, R. L. Thurlkill, S. Imura, J. M. Scholtz, K. Gajiwala, J. Sevcik, L. Urbanikova, J. K. Myers, K. Takano, E. J. Hebert, B. A. Shirley, G. R. Grimsley, *Protein Sci.* **2014**, *23*, 652-661.

[9] J. D. Watson, F. H. C. Crick, *Nature* **1953**, *171*, 737-738.

[10] J. L. Sessler, C. M. Lawrence, J. Jayawickramarajah, *Chem. Soc. Rev.* **2007**, *36*, 314-325.

[11] J.-M. Lehn, *Angew. Chem. Int. Ed.* **1988**, *27*, 89-112.

[12] J.-M. Lehn, *Science* **2002**, *295*, 2400.

[13] G. R. Desiraju, *Nature* **2001**, *412*, 397-400.

[14] W. P. J. Appel, M. M. L. Nieuwenhuizen, E. W. Meijer, in *Supramolecular Polymer Chemistry*, Wiley-VCH Verlag GmbH & Co. KGaA, **2011**, pp. 1-28.

[15] C. Bilton, F. H. Allen, G. P. Shields, J. A. K. Howard, *Acta Crystallogr. Sect. B* **2000**, *56*, 849-856.

[16] F. H. Allen, W. D. Samuel Motherwell, P. R. Raithby, G. P. Shields, R. Taylor, *New J. Chem.* **1999**, *23*, 25-34.

[17] G. Simundza, T. D. Sakore, H. M. Sobell, *J. Mol. Biol.* **1970**, *48*, 263-278.

[18] J.-M. Lehn, M. Mascal, A. Decian, J. Fischer, *J. Chem. Soc., Chem. Commun.* **1990**, 479-481.

[19] J. A. Zerkowski, C. T. Seto, G. M. Whitesides, *J. Am. Chem. Soc.* **1992**, *114*, 5473-5475.

[20] J. A. Zerkowski, J. P. Mathias, G. M. Whitesides, *J. Am. Chem. Soc.* **1994**, *116*, 4305-4315.

[21] J. A. Zerkowski, J. C. MacDonald, G. M. Whitesides, *Chem. Mat.* **1997**, *9*, 1933-1941.

[22] J. P. Mathias, C. T. Seto, E. E. Simanek, G. M. Whitesides, *J. Am. Chem. Soc.* **1994**, *116*, 1725-1736.

[23] R. F. M. Lange, F. H. Beijer, R. P. Sijbesma, R. W. W. Hooft, H. Kooijman, A. L. Spek, J. Kroon, E. W. Meijer, *Angew. Chem. Int. Ed.* **1997**, *36*, 969-971.

[24] R. F. M. Lange, E. W. Meijer, in *Supramolecular polymer chemistry based on multiple hydrogen bonding*, Wiley-VCH Verlag GmbH, **1999**, 72-77.

[25] B. Balan, C. Vijayakumar, S. Ogi, M. Takeuchi, *J. Mater. Chem.* **2012**, *22*, 11224-11234.

[26] Y.-Z. Chen, L.-Z. Wu, C.-H. Tung, Q.-Z. Yang, *Lect. N. Chem.* **2015**, *88*, 1-42.

[27] L. L. Gogin, E. G. Zhizhina, Z. P. Pai, V. N. Parmon, *Chemistry for Sustainable Development* **2009**, *17*, 331-339.

[28] J. Daniel, C. Mastrodonato, A. Sourdon, G. Clermont, J.-M. Vabre, B. Goudeau, H. Voldoire, S. Arbault, O. Mongin, M. Blanchard-Desce, *Chem. Commun.* **2015**, *51*, 15245-15248.

[29] V. K. LaMer, R. H. Dinegar, *J. Am. Chem. Soc.* **1950**, *72*, 4847-4854.

General Conclusion

General Conclusion

In this manuscript several new fluorescent molecules for bioimaging purposes have been developed, aiming to get control of their chemical and physical properties by playing on their chemical structures.

In the second chapter we synthesized four new quadrupolar dyes which satisfy the requirements of ideal two-photon ratiometric pH probes, such as large 2PA response in the biological spectral window, ratiometric behavior and pKa close to physiological pH. The latter one was achieved by exploiting the quadrupolar effect due to the structure of the dyes, therefore avoiding chemical modifications of the endgroups. Furthermore all of them display considerable 2P brightness both in basic and acidic conditions, even for deep red emitter **4**, making them very promising for monitoring of slight pH variations in biological environments, subcellular imaging and detection of cancer cells.

In the third chapter a mixed linear and divergent approach of synthesis was performed in order to develope a large series of fluorescent dyes with specific structural variations, allowing to get a wide tuning of their optical properties. The NPs prepared by them were deeply studied and displayed very interesting features for bioimaging, such as giant two-photon cross section (10^6 GM for FONs made from **Ia**) combined to deep red-NIR emission (FONs made from **IIb** and **IIIb**).

Finally in the fourth chapter, an articulated synthesis of two new dipolar chromophores containing two complementary acceptor groups was performed. With idea to take advantage from H-bond to promote molecular proximity in aggregated state, two-components NPs by direct reprecipitation method were prepared and a preliminary study of their optical properties suggested an energy transfer between the two dyes, leaving for further improvements of their features, aimed at making efficient NPs for bioimaging purposes.

Target Molecules

Chapter 2

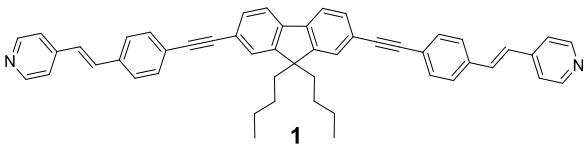

1

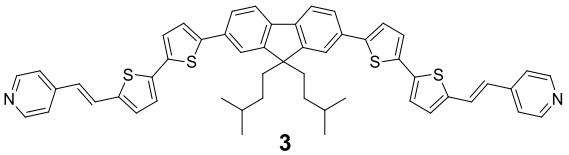

3

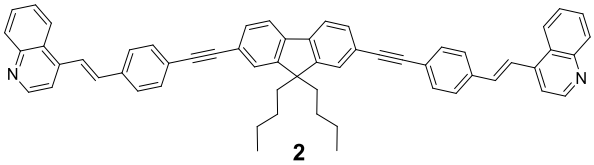

2

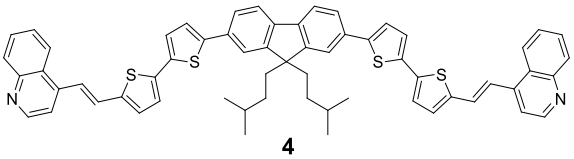

4

Chapter 3

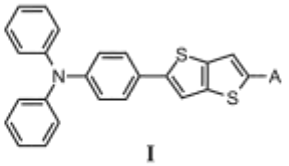

I

A: —CHO

a

b

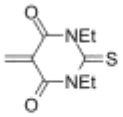

c

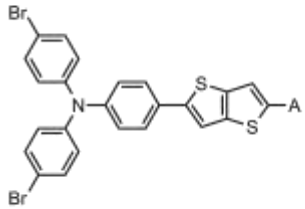

II

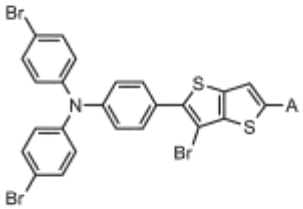

II'

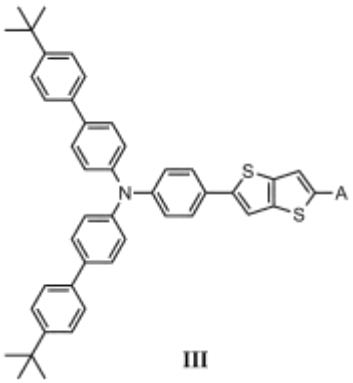

III

Chapter 4

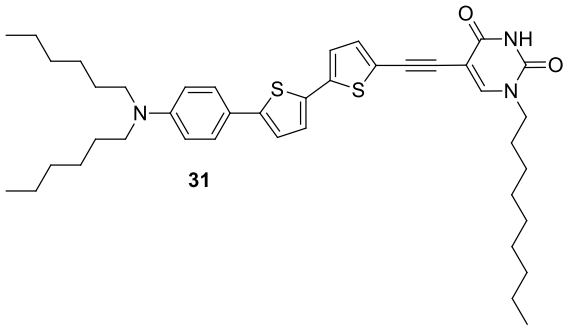

31

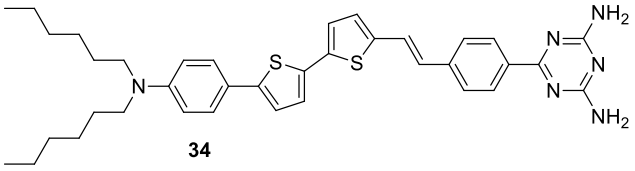

34

Experimental Part

E.1 Material and general procedures

Commercially available reagents (purchased from Aldrich, Alfa Aesar and TCI) were used without further purification. Dry solvents were distilled from the appropriate drying reagents immediately before use. All air - or water - sensitive reactions were carried out under argon. Reactions were monitored by thin layer chromatography on Merck silica gel 60 F254 precoated aluminium sheets. Column chromatography were carried out on Merck silica gel Si 60 (40–63 mm, 230–400 mesh or 63–200 mm, 70–230 mesh). Melting points were measured on Stuart SMP 10 or Electrothermal IA9300. DSC measures were carried out on Mettler Toledo DSC 1 STAReSystem. ^{1}H and ^{13}C NMR spectra were recorded on Bruker ARX 200 or Avance 200 (^{1}H: 200.13 MHz, ^{13}C: 50.31 MHz), Avance AV 300 (^{1}H: 300.19 MHz, ^{13}C: 75.47 MHz), Avance AV 400 (^{1}H : 400.25 MHz, ^{13}C : 100.63 MHz), Avance AV 500 (^{1}H : 499.89 MHz, ^{13}C : 125.68 MHz), Avance AV 600 (^{1}H : 599.95 MHz, ^{13}C : 150.83 MHz). Chemical shifts (δ) are given in parts per million with respect to solvent residual peak and coupling constants (*J*) are given in Hertz. High and low resolution mass spectra measurements were performed at the Centre Régional de Mesures Physiques de l'Ouest (C.R.M.P.O., Rennes) using a Micromass MS/MS ZABSpec TOF instrument or by CESAMO (Bordeaux, France), on a TOF mass spectrometer AccuTOFGCv using an FD emitter with an emitter voltage of 10 kV. Elemental analyses were performed at C.R.M.P.O or at "Institut de Chimie des Substances Naturelles" (Gif-sur-Yvette, France). pH of water solutions were measured on a Tacussel PHN81 instrument with a glass combined electrode and a saturated KCl calomel electrode as reference.

E.2 Photophysical studies

All photophysical studies have been performed with freshly prepared air-equilibrated solutions at room temperature (298 K). UV/Vis absorption spectra were recorded on Jasco V-570 or Jasco V-670 spectrophotometer. Steady-state fluorescence measurements were performed on dilute solutions (optical density < 0.1) contained in standard 1 cm quartz cuvettes using a Fluoromax spectrofluorometer or an Edinburgh Instruments (FLS920), and time-resolved fluorescence measurements were carried out on a Fluorolog spectrofluorometer. Fluorescence quantum yields of dilute dye solutions and of the FONs suspensions were measured according to literature procedures[1-2] using Nile Blue in EtOH (Φ_F = 0.27,

λ_{exc}= 541 nm), Cresyl Violet in MeOH (Φ_F = 0.54, λ_{exc}= 570 nm), Indocyanine Green in DMSO (Φ_F = 0.11, λ_{exc}= 678 nm), Rhodamine-6G in EtOH (Φ_F = 0.94, λ_{exc}= 488 nm), Fluorescein in NaOH 0.1 M (Φ_F = 0.9, λ_{exc}= 474 nm) depending on the emission range[3]. Fluorescence decays were measured in a time-correlated single photon counting (TCSPC) configuration, under excitation from a NanoLED (370 nm, 455 nm or 570 nm). The instrument response was determined by measuring the light scattered by a Ludox suspension. The lifetime values were obtained from the reconvolution fit analysis of the decays profiles; the quality of the fits was judged by the reduced χ^2 value ($0.9 < \chi^2 < 1.1$).

E.3 Two-photon absorption

Two-photon absorption cross sections (σ_2) were determined from the two-photon excited fluorescence (TPEF) ($\sigma_2\Phi_F$), measured at room temperature on air-equilibrated solutions, and the fluorescence quantum yield (Φ_F). TPEF cross sections were measured relative to Fluorescein in 0.01 M aqueous NaOH in the 690-1000 nm spectral range and relative to Nile Red in DMSO in the 1000-1160 nm spectral range, using the method described by Xu and Webb[4] and the appropriate solvent-related refractive index corrections. Reference values between 700 and 715 nm for Fluorescein were taken from literature. The quadratic dependence of the fluorescence intensity on the excitation power was checked at all wavelengths. Measurements were conducted using an excitation source delivering fs pulses. This allows avoiding excited-state absorption during the pulse duration a phenomenon, which has been shown to lead to overestimated two-photon absorption cross-section values. To scan the 680-1080 nm range, a Nd:YVO4-pumped Ti:Sapphire oscillator was used generating 140 fs pulses at a 80 MHz rate. To span the 1000–1400 nm range, an OPO (PP-BBO) was added to the setup to collect and modulate the output signal of the Ti:Sapphire oscillator. The excitation was focused into the cuvette through a microscope objective (10X, NA 0.25). The fluorescence was detected in epifluorescence mode via a dichroic mirror (Chroma 675dcxru) and a barrier filter (Chroma e650sp-2p) by a compact CCD spectrometer module BWTek BTC112E. Total fluorescence intensities were obtained by integrating the corrected emission.

E.4 Determination of pKa values

The pH of solutions of probes (10^{-6} M) in micellar water (SDS/butanol/water, 6 : 5 : 89 wt%) were tuned by addition of solutions of HCl (1.0 and 0.1 M) and NaOH (1.0 and 0.1 M) using a microsyringe. The values of pKa_{obs} were determined via ratiometric titrations, fitting the data with the following equation[5-6]:

$$R = \frac{R_{min} Ka\ I + R_{max} 10^{-pH}}{Ka\ I + 10^{-pH}}$$

Equation E.1

Wherein R is ratio of the the emission intensities (or absorption) at the two wavelengths chosen, therefore $R = F(\lambda^1_{ems})/F(\lambda^2_{ems})$ in emission ratiometric mode or $R = A(\lambda^1_{abs})/A(\lambda^2_{abs})$ in absorption ratiometric mode. R_{min} and R_{max} represent the limiting values of R respectively in basic and acidic conditions ($R_{min} = \lim_{[H+]\to 0} R$ and and $R_{max} = \lim_{[H+]\to \infty}$). I is the ratio of the emission intensities (or absorption) measured in basic conditions to the ones measured in acidic environment, at the wavelenght chosen for the denominator of R, therefore $I = F_{min}(\lambda^2_{ems}) / F_{max}(\lambda^2_{ems})$ in emission ratiometric mode or $I = A_{min}(\lambda^2_{abs}) / A_{max}(\lambda^2_{abs})$ in absorption ratiometric mode.

E.5 Synthesis and characterizations

2,7-Diiodo-9*H*-fluorene (5)[7]

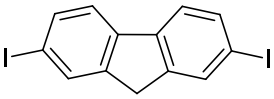

Procedure: A solution of fluorene (20.00 g, 120.38 mmol), acetic acid (100 mL), concentrated sulphuric acid (2.8 mL) and water (7 mL), was heated at 75°C. Then periodic acid (7.00 g, 30.71 mmol) and iodine (16.00 g, 63.04 mmol) were added. After 1h at 75°C, acetic acid (100 mL), periodic acid (6.44 g, 28.25 mmol) and iodine (16.00 g, 63.04 mmol) were added and the mixture was heated at 75°C for 1h more, then cooled to room temperature. CH_2Cl_2 was added and the mixture was neutralized with NaOH (3 M) until basic pH. The organic layer was washed with a saturated aqueous sodium thiosulfate solution, dried over $MgSO_4$ and then evaporated under reduced pressure. The crude product was recrystallized from heptane to yield 40.23 g (80%) of **5** as yellow solid.

Characterization: ^{1}H NMR (200.13 MHz, $CDCl_3$): δ 7.88 (s, 1H), 7.71 (d, *J* = 8.1 Hz, 2H), 7.50 (d, *J* = 8.1 Hz, 2H), 3.84 (s, 2H).

9,9-Dibutyl-2,7-diiodo-9*H*-fluorene (6)[8]

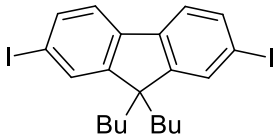

Procedure: A solution of n-Bu_4NBr (0.93 g, 2.88 mmol) and KOH (8.06 g, 143.76 mmol) in water (8 mL) was heated at 65°C. **5** (6.02 g, 14.40 mmol) and 1-bromobutane (9.3 mL, 86.10 mmol) dissolved in toluene (15 mL) were then added to the basic solution and heated at 65°C for 1h. The organic layer was extracted with CH_2Cl_2, dried over $MgSO_4$, filtered and evaporated in vacuo. The residue was purified by column chromatography (heptane) to yield 6.86 g (90%) of **6** as a white solid.

Characterization: ^{1}H NMR (200.13 MHz, $CDCl_3$): δ 7.65 (dd, *J* = 8.3 Hz, *J* = 1.7 Hz, 2H), 7.64 (d, *J* = 1.7 Hz, 2H), 7.40 (d, *J* = 8.3 Hz, 2H), 1.90 (m, 4H), 1.08 (m, 4H), 0.68 (t, *J* = 7.3 Hz, 6H), 0.56 (m, 4H); ^{13}C NMR (75.47 MHz, $CDCl_3$): δ 152.5, 139.7, 136.0, 132.0, 121.5, 93.1, 55.4, 39.9, 25.8, 22.9, 13.7.

2,7-Bis(trimethylsilylethynyl)-9,9-dibutyl-9*H*-fluorene (7)[9]

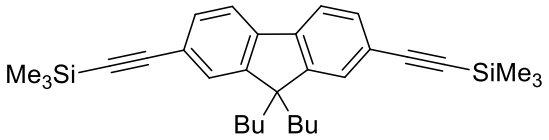

Procedure: Air was removed from a solution of **6** (2.00 g, 3.77 mmol) in toluene/Et_3N (1:1, 40 mL) by blowing argon for 20 min. Then CuI (0.03 g, 0.15 mmol), $Pd(PPh_3)_2Cl_2$ (0.11 g, 0.15 mmol) and ethynyltrimethylsilane (1.3 mL, 9.43 mmol) were added and the mixture was stirred at 40 °C for 16 h. The solvents were evaporated and the residue was purified by column chromatography (heptane) to yield 1.40 g (79%) of the title compound.

Characterization: m.p.= 180°C (decomposition); ^{1}H NMR (200.13 MHz, $CDCl_3$): δ 7.64 (d, *J* = 7.5 Hz, 2H), 7.48 (d, *J* = 7.5 Hz, 2H), 7.46 (s, 2H), 1.98 (m, 4H), 1.08 (m, 4H), 0.69 (t, *J* = 7.3 Hz, 6H), 0.55 (m, 4H), 0.33 (s, 18H); ^{13}C NMR (75.47 MHz, $CDCl_3$): δ 150.9, 140.9, 131.3, 126.2, 121.8, 119.9, 106.1, 94.3, 55.2, 40.2, 25.8, 23.1, 13.8, 0.1; elemental analysis calcd (%) for $C_{31}H_{42}Si_2$: C, 79.08, H, 8.99; found: C, 78.88, H, 9.12; HRMS (EI) m/z calcd for $C_{31}H_{42}Si_2$ [$M^{+\cdot}$]: 470.2825; found: 470.2848.

9,9-Dibutyl-2,7-diethynyl-9*H*-fluorene (8)

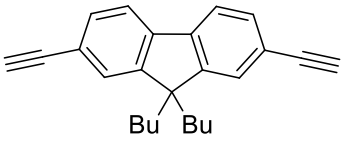

Procedure: To a solution of **7** (0.86 g, 1.83 mmol) in THF/MeOH (3:1, 44 mL) was added aqueous KOH (1 M, 13 mL), and the mixture was stirred at room temperature for 30 min. CH_2Cl_2 and water were added and the organic layer was separated. The aqueous layer was extracted with CH_2Cl_2, and the combined organic layers were dried over Na_2SO_4. The residue obtained after removal of the solvents was purified by column chromatography using heptane/CH_2Cl_2 (8:2) as eluent to yield 0.50 g (84%) of **8**.

Characterization: m.p.= 93 °C; ^{1}H NMR (200.13 MHz, $CDCl_3$): δ 7.63 (d, *J* = 8.6 Hz, 2H), 7.48 (d, *J* = 8.6 Hz, 2H), 7.46 (s, 2H), 3.15 (s, 2H), 1.94 (m, 4H), 1.07 (m, 4H), 0.67 (t, *J* = 7.2 Hz, 6H), 0.54 (m, 4H). ^{13}C NMR (50.31 MHz, $CDCl_3$): δ 151.0, 140.9, 131.2, 126.5, 120.8, 119.9, 84.5, 77.4, 55.1, 40.0, 25.8, 22.9, 13.7; elemental analysis calcd (%) for $C_{25}H_{26}$ (326.48): C, 91.97; H, 8.03; found: C, 92.17; H, 8.07; HRMS (EI) m/z calcd for $C_{25}H_{26}$ [$M^{+\cdot}$]: 326.2035; found: 326.2036.

^{1}H NMR

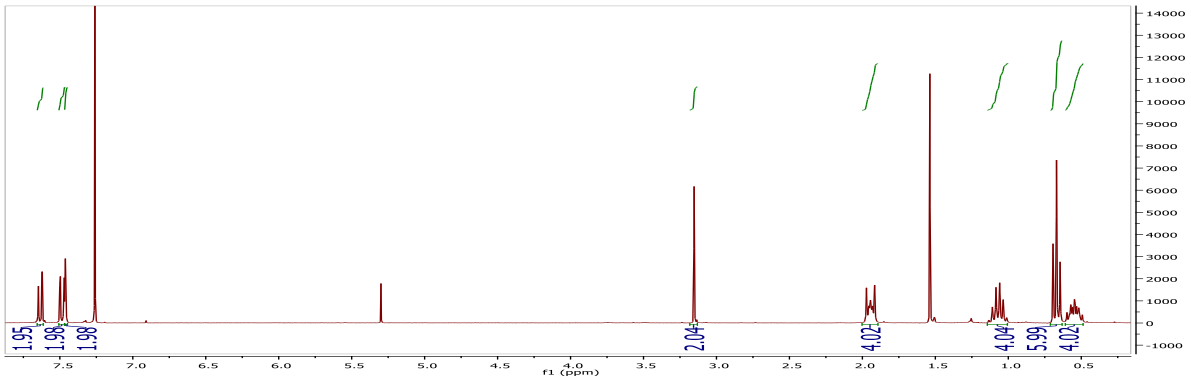

4,4'-(9,9-Dibutyl-9*H*-fluorene-2,7-diyldi-2,1-ethynediyl)bisbenzaldehyde (9)

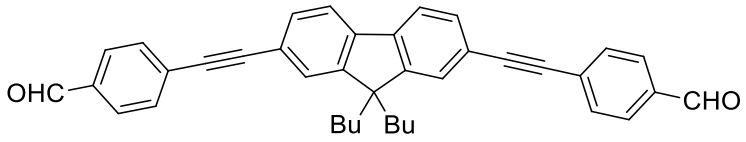

Procedure: Air was removed from a solution of **8** (251 mg, 0.77 mmol) and 4-bromobenzaldehyde (354 mg, 1.914 mmol) in toluene/Et_3N (4:1, 10 mL) by blowing argon for 20 min. Then CuI (6 mg, 0.031 mmol) and $Pd(PPh_3)_2Cl_2$ (22 mg, 0.03 mmol) were added, and argon blowing was continued for 10 min. Thereafter the mixture was stirred at 40 °C for 16 h. The solvent was evaporated in vacuo, and the crude product was purified by column chromatography using heptane/CH_2Cl_2 (gradient from 50:50 up to 40:60) as eluent to yield 307 mg (75%) of **9**.

Characterization: m.p.= 199 °C (dec.); ^{1}H NMR (300.19 MHz, $CDCl_3$): δ 9.94 (s, 2H), 7.80 (d, *J* = 8.4 Hz, 4H), 7.63 (d, *J* = 8.4 Hz, 4H), 7.62 (d, *J* = 8.7 Hz, 2H), 7.48 (d, *J* = 8.7 Hz, 2H), 7.46 (s, 2H), 1.94 (m, 4H), 1.05 (m, 4H), 0.60 (t, *J* =7.2 Hz, 6H), 0.53 (m, 4H); ^{13}C NMR (75.47 MHz, $CDCl_3$): δ 191.3, 151.2, 141.1, 135.4, 132.0, 131.1, 129.6, 126.2, 121.4, 120.3, 94.5, 89.2, 55.3, 40.2, 25.9, 22.9, 13.8; elemental analysis calcd (%) for $C_{39}H_{34}O_2$ + 0.25 CH_2Cl_2 (555.93): C, 84.80; H, 6.26; found: C, 84.87; H, 6.94. HRMS (ESI) m/z calcd for $C_{39}H_{35}O_2$ [$(M+H)^+$]: 535.2637, found 535.2638.

^{1}H NMR

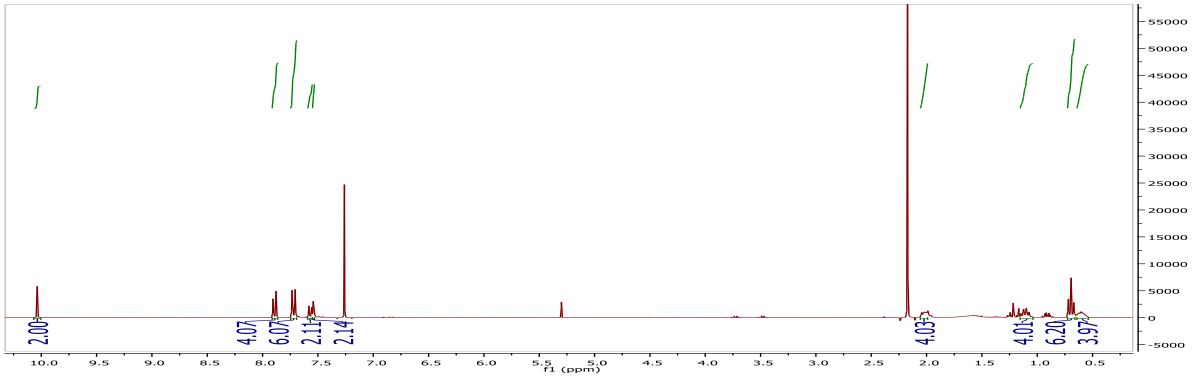

4,4'-((1*E*,1'*E*)-(((9,9-dibutyl-9*H*-fluorene-2,7-diyl)bis(ethyne-2,1-diyl))bis(4,1-phenylene))bis (ethene-2,1-diyl))dipyridine (1) and 4,4'-((1*E*,1'*E*)-(((9,9-dibutyl-9*H*-fluorene-2,7-diyl)bis(ethyne-2,1-diyl))bis(4,1-phenylene))bis(ethene-2,1-diyl))diquinoline (2)

General procedure: Air was removed from a solution of **9** (20 mg, 0.037 mmol) and 2.05 equiv of phoshine oxide (**10** or **11**) in THF (5 ml) by blowing argon for 20 min. Then NaH (4 mg, 95%) was added. The mixture was stirred at room temperature for 24 hours after which TLC revealed complete conversion. Water was added to the reaction mixture and extracted with CH_2Cl_2. The organic layer was washed with brine then dried over Na_2SO_4, filtered and evaporated in vacuo. The resulting crude yellow solids were repeatedly washed with EtOH then dried under vacuum. 20.8 mg of **1** (81.2%) and 23.3 mg of **2** (79.5%) were obtained.

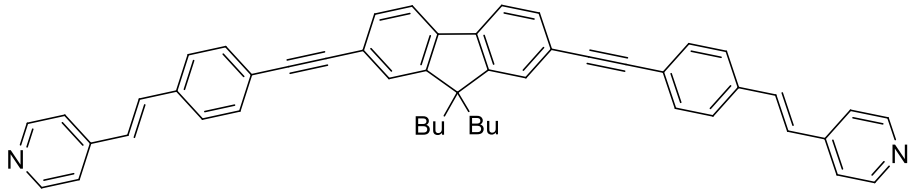

Characterization (1): m.p.= 178°C (dec.) ; ^{1}H NMR (300.19 MHz, $CDCl_3$): δ 8.60 (d, *J* = 6.2 Hz, 4H), 7.70 (d, *J* = 7.9 Hz, 2H), 7.62-7.52 (m, 12H), 7.38 (d, *J* = 6.2 Hz, 4H), 7.31 (d, *J* = 16.3 Hz, 2H), 7.06 (d, *J* = 16.3 Hz, 2H), 2.02 (m, 4H), 1.11 (m, 4H), 0.70 (t, *J* = 7.2 Hz, 6H), 0.61 (m, 4H); ^{13}C NMR (75.47 MHz, $CDCl_3$): δ 151.3, 148.8, 141.0, 135.8, 135.7, 133.9, 132.2, 131.0, 127.3, 126.3, 124.2, 121.9, 121.3, 120.2, 92.4, 89.8, 55.4, 40.3, 26.0, 23.2, 13.9; elemental analysis calcd (%) for $C_{51}H_{44}N_2$ + 1.5 H_2O: C, 86.04; H, 6.65; N, 3.93 found: C, 86.42; H, 6.65; N, 3.79. HRMS (ESI) calcd m/z for $C_{51}H_{45}N_2$ [$(M+H)^+$]: 685.3577, found 685.3575.

^{1}H NMR (1)

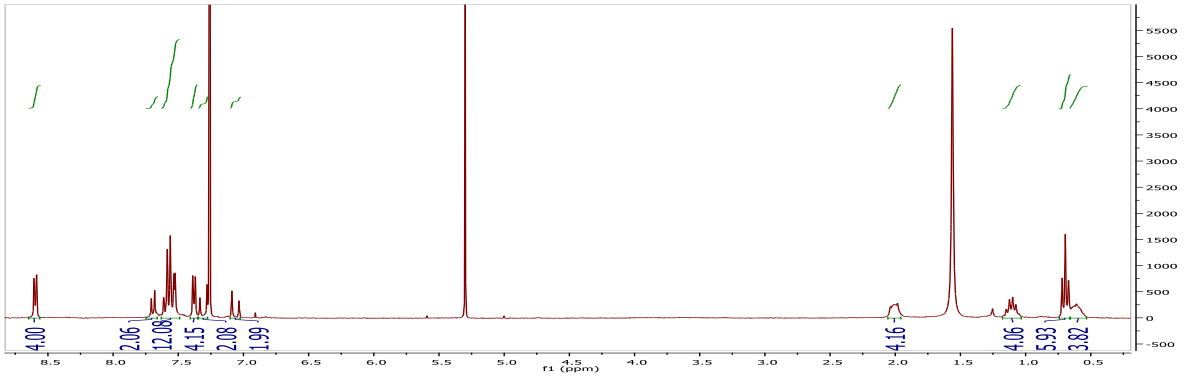

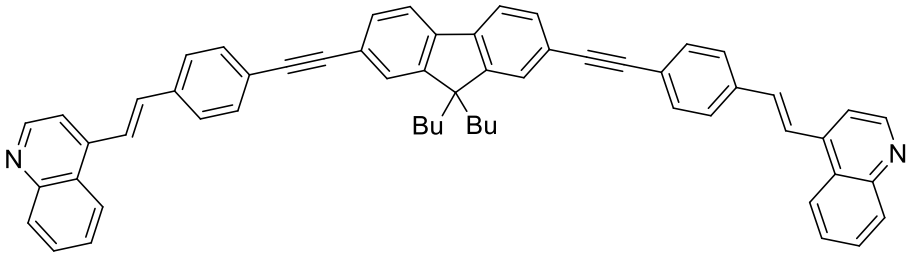

Characterization (2): m.p.=140 °C (dec.); ^{1}H NMR (300.19 MHz, $CDCl_3$): δ 8.92 (s, 2H), 8.25 (d, *J* = 8.4 Hz, 2H), 8.17 (d, *J*= 8.4 Hz, 2H), 7.89 (d, *J* = 16.2 Hz, 2H), 7.75-7.54 (m, 20H), 7.37 (d, *J* = 16.2 Hz, 2H), 2.01 (m, 4H), 1.11 (m, 4H), 0.70 (t, *J* = 7.2 Hz, 6H), 0.60 (m, 4H); ^{13}C NMR (125.68 MHz,$CDCl_3$): δ 151.3, 150.2, 148.7, 143.0, 141.0, 136.5, 134.6, 132.2, 131.0, 130.2, 129.6, 127.3, 126.8, 126.5, 126.1, 123.9, 123.8, 123.6, 122.0, 120.2, 117.2, 92.5, 90.2, 55.6, 40.7, 26.3, 23.5, 14.3; elemental analysis calcd (%) for $C_{59}H_{48}N_2$ + 0.75 CH_2Cl_2: C, 84.56; H, 5.88; N, 3.30 found: C, 84.11; H, 6.35; N, 3.24; HRMS (ESI) m/z calcd for $C_{59}H_{49}N_2$ [$(M+H)^+$]: 785.3890, found 785.3895.

^{1}H NMR (2)

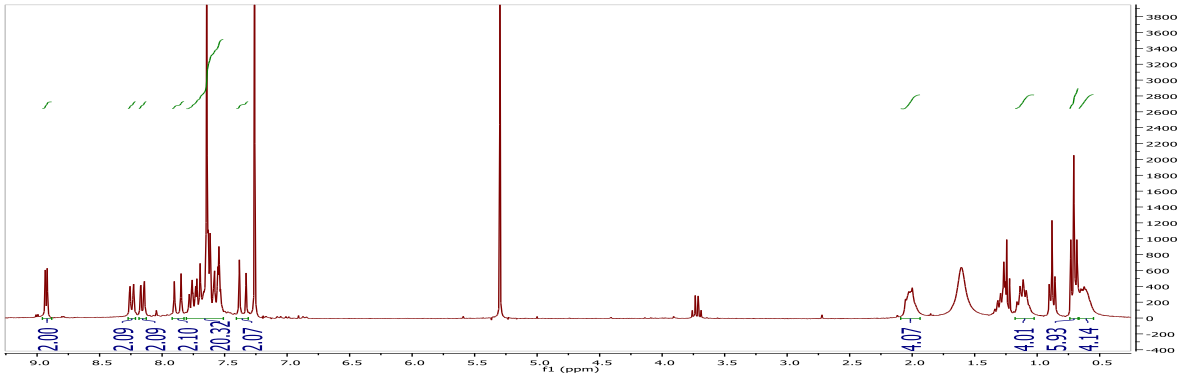

2,7-diiodo-9,9-diisopentyl-9*H*-fluorene (12)

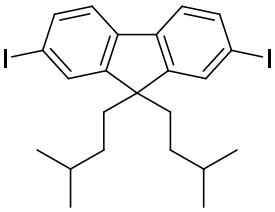

Procedure: A solution of n-Bu_4NBr (155 mg, 0.48 mmol) in 3 ml of KOH_{aq} (8 M) was stirred for 15 minutes. **5** (1.0 g, 2.40 mmol) and 1-bromo-3-methylbutane (1.72 ml, 14.40 mmol) dissolved in toluene (2.4 ml) were added and the solution was heated up to 65°C for 2 hours. The mixture was cooled to room temperature and stirred for 24 hours. After addition of water and extraction with CH_2Cl_2, the organic layer was dried over $MgSO_4$, filtered and evaporated by vacuum. The residue was purified by chromatography column (petroleum ether) affording 589 mg of **12** as a pale yellow solid (44%).

Characterization: m.p. = 127°C (dec.); ^{1}H NMR (400.25 MHz, $CDCl_3$): δ 7.64-7.66 (m, 2H), 7.61-7.63 (m, 2H), 7.41 (d, *J*= 8.0 Hz, 2H), 1.86-1.93 (m, 4H), 1.25-1.33 (m, 2H), 0.69 (d, *J*= 6.6 Hz, 12H), 0.39-0.45 (m, 4H); ^{13}C NMR (151 MHz, $CDCl_3$): δ 152.5, 139.9, 136.1, 132.0, 121.7, 93.3, 55.3, 38.1, 32.4, 28.3, 22.5; HRMS (EI) m/z calcd for $C_{23}H_{28}I_2$ [$M^{+\cdot}$]: 558.0280, found 558.0275.

^{1}H NMR

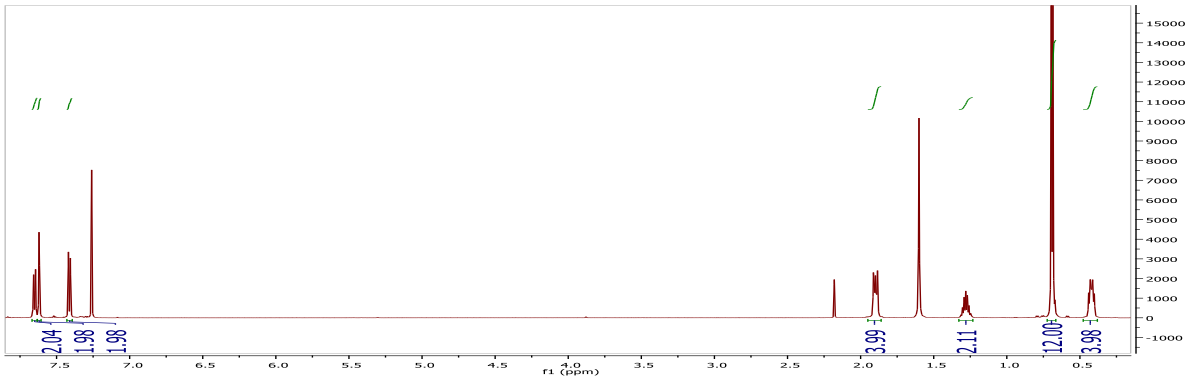

5',5'''-(9,9-diisopentyl-9*H*-fluorene-2,7-diyl)bis([2,2'-bithiophene]-5-carbaldehyde) (13)

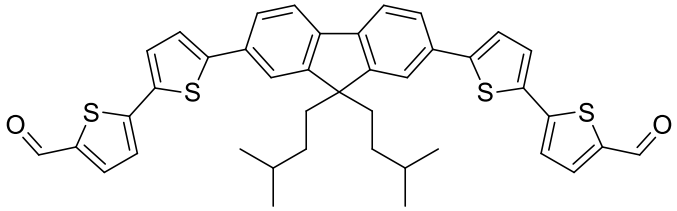

Procedure: 12 (500 mg, 0.90 mmol) and (5'-formyl-[2,2'-bithiophen]-5-yl)boronic acid (643 mg, 2.7 mmol) were transferred into a flask under Argon. A mixture of toluene/MeOH = 3:2 (degassed by blowing Ar for 30 minutes) was added until completely dissolution. K_2CO_3 (1.64 g, 11.8 mmol) and Pd(dppf)Cl_2 (147 mg, 0.18 mmol) was added and the mixture was heated up to 70 °C for 48 hours. After addition of water and extraction with CH_2Cl_2 the organic phase was dried over Na_2SO_4 and concentrated by vacuum. The residue was purified by chromatography column (CH_2Cl_2) affording 240 mg of **13** as orange solid (39%).

Characterization: m.p. = 208°C (decomp.); ^{1}H NMR (300.49 MHz, CD_2Cl_2): δ 9.86 (s, 2H), 7.68-7.76 (m, 4H), 7.60-7.67 (m, 4H) 7.36-7.44 (m, 4H), 7.32 (d, *J*= 3.9 Hz, 2H), 2.05-2.20 (m, 4H), 1.24-1.40 (m, 2H), 0.71 (d, *J*= 6.6 Hz, 12H), 0.48-0.62 (m, 4H); ^{13}C NMR (75.47 MHz, CD_2Cl_2): δ 182.8, 152.3, 147.1, 147.0, 142.0, 141.3, 137.9, 135.2, 133.0, 127.6, 125.3, 124.6, 124.5, 120.8, 120.3, 55.6, 38.5, 33.0, 28.6, 22.5; IR (KBr): ν= 1662 cm^{-1} (C=O); HRMS (FD) m/z calcd for $C_{41}H_{38}O_2$ [$M^{+\cdot}$]: 690.1755, found 690.1763.

^{1}H NMR

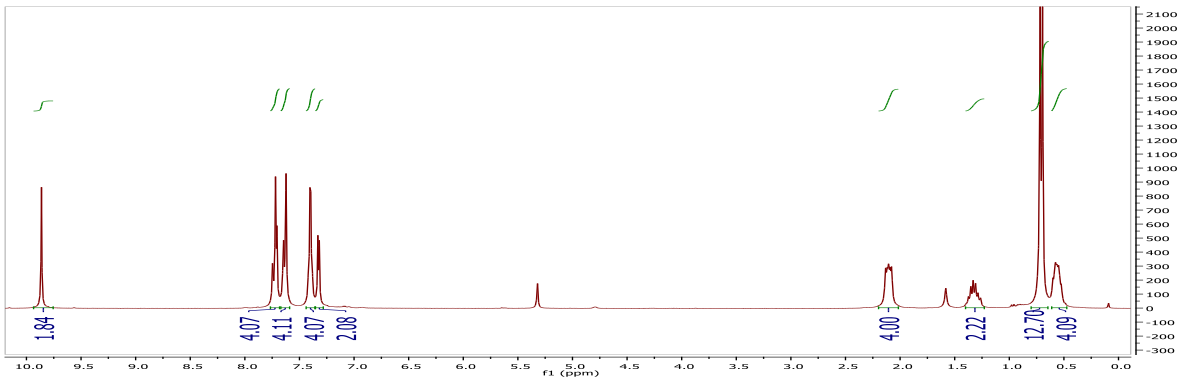

4,4'-((1*E*,1'*E*)-(5',5'''-(9,9-diisopentyl-9*H*-fluorene-2,7-diyl)bis([2,2'-bithiophene]-5',5-diyl))bis(ethene-2,1-diyl))dipyridine (3)

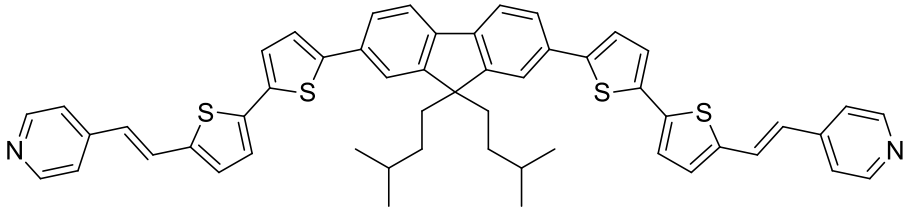

Procedure: Air was removed from a solution of **13** (30 mg, 0.043 mmol) and 1.02 eq. of **10** in THF (5 ml) by blowing argon for 20 min. Then NaH (4 mg, 95%) was added. The mixture was stirred at room temperature for 24 hours then poured into ice; after melting the suspension was centrifuged and the residue was purified by chromatography column (CH_2Cl_2:MeOH = 93:7) affording 23 mg of **3** as a reddish powder (64%).

Characterization: m.p. = 249°C (decomp.); ^{1}H NMR (300.19 MHz, $CDCl_3$): δ 8.53-8.60 (m, 4H), 7.74-7.77 (m, 2H), 7.59-7.64 (m, 2H), 7.53-7.56 (m, 2H), 7.39 (d, *J*= 16.0 Hz, 2H), 7.29-7.35 (m, 6H), 7.23 (d, *J*= 3.7 Hz, 2H), 7.13 (d, *J*= 3.7 Hz, 2H), 7.09 (d, *J*= 3.7 Hz, 2H), 6.79 (d, *J*= 16.0 Hz, 2H), 1.99-2.11 (m, 4H), 1.28-1.38 (m, 2H), 0.71 (d, *J*= 6.6 Hz, 12H), 0.50-0.62 (m, 4H); ^{13}C NMR (75.47 MHz, CD_2Cl_2): δ 152.1, 150.2, 144.7, 144.6, 140.8, 140.7, 138.2, 136.2, 133.1, 129.9, 126.2, 125.6, 125.4, 124.9, 124.4, 124.2, 120.8, 120.6, 120.0, 55.4, 38.5, 32.8, 28.5, 22.5; IR (KBr): ν = 1619 cm-1 (C=C); HRMS (ESI) m/z calcd for $C_{53}H_{48}N_2S_4$ [$M^{+\cdot}$]: 840.2700, found 840.2715; elemental analysis calcd (%) for $C_{53}H_{48}N_2S_4$ + 0.56 CH_2Cl_2: C 72.38, H 5.57, N 3.15; found: C 72.34, H 5.82, N 3.13.

^{1}H-NMR

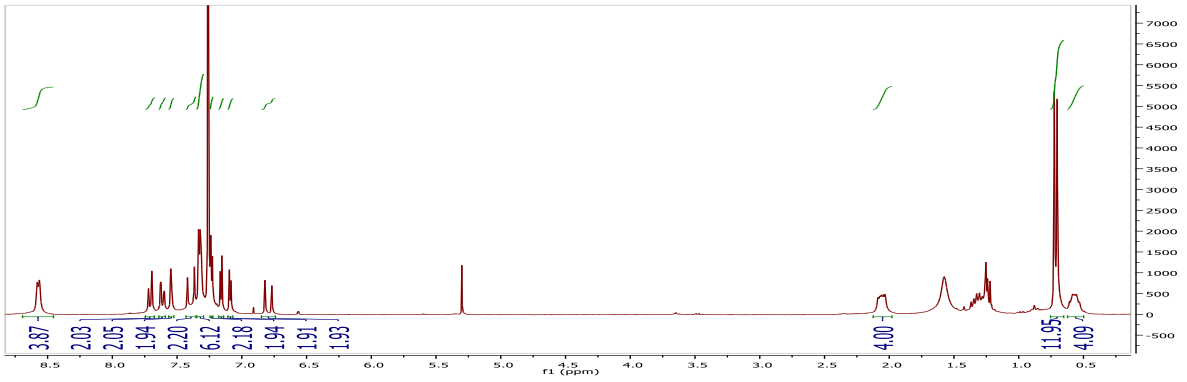

4,4'-((1*E*,1'*E*)-(5',5'''-(9,9-diisopentyl-9*H*-fluorene-2,7-diyl)bis([2,2'-bithiophene]-5',5-diyl))bis(ethene-2,1-diyl))diquinoline (4)

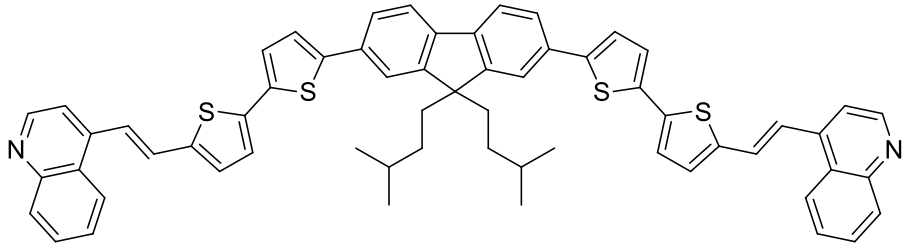

Procedure: Air was removed from a solution of **13** (30 mg, 0.043 mmol) and 1.02 eq. of **11** in THF (5 ml) by blowing argon for 20 min. Then NaH (4 mg, 95%) was added. The mixture was stirred at room temperature for 24 hours then poured into ice; after melting the suspension was centrifuged and the residue dried and crystallized from CH_2Cl_2/EtOH, affording 24 mg of **4** as a red powder (59%).

Characterization: m.p. = 145°C (decomp.); ^{1}H NMR (599.95 MHz, $CDCl_3$): δ 8.90 (d, *J*= 4.5Hz, 2H), 8.22-8.25 (m, 2H), 8.13-8.15 (m, 2H), 7.74-7.77 (m, 2H), 7.71-7.73 (m, 2H), 7.62-7.65 (m, 4H), 7.58-7.61 (m, 4H), 7.56-7.57 (m, 2H), 7.47 (d, *J*= 15.3 Hz, 2H), 7.35 (d, *J*= 3.8Hz, 2H), 7.27 (d, *J*= 3.7Hz, 2H), 7.20 (d, *J*= 3.7 Hz, 2H), 7.15 (d, *J*= 3.8 Hz, 2H), 2.04-2.10 (m, 4H), 1.29-1.38 (m, 2H), 0.73 (d, *J*= 6.6 Hz, 12H), 0.55-0.61 (m, 4H); ^{13}C NMR (150.83 MHz, CD_2Cl_2): δ 152.1, 150.4, 149.0, 144.8, 142.4, 141.2, 140.9, 138.3, 136.3, 133.1, 130.3, 130.0, 129.7, 127.8, 126.8, 126.3, 125.6, 125.0, 124.5, 124.3, 123.6, 121.9, 120.6, 120.1, 116.6, 55.5, 38.6, 32.9, 28.6, 22.5; IR (KBr): ν = 1615 cm-1 (C=C); HRMS (ESI) m/z calcd for $C_{61}H_{52}N_2S_4$ [$M^{+\cdot}$]: 940.3013, found 940.2999; elemental analysis calcd (%) for $C_{61}H_{52}N_2S_4$ + 0.40 CH_2Cl_2: C 75.61, H 5.46, N 2.87; found: C 75.55, H 5.31, N 2.61.

^{1}H NMR

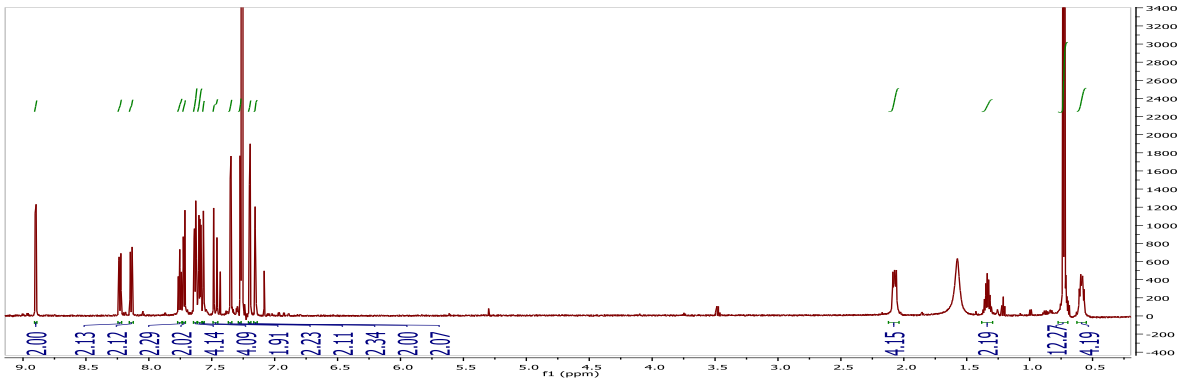

5-(4-(diphenylamino)phenyl)thieno[3,2-b]thiophene-2-carbaldehyde (14)

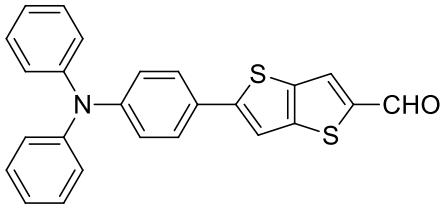

Procedure: To a solution of **1** (1.00 g, 3.450 mmol) in 16.0 ml of anhydrous and degassed toluene/MeOH mixture (1:1), 5-bromothieno[3,2-b]thiophene-2-carbaldehyde (0.812 g, 3.280 mmol), K_2CO_3 (1.13 g, 8.210 mmol), Pd(dppf)Cl_2 (134.0 mg, 0.154 mmol) were added and the mixture was stirred overnight at 75 °C. After cooling down to room temperature, the crude was concentrated and few milliliters of CH_2Cl_2 were added. The suspension was filtered and plenty rinsed with CH_2Cl_2. The filtered was purified by means of chromatography column (petroleum ether: CH_2Cl_2 = 6:4) obtaining 1.03 g of **14** as a yellow powder (76%).

Characterization: ^{1}H NMR (300.19 MHz, DMSO-d6): δ 9.95 (s, 1H), 8.37 (s, 1H), 7.87 (s, 1H), 7.65 (d, *J*= 8.5 Hz, 2H), 7.30-7.41 (m, 4H), 7.05-7.17 (m, 6H), 6.99 (d, *J*= 8.5 Hz, 2H).

^{1}H NMR

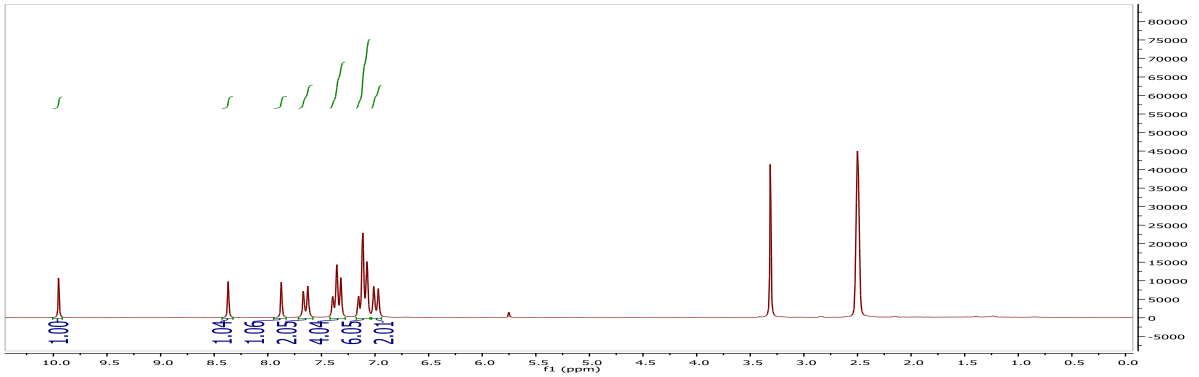

5-(4-(bis(4-bromophenyl)amino)phenyl)thieno[3,2-b]thiophene-2-carbaldehyde (15)

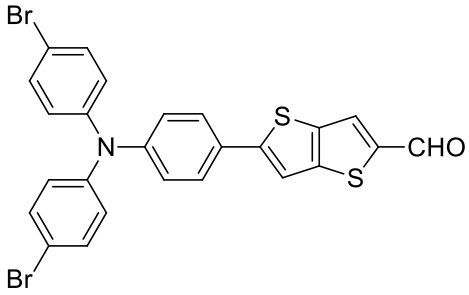

Procedure: To a solution of **14** (200.0 mg, 0.486 mmol) in 22.0 ml of anhydrous THF cooled at 0°C, NBS (176.5 mg, 0.991 mmol) was added and the mixture was stirred for 6 h. The solution was slowly warmed to room temperature and stirred for 12 h. 22.0 ml of water were added and extraction with CH_2Cl_2 was done. The organic layer was washed with $NaHCO_3$(sat), water, dried over Na_2SO_4 and filtered. Evaporation of the solvents gave a yellow powder which is purified by means of chromatography column (CH_2Cl_2), obtaining 244.0 mg of **15** as a yellow powder (88%).

Characterization: m.p./DSC= 204°C (dec.); ^{1}H NMR (200.13 MHz, acetone-d6): δ 10.01 (s,1H), 8.28 (s,1H), 7.84 (s,1H), 7.72 (d, *J*= 8.6 Hz, 2H), 7.51 (d, *J*= 8.8 Hz, 4H), 7.14 (d, *J*= 8.6 Hz, 2H), 7.09 (d, *J*= 8.8Hz, 4H); ^{13}C NMR (50.31 MHz, acetone-d6): δ 184.3, 152.9, 148.6, 147.3, 147.1, 145.7, 138.8, 133.5, 131.1, 129.4, 128.1, 127.3, 124.7, 116.9, 116.6; ATR (cm^{-1}): 1657 ν(C=O); HRMS (FD) calcd m/z for $C_{25}H_{15}Br_2NOS_2$ [$M^{+\cdot}$]: 566.8962, found: 566.8935; elemental analysis calcd (%) for $C_{25}H_{15}Br_2NOS_2$ + 0.04 CH_2Cl_2: C 52.51, H 2.65, N 2.45, found: C 52.25, H 2.59, N 2.58.

^{1}H NMR

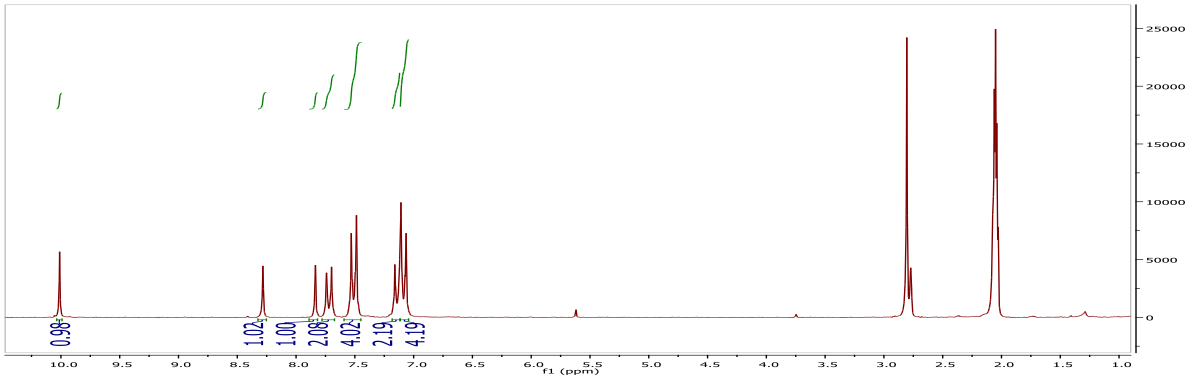

5-(4-(bis(4-bromophenyl)amino)phenyl)-6-bromothieno[3,2-b]thiophene-2-carbaldehyde (16)

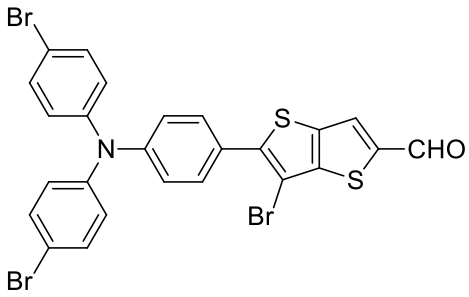

Procedure: To a solution of **14** (30.0 mg, 0.073 mmol) in 3.5 ml of anhydrous THF cooled at 0°C, NBS (43.0 mg, 0.240 mmol) was added and the mixture was stirred for 0.5 h. The solution was warmed to room temperature and stirred for 72 h. 4.0 ml of water were added and extraction with CH_2Cl_2 was done. The organic layer was washed with $NaHCO_3$(sat), water, dried over Na_2SO_4 and filtered. Evaporation of the solvents gave a yellow powder which is purified by means of a short pad of silica (CH_2Cl_2), obtaining 42.0 mg of **16** as a yellow powder (89%).

Characterization: m.p./DSC= 240°C (dec.); ^{1}H NMR (200.0 MHz, CD_2Cl_2): δ 9.96 (s,1H), 8.00 (s,1H), 7.64 (d, J=8.7 Hz, 2H), 7.43 (d, J=8.8 Hz, 4H), 7.11 (d, J= 8.7 Hz, 2H), 7.03 (d, J= 8.8 Hz, 4H); 13C NMR (150 MHz, CD2Cl2): δ 183.6, 155.7, 148.8, 148.4, 146.3, 146.1, 144.7, 135.6, 133.0, 130.3, 129.9, 126.9, 123.1, 117.0, 100.2; ATR (cm-1): 1663 ν(C=O); HRMS (FD) calcd m/z for $C_{25}H_{14}Br_3NOS_2$ [$M^{+\cdot}$]: 644.8067, found: 644.8062; elemental analysis calcd (%) for $C_{25}H_{14}Br_3NOS_2$: C 46.32, H 2.18, N 2.16, found: C 46.41, H 1.84, N 2.09.

^{1}H NMR

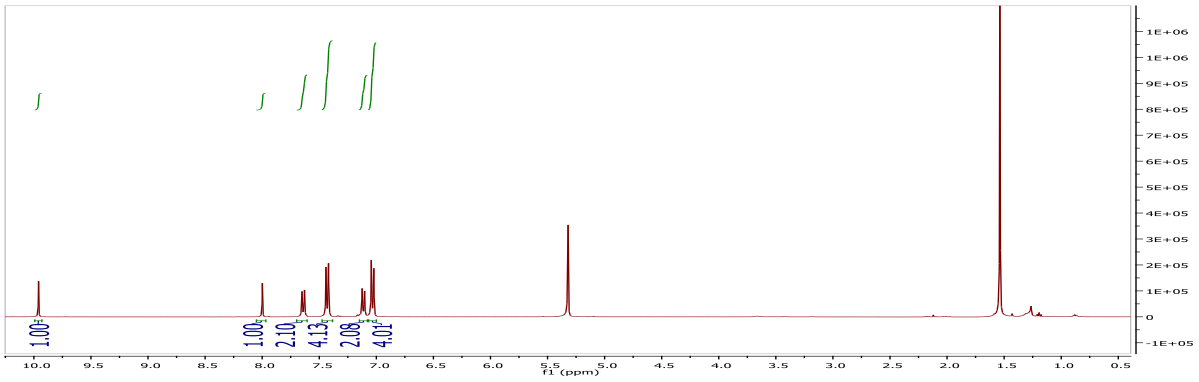

5-(4-(bis(4'-(tert-butyl)-[1,1'-biphenyl]-4-yl)amino)phenyl)thieno[3,2-b]thiophene-2-carbaldehyde (17)

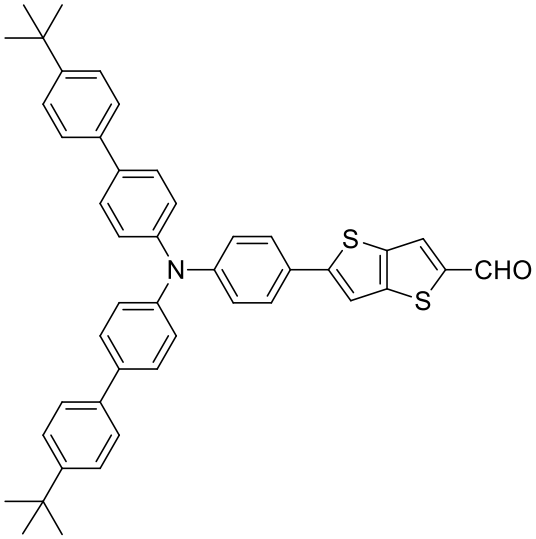

Procedure: Air was removed from a mixture of **15** (250.0 mg, 0.440 mmol), 4-tert-butylphenylboronic acid (215.0 mg, 1.208 mmol), Pd(dppf)Cl_2 (72.0 mg, 0.088 mmol) and K_2CO_3 (365.0 mg, 2.641 mmol) in 6.0 ml of toluene/MeOH (1:1) by blowing argon for 30 min. The mixture was warmed to 75°C for 24 h. The reaction was cooled to room temperature and quenched by addition of water. After extraction with CH_2Cl_2, drying over Na_2SO_4 and filtering through a short pad of Celite, the crude was concentrated under vacuum and purification was achieved by chromatography column using gradient elution (petroleum ether, petroleum ether:CH_2Cl_2 = 75:25, 60:40) to yield 211.0 mg of **17** as an orange powder (71%).

Characterization: m.p./DSC= 155°C (dec.); ^{1}H NMR (300.19 MHz, CD_2Cl_2): δ 9.96 (s,1H), 8.39 (s,1H), 7.92 (s,1H), 7.71 (d, *J*= 8.6 Hz, 2H), 7.65 (d, *J*= 8.5 Hz, 4H), 7.59 (d, *J*= 8.4 Hz, 4H), 7.47 (d, *J*= 8.4 Hz, 4H), 7.20 (d, *J*= 8.5 Hz, 4H), 7.13 (d, *J*= 8.6 Hz, 2H), 1.32 (s, 18H); ^{13}C NMR (75.47 MHz, CD_2Cl_2): δ 183.4, 153.4, 150.6, 148.9, 147.3, 146.5, 144.6, 138.1, 137.8, 136.7, 129.8, 128.2, 127.7, 127.5, 126.7, 126.2, 125.5, 123.4, 115.1, 34.8, 31.5; ATR (cm^{-1}): 1660 ν(C=O); HRMS (FD) calcd m/z for $C_{45}H_{41}NOS_2$ [$M^{+\cdot}$]: 675.2630, found: 675.2614; elemental analysis calcd (%) for $C_{45}H_{41}NOS_2$ + 0.05 CH_2Cl_2: C 79.55, H 6.09, N 2.06, found: C 79.18, H 6.17, N 1.90.

^{1}H NMR

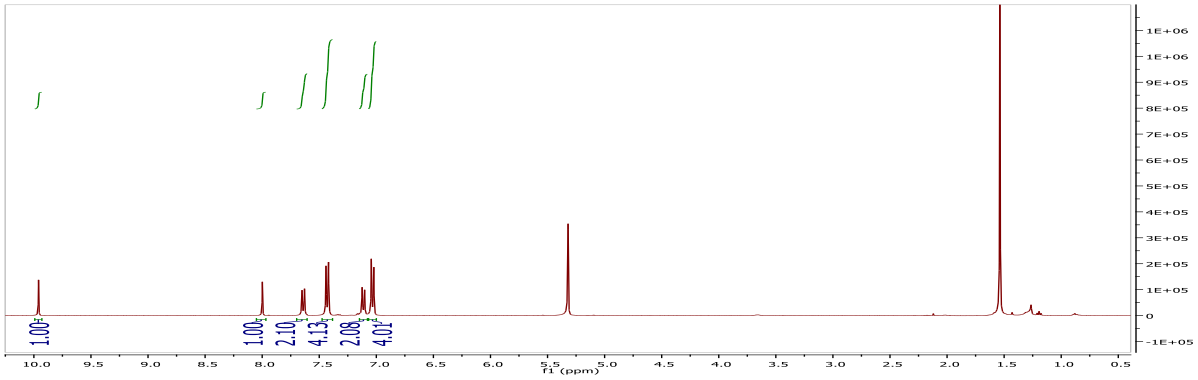

2-((5-(4-(diphenylamino)phenyl)thieno[3,2-b]thiophen-2-yl)methylene)malononitrile (18)

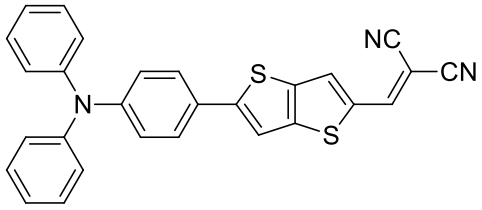

Procedure: To a round flask containing **14** (46.3 mg, 0.112 mmol) dissolved in 4.5 ml of toluene were added and the solution was stirred for 5 minutes. Then malononitrile (14.5 mg, 0.220 mmol), 3.0 ml of absolute EtOH and a catalytic amount of β-alanine were added and the mixture was warmed up to reflux for 24 h. Solvents were evaporated and the crude was dissolved in a small amount of CH_2Cl_2 and purified by chromatography column (CH_2Cl_2) to yield 46.0 mg of **18** as a dark powder (91%).

Characterization: m.p./DSC= 158°C (dec.); ^{1}H NMR (599.95 MHz, acetone-d6): δ 8.46 (s,1H), 8.22 (s,1H), 7.88 (s,1H), 7.68 (d, *J*= 8.7Hz, 2H), 7.38 (d, *J*= 8.4Hz, 2H), 7.36 (d, *J*= 8.4Hz, 2H), 7.13-7.17 (m, 6H), 7.05 (d, *J*= 8.7Hz, 2H); ^{13}C NMR (150.83 MHz, $CDCl_3$): δ 155.8, 150.9, 149.7, 149.5, 147.0, 138.5, 135.8, 130.5, 129.7, 127.3, 126.3, 125.5, 124.2, 122.3, 114.6, 114.1, 113.9, 75.4; ATR (cm^{-1}): 2213 ν(C≡N); HRMS (FD) calcd m/z for $C_{28}H_{17}N_3S_2$ [$M^{+\cdot}$]: 459.0864, found: 459.0879; elemental analysis calcd (%) for $C_{28}H_{17}N_3S_2$: C 73.17, H 3.73, N 9.14, found: C 72.84, H 3.67, N 9.19.

^{1}H NMR

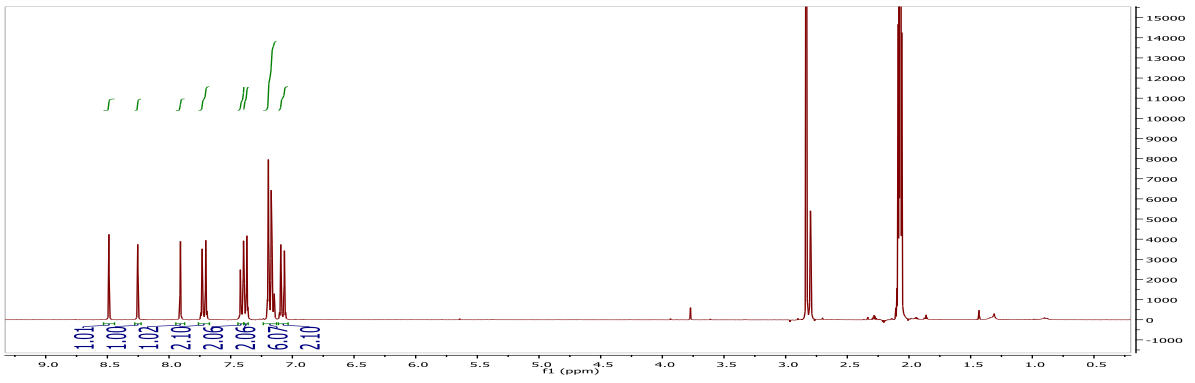

2-((5-(4-(bis(4-bromophenyl)amino)phenyl)thieno[3,2-b]thiophen-2-yl)methylene)malononitrile (19)

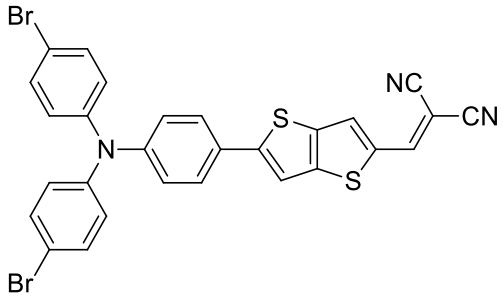

Procedure: To a round flask containing **15** (31.8 mg, 0.056 mmol) in 42.0 ml of absolute EtOH, malononitrile (8.4 mg, 0.123 mmol) and a catalytic amount of β-alanine were added and the mixture was warmed up to reflux for 48 h. After cooling down to room temperature, filtration and washing with pentane, 30.1 mg of **19** as a dark powder (87%) were obtained.

Characterization: m.p./DSC= 183°C (dec.); ^{1}H NMR (300.19 MHz, DMSO-d6): δ 8.73 (s,1H), 8.25 (s,1H), 7.98 (s,1H), 7.70 (d, *J*= 8.7Hz, 2H), 7.52 (d, *J*=8.8Hz, 4H), 7.07 (d, *J*= 8.7Hz, 2H), 7.04 (d, *J*=8.8Hz, 4H); ^{13}C NMR (150.83 MHz, CD_2Cl_2): δ 155.3, 151.5, 149.7, 148.7, 146.2, 139.0, 136.4, 133.0, 131.3, 128.0, 127.8, 126.9, 123.6, 117.0, 115.0, 114.9, 114.2, 76.0; ATR (cm^{-1}): 2218 ν(C≡N); HRMS (FD) calcd m/z for $C_{28}H_{15}Br_2N_3S_2$ [$M^{+\cdot}$]: 614.9074, found: 614.9052; elemental analysis calcd (%) for $C_{28}H_{15}Br_2N_3S_2$ + 0.05 C_5H_{12}: C 54.64, H 2.53, N 6.77, found: C 55.02, H 2.26, N 6.69.

^{1}H NMR

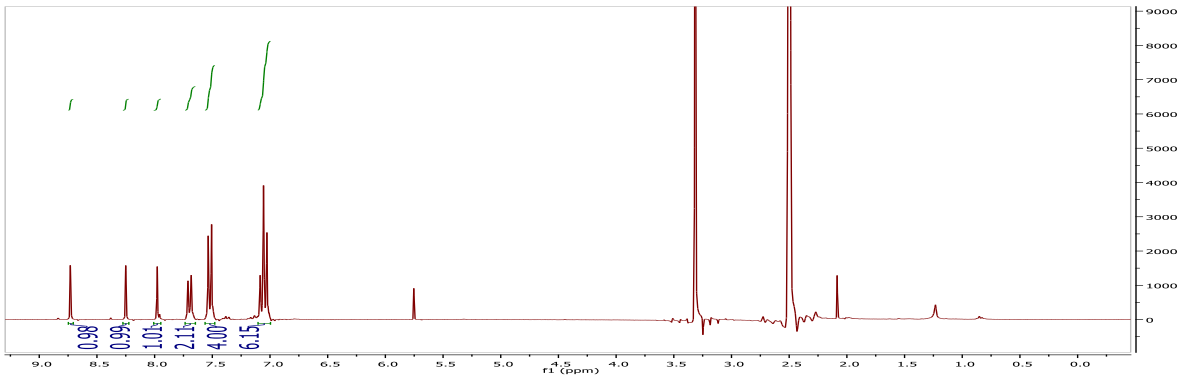

2-((5-(4-(bis(4-bromophenyl)amino)phenyl)-6-bromothieno[3,2-b]thiophen-2-yl)methylene) malononitrile (20)

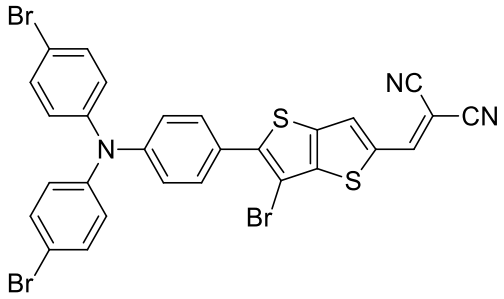

Procedure: To a round flask containing **16** (40.0 mg, 0.062 mmol) in 85.0 ml of absolute EtOH, malononitrile (4.5 mg, 0.068 mmol) and a catalytic amount of β-alanine were added and the mixture was warmed up to reflux for 72 h. EtOH was distilled until appearing of solid, then the crude was slowly cooled to room temperature and left for 3 h. Filtration and washing with pentane gave 28.2 mg of **20** as a dark powder (66%).

Characterization: m.p./DSC= 230°C (dec.); ^{1}H NMR (400.25 MHz, CD_2Cl_2): δ 7.98 (s,1H), 7.90 (s,1H), 7.66 (d, *J*= 8.8 Hz, 2H), 7.44 (d, *J*= 8.8 Hz, 4H), 7.11 (d, *J*= 8.8 Hz, 2H), 7.03 (d, *J*= 8.8 Hz, 4H); ^{13}C NMR (150.83 MHz, CD_2Cl_2): δ 151.5, 150.8, 148.8, 148.1, 146.1, 136.3, 136.1, 133.1, 131.4, 130.3, 127.1, 126.4, 122.8, 117.2, 114.5, 113.7, 99.7, 77.8; ATR (cm^{-1}): 2225 ν(C≡N); HRMS (FD) calcd m/z for $C_{28}H_{14}Br_3N_3S_2$ [$M^{+\cdot}$]: 692.8180, found: 692.8179; elemental analysis calcd (%) for $C_{28}H_{14}Br_3N_3S_2$: C 48.30, H 2.03, N 6.04, found: C 47.99, H 1.86, N 6.05.

^{1}H NMR

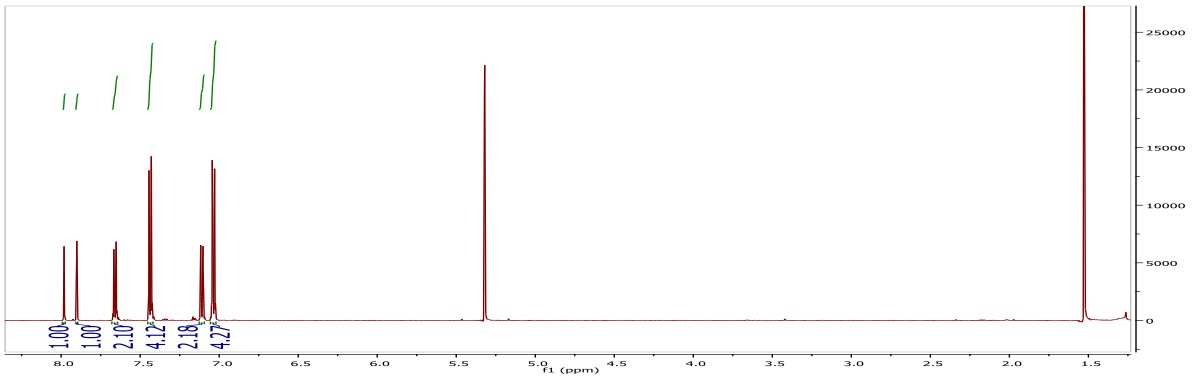

2-((5-(4-(bis(4'-(tert-butyl)-[1,1'-biphenyl]-4-yl)amino)phenyl)thieno[3,2-b]thiophen-2-yl)methylene)malononitrile (21)

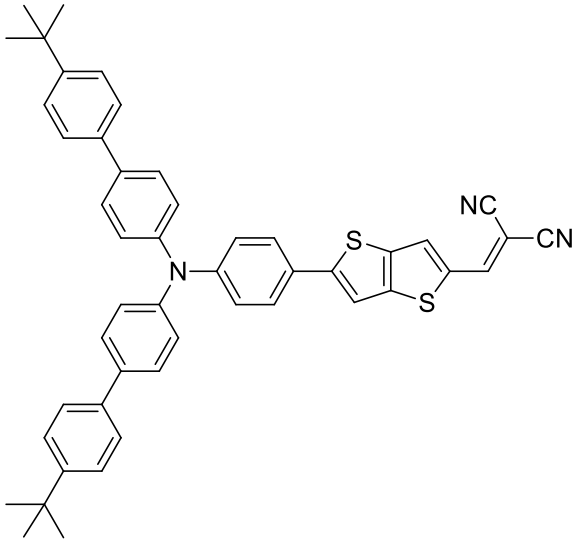

Procedure: To a round flask containing **17** (30.0 mg, 0.044 mmol) in 7.0 ml of toluene, malononitrile (27.0 mg, 0.409 mmol), 4.0 ml of absolute EtOH and and a catalytic amount of β-alanine were added. The mixture was warmed up to reflux for 24 h. Solvents were evaporated and the crude was dissolved in CH_2Cl_2 and purified by chromatography column (CH_2Cl_2) to yield 24.0 mg of **21** as a dark powder (75%).

Characterization: m.p./DSC= 145 (dec.); ^{1}H NMR (300.19 MHz, acetone-d6): δ 8.46 (s,1H), 8.22 (s,1H), 7.89 (s,1H), 7.72 (d, *J*= 8.6Hz, 2H), 7.66 (d, *J*=8.5 Hz, 4H), 7.59 (d, *J*= 8.3Hz, 4H), 7.49 (d, *J*= 8.3Hz, 4H), 7.23 (d, *J*= 8.5Hz, 4H), 7.15 (d, *J*= 8.6 Hz, 2H), 1.34 (s, 18H); ^{13}C NMR (75.47 MHz, acetone-d6): δ 155.7, 153.2, 150.9, 150.2, 149.8, 146.8, 139.1, 138.1, 137.4, 137.2, 133.6, 128.7, 128.2, 127.9, 127.1, 126.7, 126.3, 123.5, 116.0, 115.4, 114.8, 75.4, 35.1, 31.6; ATR (cm^{-1}): 2216 ν(C≡N); HRMS (FD) calcd m/z for $C_{48}H_{41}N_3S_2$ [$M^{+\cdot}$]: 723.2742, found: 723.2708; elemental analysis calcd (%) for $C_{48}H_{41}N_3S_2$ + 0.04 CH_2Cl_2: C 79.32, H 5.69, N 5.78, found: C 79.63, H 5.71, N 5.75.

^{1}H NMR

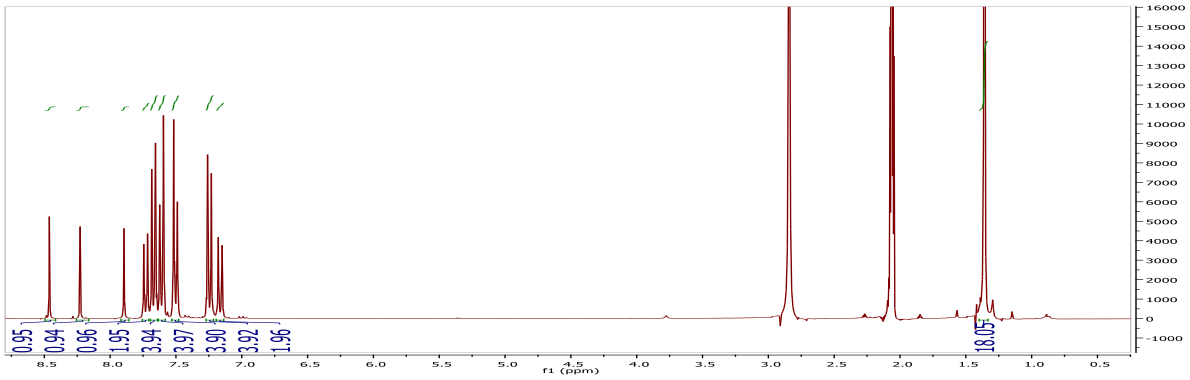

5-((5-(4-(diphenylamino)phenyl)thieno[3,2-b]thiophen-2-yl)methylene)-1,3-diethyl-2-thioxodihydropyrimidine-4,6(1*H*,5*H*)-dione (22)

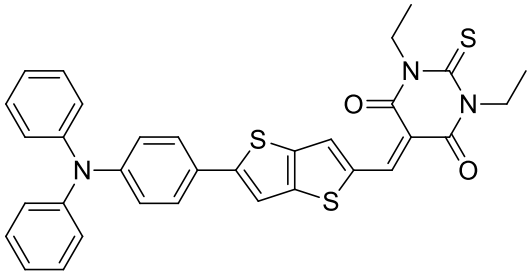

Procedure: To a round flask containing **14** (30.0 mg, 0.073 mmol) in 25.0 ml of absolute EtOH, 1,3-diethyl-2-thiobarbituric acid (16.1 mg, 0.080 mmol) and a catalytic amount of β-alanine were added and the mixture was warmed up to reflux for 24 h. Filtration of the precipitate obtained after cooling to room temperature, gave 36.0 mg of **22** as a dark powder (83%).

Characterization: m.p./DSC= 180°C (dec.); ^{1}H NMR (599.95 MHz, CD_2Cl_2): δ 8.71 (s,1H), 8.09 (s,1H), 7.57 (d, *J*= 8.7Hz, 2H), 7.50 (s, 1H), 7.30-7.34 (m, 4H), 7.10-7.17 (m, 6H), 7.06 (d, *J*= 7.0Hz, 2H), 4.59 (q, *J*= 7.0Hz, 2H), 4.55 (q, *J*= 7.0Hz, 2H), 1.32 (t, *J*= 7.0Hz, 3H), 1.29 (t, *J*= 7.0Hz, 3H); ^{13}C NMR (150.83 MHz, CD_2Cl_2): δ 179.2, 161.3, 160.2, 156.6, 156.4, 150.0, 149.8, 147.3, 139.4, 139.0, 138.1, 129.9, 127.7, 126.9, 125.8, 124.5, 122.4, 114.8, 110.3, 44.2, 43.5, 12.6, 12.5; ATR (cm^{-1}): 1655 ν(C=O); HRMS (FD) calcd m/z for $C_{33}H_{27}N_3O_2S_3$ [$M^{+\cdot}$]: 593.1265, found: 593.1268; elemental analysis calcd (%) for $C_{33}H_{27}N_3O_2S_3$: C 66.75, H 4.58, N 7.08, found: C 66.53, H 4.62, N 6.73.

^{1}H NMR

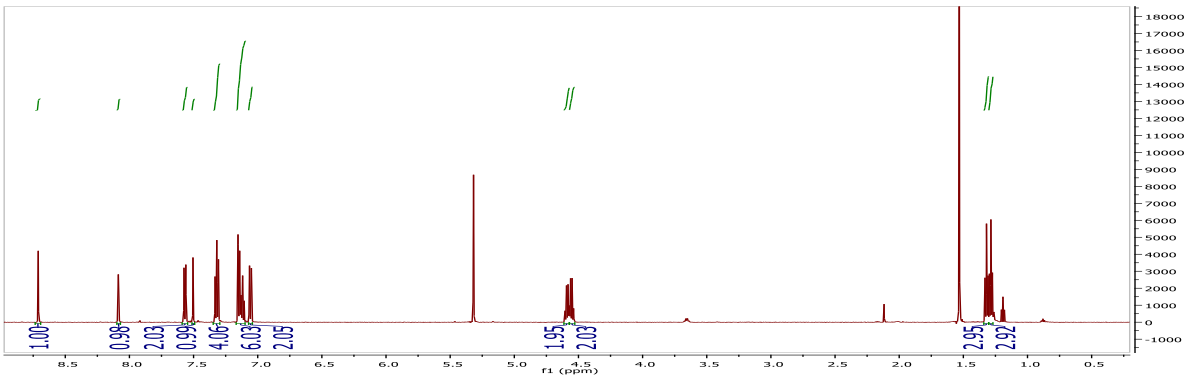

5-((5-(4-(bis(4-bromophenyl)amino)phenyl)thieno[3,2-b]thiophen-2-yl)methylene)-1,3-diethyl-2-thioxodihydropyrimidine-4,6(1*H*,5*H*)-dione (23)

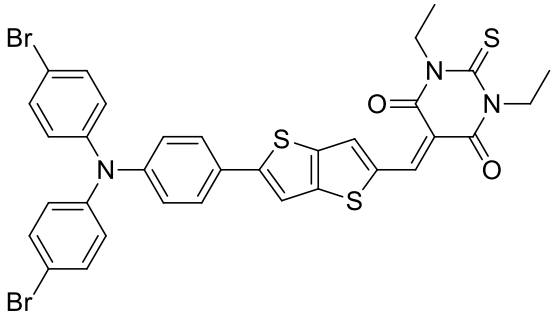

Procedure: To a round flask containing **15** (35.0 mg, 0.061 mmol) in 40.0 ml of absolute EtOH, 1,3-diethyl-2-thiobarbituric acid (12.9 mg, 0.064 mmol) and a catalytic amount of β-alanine were added and the mixture was warmed up to reflux for 24 h. Filtration of the precipitate obtained after cooling to room temperature, gave 39.5 mg of **23** as a dark powder (86%).

Characterization: m.p./DSC= 250°C (dec.); ^{1}H NMR (599.95 MHz, CD_2Cl_2): δ 8.72 (s,1H), 8.10 (s,1H), 7.61 (d, *J*= 8.7Hz, 2H), 7.53 (s, 1H), 7.43 (d, *J*= 8.8Hz, 4H), 7.08 (d, *J*= 7.0Hz, 2H), 7.02 (d, *J*= 8.8Hz, 4H), 4.59 (q, *J*= 7.0 Hz, 2H), 4.56 (q, *J*= 7.0 Hz, 2H), 1.32 (t, *J*= 7.0Hz, 3H), 1.29 (t, *J*= 7.0Hz, 3H); ^{13}C NMR (150.83 MHz, CD_2Cl_2): δ 179.2, 161.3, 160.2, 156.1, 155.9, 150.1, 148.7, 146.2, 139.6, 139.1, 138.0, 133.0, 128.2, 127.9, 126.9, 123.5, 117.0, 115.4, 110.6, 44.2, 43.5, 12.6, 12.5; ATR (cm^{-1}): 1660 ν(C=O); HRMS (FD) calcd m/z for $C_{33}H_{25}Br_2N_3O_2S_3$ [$M^{+\cdot}$]: 748.9476, found: 748.9475; elemental analysis calcd (%) for $C_{33}H_{25}Br_2N_3O_2S_3$: C 52.74, H 3.35, N 5.59, found: C 53.06, H 3.11, N 5.54.

^{1}H NMR

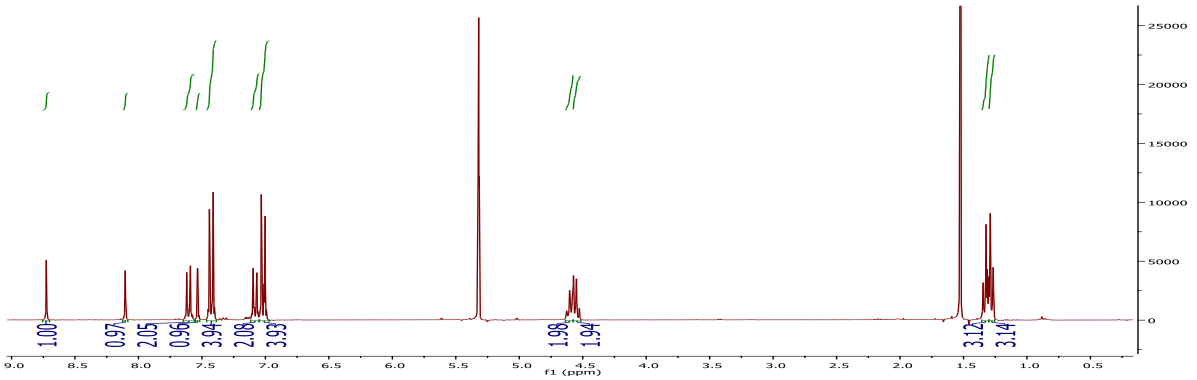

5-((5-(4-(bis(4-bromophenyl)amino)phenyl)-6-bromothieno[3,2-b]thiophen-2-yl)methylene)-1,3-diethyl-2-thioxodihydropyrimidine-4,6(1*H*,5*H*)-dione (24)

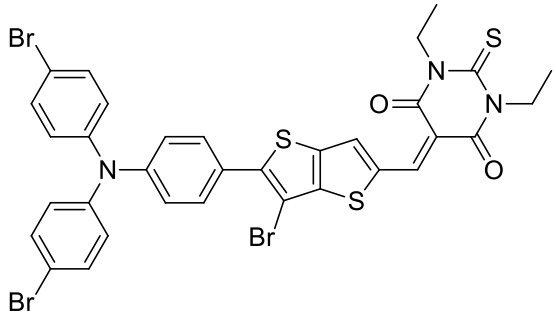

Procedure: To a round flask containing **16** (30.0 mg, 0.046 mmol) in 65.0 ml of absolute EtOH, 1,3-diethyl-2-thiobarbituric acid (10.2 mg, 0.051 mmol) and a catalytic amount of β-alanine were added and the mixture was warmed up to reflux for 24 h. After cooling to room temperature the solid was filtered, washed with pentane and dried, leading to 31.0 mg of **24** as a dark solid (81%).

Characterization: m.p./DSC= 265°C (dec.); ^{1}H NMR (300.19 MHz, CD_2Cl_2): δ 8.73 (s,1H), 8.14 (s,1H), 7.69 (d, *J*= 8.9 Hz, 2H), 7.44 (d, *J*= 8.9 Hz, 4H), 7.11 (d, *J*= 8.8 Hz, 2H), 7.04 (d, *J*= 8.8 Hz, 4H), 4.60 (q, *J*= 7.0 Hz, 2H), 4.56 (q, *J*= 7.0 Hz, 2H), 1.34 (t, *J*= 7.0 Hz, 3H), 1.29 (t, *J*= 7.0 Hz, 3H); ^{13}C NMR (150.83 MHz, CD_2Cl_2): δ 179.2, 161.3, 160.2, 156.1, 155.9, 150.1, 148.7, 146.2, 139.6, 139.1, 138.0, 133.0, 128.2, 127.9, 126.9, 123.5, 117.0, 115.4, 110.6, 44.2, 43.5, 12.6, 12.5; ATR (cm^{-1}): 1687 ν(C=O); HRMS (FD) calcd m/z for $C_{33}H_{24}Br_3N_3O_2S_3$ [$M^{+\cdot}$]: 826.8581, found: 826.8584; elemental analysis calcd (%) for $C_{33}H_{24}Br_3N_3O_2S_3$: C 47.73, H 2.91, N 5.06, found: C 47.68, H 2.80, N 5.05.

^{1}H NMR

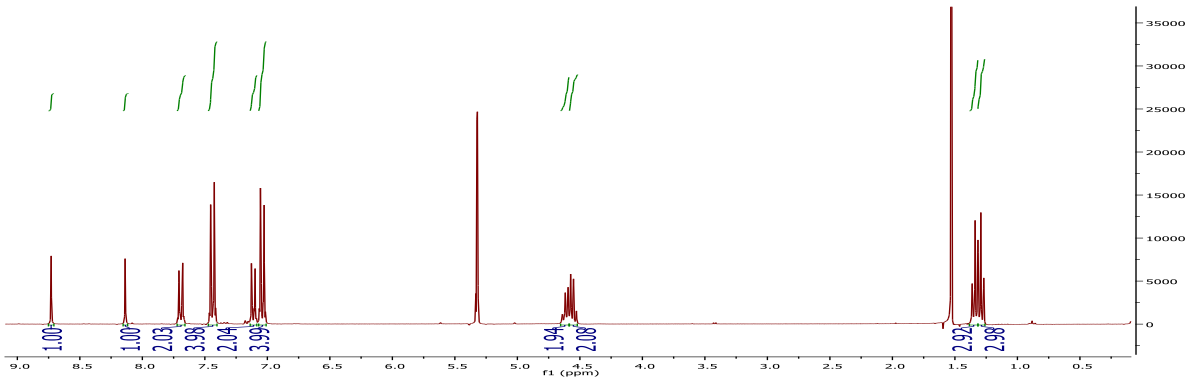

5-((5-(4-(bis(4'-(tert-butyl)-[1,1'-biphenyl]-4-yl)amino)phenyl)thieno[3,2-b]thiophen-2-yl)methylene)-1,3-diethyl-2-thioxodihydropyrimidine-4,6(1*H*,5*H*)-dione (25)

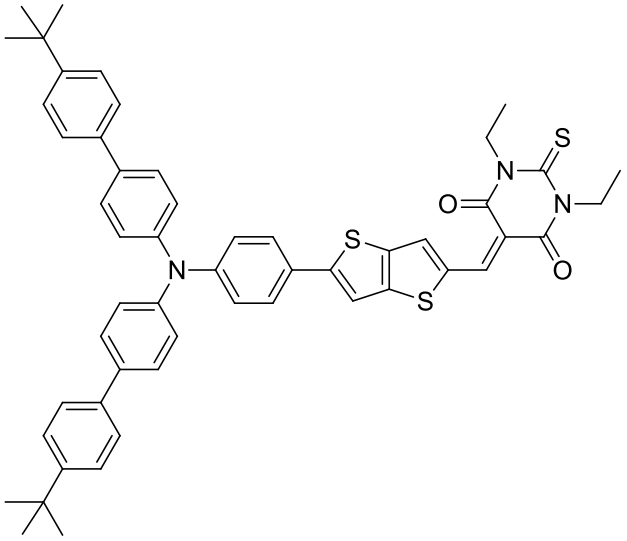

Procedure: To a round flask containing **17** (40.0 mg, 0.059mmol) in 5.0 ml of toluene, 1,3-diethyl-2-thiobarbituric acid (13.0 mg, 0.065 mmol), 6.6 ml of absolute EtOH, and a catalytic amount of β-alanine were added and the mixture was warmed up to reflux for 24 h. Solvents were evaporated until 0.5 ml then, 10 ml of absolute EtOH were added obtaining a dark green precipitate which was collected by means of filtration. After washing with pentane and drying, 39.0 mg of **25** (77%) as a dark green solid were obtained.

Characterization: m.p./DSC= 230°C (decomp.); ^{1}H NMR (599.95 MHz, CD_2Cl_2): δ 8.72 (s,1H), 8.10 (s, 1H), 7.62 (d, *J*= 8.8 Hz, 2H), 7.58 (d, *J*= 8.6 Hz, 4H), 7.55 (d, *J*= 8.5 Hz, 4H), 7.53 (s, 1H), 7.47 (d, *J*= 8.5 Hz, 4H), 7.24 (d, *J*= 8.6 Hz, 4H), 7.17 (d, *J*= 8.8 Hz, 2H), 4.59 (q, *J*= 7.0 Hz, 2H), 4.56 (q, *J*= 7.0 Hz, 2H), 1.36 (s, 18H), 1.32 (t, *J*= 7.0 Hz, 3H), 1.29 (t, *J*= 7.0 Hz, 3H); ^{13}C NMR (150.83 MHz, CD_2Cl_2): δ 179.2, 161.3, 160.2, 156.5, 156.4, 150.7, 150.0, 149.5, 146.2, 139.4, 139.0, 138.0, 137.8, 137.0, 128.3, 127.8, 127.2, 126.7, 126.2, 125.8, 122.9, 115.0, 110.4, 44.2, 43.5, 34.8, 31.5, 12.6, 12.5; ATR (cm^{-1}): 1646 ν(C=O); HRMS (FD) calcd m/z for $C_{53}H_{51}N_3O_2S_3$ [$M^{+\cdot}$]: 857.3143, found: 857.3134; elemental analysis calcd (%) for $C_{53}H_{51}N_3O_2S_3$: C 74.18, H 5.99, N 4.90, found: C 73.82, H 5.80, N 4.87.

^{1}H NMR

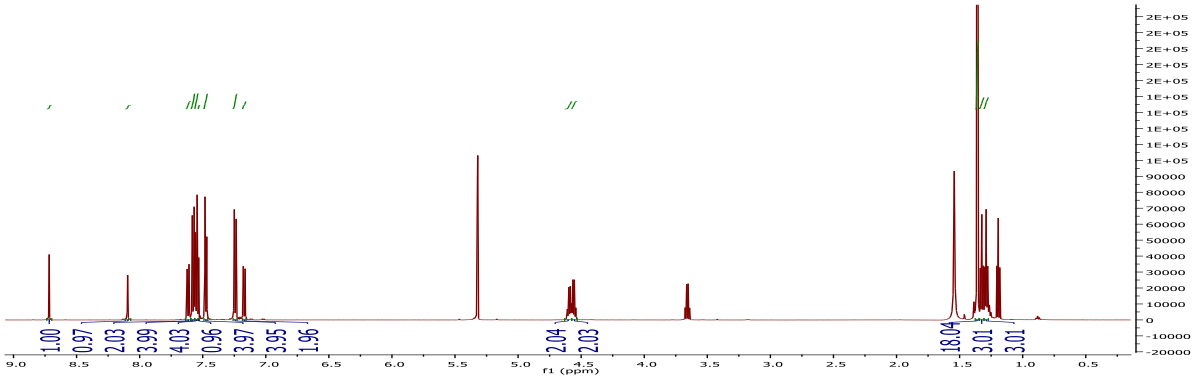

***N*,*N*-dihexylaniline (26)**

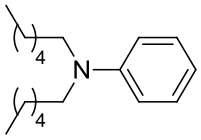

Procedure: 1.20 g (12.9 mmol) of aniline, 14.90 g of hexylbromide (90.6 mmol) and 485 mg of tetrabutylammonium iodide (1.3 mmol) were transferred into a round flask. 13 ml of $NaOH_{aq}$ (50% w/v) were added and the reaction was warmed up to 60°C and left under stirring overnight.After extraction with CH_2Cl_2, the organic layer was dried over Na_2SO_4, filtered and reduced by vacuum up to 5 g. The residue was purified by chromatography column (CH_2Cl_2:petroleum ether = 1:9) affording 3.10 g of **26** as a colorless liquid (91%).

Characterization: ^{1}H NMR (200.13 MHz, $CDCl_3$): δ 7.18-7.28 (m, 2H), 6.60-6.71 (m, 3H), 3.23-3.33 (m, 4H), 1.52-1.70 (m, 4H), 1.28-1.42 (m, 12H), 0.88-0.99 (m, 6H); ^{13}C NMR (50.31 MHz, $CDCl_3$): δ 148.3, 129.3, 115.1, 111.8, 51.2, 31.9, 27.3, 27.0, 22.8, 14.2.

^{1}H NMR

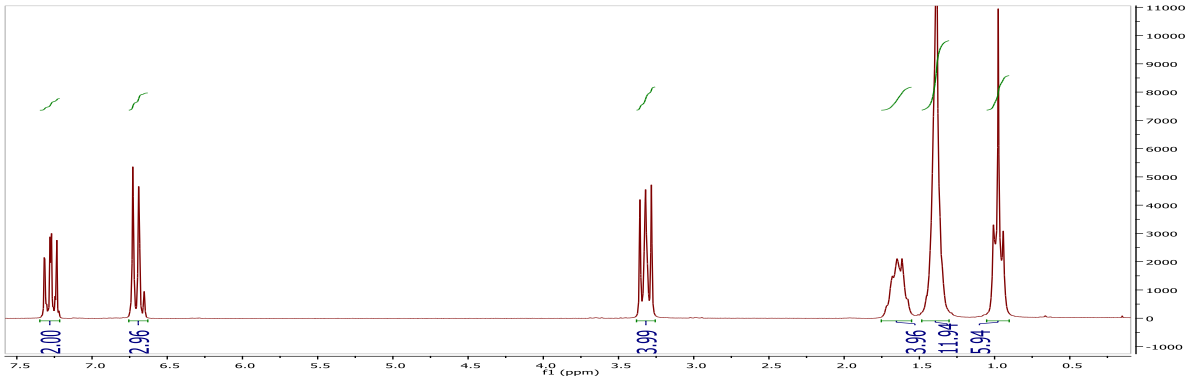

***N*,*N*-dihexyl-4-iodoaniline (27)**

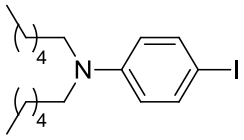

Procedure: To a solution of $NaHCO_3$ in 40 ml of water, 3.00 g (11.5 mmol) of **26** were added. The mixture was cooled to 0°C and 3.50 g (13.8 mmol) of I_2, dissolved in 140 ml of CH_2Cl_2 were slowly added. The reaction was slowly warmed up to room temperature and left under stirring overnight. After reduction of the excess of I_2 by addition of $Na_2S_2O_{3aq}$, the organic layer was washed with water, dried over Na_2SO_4 and concentrated by vacuum. The residue was purified by chromatography column (CH_2Cl_2:petroleum ether = 3:7) affording 3.05 g of **27** as a pale yellow liquid (70%).

Characterization: ^{1}H NMR (200.13 MHz, $CDCl_3$): δ 7.38-7.48 (m, 2H), 6.37-6.48 (m, 2H), 3.17-3.29 (m, 4H), 1.47-1.66 (m, 4H), 1.26-1.40 (m, 12H), 0.86-0.98 (m, 6H); ^{13}C NMR (50.31 MHz, $CDCl_3$): δ 147.7, 137.7, 114.1, 75.4, 51.1, 31.8, 27.1, 26.9, 22.8, 14.2.

^{1}H NMR

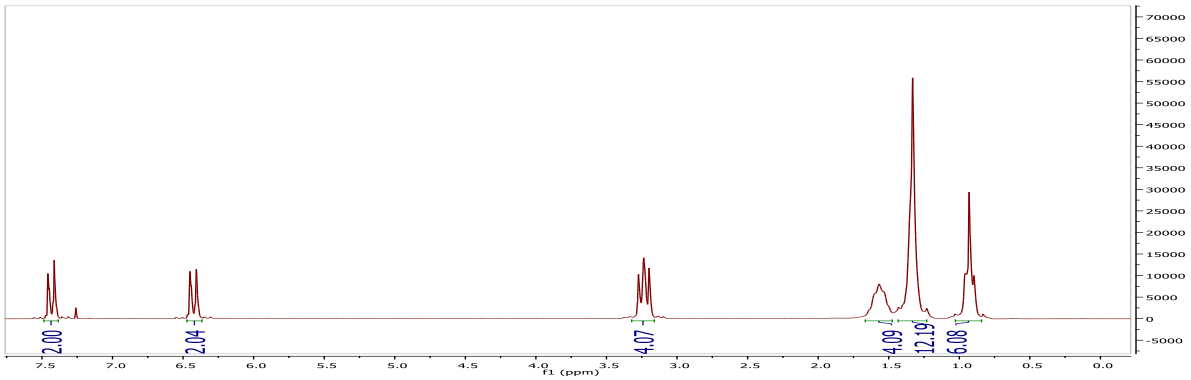

5'-(4-(dihexylamino)phenyl)-[2,2'-bithiophene]-5-carbaldehyde (28)

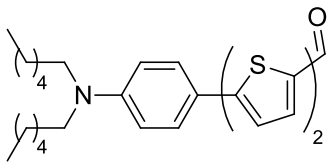

Procedure: 1.00 g of **27** (2.58 mmol), 985 mg (4.13mmol) of (5'-formyl-[2,2'-bithiophen]-5-yl)boronic acid, 4.7 g (34.06 mmol) of K_2CO_3 and 63 mg of $Pd(dppf)Cl_2$ (0.1 mmol) were transferred into a round flask. 50 ml of Tol:MeOH = 2:1 (previously degassed by blowing Ar for 30 min). The mixture was warmed up to 70 °C and stirred overnight. Solvents were removed by vacuum and the residue treated with CH_2Cl_2 and transferred into an extraction funnel. After washing with NH_4Cl_{sat} and water, the organic layer was dried over Na_2SO_4, filtered and reduced by vacuum. The residue was purified by chromatography column (CH_2Cl_2), then by crystallization from CH_3CN, affording 750 mg of **28** as an orange solid (64%).

Characterization: m.p./DSC= 84°C (dec.); ^{1}H NMR (300.19 MHz, CD_2Cl_2): δ 9.82 (s, 1H), 7.68 (d, *J*= 3.9 Hz, 1H), 7.42-7.49 (m, 2H), 7.32 (d, *J*= 3.9 Hz, 1H), 7.24 (bs, 1H), 7.10 (bs, 1H), 6.64 (bs, 2H), 3.16-3.39 (m, 4H), 1.55-1.66 (m, 4H), 1.29-1.38 (m, 12H), 0.86-0.95 (m, 6H); ^{13}C NMR (150.83 MHz, CD_2Cl_2): δ 182.8, 148.9, 148.4, 148.1, 141.4, 138.2, 132.7, 127.9, 127.4, 123.9, 121.8, 120.6, 112.2, 51.5, 32.30, 27.77, 27.33, 23.3, 14.4; IR (KBr, cm^{-1}): 1673 ν(C=O).

^{1}H NMR

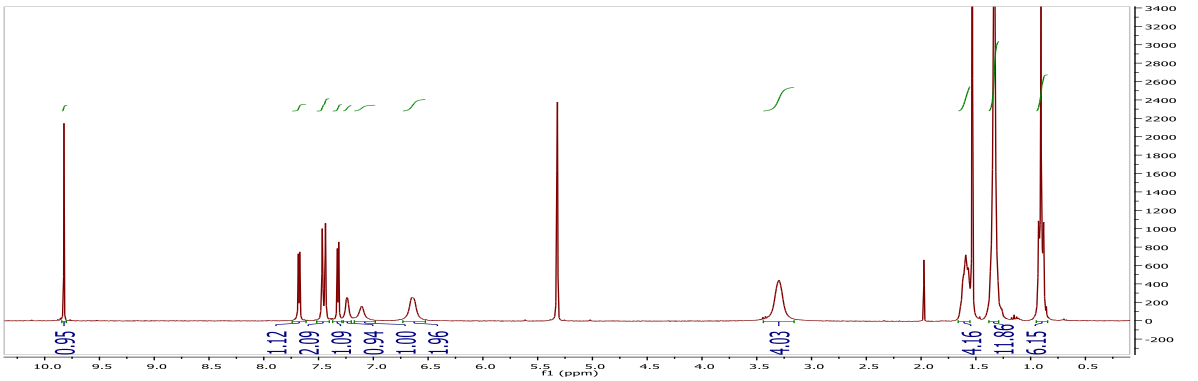

4-(5'-ethynyl-[2,2'-bithiophen]-5-yl)-*N*,*N*-dihexylaniline (29)

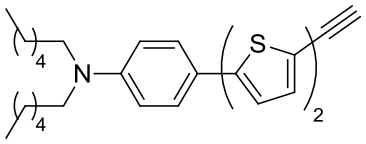

Procedure: 120 mg of **28** (0.26 mmol) and 94 mg of K_2CO_3 (0.61 mmol) were transferred into a round flask with 2.0 ml of MeOH. THF was added until total dissolution (1.6 ml). Then 104 mg of dimethyl (1-diazo-2-oxopropyl)phosphonate (0.54 mmol) were added and the mixture was stirred at room temperature for 48 h. After removal of solvents by vacuum, the residue was treated with CH_2Cl_2 and washed with water. The organic phase was dried over Na_2SO_4, filtered and concentrated by vacuum; the residue was purified by chromatography column (petroleum ether:CH_2Cl_2 = 7:3), affording 81 mg **29** as a brown solid (69%).

Characterization: m.p./DSC= 73°C (dec.); ^{1}H NMR (300.19 MHz, CD_2Cl_2): δ 7.42 (d, *J*= 8.6 Hz, 2H), 7.18 (d, *J*= 3.6 Hz, 1H), 7.13 (d, *J*= 3.6 Hz, 1H), 7.04 (d, *J*= 3.7 Hz, 1H), 7.01 (d, *J*= 3.7 Hz, 1H), 6.63 (d, *J*= 8.6 Hz, 2H), 3.47 (s, 1H), 3.25-3.34 (m, 4H), 1.51-1.67 (m, 4H), 1.27-1.38 (m, 12H), 0.87-0.95 (m, 6H); ^{13}C NMR (150.83 MHz, CD_2Cl_2): δ 148.7, 146.2, 140.4, 134.7, 133.2, 127.2, 1256.0, 122.9, 121.5, 121.0, 120.1, 112.2, 82.5, 77.38, 51.5, 32.3, 27.8, 27.3, 23.3, 14.4; IR (KBr, cm^{-1}): 2094 ν(C≡C).

^{1}H NMR

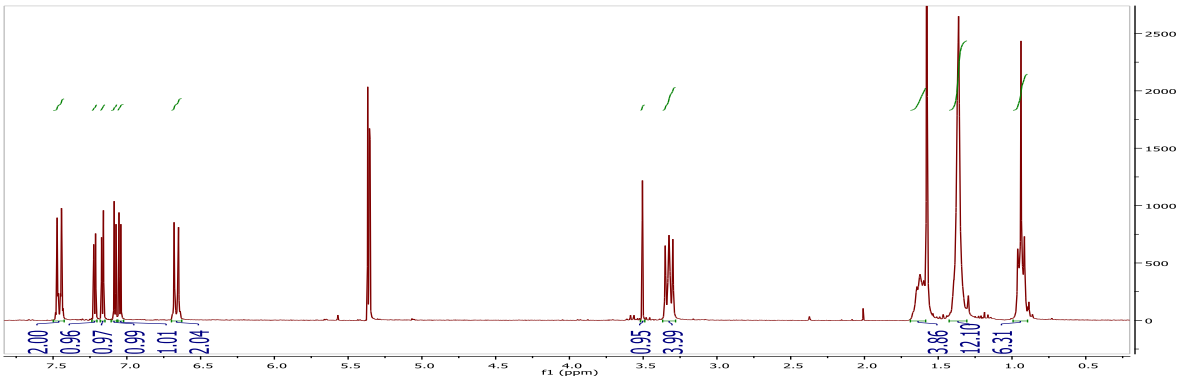

5-iodo-1-nonylpyrimidine-2,4(1*H*,3*H*)-dione (30)

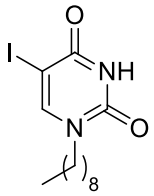

Procedure: 0.50 g of 5-iodouracil (2.1 mmol), 8 mg of $(NH_4)_2SO_4$ (0.06 mmol) and 1.00 g of bis(trimethylsilyl)amine (6.3 mmol) were transferred into a round flask and heated up to reflux overnight with vigorous stirring. After cooling to room temperature, the mixture was concentrated by vacuum and 3 ml of DMF and 0.60 g of 1-bromononane (2.9 mmol) were added. The reaction was heated up to 80°C for 24 hours then, it was quenched by addition of ice and extracted with AcOEt. The organic phase was filtered, dried over Na_2SO_4 and concentrated by vacuum. The residue was purified by chromatography column (petroleum ether:AcOEt = 7:3), then by crystallization from $CHCl_3$/cyclohexane, affording 860 mg of **30** as a white solid (25%).

Characterization: m.p./DSC= 151°C (dec.); ^{1}H NMR (300.19 MHz, $CDCl_3$): δ 8.31 (bs, 1H), 7.6 (s, 1H), 3.69-3.76 (m, 2H), 1.62-1.74 (m, 2H), 1.22-1.36 (m, 12H), 0.84-0.92 (m, 3H); ^{13}C NMR (50.31 MHz, $CDCl_3$): δ 160.6, 150.5, 149.0, 67.6, 49.4, 31.9, 29.5, 29.3, 29.3, 29.2, 26.5, 22.8, 14.2.

^{1}H NMR

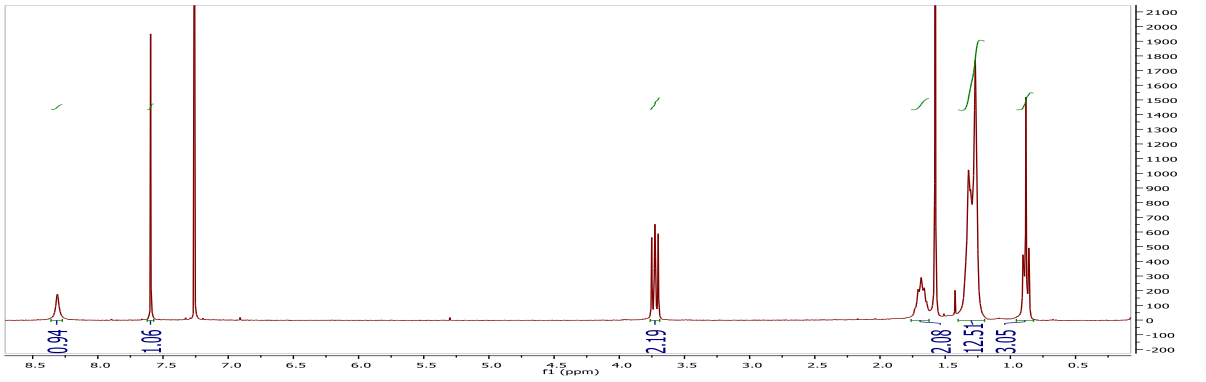

5-((5'-(4-(dihexylamino)phenyl)-[2,2'-bithiophen]-5-yl)ethynyl)-1-nonylpyrimidine-2,4(1*H*,3*H*)-dione (31)

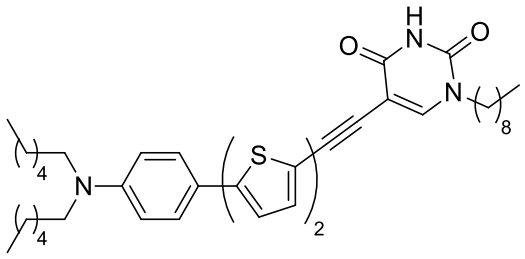

Procedure: 50 mg of **29** (0.11mmol), 32 mg of **30** (0.09 mmol), 10 mg of $Pd(PPh_3)_4$ ($9 \cdot 10^{-3}$ mmol) and 5 mg of CuI (0.03 mmol) were transferred into a round flask. 6 ml of DMF and 25 µl of Et_3N were added and the mixture was stirred for 48 hours. The reaction was quenched with water and extracted with CH_2Cl_2. The organic layer was dried over Na_2SO_4, filtered and concentrated by vacuum. The residue was purified by chromatography column (AcOEt:petroleum ether = 52:68) and crystallization from CH_2Cl_2/cyclohexane, affording 54 mg of 6 as a reddish powder (72%).

Characterization: m.p./DSC= 204°C (dec.); ^{1}H NMR (599.95 MHz, CD_2Cl_2): δ 7.58 (s, 1H), 7.38-7.42 (m, 3H), 7.08-7.12 (m, 2H), 7.02 (bs, 1H), 6.58-6.64 (m, 2H), 3.95-4.05 (m, 1H), 3.73-3.82 (m, 1H), 3.23-3.32 (m, 4H), 1.65-1.71 (m, 2H), 1.56-1.61 (m, 4H), 1.30-1.35 (m, 12H), 1.19-1.25 (m, 6H), 1.15-1.18 (m, 6H), 0.88-0.92 (m, 6H), 0.82 (t, *J*= 7.2 Hz, 3H); ^{13}C NMR (150.83 MHz, CD_2Cl_2): δ 171.4, 155.4, 148.6, 148.4, 146.8, 142.5, 140.4, 132.5, 129.7, 127.1, 126.8, 126.5, 123.7, 121.4, 120.6, 112.0, 107.1, 100.0, 52.7, 51.4, 32.2, 32.1, 29.8, 29.7, 29.6, 29.5, 27.6, 27.2, 26.9, 23.10, 23.0, 14.3, 14.2; IR (KBr, cm^{-1}): 1670 ν(C=O).

^{1}H NMR

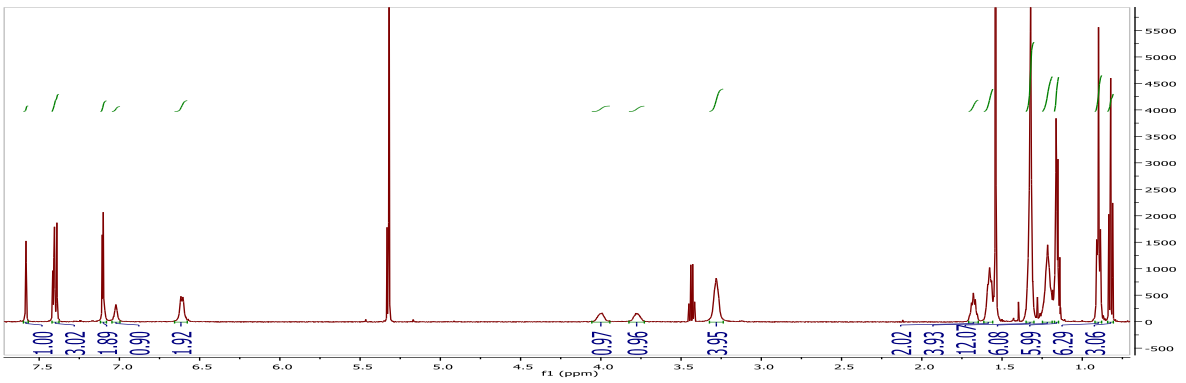

Diethyl (*p*-cyanobenzyl)phosphonate (32)[10]

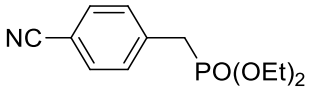

Procedure: To a solution of 4-(bromomethyl)benzonitrile (1.0 g, 5.1 mmol) in $CHCl_3$ (20 ml), 2.2 ml of triethylphosphite were added and the mixture was heated up to reflux and stirred overnight. The crude was concentrated by vacuum leading to viscous liquid. Few milliliters of pentane were added and the mixture was sonicated for few minutes, leading to a white solid. The operation was repeated one more time and after dry by vacuum, 790 mg of **32** (62%) were obtained.

Characterization: 7.49 (AA'BB', 4H), 3.92-4.08 (m, 4H) 3.16 (d, *J*= 22.3 Hz, 2H), 1.22 (t, *J*= 7.0 Hz, 6H).

^{1}H NMR

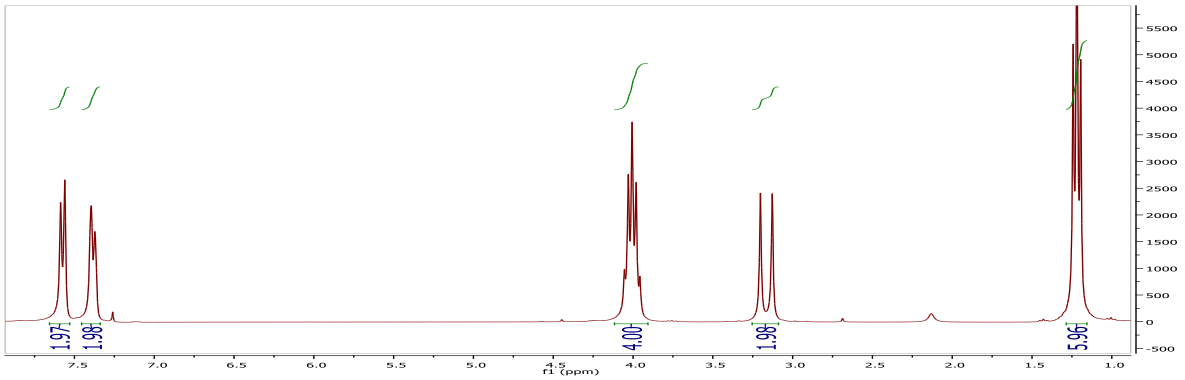

(*E*)-4-(2-(5'-(4-(dihexylamino)phenyl)-[2,2'-bithiophen]-5-yl)vinyl)benzonitrile (33)

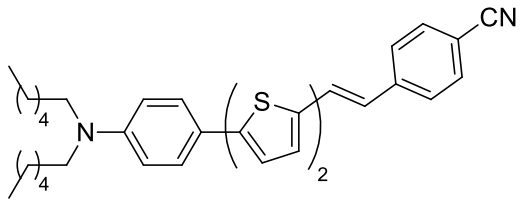

Procedure: 100 mg of **28** (0.22 mmol) and 64 mg of **32** (0.25 mmol) were dissolved in 8 ml of THF. 80 mg of NaH (60% in mineral oil) were added and the mixture was left under stirring overnight. The crude was poured into ice and after total melting it was filtered and washed with pentane, affording 105 mg of **33** as a reddish solid (82%).

Characterization: m.p./DSC= 179°C; ^{1}H NMR (300.19 MHz, CD_2Cl_2): δ 7.59 (AA'BB', 4H), 7.40-7.46 (m, 2H), 7.33 (d, *J*= 16.0 Hz, 1H), 7.14-7.17 (m, 1H), 7.04-7.11 (m, 3H), 6.87 (d, *J*= 16.0 Hz, 1H), 6.60-6.67 (m, 2H), 3.24-3.35 (m, 4H), 1.53-1.66 (m, 4H), 1.27-1.39 (m, 12H), 0.86-0.94 (m, 6H); ^{13}C NMR (75.47 MHz, CD_2Cl_2): δ 148.6, 146.0, 142.1, 140.5, 138.9, 134.0, 133.1, 129.7, 127.2, 127.1, 126.2, 125.7, 125.7, 123.9, 121.6, 121.1, 119.5, 112.2, 110.9, 51.5, 32.3, 27.8, 27.3, 23.3, 14.4; IR (KBr, cm^{-1}): 2222 ν(C≡N).

^{1}H NMR

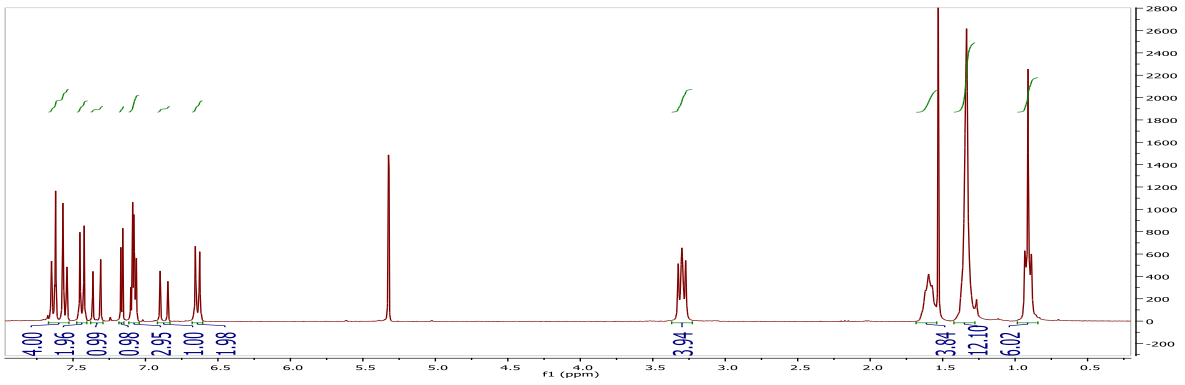

(*E*)-6-(4-(2-(5'-(4-(dihexylamino)phenyl)-[2,2'-bithiophen]-5-yl)vinyl)phenyl)-1,3,5-triazine-2,4-diamine (34)

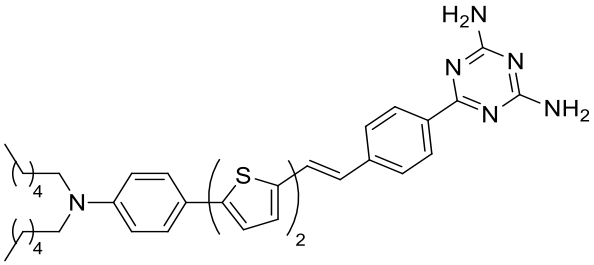

Procedure: 70 mg of **33** (0.13 mmol), 44 mg of dicyandiamide (0.52 mmol) and 8.9 mg (0.16 mmol) of KOH were dissolved in 10 ml of BuOH and stirred for 48 hours. Solvents were removed by vacuum and the residue was treated with CH_2Cl_2 and washed with NH_4Cl_{aq} and water. The organic layer was dried over Na_2SO_4, filtered and concentrated by vacuum; the crude was purified by chromatography column (CH_2Cl_2:AcOEt = 6:4) and trituration with pentane, leading 55 mg of **34** as red powder (66%).

Characterization: m.p./DSC= 217°C (dec.); ^{1}H NMR (599.95 MHz, CD_2Cl_2): δ 8.30-8.34 (m, 2H), 7.55 (d, *J*= 8.2 Hz, 2H), 7.42-7.46 (m, 2H), 7.33 (d, *J*= 16.0 Hz, 1H), 7.15 (d, *J*= 3.7 Hz, 1H), 7.08 (d, *J*= 3.7 Hz, 1H), 7.06 (d, *J*= 3.7 Hz, 1H), 7.04 (d, *J*= 3.7 Hz, 1H), 6.94 (d, *J*= 16.0 Hz, 1H), 6.62-6.66 (m, 2H), 5.14 (bs, 4H), 3.27-3.32 (m, 4H), 1.58-1.62 (m, 4H), 1.31-1.35 (m, 12H), 0.89-0.93 (m, 6H); ^{13}C NMR (150.83 MHz, CD_2Cl_2): δ 171.9, 168.3, 148.4, 145.5, 141.2, 140.6, 137.8, 135.9, 134.1, 129.1, 128.6, 127.5, 127.0, 126.4, 125.3, 123.7, 123.6, 121.4, 121.0, 112.0, 51.4, 32.2, 27.6, 27.2, 23.1, 14.2; HRMS (FD) calcd m/z for $C_{37}H_{44}N_6S_2$ [$M^{+\cdot}$]: 636.30689, found m/z 636.30765; IR (KBr, cm-1): 1527, 1543 ν(CN) + δ(NH_2).

^{1}H NMR

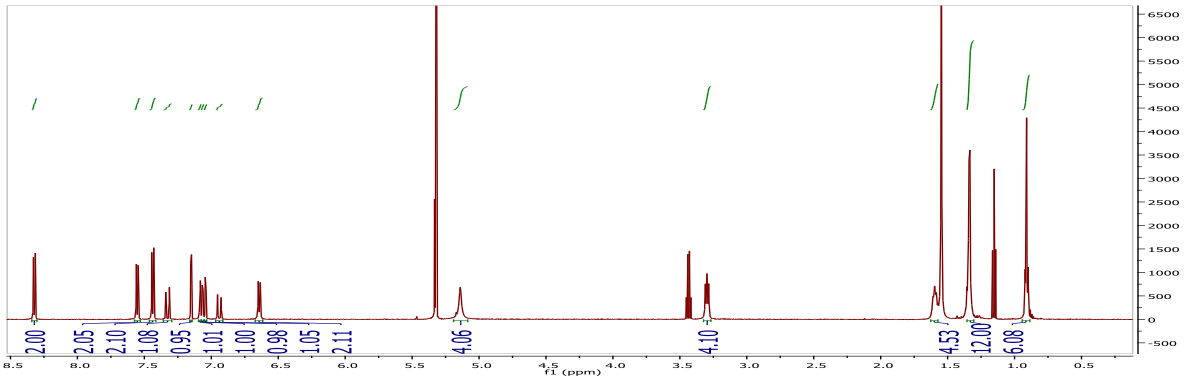

Bibliographic references

[1] C. Würth, M. Grabolle, J. Pauli, M. Spieles, U. Resch-Genger, *Nat. Protoc.* **2013**, *8*, 1535-1550.

[2] U. Resch-Genger, K. Rurack, *Pure Appl. Chem.* **2013**, *85*, 2005-2013.

[3] A. M. Brouwer, *Pure Appl. Chem.* **2011**, *83*, 2213-2228.

[4] C. Xu, W. W. Webb, *J. Opt. Soc. Am. B*, *13*, 481-491

[5] N. Boens, V. Leen, W. Dehaen, *Chem. Soc. Rev.* **2012**, *41*, 1130-1172.

[6] J. E. Whitaker, R. P. Haugland, F. G. Prendergast, *Anal. Biochem.* **1991**, *194*, 330-344.

[7] O. Mongin, M. Sankar, M. Charlot, Y. Mir, M. Blanchard-Desce, *Tetrahedron Lett.* **2013**, *54*, 6474-6478.

[8] E. J. Cueto Díaz, S. Picard, V. Chevasson, J. Daniel, V. Hugues, O. Mongin, E. Genin, M. Blanchard-Desce, *Org. Lett.* **2015**, *17*, 102-105.

[9] J. Daniel, C. Mastrodonato, A. Sourdon, G. Clermont, J.-M. Vabre, B. Goudeau, H. Voldoire, S. Arbault, O. Mongin, M. Blanchard-Desce, *Chem. Commun.* **2015**, *51*, 15245-15248.

[10] Y. Yao, W. Shen, B. Nohra, C. Lescop, R. Réau, *Chem. Eur. J.* **2010**, *16*, 7143-7163.

Annex

Organic Synthesis Review

A.1 Organic synthesis overview

In this section will be elucidated some main aspects about chemical reactions of particular relevance that have been used to prepare the target compounds described in this manuscript, in order to understand their features in relation to the synthetic protocols adopted.

A.2 Palladium catalysed cross coupling

Nowdays cross coupling reactions are a very powerful tools in organic synthesis largely used both in industry and academia. The birth and evolution of these reactions are the result of over a century of scientific research (Figure A.1) and the interested reader can find more detailed information in the nice review by Snieckus et al[1] and cited literature in it.

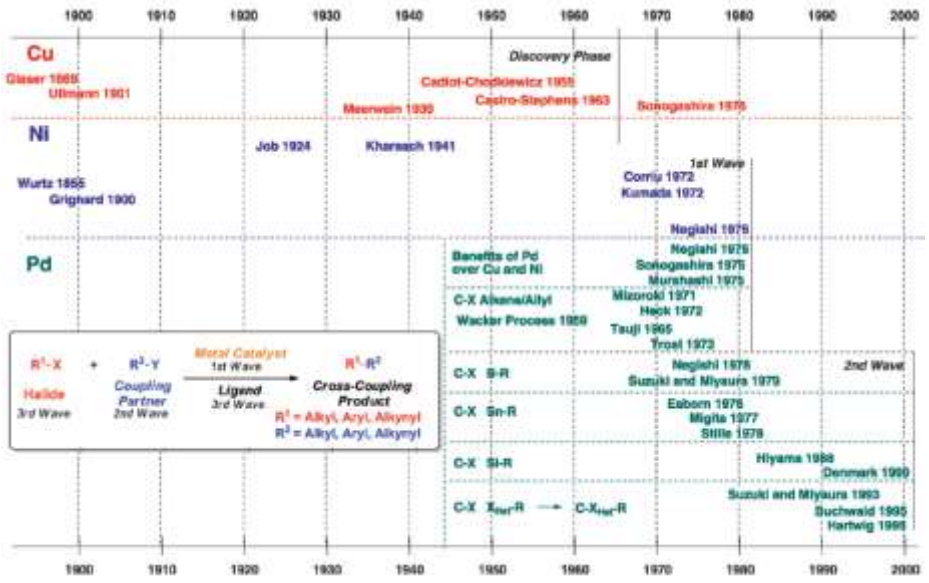

Figure A.1 Time evolution of metal catalyzed cross coupling reactions[1]

Since the pioneering works of Glaser[2] in the middle of the 19th century about oxidative dimerization of phenylacetylene (Scheme A.1), the interest towards the reactions that bring to the selective formation of carbon-carbon bonds has soared.

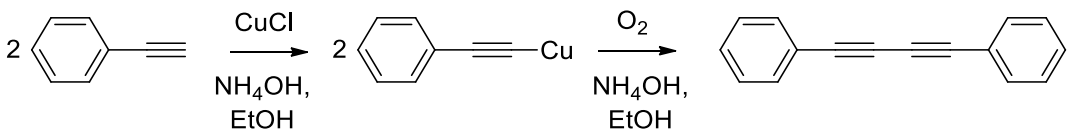

Scheme A.1 Glaser's coupling

The extension of those dimerization reactions to halogenated aryl compounds [3], the possibility of using substoichiometric or catalytic metal amount [4-6], the advent of the palladium complexes[7], were some of the most important input (Scheme A.2) that made such reactions more and more useful in organic synthesis, attracting the interest of different people and spurring the research in this field, leading to the development of the cross coupling reactions as we know it today.

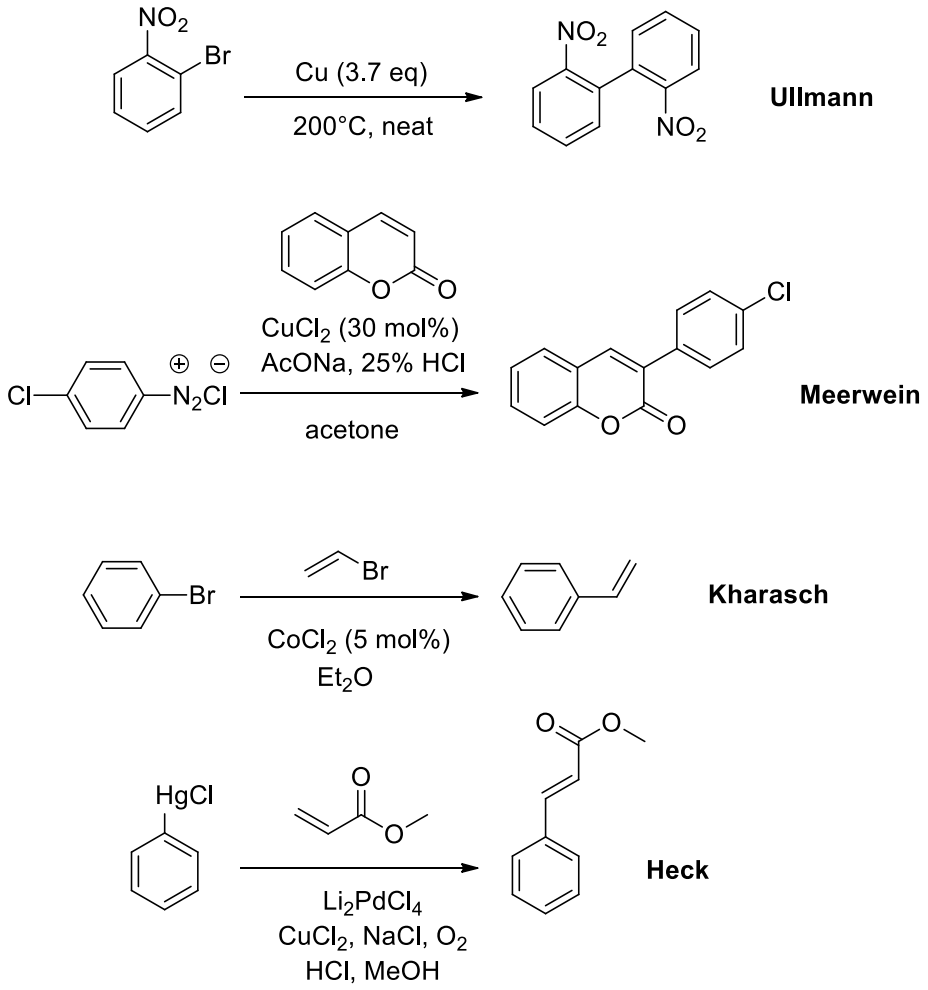

Scheme A.2 Key examples of coupling reactions

Pd-catalysed cross couplings can be referred to the general equation in the following scheme wherein X represents an halide (typically bromide or iodide) or a pseudohalide (e.g., triflate); the nature of Y, R and R' determines the kind of coupling (Figure A.2).

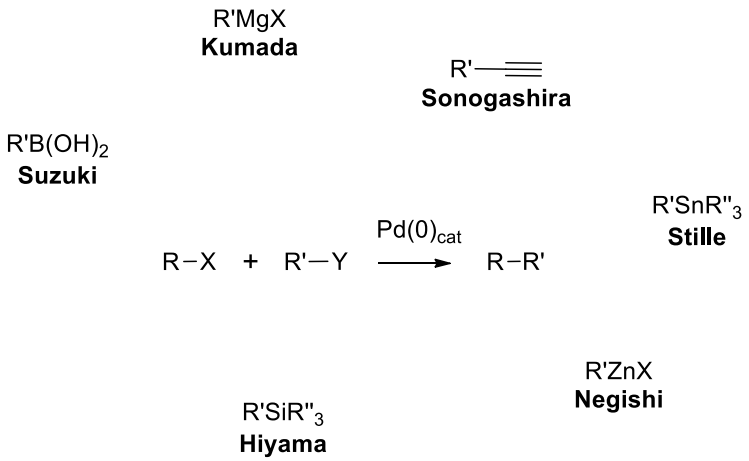

Figure A.2 General equation for Pd catalysed cross couplings, with some examples according to nature of R'

Many of these reactions follow the catalytic cycle depicted in the Scheme A.3.

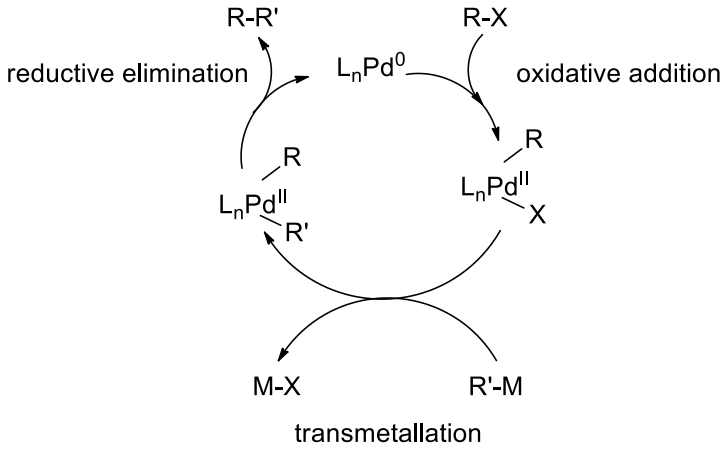

Scheme A.3 General catalytic cycle for many Pd catalysed cross coupling

The first step is an oxidative addition of the specie R-X to the palladium leading to a Pd(II) specie; at this point a transmetallation takes place leading the R' moiety on the metal center. The last step consist in a reductive elimination which leads to the cross coupling product and restores the catalyst. Besides to the general mechanism exposed, each kind of cross coupling has its specific features according to the nature of the substrates (i.e., R-X and R'-Y), which involves the need to optimize the reaction conditions in order to obtain satisfactory results (i.e., nature of the catalyst, solvent, temperature, bases).

A.2.1 Suzuki cross coupling

When R'-Y is an organoboron derivative (usually a boronic ester or, as in this chapter, a boronic acid) the cross coupling comes to Suzuki-Miyaura reaction. Generally such reactions have significant

synthetic advantages, as they are compatible with a variety of potentially susceptible functional groups[8-9] (i.e., the preparation of **13** in this chapter involved the use of (5'-formyl-[2,2'-bithiophen]-5-yl)boronic acid, bearing itself a formyl group) and may be carried out under mild conditions[8-9]; moreover boronic acids and esters are generally rather stable and therefore easy to manipulate. The catalytic cycle of the Suzuki cross coupling is analogous to the one depicted in the Scheme A.3, however some more clarification are necessary (Scheme A.4)[9].

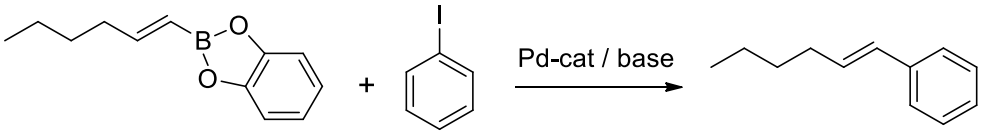

base (eq)	time (h)	yield (%)
none	6	0
NaOEt (2)	2	99
NaOH (2)	2	99

Reactions performed in benzene at 80°C, using $Pd(PPh_3)_4$ (3 mol%), boronic ester (1 eq) and PhI (1.1 eq).

Scheme A.4 Example of Suzuki cross coupling performed with and without base[9]

In the previous scheme is reported an example that helps to better understand some features of the reaction. In absence of a base the transformation doesn't take place, whereas adding sodium alkoxyde or hydroxide, the reaction leads to coupled products quantitatively. The reason of this behavior lies in the fact that the R group in organoboran derivatives have weak nucleophilic properties and turns out to be low reactive in the transmetallation step , whereas upon complexation with a base (typically oxygen based one), it results activated and the transfer of the R group (now with enhanced nucleophilic character) to the palladium center is promoted[10] (Scheme A.5).

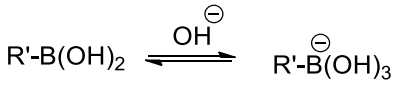

Scheme A.5 Activation of a boronic acid by action of hydroxide formation of the "ate" complex[10]

This also explains the conditions tipically used for Suzuki reactions carried out in this manuscript: toluene/methanol in the presence of a base such as potassium carbonate, allowing the formation of the methoxyde which activates the organoboron.

A.2.2 Sonogashira cross coupling

The synthesis of the compound **1** and **2** involved what so called a Heck-Cassar-Sonogashira reaction[11-13], or more briefly known as Sonogashira. This most likely represents the main cross coupling method for linking of the kind sp-sp^2 carbon (both vinyl or aryl)[14-15]. Considering the Figure A.2, you may notice immediately a first difference compared to the previous described Suzuki cross coupling, in the Sonogashira reaction the organometallic specie, a copper acetylide, is not preformed and is not stoichiometric, but is generated in situ in catalytic amounts through the use of a copper(I) salt as cocatalyst. This specie then enter in the catalytic cyle in the Scheme A.3; in the following one is reported the proposed path[16] which is responsible for the generation of this specie (Scheme A.6).

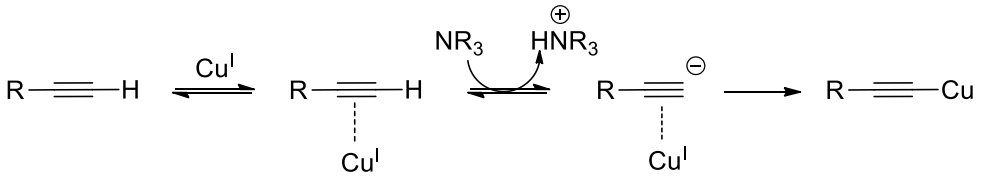

Scheme A.6 Mechanism for copper acetylide formation[16]

The mechanism proposed consists into a first coordination of the copper to the triple bond; this interaction leads to an increase in acidity of the acetylenic proton, which is subsequently extracted by a base (typically an amine) with formation of the organometallic species, which then accesses the transmetallation process restoring the copper(I) salt.

Sonogashira reactions are quite robust and can be achieved in mild condition (e.g., acqueous conditions, low temperatures, weak bases), for instance in the synthesis of the intermediate **7** and **9** in this chapter, they were performed at room temperature with good yield. However there are some important practical aspects to be taken into account; in particular the presence of oxidizing agents[14-15] (e.g., oxygen) must be excluded, as it promotes the formation of homocoupling products due to Glaser coupling, therefore Sonogashira reactions have to be performed rigorously under inert atmosphere.

A.3 Knoevenagel condensations (KC)

The synthesis of the compounds in third chapter was divided into two parts: the preparation of the **a** series, in which we made use of cross coupling reactions and electrophilic aromatic substitutions, and the conversion of its constituents into the derivatives of the series **b** and **c**. These steps were carried out

by Knoevenagel condensations, which have represented the cornerstone of the synthetic approach that led to the desired dipolar dyes.

The first historical example of Knoevenagel reaction was reported by the homonymous German chemist in 1896[17] about condensation of malonic acid with aromatic aldehydes. Today KC represents a relevant method of carbon-carbon bond formation which is widely used in organic synthesis for the preparation of a wide variety of chemical intermediates used in different areas, such as pharmaceutical, cosmetics, perfume and polymer industry[18-20], therefore a lot of research have been dedicated to the subject aiming to improve the synthetic methodologies. Such condensations take place between an aldehyde or a ketone with a compound with active methylene usually in presence of a base[18], according to the following scheme.

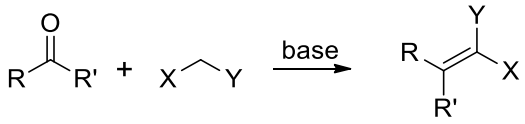

Scheme A.7 General equation for Knoevenagel condensation

Wherein both X and Y, or just one of them, has electron withdrawing character (e.g., CN, COOR, CHO, COR, SO_2R) capable of increasing the acidity of the methylene protons, in our specific case the nitrile groups of the malononitrile and the carbonyl ones of the 1,3-diethyl-2-thiobarbituric acid.

KC can be catalyzed by a variety of chemical species such as amines[18, 21] (the most common), ammonium salts[22], aminoacids[23] and many other species, that can be readily found in the literature. Made this premise, it is possible to discuss the course of these reactions that, according to the nature of the substrates and conditions (i.e., type of catalyst, solvent), can basically follow two paths[18] (Scheme A.8).

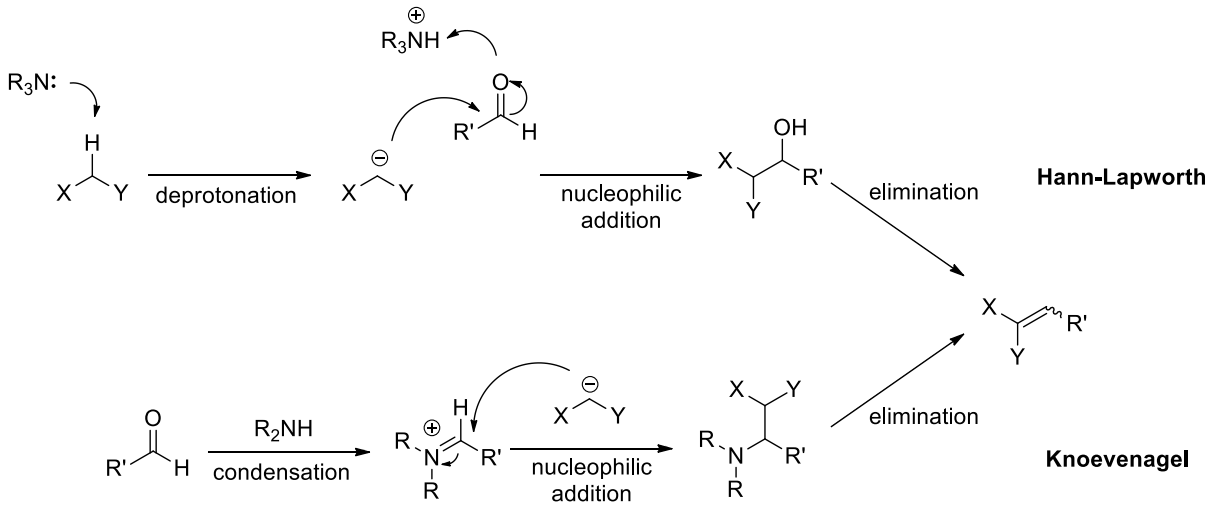

Scheme A.8 Hann-Lapworth and Knoevenagel mechanisms for KC

The mechanism on the top is known as Hann-Lapworth[24]. When the catalyst is a tertiary amine (e.g., triethylamine), it represents the main way that leads to the condensed product[18]; the base is responsible for deprotonation of the specie bearing the active hydrogens, generating a stabilized anion that gives addition to the carbonyl with formation of hydroxy intermediate, followed by dehydration to the final alkene. The mechanism on the bottom is known as Knoevenagel[17] one that, when the base chosen is a primary or secondary amine, represents a competitive path with the Hann-Lapworth one that leads to the same condensed product through the formation of an iminium salt. Concerning the cases in this manuscript, a study in the literature by Prout et al.[25] about KC condensation between 3-methylcyclohexanone and malononitrile, carried out in a mixture of water/ethanol and catalyzed by β-alanine, showed that Hann-Lapworth type course was favoured.

Regarding the experimental protocols used, the first KC carried out was the one for the synthesis of **18** (**Ib**). In this case the reaction was carried out by dissolving **14** (**Ia**) in toluene then adding malononitrile that, being not completely soluble in the reaction medium, has required the addition of absolute EtOH up to complete dissolution. After warming up the reaction the product precipitated (the reaction does not lead to the formation of other non soluble byproducts, but just water). After purification qualitative assays showed that the condensed product was not soluble in pure EtOH. In this view the subsequent protocols were implemented by performing the reactions exclusively in absolute EtOH. In the cases of the synthesis of **21** and **25** (respectively **IIIb** and **IIIc**), the starting aldehyde **17** (**IIIa**), was only sparingly soluble in EtOH, as for the preparation of **18** (**Ib**), these condensations were carried out by

dissolving **IIIa** in a minimum amount of toluene and, after the addition of the active methylene compounds, ethanol was added till completely solubilization of all the reagents.

In the fourth chapter several organic reactions have been carried out, aimed at multisteps synthesis of the two final compounds (**31** and **34**). Among them are found to be of particular interest the homologation of the aldehyde (**28**) and the Horner-Wadsworth-Emmons reaction for the preparation of **33**. Therefore in the next sections they will be briefly discussed in a broader context of belonging, respectively, the conversion of an aldehyde into a terminal alkyne and the olefination of carbonyl compounds through Wittig type reactions, describing also the Horner-Wittig ones which have been used in the synthesis of the pH-probes (**1-4**) exposed in the second chapter

A.4 Seyferth-Gilbert homologation / Bestmann-Ohira modification

The conversion of an aldehyde into a terminal alkyne falls within the group of homologation reactions, in which the carbon chain is lengthened by one unit. Preparation of alkyne from carbonyl derivatives is an important methodology in organic chemistry, allowing the synthesis of aldehyde and ketones that, in this view, can be therefore considered to be precursors of target acetylenes. A broad discussion on the key methods for such transformations has been described by Koshinen et al.[26]; they are the Corey-Fuchs (Scheme A.9), the Colvin rearrangement (Scheme A.9) and the Seyferth-Gilbert homologation.

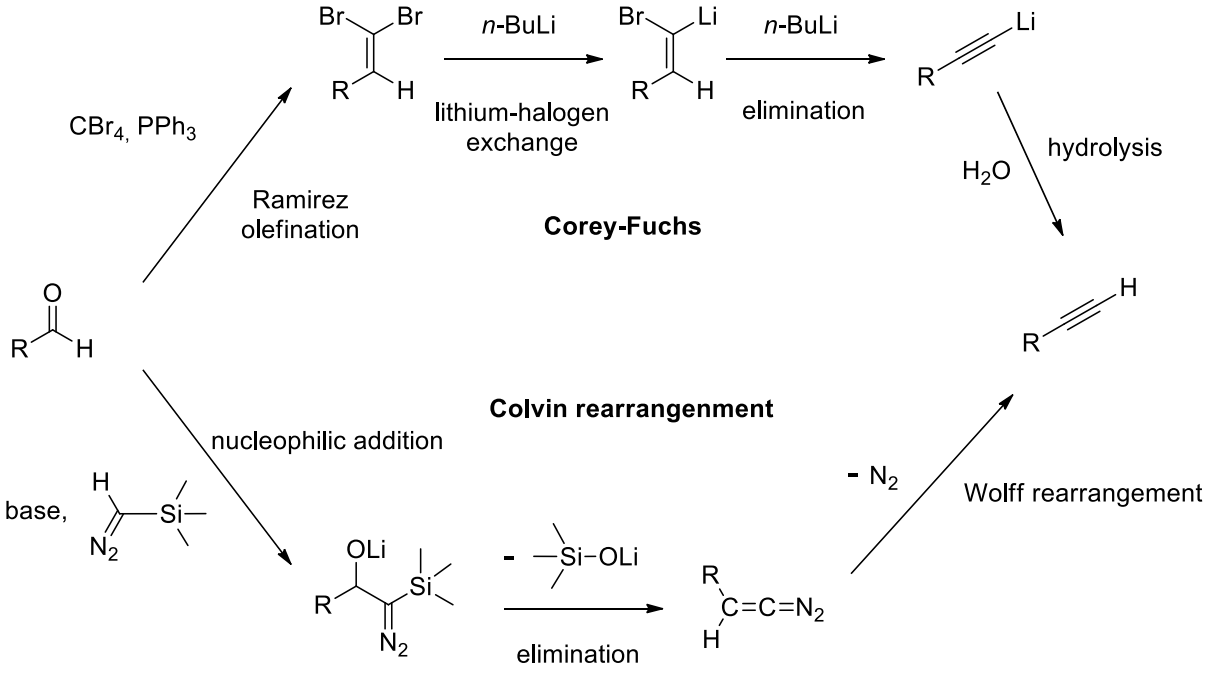

Scheme A.9 Corey-Fuchs (top) and Colvin rearrangement (bottom) for aldehyde homologation

Corey-Fuchs[27] are performed by generating a phosphorous ylide by reaction of triphenylphosphine with tetrabromomethane, to which the carbonyl compound is added. A Wittig type reaction[26], known as Ramirez olefination[28], leads to the formation of a dibromoolefin. Then the latter one is reacted with *n*-BuLi, getting lithium acetylide by halogen-lithium exchange followed by elimination. The hydrolysis of the organometallic species returns the desired alkyne.

The Colvin rearrangement[29] takes place by treating the aldehyde or the ketone with trimethylsilyldiazomethane lithium salt (thermally unstable and therefore usually generated in situ), that gives nucleophilic attack followed by elimination of lithium trimethylsilanolate leading to a diazoalkene. The latter one undergoes Wolff rearrangement[26] to afford the alkyne.

The Seyfert-Gilbert[30-31] homologation is reported in the Scheme A.10.

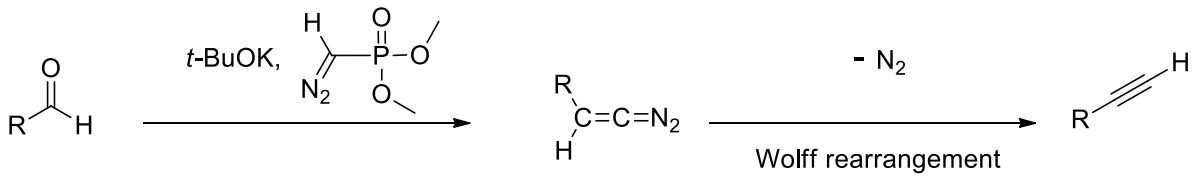

Scheme A.10 Seyferth-Gilbert homologation

The reaction involve the use of dimethyldiazomethylphosphonate which is deprotonated by a steric hindered base (tipically *t*-BuOK), leading to the corresponding anion. It's assumed a nucleophilic attack on the carbonyl group affording an intermediate, that collapses to oxaphosphethane and eliminates dimethylphosphate (similarly to Horner-Wittig-Emmons reaction) leading to a diazoalkene. The latter one undergoes nitrogen extrusion and 1,2-shift of the alkyl moiety (Wolf rearrangement) as in the Colvin rearrangement affording the desired alkyne. However both trimethysilyldiazomethane and dimethyldiazomethylphosphonate lithium salt are sensitive to temperature and can undergo thermal decomposition[26]; in fact common protocols for the two processes are carried out at low temperature (i.e., THF solution at -78°C). Furthermore dimethyldiazomethylphosphonate is not commercially available and requires synthesis. In this view the Bestmann-Ohira[32-33] modification of the Seyferth-Gilbert homologation represents an improvement of the latter points. In particular Ohira demonstrated that treatment of dimethyl (1-diazo-2-oxopropyl)phosphonate with K_2CO_3 (substoichiometric) in

MeOH, leads to dimethyldiazomethylphosphonate (Scheme A.11) in high yield and, in parallel, the stability of the latter one is improved by the low concentration of methoxide in the solution[26, 33].

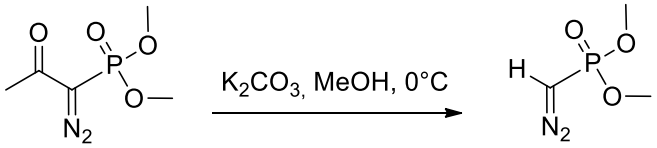

Scheme A.11 Bestmann-Ohira conditions for in situ generation of dimethyldiazomethylphosphonate

These conditions have been adopted in the protocol for the synthesis of **29**. However the starting aldehyde (**28**) was only partially soluble in pure MeOH, therefore a cosolvent (THF) was added till completely solubilization. The reaction represents a good alternative to the most common Corey-Fuchs with positive features in terms of experimental protocol (no *n*-BuLi manipulation), conditions (mild base) and purification, in fact the reaction leads to the formation of dimethylphosphate (water soluble), whereas in the Corey-Fuchs the formation of the dibromoolefin affords triphenylphosphine oxide as byproduct. Finally the Bestmann-Ohira reagent allows a certain synthetic flexibility, in facts under suitable conditions the alkyne generated can directly undergo 1,3-dipolar cycloaddition with azide in click chemistry fashion, without previous isolation and purification[34-35] (Scheme A.12).

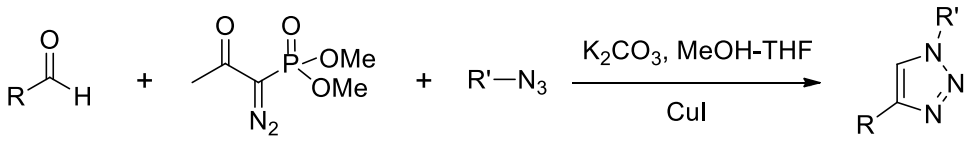

Scheme A.12 One-pot synthesis of 1,4-disubstituted tryazole

A.5 Wittig type reactions

Wittig type reactions represent a versatile and efficient way for carbonyl olefination, allowing the formation of carbon-carbon double bonds from aldehyde and ketones. The amount of studies carried out for such transformation is literally huge[36-38], due to the interest of understanding what are the factors that regulate some aspects of these versatile reactions such as reactivity and stereoselectivity.

A.5.1 Classical Wittig reactions

Reported for the first time in 1953 by G. Wittig[39], the reaction involves the use of a phosphorous ylid (generated by the action of a base on a suitable phosphonium salt) which is reacted with an aldehyde or a ketone as reported in the Scheme A.13[38].

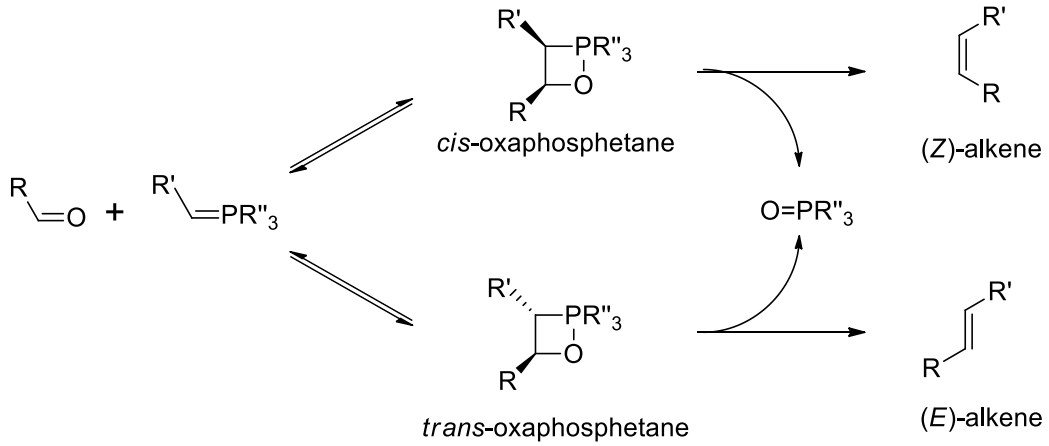

Scheme A.13 Wittig reaction reaction[38]

As depicted the reaction can, when allowed by the nature of the reagents, lead to the two stereoisomers of alkene (*E*/*Z*). The mechanism of the reaction has been debated for several years and many paths have been proposed[40], such has the formation of a betaine intermediate[41] due to nucleophilic attack of the ylid on the carbonyl moiety, followed by ring closure to oxaphosphetane. However nowadays it has been generally assumed that the formation of the four membered ring proceeds through a concertated cycloaddition that can lead to the *cis* or *trans*-oxaphosphetane[42-43]. From these intermediates a *syn*-elimination affords the target alkene with formation of phosphinoxide as byproducts.

The factors that contribute to determining the type of the cyclic intermediate, and then the stereoselectivity of the reaction, are wide and depend on several parameters (e.g., nature of the ylids, of the carbonyl compounds, conditions of the reaction). When the ylids bear an electronwithdrawing group (R') on the α-carbon (e.g., -CN, -COR, -SO_2R) able to give a conjugative stabilization, they are referred to stabilized ones. Such ylids are less reactive and tend to promote the formation of the *trans*-oxaphosphetane and consequently the formation of the *E*-alkene. Vice versa when ylids are not stabilized (e.g., R= alkyl group) they are more reactive than the previous ones, and in this case the

stereoselectivity towards *Z*-alkene is favoured, especially with bulky aldehyde and bulky phosphine ligands.

A.5.2 Horner-Wadsworth-Emmons (HWE)

The HWE[44-45] are a particular variant of the Wittig reactions in which the phosphorus derivative used for the olefination of aldehydes and ketones consists of a phosphonate (Scheme A.14[38]).

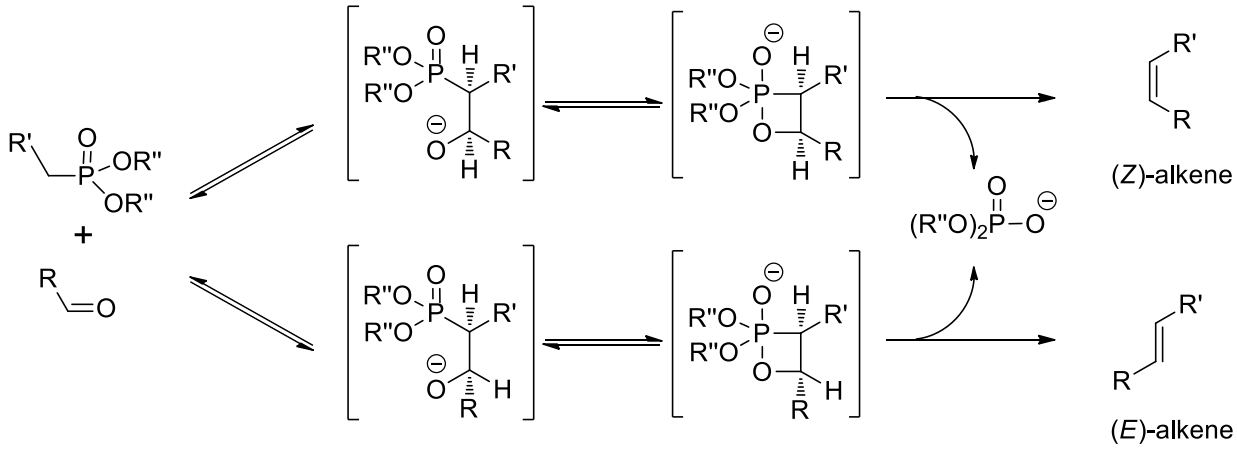

Scheme A.14 Horner-Wadsworth-Emmons reaction[38]

Such reactions are carried out in the presence of a base able to deprotonate the phosphonate, resulting in a nucleophilic addition to the carbonyl and formation of a β-oxyanion intermediate which may have *erythro* or *threo* character. These are in equilibrium, as a result of ring closure, with cyclic oxaphosphethane derivatives (respectively *cis* or *trans*), which eliminate phosphate affording the alkene with *E* or *Z* configuration.

As for classical Wittig reactions, for such the stereochemical feature is fundamental too. The use of phosphonate tends to promote an *E*-selectivity, which is increased by the use of sterically hindered and/ or stabilized phosphonates. Among the advantages of HWE there is also a usually more simple purification of the products, as the phosphate produced is water soluble. Finally the phosphonates can be readily prepared by means of Michaelis-Arbuzov reaction[46], treating suitable alkyl halide with triphenylphosphite.

The combination of the two processes represents the protocol which have been exploited for the synthesis of **33**, wherein the phosphonate **32** was prepared by Arbuzov-Michaelis on the 4-(bromomethyl)benzonitrile and then reacted with the aldehyde **28**.

A.5.3 Horner-Wittig (HW)

In this class of Wittig reactions the phosphorus derivative involved is a phosphin oxide[47] that, although it may seem similar to phosphonate in HWE, it provides some specific properties that make HW reactions unique and very useful (Scheme A.15[38]).

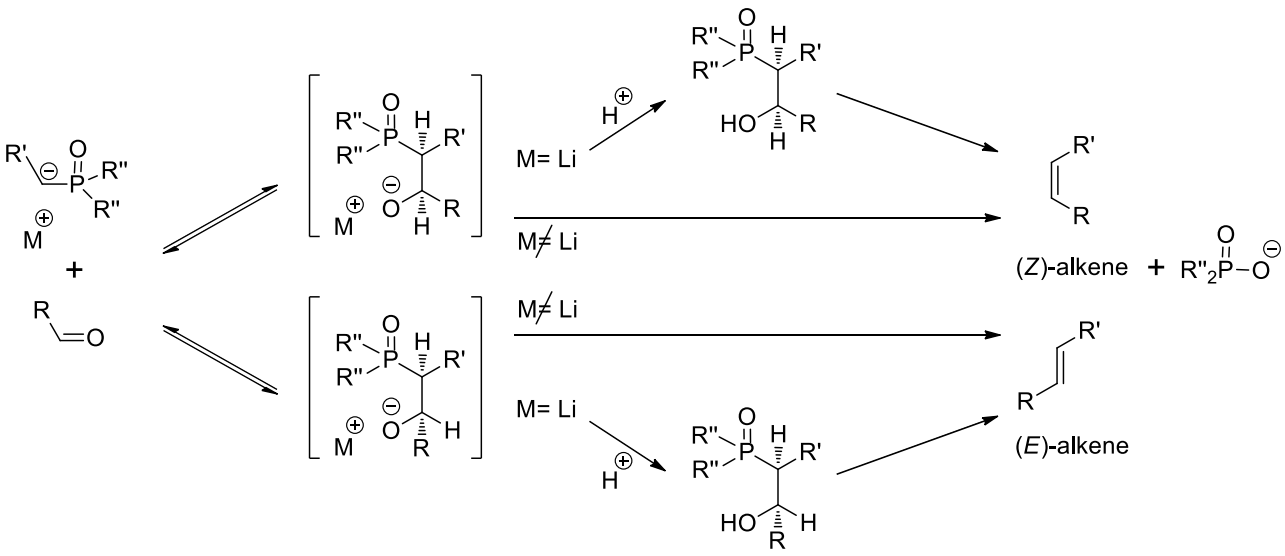

Scheme A.15 Horner-Wittig reaction[38, 48]

The illustrated mechanism may be discussed by dividing it into two parts[48], depending on whether the base used to deprotonate the phosphin oxide is a lithium-based one or not. In the case of non-lithiated (e.g., KOH, NaH), the reaction proceeds with nucleophilic addition, leading to the formation of a β-hydroxy phosphin oxide which may be *erythro* or *threo* type, that undergoes ring closure and *syn*-elimination, affording *Z* or *E*-alkene. Considering that the nucleophilic addition is reversible and the elimination leading to the *E*-alkene faster, these reactions usually display good *E*-stereoselectivity when the phosphin oxide bears a stabilizing group otherwise, with non-stabilizing ones (e.g., R'= H, Me) the stereoselectivity is reduced. However in this case the character of the phosphin oxide plays a key role; in particular the use of a lithium-base leads to the formation of stable intermediates, which allows to

quench the reaction and isolate the two diastereoisomers. After separation they can be subjected again to *syn*-elimination in a stereocontrolled manner, allowing to get pure *E* or *Z* alkene.

Bibliography references

[1] C. C. C. Johansson Seechurn, M. O. Kitching, T. J. Colacot, V. Snieckus, *Angew. Chem. Int. Ed.* **2012**, *51*, 5062-5085.

[2] C. Glaser, *Ann. Chem. Pharm.* **1870**, *154*, 137-171.

[3] F. Ullmann, J. Bielecki, *Ber. Dtsch. Chem. Ges.* **1901**, *34*, 2174-2185.

[4] H. Meerwein, E. Büchner, K. van Emster, *J. Prak. Chem.* **1939**, *152*, 237-266.

[5] M. S. Kharasch, E. K. Fields, *J. Am. Chem. Soc.* **1941**, *63*, 2316-2320.

[6] M. S. Kharasch, C. F. Fuchs, *J. Am. Chem. Soc.* **1943**, *65*, 504-507.

[7] R. F. Heck, *J. Am. Chem. Soc.* **1968**, *90*, 5518-5526.

[8] A. Suzuki, *J. Organomet. Chem.* **1999**, *576*, 147-168.

[9] N. Miyaura, A. Suzuki, *Chem. Rev.* **1995**, *95*, 2457-2483.

[10] J. Clayden, N. Greeves, S. Warren, P. Wothers, *Organic Chemistry*, Oxford University Press Inc., **2001**.

[11] K. Sonogashira, Y. Tohda, N. Hagihara, *Tetrahedron Lett.* **1975**, *16*, 4467-4470.

[12] L. Cassar, *J. Organomet. Chem.* **1975**, *93*, 253-257.

[13] H. A. Dieck, F. R. Heck, *J. Organomet. Chem.* **1975**, *93*, 259-263.

[14] R. Chinchilla, C. Nájera, *Chem. Soc. Rev.* **2007**, *107*, 874-922.

[15] R. Chinchilla, C. Najera, *Chem. Soc. Rev.* **2011**, *40*, 5084-5121.

[16] P. Bertus, F. Fecourt, C. Bauder, P. Pale, *New J. Chem.* **2004**, *28*, 12-14.

[17] E. Knoevenagel, *Ber. Dtsch. Chem. Ges.* **1898**, *31*, 2596-2619.

[18] L. F. Tietze, U. Beifuss, *Comprehensive Organic Synthesis, Vol. 2*, Pergamon Press, Oxford, **1991**.

[19] R. D. Murray, J. Mendez, S. A. Brown, *The Natural Coumarins; Occurrence, Chemistry and Biochemistry*, Wiley, New York, **1982**.

[20] W. C. Meuly, K. Othmer, *Encyclopedia of Chemical Technology, Vol. 7*, John Wiley and Sons, New York, **1979**.

[21] G. Jones, *Organic Reactions, Vol. 15*, Wiley, New York, **1967**.

[22] N. Mase, T. Horibe, *Org. Lett.* **2013**, *15*, 1854-1857.

[23] F. S. Prout, *J. Org. Chem.* **1953**, *18*, 928-933.

[24] A. C. O. Hann, A. Lapworth, *J. Chem. Soc., Trans.* **1904**, *85*, 46-56.

[25] F. S. Prout, V. D. Beaucaire, G. R. Dyrkacz, W. M. Koppes, R. E. Kuznicki, T. A. Marlewski, J. J. Pienkowski, J. M. Puda, *J. Org. Chem.* **1973**, *38*, 1512-1517.

[26] D. Habrant, V. Rauhala, A. M. P. Koskinen, *Chem. Soc. Rev.* **2010**, *39*, 2007-2017.

[27] E. J. Corey, P. L. Fuchs, *Tetrahedron Lett.* **1972**, *13*, 3769-3772.

[28] N. B. Desai, N. McKelvie, F. Ramirez, *J. Am. Chem. Soc.* **1962**, *84*, 1745-1747.

[29] E. W. Colvin, B. J. Hamill, *J. Am. Chem. Soc.* **1973**, 151-152.

[30] D. Seyferth, P. Hilbert, R. S. Marmor, *J. Am. Chem. Soc.* **1967**, *89*, 4811-4812.

[31] J. C. Gilbert, U. Weerasooriya, *J. Org. Chem.* **1982**, *47*, 1837-1845.

[32] G. J. Roth, B. Liepold, S. G. Müller, H. J. Bestmann, *Synthesis* **2004**, *2004*, 59-62.

[33] S. Ohira, *Synth. Commun.* **1989**, *19*, 561-564.

[34] S. Mohapatra, C. Bhanja, S. Jena, S. Chakroborty, S. Nayak, *Synth. Commun.* **2013**, *43*, 1993-2007.

[35] D. Luvino, C. Amalric, M. Smietana, J.-J. Vasseur, *Synlett* **2007**, *2007*, 3037-3041.

[36] A. W. Johnson, *Ylid Chemistry*, Academic Press, New York, **1966**.

[37] M. B. Smith, J. March, *March's Advanced Organic Chemistry: Reactions, mechanisms and structure*, Wiley, **2007**.

[38] M. Edmonds, A. Abell, *Modern Carbonyl Olefination*, Wiley-VCH, **2004**.

[39] G. Wittig, G. Gleisser, *Liebigs Ann.* **1953**, *580*.

[40] P. A. Byrne, D. G. Gilheany, *Chem. Soc. Rev.* **2013**, *42*, 6670-6696.

[41] G. Wittig, A. Haag, *Ber. Dtsch. Chem. Ges.* **1963**, *96*.

[42] E. Vedejs, T. J. Fleck, *J. Am. Chem. Soc.* **1989**, *111*, 5861-5871.

[43] E. Vedejs, C. F. Marth, *J. Am. Chem. Soc.* **1988**, *110*, 3948-3958.

[44] W. S. Wadsworth, W. D. Emmons, *J. Am. Chem. Soc.* **1961**, *83*, 1733-1738.

[45] W. S. Wadsworth, *Org. React.* **1977**, *25*, 73-253.

[46] A. K. Bhattacharya, G. Thyagarajan, *Chem. Rev.* **1981**, *81*, 415-430.

[47] L. Horner, *Pure Appl. Chem.* **1964**, *9*, 225-244.

[48] J. Clayden, S. Warren, *Angew. Chem. Int. Ed.* **1996**, *35*, 241-270.